CRANFIELD UNIVERSITY

DAVIDE DI PASQUALE

Aerodynamic and Cost Modelling for Aircraft in a Multi-Disciplinary Design Context

SCHOOL OF AEROSPACE, TRANSPORT AND MANUFACTURING

PhD Thesis
Academic Year: 2011 - 2015

Academic Supervisors: Prof. A. Mark Savill
Dr. Timoleon Kipouros
Industrial Supervisor: Dr. Carren Holden

December 2015

CRANFIELD UNIVERSITY

SCHOOL OF AEROSPACE, TRANSPORT AND MANUFACTURING

PhD Thesis

Academic Year 2011 - 2015

DAVIDE DI PASQUALE

Aerodynamic and Cost Modelling for Aircraft in a Multi-Disciplinary Design Context

Academic Supervisors: Prof. A. Mark Savill
Dr. Timoleon Kipouros
Industrial Supervisor: Dr. Carren Holden

December 2015

This thesis is submitted in partial fulfilment of the requirements for the degree of Doctor of Philosophy

ABSTRACT

A challenge for the scientific community is to adapt to and exploit the trend towards greater multidisciplinary focus in research and technology. This work is concerned with multi-disciplinary design for whole aircraft configuration, including aero performance and financial considerations jointly for an aircraft program. A Multi-Disciplinary (MD) approach is required to increase the robustness of the preliminary design data and to realise the overall aircraft performance objectives within the required timescales. A pre-requisite for such an approach is the existence of efficient and fully integrated processes.

For this purpose an automatic aero high-speed analysis framework has been developed and integrated using a commercial integration/building environment. Starting from the geometry input, it automatically generates aero data for loads in a timescale consistent with level requirement, which can afterwards be integrated into the overall multi-disciplinary process.

A 3D Aero-solution chain has been implemented as a high-speed aerodynamic evaluation capability, and although there is not yet a complementary fully automated Aerodynamic design process, two integrated systems to perform multi-objective optimisation have been developed using different optimisation approaches.

In addition to achieving good aircraft performance, reducing cost may be essential for manufacturer survival in today's competitive market. There is thus a strong need to understand the cost associated with different competing concepts and this could be addressed by incorporating cost estimation in the design process along with other analyses to achieve economic and efficient aircraft. For this reason a pre-existing cost model has been examined, tested, improved, and new features added. Afterwards, the cost suite has been integrated using an integration framework and automatically linked with external domains, providing a capability to take input from other domain tool sets. In this way the cost model could be implemented in a multi-disciplinary process allowing a trade-off between weight, aero performance and cost. Additionally, studies have been performed that link aerodynamic characteristics with cost figures and reinforce the importance of considering aerodynamic, structural and

cost disciplines simultaneously. The proposed work therefore offers a strong basis for further development. The modularity of the aero optimisation framework already allows the application of such techniques to real engineering test cases, and, in future, could be combined with the 3D aero solution chain developed. In order to further reduce design wall-clock time the present multi-level parallelisation could also be deployed within a more rapid multi-fidelity approach. Finally the 3D aero-solution chain could be improved by directly incorporating a module to generate aero data for performance, and linking this to the cost suite informed by the same geometrical variables.

ACKNOWLEDGEMENTS

I would like to express my profound gratitude to my supervisor Prof. Mark Savill who gave me the great opportunity of working in the challenging field of multi-disciplinary design and optimisation and also for his support and suggestions over this period of time. I would also like to especially thank Dr. Timos Kipouros for his assistance and advices on the subject. He has continuously motivated and encouraged me through the entire research period. A special thanks goes to all my Cranfield colleagues, especially, Giuseppe Trapani, Giovanna Ferraro and Ritesh Amin. I would further acknowledge Dave Gore from Airbus for his expert guidance on cost modelling. I wish extend my gratitude to Airbus Operation Ltd, and especially to the entire Methods and Tools Department in Filton (UK). Finally, my gratitude goes to Anthony Mosquera from Applied Computing&Engineering and Steve Dean from Qinetiq for their help and support with Model Center integration software. Finally, I want to express my sincere gratitude to my industrial supervisor Dr. Carren Holden for providing me the opportunity to blend the academic research in an industrial context and for her guidance and support. Of course, I would like also to thank my family for the never ending support they rendered to me throughout my life. They gave me the opportunity to travel as well as study a subject that I am passionate about, without regrets and without questioning my choice.

This research project has been supported by Airbus Operation Ltd/Engineering and Physical Science Research Council (EPSRC) PhD Industrial case fellowship. Financial support from both institutions is here gratefully acknowledged.

TABLE OF CONTENTS

LIST OF FIGURES

LIST OF TABLES

NOMENCLATURE

α	Angle of attack
$b/2$	Wing semi span
$B_{i,p}(u)$	Bernstein polynomials of degree p
$\overline{c}_i$	Coefficient vector corresponding with the three dimensional coordinates
Λ	Sweep angle
c	Chord
$\bar{c}$	Mean aerodynamic chord
c_p	Gas constant pressure specific heat
c_v	Gas constant volume specific heat
C_D	Drag coefficient
C_L	Lift Coefficient
C_M	Moment coefficient
C_N	Normal force coefficient
C_P	Pressure coefficient
D	Drag
D_i	Induced drag
D_f	Friction drag on skin
D_p	Pressure drag on skin
D_v	Viscous drag
D_{vp}	Viscous pressure drag
D_w	Wave drag
ε	Turbulent dissipation
$\vec{f}$	Dynalpy like-vector
$\boldsymbol{F}_C$	Inviscid flux vector
$\boldsymbol{F}_V$	Viscous flux vector
L	Lift
M	Mach Number
M_∞	Free-stream Mach number
M_{crit}	Critical Mach number
M_{eff}	Effective Mach number

N	Number of snapshots
p	Pressure
Pr	Prandlt number
R	Gas constant
Re	Reynolds number
R_{le}	Leading edge radius
$\overline{R}$	New design shape
$\overline{r}$	Datum shape
S_s	Skin surfaces
S_w	Wave drag integration surface
S_v	Viscous drag integration surface
S_i	Induced drag integration surface
V	Mean velocity of the object relatively to the fluid
V_∞	Free-stream Velocity
$\overline{v}_n$	Design variable vector
t/c	thickness over chord
T	Temperature
$\boldsymbol{u}$	Velocity vector
$\overline{\boldsymbol{u}}$	Mean component
$\boldsymbol{u}'$	Fluctuating component
$\boldsymbol{U}$	Conservative variables vector
$\overline{U}_n$	Design perturbation vector
θ	Trailing edge angle
ω	Specific rate of dissipation (of the turbulence kinetic energy k)
W_{fuel}	Fuel weight
W_{PL}	Payload weight
W_o	Empty weight
γ	c_p/c_v
K_B	Boltzmann constant
k_t	Fluid thermal conductivity
$\boldsymbol{\tau}$	Viscous stress tensor

$\overline{\boldsymbol{\tau}}_{\boldsymbol{r}}$	Reynolds stress tensor
h_0	Specific stagnation enthalpy
e_o	Specific total energy
E	Oswald efficiency factor
Γ	Circulation
$\overline{k}$	Kinetic energy
Δt	Time step in the CFD computation
ΔH	Variations of enthalpy
ΔS	Variations of entropy
q	Dynamic pressure
$\boldsymbol{q}$	Conduction heat flux vector
$\boldsymbol{q}_t$	Turbulent heat flux vector
ρ	Density of the fluid
μ	Dynamic viscosity
μ_l	Laminar viscosity
μ_t	Eddy viscosity
ν	Kinematic viscosity
∇	Nabla operator
$\otimes$	Tensor product
A/C	Aircraft
ACARE	Advisory Council for Aviation Research and Innovation in Europe
ALC	Airplane Life Cycle
ACT	Architect Cockpit Tool
ATL	Automated-Tape Laying
AFP	Automated Fibre Placement
AFW	Airframe Weight
ANN	Artificial Neural Network
AR	Aspect Ratio (b^2/S)
CAD	Computer Aided Design
CEM	Common Engineering Model
CERs	Cost Estimating Relationships

COC	Cash Operating Cost
CPU	Central Processing Unit
CST	Classic Shape Transformation
DDL	Drag Due to Lift
DOC	Direct Operating Cost
DM	Decision Maker
DNS	Direct Numerical Simulation
DVs	Design Variables
ERR	Economic Rate of Return
ESDU	Engineering Science Date Unit
FBSM	Feature-Based Solid Modelling
FDM	Finite Difference Method
FEM	Finite Element Method
FFD	Free Form Deformation
FIFO	First-Input-First-Output
FVM	Finite Volume Method
GA	Genetic Algorithm
HLF	Hybrid Laminar Flow
IOC	Indirect Operating Cost
IPTs	Integrated Project Teams
IS	Information System
LCC	Life Cycle Cost
LG	Landing Gear
LTM	Long Term Memory
CFD	Computational Fluid Dynamics
MD	Multi-Disciplinary
MDD	Multi-Disciplinary Design
MDO	Multi-Disciplinary Optimisation
MDTOCs	Multi-Disciplinary Trade-Off Capabilities
MOTS	Multi-Objective Tabu Search
MSO	Multi-Shape Optimisation
MTM	Medium Term Memory
NSGA-II	Non-dominated Sorting Genetic Algorithm II

NPV	Net Present Value
NPW	Net Present Worth
NRC	Non-Recurring Cost
NURBS	Non-Uniform Rationale B-Spline
PDE	Partial Differential Equation
POD	Proper Orthogonal Decomposition
PVs	Present Values
RAM	Random Access Memory
RANS	Reynolds-Averaged Navier-Stokes
RBF	Radial Basic Function
ROI	Return of Investment
ROM	Reduced Order Model
SA	Simulated Annealing
SD	Search Diversification
SFC	Specific Fuel Consumption
SI	Search Intensification
SSR	Step Size Reduction
STM	Short Term Memory
TP	Technological Product
TS	Tabu Search
VII	Viscous-Inviscid Interaction

1 The Research Project

1.1 Aims and Objectives

Multi-disciplinary approach is essential in the design process of real world applications. The aim of the research project is to support the development of a new aircraft preliminary multi-disciplinary design process by increasing the fidelity of the elements of the existing conceptual design process through exploitation of appropriate domain tools. A Multi-Disciplinary approach is required to increase the robustness of the preliminary design data and to realise aircraft performance objectives within the required timescales. A pre-requisite for such an approach is the existence of efficient and fully automated and integrated processes. Specifically, within it the multi-disciplinary process the research work is focused on the aero and cost part of the process.

In addition to achieving good aircraft performance, reducing cost may be essential for manufacturer survival in today's competitive market. There is thus a strong need to understand the cost associated with different competing concepts and this could be addressed by incorporating cost estimation in the design process along with other analyses to achieve economic and efficient aircraft.

The objectives are therefore the development on a 3D aero automatic design process and the development of a cost estimation model fully integrated with other domain tool sets.

Additionally, studies have been performed that link aerodynamic characteristics with cost figures to understand the interactions between the two disciplines.

1.2 Context

The Strategic Research Agenda [1], prepared by ACARE (Advisory Council for Aeronautical Research in Europe), initiative has posed a series of challenging goals for aeronautical industry, calling for a drastic reduction in both noise and pollution levels for future aircrafts. It set the direction for European research to reduce the environmental impact of aircraft and to improve safety and operational efficiency. ‘Vision2050’ for commercial transport aircraft sets a

target of a 75% reduction in fuel consumption and CO_2 emissions, with a 20-25% reduction to be achieved through airframe improvements. This is a huge challenge to aircraft designers, since modern aircraft comprise a large number of highly complicated systems. The traditional manual approach would find it difficult, if not impossible, to satisfy future design requirements. This step change in performance is in part dependent on the successful integration of Multi-Disciplinary Design Capabilities (MDDC) at the preliminary design stage.

In order to achieve such improvement in aircraft performance, a paradigm shift in the capability of simulation-based design process is necessary. Hence, numerical optimisation techniques based on computational solutions have become a critical tool for the aircraft industry to help designers to meet future design challenges.

That is the reason why industry invests substantial money and resource in developing new multi-disciplinary optimisation capability. It seems inevitable that a method of this type will provide the basis for aircraft designs of the future. Even though, one of the stumbling blocks is still the mind-set of the designers that are often not inclined to change their way of working. This research is aimed at providing a contribution towards the development of innovative methodologies and simulation capability in a multi-disciplinary context.

1.3 Thesis Contents Outline

The thesis is structured as follows. **Chapter 1** describes the aim and objectives of the research and gives a short overview of the context in which the research has been carried out. **Chapter 2** briefly describes the aims and objectives of this research and also gives an introduction to multi-disciplinary design and optimisation approach explaining the reasons of its wide interests from the engineering community and some historical aspects. Additionally, it describes the wing design process in an industrial context.

Chapter 3 describes the current geometry data management issues in a MDO framework and proposes a new paradigm for geometry management across the various stages of aircraft design.

Chapter 4 provides a description of one of the most important tasks to be performed within the optimisation process, which is the Computation Fluid Dynamics (CFD) analysis. Moreover, some information about different CFD methods and their industrial usage are given.

Chapter 5 introduces aircraft drag and its implications on the performance of the aircraft, provides a basic classification of drag sources. Moreover it gives an overview of drag prediction methods. **Chapter 6** provides a detailed technical description of the integrated automatic aero high-speed analysis framework. The main modules that make up the automated process are presented and discussed and some results shown. **Chapter 7** offers a literature review of geometry parameterisation techniques used for optimisation purposes. **Chapter 8** gives an overview of the optimisation background theory and the optimisation algorithms used in the two integrated multi-objectives optimisation systems developed and presented later on in the chapter. The differences between these two are discussed and results analysed. **Chapter 9** gives an introduction to cost engineering and the reasons for its wide interest to the engineering community. Furthermore it gives some insight into the most used cost modelling in aerospace industry together with a detailed description of the in-house cost suite retrieved and improved. Moreover the work performed in integrating this model within an integration framework and automatically linked with external domains is described. **Chapter 10** deals with coupling aero performance and financial design. Specifically, a trade study is conducted in order to see the impact on the Direct Operating Cost (DOC) and manufacturing cost varying parametrically the wing thickness over the chord along the wing span. While the process is not automated, the purpose is to establish a useful foundation for further study and to gain insight into the interactions between technical and program design. Finally, **Chapter 11** summarises the results of this work and identifies future development directions to improve the effectiveness of an automated preliminary multi-disciplinary process.

2 Introduction to Multi-disciplinary Design Optimisation

2.1 Historical Review

The design of a large commercial aircraft is a daunting task. It represents the synthesis of a staggering array of technologies, concepts, material and subsystem into a functioning machine.

A complete commercial aircraft is one of the most complex systems in operation today. Moreover, its design is rendered all the more complex, because it is not only an engineering system, which performs a set of specified functions, but it, is also a value-creating mechanism for the manufacturer, and furthermore, it generates revenue to the operator, the airline.

Thus, there is an imperative to design commercial aircraft not for maximum range or maximum speed or maximum payload, or even for minimum cost, but rather for maximum value for the entire program [2]. The design for value has been addressed in various forms by several authors. Reinhardt [3] discusses a historical case study: the valuation techniques used for the Lockheed Tri Star commercial aircraft, and their effects on the program. Dickinson et al. [4] discuss portfolio optimisation: “the problem of managing multiple interdependent development projects” and illustrate several aircraft development techniques used at Boeing to maximize. Slack [5] discussed the concept of value directly, and Browning [6] addresses value through consideration of the interactions between, cost, schedule and performance. The field of technical aircraft design is a very well established and thoroughly documented. Engineers developing new aircraft have performed the problem of meeting a set of technical requirements with a system design hundreds of time. Recently, there have been advances in performing these design tasks from a multi-disciplinary standpoint, where several different types of analysis are combined into an optimisation simulation process. In the design of complex engineering systems, such as a large transport aircraft, it is critical that the interactions between the subsystems of the problem are accounted for. Only by considering the fully coupled system can an optimal design emerge [7, 8, 9]. Several examples of these multidisciplinary analysis and optimisation techniques may be found in the

literature, see for instance the work of Wakayama [10, 11], Kroo [12], Baker [13], Perez [14] or Peoples [15].

One of the earliest disciplines to embrace optimisation in a relevant way was aerospace design. It was motivated from the requisite to reduce the large cost associated with carrying “unnecessary” weight in aerospace vehicles. To minimize mass structure is the requirement emanating from the need to save fuel through trajectory design. In this context recognizing the desire/need of optimisation and actual implementation becomes an important issue. At present, optimisation is an enabling technology in innovation. Multi-Objective and Multi-Disciplinary optimisation tools are essential in the design of real word applications. Optimisation has become a part of the design activity in all major disciplines, that are not only restricted to engineering. The motivation behind this is the need to produce economically relevant products or services with embedded quality. Improved production and design tools, supported by the advancement of computational resources have aided the consideration of optimisation methods in new developments and different applications. Optimisation is usually associated with design, and it implies the identification of the best solution for the given circumstances including a particular set of constraints on the development resources, current knowledge and so on, exploiting interdisciplinary interactions to achieve a better overall system than can be achieved by ignoring the interactions [16]. The rapid evolution of computing technology offers great potential to the engineers in facilitating the use of optimisation in design in a real-word application framework [17].

2.2 Rationale

Nowadays, economic and safety reasons govern the actual design of commercial aircraft. In the highly competitive commercial aviation market of today, the transport aircraft design is driven by the minimisation of Direct Operating Cost (DOC). In fact, the strict link between aircraft performance, volume of passengers, and the nearly constant increase in fuel costs, has underlined the paramount importance of reducing DOC for airlines to be able to transform revenues in profits. Indeed, the low profit margin that airlines continue

to face is a major challenge for the civil aircraft sector [18]. In the aircraft industry, aggressive weight targets, shortened development time scale and reduced costs to be competitive in today's global market require different approach for the design process [19].

A Multi-Disciplinary wing design and Optimisation (MDO) assessment has to be performed for the improvements to be pursued. Since the design of wings is a real-world problem, the aerodynamic performances are dependent on several parameters, which mean that the optimisation is also multi-objective. Finding an optimum solution to the problem is a complex and iterative procedure that demands the intervention and judgment of the designer. This implies that every design process is time-consuming and also that the results obtained depend on the expertise of the designer himself. In this context the use of numerical optimisation methods reduce drastically the design processing time and resources employed as well as the dependence of the solution on the designer's abilities and experience.

The motivations mentioned above, highlight the importance of the development of an integrated automated multi-disciplinary optimisation framework for aircraft design. Optimisation is practiced through software programs and requires relevant computer resources. The techniques of optimisation in the recent years have not changed significantly but the areas in which they are applied have increased at considerable rate.

Successful use of optimisation requires the prerequisites of a mathematical modelling of the design problem, knowledge of the computer software, and of the optimisation technique. In this context the significant progress and improvement of the digital computation have aided the continuous soaring application of the optimisation to a variety of disciplines, especially for the engineering optimisation these resources were necessary to handle the non-linear problems associated with it.

The correct implementation of such an analysis hence involves the utilisation of the most advanced numerical simulation methods in a wide variety of disciplines. It is clear that from a technical point of view it represents a very challenging task.

2.3 Wing design in an industrial environment

The complete aircraft design process, ahead of manufacturing, goes through three distinct phases that are carried out in sequence. These phases are, in chronological order: conceptual design, preliminary design and final detailed design, as illustrated in Figure 2.1. Discrimination between the three design phases is related to the differences in activities, tools, amount of people and expertise, time scales, etc. that take place in each part of the process.

Figure 2.1: Higher level view of a design process

The conceptual design stage defines the mission in the light of anticipated market requirements, and determines a general preliminary configuration, together with first estimates of size, weight and performance. Once the decision to proceed further with the design is taken, the preliminary design stage can begin. The preliminary design phase starts when the major changes in the design solutions are over. The preliminary phase uses the baseline configuration that was elaborated and selected during the conceptual phase. The purpose of this phase is to further develop and mature the baseline design, until sufficient understanding of the design quality is achieved. At that point, the design can be frozen and the detail design phase can start. In the preliminary design phase, only minor changes are made to the conceptual design. If major changes were to be demanded during this phase, the conceptual design process would have been flawed initially.

In the preliminary design stage the aerodynamic shape and structural skeleton progress to the point where detailed performance estimates can be made and guaranteed to potential customers. While the costs are still fairly moderate, because resource has not yet ramped up, decisions made at this stage essentially determine both the final performance and the development costs. At the end of the preliminary design phase, the configuration is frozen and precisely defined. Moreover, the end of this phase brings a major decision – to

commit the aircraft to the manufacturer or not. In the final design stage the structure must be defined in complete detail, together with complete systems, including control systems, avionics, electrical and hydraulic systems, landing gear, and cabin layout for commercial aircraft. This stage will also focus on design verification and formal approval or acceptance of the designs. The verification and acceptance process may well involve prototype manufacture and testing. Apart from concerns over product performance, issues such as reliability, safety and maintainability will be major priorities at this stage. The objective of the detailed design phase is a completely specified product that meets both customer and business needs. At this stage in the process, the number of staff involved in the design team will increase greatly. Major costs are incurred at this stage, during which it is also necessary to prepare a detailed manufacturing plan.

Designing a good airplane is not a trivial process. The problem arises both from the complexity of the flow over the airplane and from the need to treat complex multi-disciplinary interactions such as the trade-off between aerodynamic performance and structural weight. Flow past the airplane is governed by a system of highly non-linear equations, and for various problems such as viscous separated flows, their solution is still beyond our reach. This problem is mitigated using experience and empirical rules determined after studying many aircrafts.

It is traditional for the different aspects or components of the design to be considered by dedicated teams. For aircraft, this might consist of an aerodynamics division, a structures division, a control systems division, costing teams, and so on, or it might consist of a team considering the fuselage, another considering wing design, others looking at the tail plane, propulsion systems, and so on. Managing the interrelationships between such teams becomes a key part of managing the design process, especially if they are geographically widely dispersed, as is now often the case.

In the Civil Aeronautical Industry, the trend nowadays is to consider from the beginning in an integrated design process, a large number of design requirements and constraints from the engineering and manufacturing

disciplines. So an alternative, and more modern, approach to managing design is via the use of Integrated Project Teams (or IPTs). Such teams are normally formed specifically for the product being designed and grow in size progressively throughout the preliminary design phase. If an IPT-based approach is used, it is then usually supported by specialist divisions that are charged with providing technical input across a range of project teams. These specialist divisions are responsible for the retention and development of core technologies and capabilities. They will also interface directly with any research activities and engage in technology-acquisition programs. The tools used by designers will be much more sophisticated than during concept work. For example, the designers considering structures will, as a matter of routine, make use of quite detailed stress analysis, normally by means of Finite Element Analysis (FEA). Those considering the wings will pay close attention to predictions of the airflow. This may involve extensive use of computational methods (CFD).

At the present time, preparing the input for computational analysis is commonly far from automated. It is quite normal for the design team to take from days to weeks, depending on the complexity of the model, to prepare the meshes needed for the CFD analysis of a complete aircraft configuration, to run the analysis, and to assimilate the results. This severely restricts the number of different configurations that can be considered during preliminary design [20]. Hence, there is also a strong desire that different toolsets are fully chained together, with automatic data transmission and interpretation along the chain.

The wing may be considered as the most important component of an aircraft, since a fixed-wing aircraft is not able to fly without it. Moreover, the wing geometry and its features influence all other aircraft components**.** The primary function of the wing is to generate sufficient lift force or simply lift (L). However, the wing tends to generate two unwanted aerodynamics effects, namely drag force or drag (D) and nose-down pitching moment (M), see Figure 2.2. While a wing designer is looking to maximize the lift, the other two (drag and pitching moment) must be minimized. The pitching moment on the wing is part of the total moment that must be balanced using the lift on the horizontal stabilizer.

Normal aircraft require downforce on the tail to lift the nose up. The increment in drag resulting from the tail aerodynamic forces required to trim the aircraft about its centre of gravity. Trim drag usually is a form of induced and form drag on the horizontal tail. Strictly, the absolute value of moment is controlled/kept small to avoid large trim drag penalty.

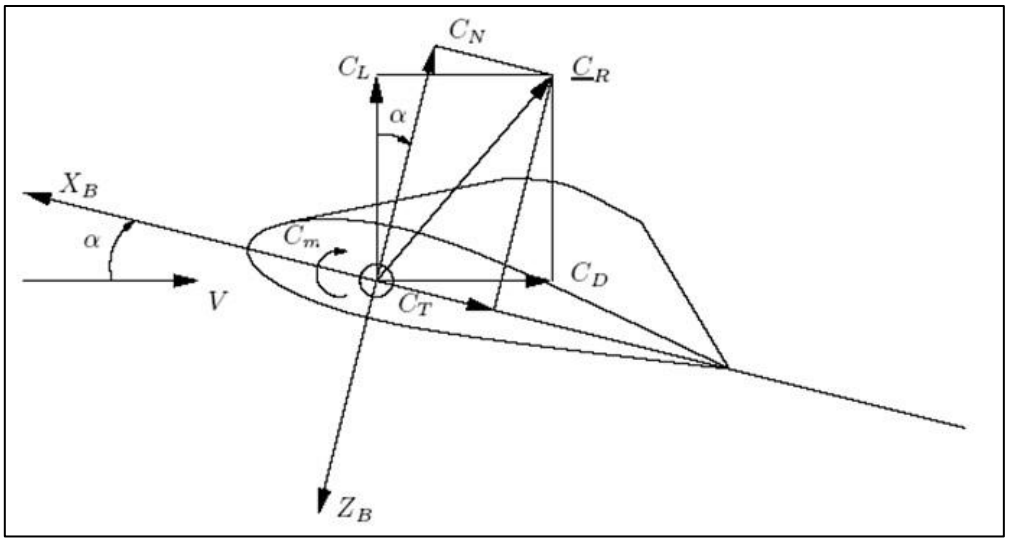

Figure 2.2: The forces and moments acting on a wing [21]

Transport aircraft wings are designed to meet a set of multidisciplinary technical requirements which cover aerodynamic performance, propulsion, stability and control, weight, structures, aeroelasticity, systems, production techniques, etc. In principle, all requirements are equally important and a change in any one of them (for instance, structures) could lead to significant consequences for the accomplishment of another (for instance, aerodynamics). Optimal overall design will always involve a compromise between these requirements. Hence, the evolution and the final aerodynamic configuration of an aircraft wing are determined by several factors, only one of which is aerodynamics itself. These design goals must be collectively satisfied throughout all flight operations and missions. An essential element of the design process is that it is always made up of iterations. Figure 2.3 shows the usual iterative design procedure.

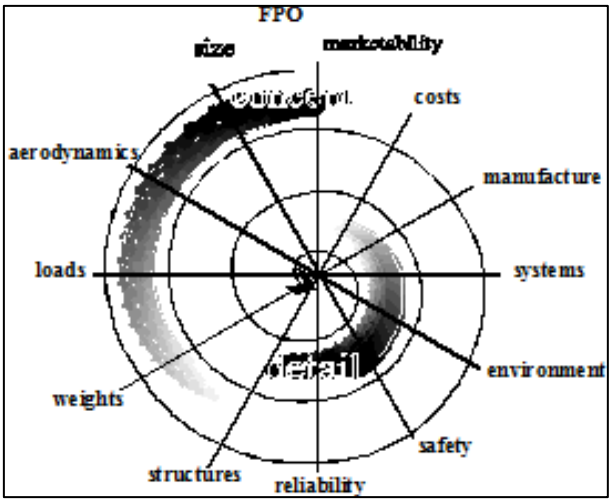

Figure 2.3: Spiral design process [22]

After a trial configuration has been subjected to a first analysis of its characteristics, it will be seen either that it does not meet all the requirements, or that it does comply with them, but improvements in some respect are possible. Only after a number of configuration changes have been incorporated will the designer be able to determine whether the final configuration may be regarded as the best conceivable design, bearing in mind the inevitable uncertainties peculiar of the engineering design [23]. Design is much more subjective, there is rarely a single “correct” answer. For instance, 76 wings were designed for Boeing 767 in 1986 until the best wing was eventually finalized. However, only 11 wings were designed for Boeing 787 Dreamliner in 2008 [24]. A reduction in the number of iterations is evident which is partially due to the advances in software/hardware in recent years, and partly due to the years of experience of wing designers.

The design and analysis of the wings of aircraft is one of the principal applications of the science of aerodynamics, which is a branch of fluid mechanics. Small modification in the airfoil has a direct impact on the performance of an aircraft. A lot of disturbances are generated in the air when an aeroplane flies. It is through the study of these disturbances of the flow past the airfoil, lot of design considerations can be done.

Planform selection is one major element in wing design. The initial specification of the overall wing planform parameters is a crucial stage in the development of

any aircraft, since changes to planform further down the design process are often extremely difficult to accommodate and usually represent an unacceptable delay or cost to the process. The wing planform is the shape when seen from above. To be aerodynamically efficient, a wing should be straight with a long span from side to side but have a short chord (high aspect ratio). But to be structurally efficient and hence light weight, a wing must have a short span but still enough area to provide lift (low aspect ratio). Selecting the wing span is one of the most basic decisions to make in the design of a wing. The span is sometimes constrained by contest rules, hangar size, or ground facilities but when it is not we might decide to use the largest span consistent with structural dynamic constraints (flutter: a rapid self-feeding motion, potentially destructive, excited by aerodynamic forces, in on an object couple with a structure's natural mode of vibration to produce rapid periodic motion). This would reduce the induced drag directly. However, as the span is increased, the wing structural weight also increases and at some point the weight increase offsets the induced drag savings. The selection of optimum wing span thus requires an analysis of much more than just cruise drag and structural weight. The interaction between the inertial, elastic, and aerodynamic forces that occur when an elastic body is exposed to a fluid flow have to take into account, therefore the aeroelasticity, which is the branch of physics and engineering that studies these interactions is part of the design problem. See Figure 2.4.

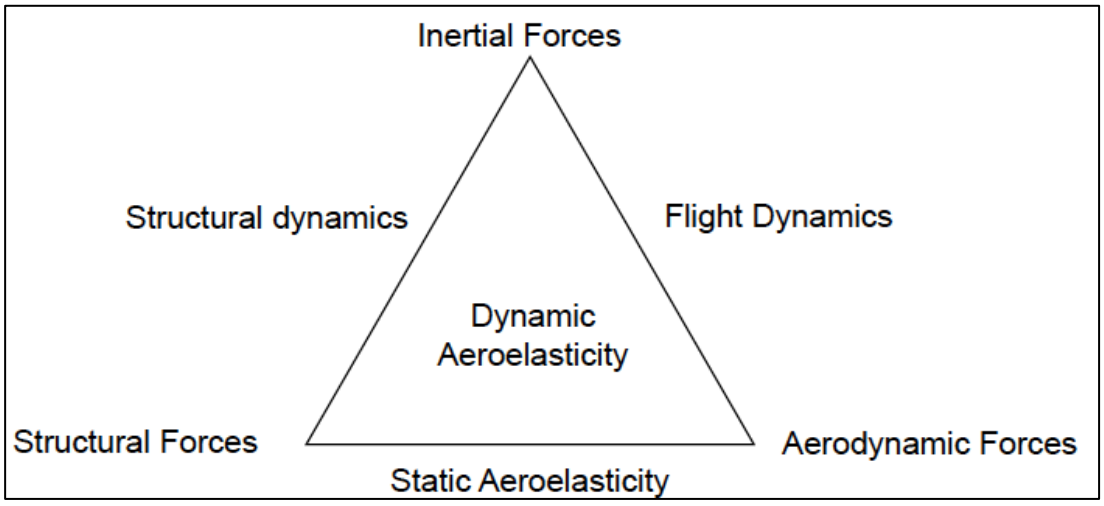

Figure 2.4: Schematic of the forces interactions that arise aeroelasticity problems [25]

Although the elliptic wing is ideal for minimizing induced drag, it is difficult to manufacture. Tapered wings are easier to manufacture and, if properly designed, can have similar drag minimization characteristics to elliptical wings. Rectangular wings are the easiest to manufacture but can be heavier than necessary since lift loads decrease near the tip, there is more structure at the tip than necessary. The planform must provide the necessary space for both high-lift systems and control surfaces outside the main structural box, and it must also accommodate the landing gear. The maximum thickness and thickness distribution are chosen to yield the required strength and structural efficiency of the wing, and to provide enough space for fuel tank volume, see Figure 2.5.

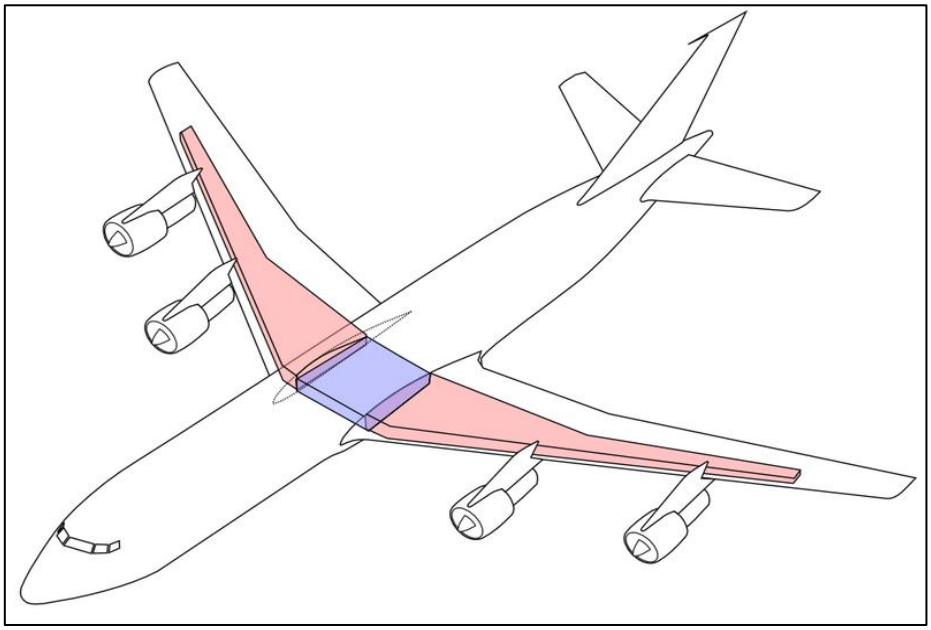

Figure 2.5: Layout of a modern airliner's main fuel tanks [26]

After the planform, the airfoil section is the second most important wing parameter. The detailed shapes of the individual sections of the wing are the critical elements that define its performance. The airfoil section is responsible for the generation of the optimum pressure distribution on the top and bottom surfaces of the wing such that the required lift is created with the lowest aerodynamic cost (i.e. drag and pitching moment). The design of the airfoil is a complex and time-consuming process and needs expertise in fundamentals of aerodynamics.

A regular flight operation consists of take-off, climb, cruise, turn, manoeuvres, descent, approach and landing (Figure 2.6)

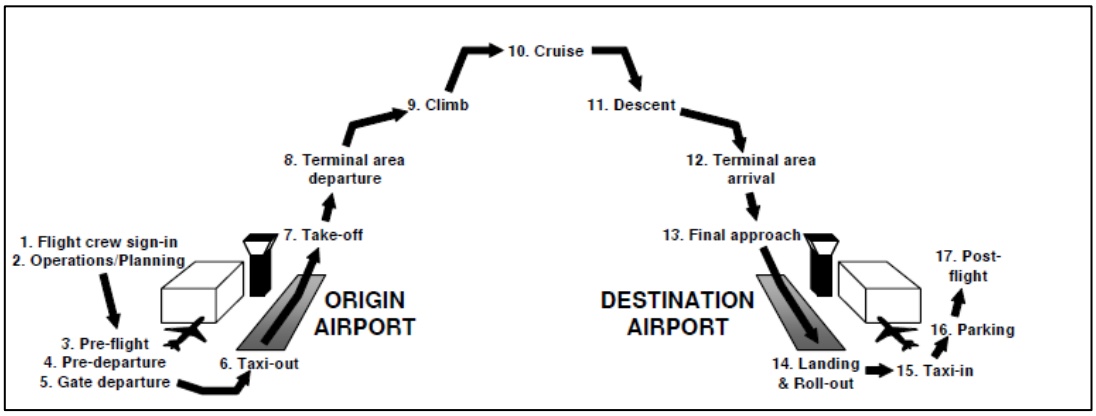

Figure 2.6: Simplified regular flight operation [27]

Basically, the airfoil's optimum function is in the cruise phase of the mission in which an aircraft spends much of its flight time. Selecting an airfoil is a key part of the overall wing design process. Selection of an airfoil for a wing begins with the clear statement of the flight requirements. For instance, subsonic flight design requirements are very different from supersonic flight design objectives. On the other hand, flight in the transonic region requires a special airfoil that meets Mach divergence requirements.

2.3.1 A short insight into transonic aerodynamics

Since the advent of the jet engine, virtually all commercial transports now cruise in the transonic speed range, because this allows the range of the aircraft to be maximised, as shown below by the Breguet range equation (2.1). From this equation it is possible to gather that technology advances reduce specific fuel consumption (SFC), increase Lift over Drag ratio (L/D) and lower empty weight (W_0). Given these technological characteristics and the amount of payload and fuel on board, the Breguet range equation determines the maximum flight distance.

$$Aircraft\ Range = \frac{V\ L/D}{SFC} ln\left(1 + \frac{W_{fuel}}{W_{PL} + W_0}\right) \quad (2.1)$$

A mixture of supersonic and subsonic flow characterizes the transonic regime, and in some cases there are also large areas of separation at off-design conditions.

As the Mach number increases, shock waves appear in the flow field, getting stronger as the speed increases. The shock waves lead to a rapid increase in drag, both due to the emergence of wave drag, due to the loss of total pressure through the shock, and also because the pressure rise through a shock wave thickens the boundary layer, leading to increased viscous drag. Thus cruise speed is limited by the rapid drag rise. An example of drag rise characteristics for the RAE2822 transonic airfoil is depicted in Figure 2.7.

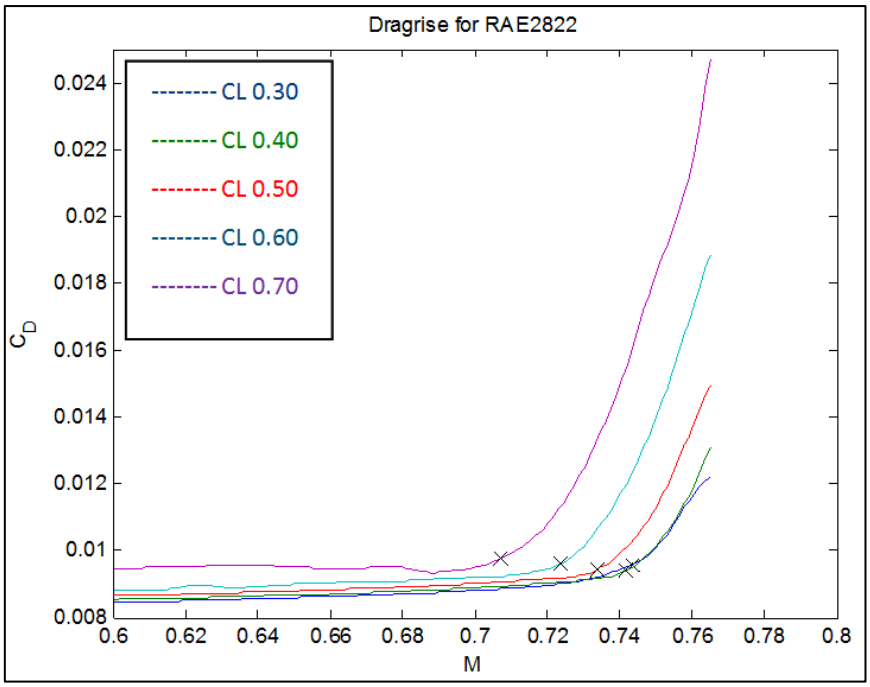

Figure 2.7: Drag rise curves for RAE2822

Usually, the supersonic region of the flow is terminated by a shock wave, allowing the flow to slow down to subsonic speeds, (see Figure 2.8 and Figure 2.9). This complicates both computations and wind tunnel testing.

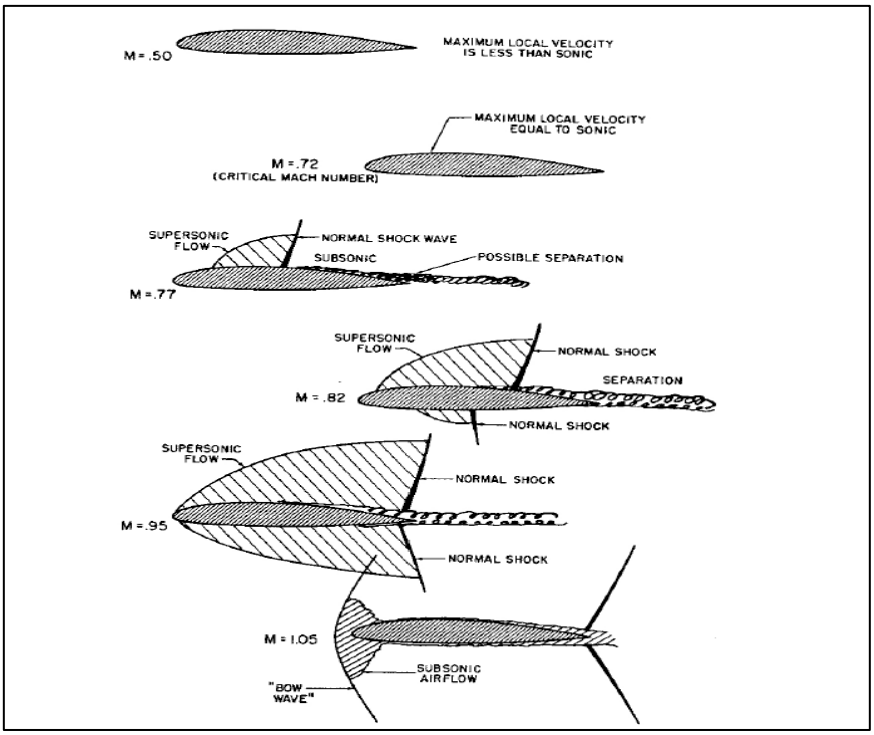

Figure 2.8: Progression of shock waves with increasing Mach number [28]

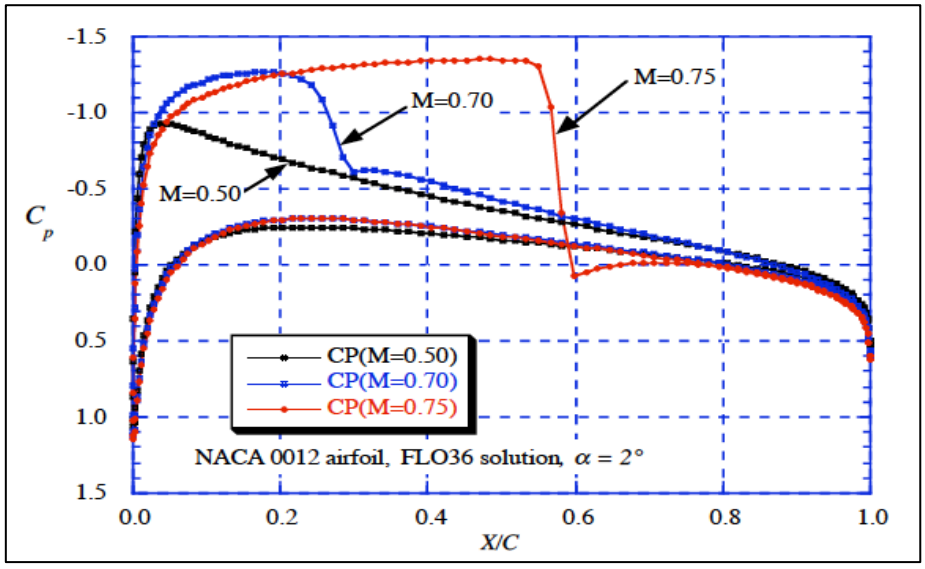

Figure 2.9: Pressure distribution change with increasing Mach number, NACA 0012 airfoil, α = 2° [28]

These characteristics are better explained by a comparison of a conventional sub-sonic aerofoil with a supercritical aerofoil as shown in Figure 2.10. As an aerofoil designed for sub-sonic flow approaches the speed of sound, the flow that accelerates around the upper surface continues to accelerate until it

reaches super-sonic speed due to the continuous curvature along the upper surface.

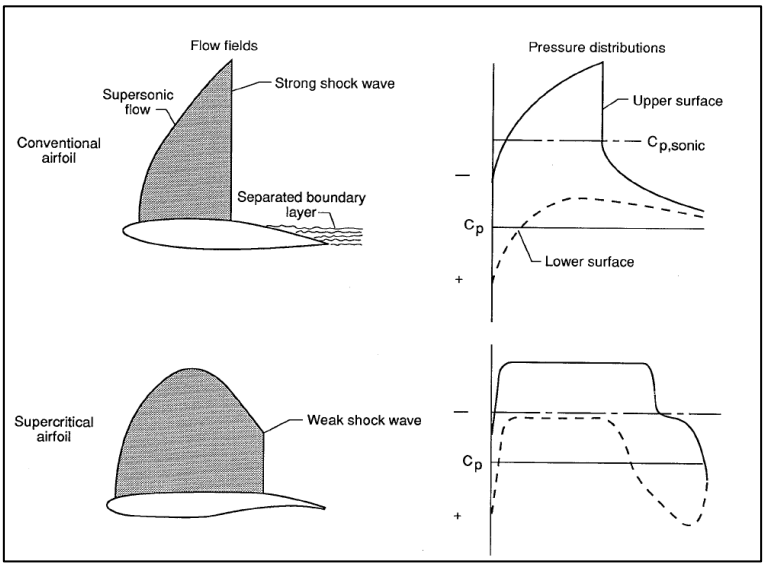

Figure 2.10: Flow fields and *Cp* distribution around conventional and supercritical aerofoils. [29]

This region of local supersonic flow is terminated near the mid-chord by a strong shock wave, which decelerates the flow to subsonic speeds. The adverse pressure change caused by the shock may cause the boundary layer to separate causing buffeting and stability problems. Low amount of aft camber also results in lower loading at the trailing edge. Applying the super-critical aerofoil elements decreases the shock strength and moves it aft of the mid-chord. The larger leading edge radius rapidly accelerates the flow resulting in a more 'filled out' pressure distribution. The acceleration is haltered by the flattened upper surface and results in a significantly weaker shock wave, which could be weakened further by shaping the aerofoil for decelerating the flow ahead of it. The additional aft camber on the supercritical section is also shown to increase aft loading.

Transonic wings are usually swept back, see Figure 2.11, to reduce the effective Mach number normal to leading edge, resulting in lower wave drag.

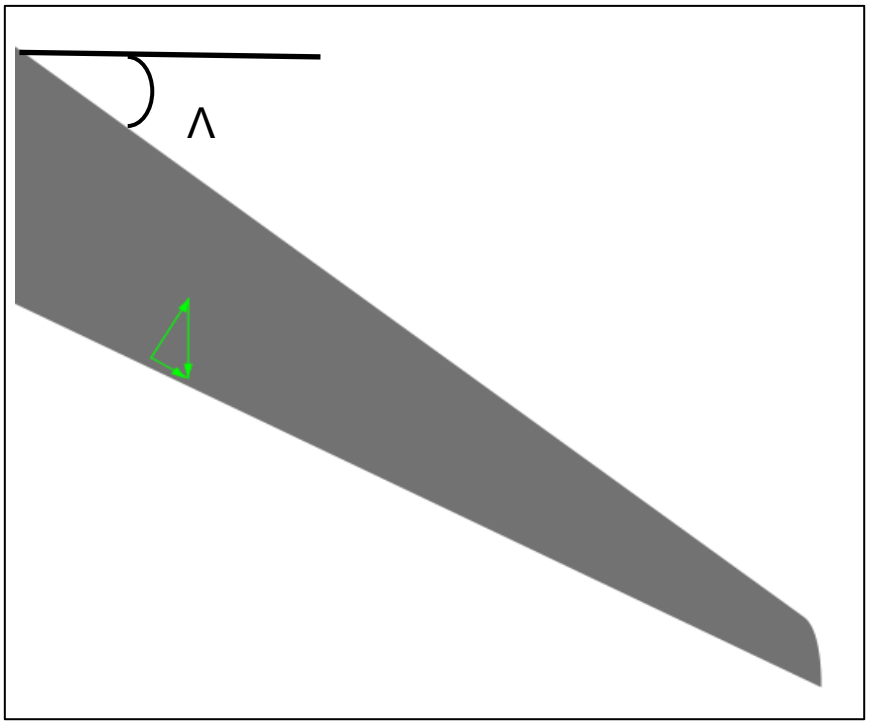

Figure 2.11: Example of Swept back wing [30]

Wing sweep is chosen almost exclusively for its desirable effect on transonic wave drag. (Sometimes for other reasons such as a c.g. problem or to move winglets back for greater directional stability.) The free-stream velocity vector can be resolved into components normal and parallel to the leading edge. The normal component is responsible for the aerodynamic characteristics, and its associated Mach number is:

$$M_n = M_\infty \cos \Lambda. \tag{2.2}$$

It follows that if the critical Mach number for the same wing, but unswept, is denoted with M^*, then the critical Mach number for the swept wing would be given by the relation

$$M_{crit} \cos \Lambda = M^* or\ M_{crit} = M^* \,/\, cos\, \Lambda \tag{2.3}$$

This result can also be interpreted as follows. In a flow with M_∞, the sectional characteristics would correspond to an effective lower Mach number given by:

$$M_{eff} = M_\infty \cos \Lambda \tag{2.4}$$

Although swept wings delay drag rise, there are other problems associated with swept wings. Even at subsonic speed, wing sweep will tend to shift the load outboard, leading to high section C_L, and the possibility of outboard stall, accompanied by pitch up. The wing is twisted (washed out) to unload the tip. The lift curve slope also decreases. In addition, for a given span, the actual wing length is longer, and hence heavier. High lift devices are not as effective if the trailing edge is swept, and finally, swept wings are prone to flutter. Thus the total system design must be considered when selecting the wing sweep. One of the benefits of advanced airfoils is that they can achieve the same performance as a wing with a less capable airfoil using less sweep. This explains the general trend to modern transports having less sweep than earlier transports.

The transonic problem is difficult because it is inherently nonlinear, and the governing equations change the mathematical formulation, being elliptic in the subsonic portion of the flow and hyperbolic in the supersonic part of the flow. This is much more difficult than the subsonic case, where the equations for panel methods are linear.

There is very little analytic theory available for guidance in designing for transonic flow conditions. Importantly, not only is the outer inviscid portion of the flow governed by nonlinear flow equations, but the nonlinear flow features typically require that viscous effects be included immediately in the flow field analysis for accurate design and analysis work.

For civil transonic aircraft, the main problems of aerodynamic design is mainly related to attaining a high drag divergence Mach number, avoiding undesirable flight characteristics at off-design conditions and providing good low speed characteristics of the swept wing.

For transonic designs perhaps the most important aspect of aerodynamic performance considered is the position and nature of the compression shock on the upper surface and how this can be controlled. Essentially, the key to transonic airfoil design to is to control the expansion of the flow to supersonic speed and its subsequent recompression. Key elements of supercritical airfoils are:

- A relatively large leading edge radius is used to expand the flow at the upper surface leading edge, thus obtaining more lift. The generation of this suction peak is mainly due to security purpose.
- To maintain the supersonic flow along a constant pressure plateau, or even have it slow down slightly approaching the shock. By slowing the flow going into the shock, a relatively weak shock, compared to the amount of lift generated, is used to bring the flow down to subsonic speed. Where the goal is have an isentropic compression.
- Another means of obtaining lift without strong shocks at transonic speed is to use aft camber. One potential drawback to the use of aft camber is the large zero lift pitching moment.
- Finally, to avoid flow separation, the upper and lower surfaces at the trailing edge are nearly parallel, resulting in a finite thickness trailing edge, which is also good for the manufacturing process.

The base drag is small at transonic speeds compared to the reduction in profile drag. These are the essential ingredients in supercritical airfoil design, and modern aerodynamic designers pick the best aspect of these elements to fit their particular application. Unfortunately, airfoil sections are some of the most critical shapes encountered in engineering and their design is never simple. Describing these sections in an efficient way is a critical part of any optimal design process.

2.3.2 Design methods applicable to aerodynamic design

They can be categorized into two classes: inverse design methods and direct optimisation methods. The inverse design method determines the shape of an airfoil or a wing that produces a prescribed pressure distribution on its contour at a specified flow condition, whereas a direct optimisation method tries to design an aerodynamic configuration by minimizing a given objective function by iterating directly on the geometry. However, inverse design methods have a few drawbacks compared to the direct optimization methods. First, inverse design methods require aerodynamic designers to specify a target pressure distribution producing improved aerodynamic performance and satisfying

structural and manufacture constraints. Although experienced aerodynamicists can identify desirable flow characteristics, for example, reduced shock strength and/or elimination of flow separation, it is not a trivial task to develop a target pressure distribution that will provide these benefits while maintaining other aerodynamic requirements such as lift and pitching moment. Moreover, inverse design methods have difficulty in enforcing geometric constraints. For example, the wing thickness cannot be easily specified. For instance, when a shock-free wing is designed, the resulting wing tends to be too thin. This leads to penalties for the complete aircraft design, such as increased structural weight and reduced fuel volume. Another drawback of the inverse design method is the lack of versatility in a sense that it is difficult for the inverse method to be extended to more general design problems, such as multipoint design, wing planform design and multidisciplinary design optimisation. The clearest benefit offered by inverse methods is the speed with which a design can be achieved. Other benefits come from the inverse method indicating, directly or indirectly, that particular combinations of pressure and geometric constraints are incompatible, saving otherwise-wasted design effort. The direct optimisation methods, on the other hand, are very versatile, that is, they can be extended to other design problems and combined with other design tools with relative ease. This not only allows the wing to be designed in a controlled manner (from inboard to outboard) but also can be useful in exploring sensitivities of the flow to particular features of the geometry. But there are no models or guides that determine whether the “perfect” design has been achieved.

2.3.3 Actual Wing Aero Design

Generally, the aerodynamic designer is given the planform and maximum thickness and told to design the twist and camber under certain design condition. The best starting point for the wing design is an existing design, which is not too different, in terms of planform and performance, from the target. If this is not possible, a long iterative process is involved, starting in two dimensions.

The aerodynamicist usually tends to design a number of sections between 9 and 12 normally function of the wing span length, in order to accurately capture the span-wise geometry variation of the wing. The wing surface is constructed as an interpolation/extrapolation of these airfoil shapes along the span as needed. Among these sections to be designed the main ones are the root section, the crank section, the tip section and the section with the maximum local loading.

The aerodynamic design process starting point is an initial geometry definition resulting from the conceptual design. It usually consists of planform geometry and thickness distribution along the span and dihedral information.

Wing design often proceeds by selecting a desirable wing lift distribution and then finding the geometry that achieves this distribution. The conceptual design office usually provides this wing lift distribution. If it is not given the optimum lift distribution is predicted fairly well with an algorithm based on Lifting line theory, developed by Prandtl during the early 20th century [31], which also gives a first approximation to the twist distribution. The lift distribution predicted is usually close to the elliptical distribution (see Figure 2.12) in order to minimize the induced drag, associated with wing lift generation, at cruise condition, although it might be better for the design if the load is shifted inboard slightly, reducing the root bending moment and hence wing structural weight. In any case, a good target pressure distribution along the span should yield an elliptic loading, a straight isobar pattern and low drag profile. Favourable to the maintenance of low drag flows over a range of cruise Mach numbers; the reduction of the shock wave over the upper surface of the wing is the primary target. A decrease in the amplitude of the shock wave induces a decrease of the shock drag, which is related to a reduction of fuel consumption.

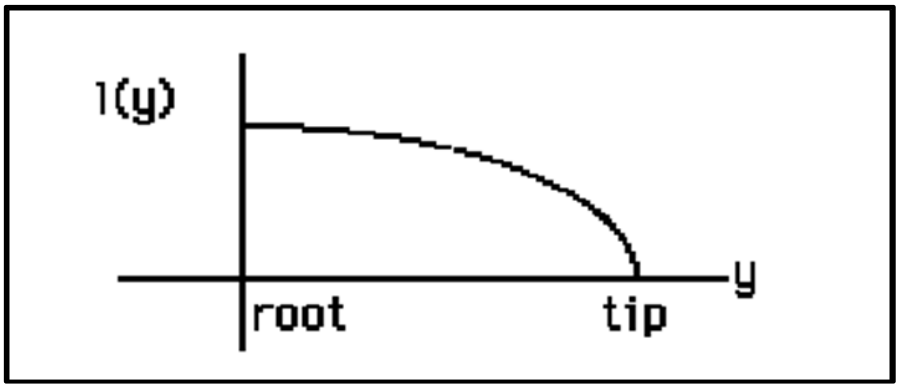

Figure 2.12: Elliptical lift distribution [32]

Once the lift distribution is known, given that the section lift coefficient is related to the lift distribution by:

$$C_{ll}(y) = \frac{l(y)}{qc[y]} \tag{2.5}$$

It is possible to find the three dimensional Cll distribution, knowing the lift distribution, the desired flight conditions (q) and the planform shape.

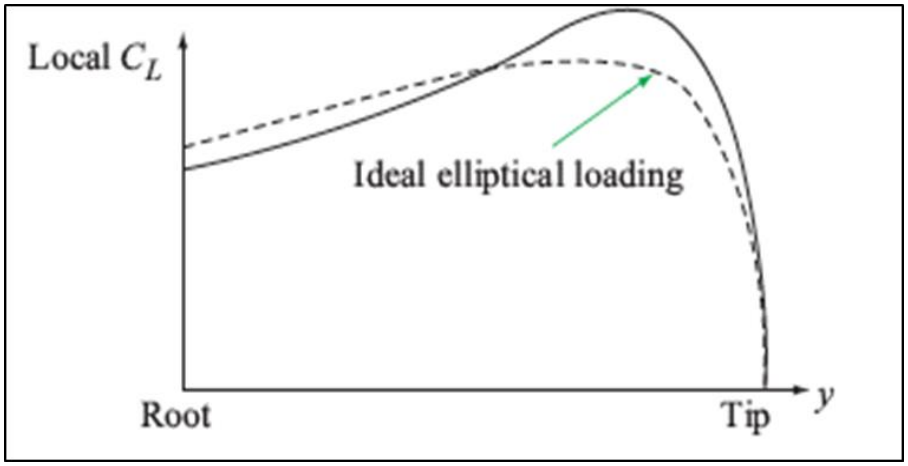

Figure 2.13: Elliptical loading distribution [33]

An initial section must be chosen, usually a 2D profile with low drag for all cruise range, for which its shape should delay the drag rise and checked. This could be an existing airfoil or, a section taken from an existing swept wing. If the latter is the case, it is necessary to obtain an equivalent two-dimensional section, which can be derived from the sweep laws and the concept of equivalence in three- and two-dimensional flow. A streamwise section of a wing and an airfoil

may be said to be equivalent if the distributions of M_n the local Mach number normal to isobars are the same in both cases. Isobars lines on wing surface are line of identical pressure and therefore identical velocity. In the case of the airfoil M_n is simply the surface local Mach number whilst in the case of the wing it is the surface local Mach number normal to the local isobars. The wing is a three-dimensional entity, while an airfoil is a two-dimensional section. If the wing chord is constant, with no sweep angle, no dihedral, and the wingspan is assumed to be infinity, theoretically, the wing lift coefficient would be the same as wing airfoil lift coefficient. In order to design the airfoil at a specified span position, the airfoil theoretical C_l has to be predicted, hence, it is necessary to relate the three-dimensional lift coefficient and flow characteristics (Mach and Reynolds number) into 2D characteristics to take into account for the wing sweep, making use of simple sweep rules [34]:

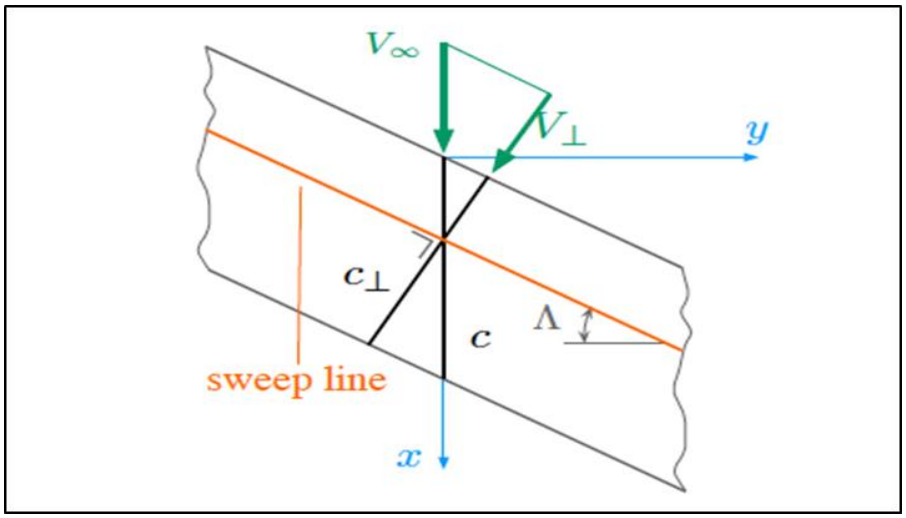

Figure 2.14: Simple sweep theory of an infinite wing (untapered wing) [33]

The following relations were derived from geometric considerations:

$$c_\perp = c \cos \Lambda \tag{2.6}$$

$$z_\perp = z \tag{2.7}$$

So that:

$$\left(\frac{z}{c}\right)_{\perp} = \left(\frac{z}{c}\right)\sec\Lambda \tag{2.8}$$

$$\left(\frac{t}{c}\right)_{\perp} = \left(\frac{t}{c}\right)\sec\Lambda \tag{2.9}$$

where z represents the ordinates perpendicular to the x − y plane. From the aerodynamics of the flow cases, the following was derived:

$$M_{\infty,2D} = M_{\infty,3D}\cos\Lambda \tag{2.10}$$

$$C_{L,2D} = C_{L,3D}\sin^2\Lambda \tag{2.11}$$

These relations demonstrate that the equivalent two-dimensional airfoil is thicker, operates at a lower Mach number, and at a higher lift coefficient than the three-dimensional wing airfoil section.

As the Reynolds number changes with varying chord length, the actual Reynolds number acting on the airfoil section perpendicular to the sweep line needs to be calculated. The Reynolds number is defined as follows:

$$Re_{\infty} = \left(\frac{\rho V_{\infty}\bar{c}}{\mu}\right) \tag{2.12}$$

Where $\bar{c}$ and μ represent respectively the mean aerodynamic chord (MAC) and the dynamic viscosity. Only the velocity and the chord length vary in (2.5), whereas the density ρ and μ are altitude dependent and are constant. Knowing that, the Reynolds number Re⊥ can be scaled by:

$$Re_{\perp} = Re_{\infty}\frac{V_{\perp}}{V_{\infty}}\frac{c_{\perp}}{\bar{c}} \tag{2.13}$$

It is important to note that the simple sweep theory is based on infinite wings and since it relates the swept wing flow to an equivalent two-dimensional flow, it does not include real three-dimensional flow characteristics such as boundary layer movements and others.

Wings are designed such that the flow (except in root and tip regions) is of quasi-two- dimensional nature, in the sense that it varies slowly across the

span. This is true for sweep wings and high aspect ratio, which is typical for modern transport aircraft.

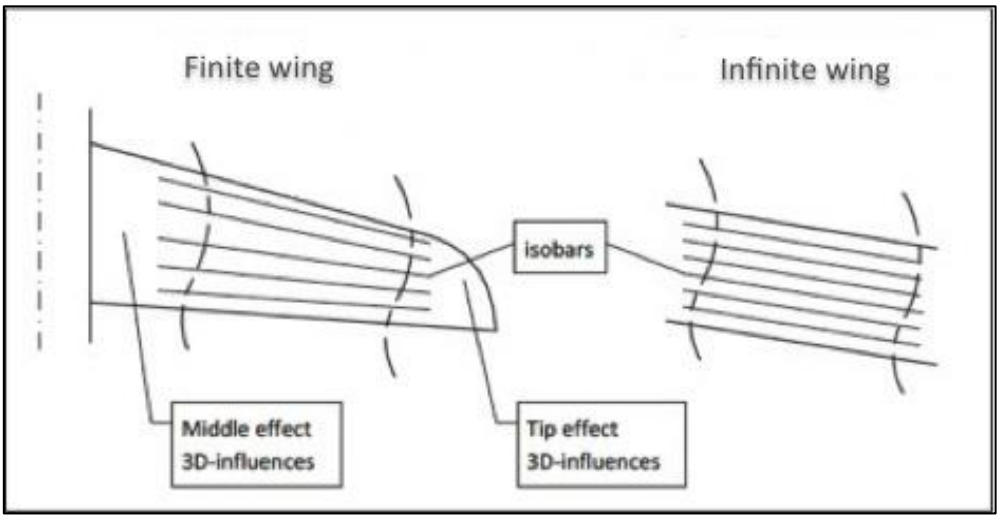

Figure 2.15: Comparison of infinite wing and finite wing with high aspect Ratio (AR>6) [33]

In these regions, the semi-mid-span regions, the idealized concept of an “infinite yawed wing” is a useful starting point that relates the swept wing flow to an equivalent two-dimensional flow over a transformed airfoil section, taken normal to the sweep line of the actual wing.

The second step is checking the airfoil for the target value of thickness/chord ratio and adjusts sections for t/c if necessary at span stations. After the CFD code is run the C_l has be checked. If it is not satisfactory the angle of attack is varied and continuing the loop until the C_l is satisfactory. Afterwards, the coefficient of pressure distribution is checked and if it is not satisfactory it is possible to adjust the curvature. Figure 2.16 illustrates one algorithm for the design of a two-dimensional wing section as a series of steps with the necessary feedback loops.

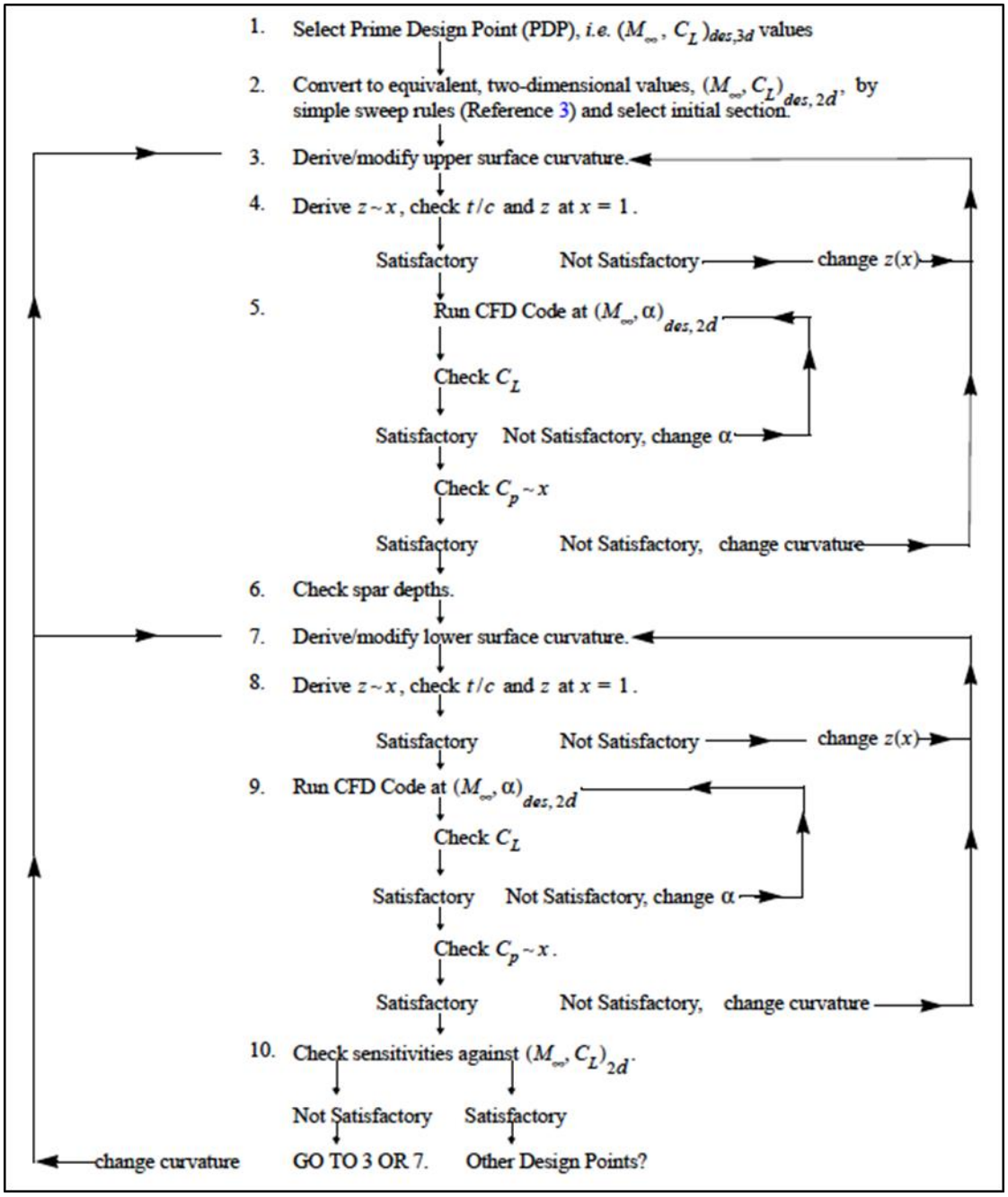

Figure 2.16: Two-dimensional design process as starting point for the three-dimensional design [35]

When the different sections have been designed, they are converted to three dimensions using again simple sweep theory, and modified by any required spanwise variation of thickness and then will be extrapolate and interpolate as needed for complete wing definition. For a finite wing where root and tip effects propagate along the span there may be section changes across the span the isobars, in contrast to those for an infinite tapered wing, it is no longer

necessary to follow the local geometric sweep, furthermore, an additional characteristic feature of swept wing flows, is the appearance of an extra shock wave over the forward part of the wing near the root, leading to a shock wave pattern, the so called Lambda shock pattern, as illustrated in Figure 2.17.

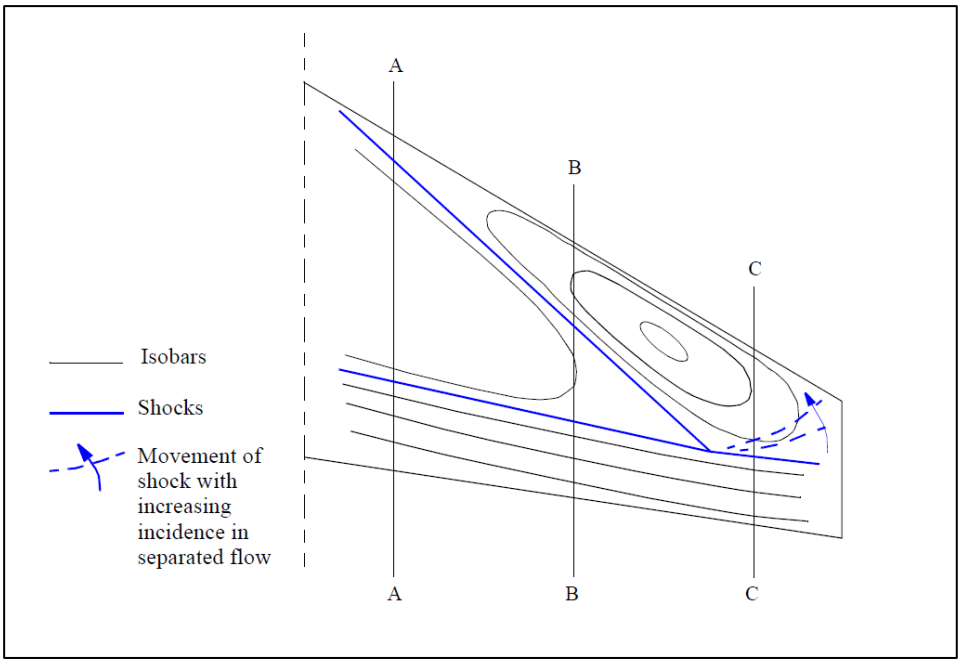

Figure 2.17: Three-dimensional isobar pattern and lambda shock pattern [35]

For the concept that an airfoil exists that is equivalent to the streamwise section of a finite tapered wing to have substantial validity a necessary condition is that the isobar sweep over that part of the wing in which the streamwise section lies should approximately correspond to the local geometric sweep. When local isobar sweeps do not closely follow the local geometric sweep, as may be the case on wings of lower aspect ratio, the concept of equivalence is more obscure. The natural tendency is for the flow to unsweep at the root and tip. So the designer tries to reduce this tendency to obtain an effective aerodynamic sweep as large as the geometric sweep. Therefore, special attention to root and tip sections to maintain isobar sweep has to be taken, bearing in mind that the tip section should have a fairly high maximum lift coefficient and gradual stalling characteristics and the tip chord should not be too small as Reynolds number effects cause reduced C_l capability.

A great deal of the art of swept-wing design consists of shaping the wing (by the incorporation of spanwise variations of twist and of the thickness and camber distributions) in order to counteract the adverse features described here but, even if this can be done successfully for one particular combination of Mach number and lift coefficient (at 'cruise' conditions, say), it is difficult to avoid similar adverse effects at higher, off-design, lift coefficients, even if it is possible to alleviate this effect making use of Kuchemann wing tips, shown in Figure 2.18.

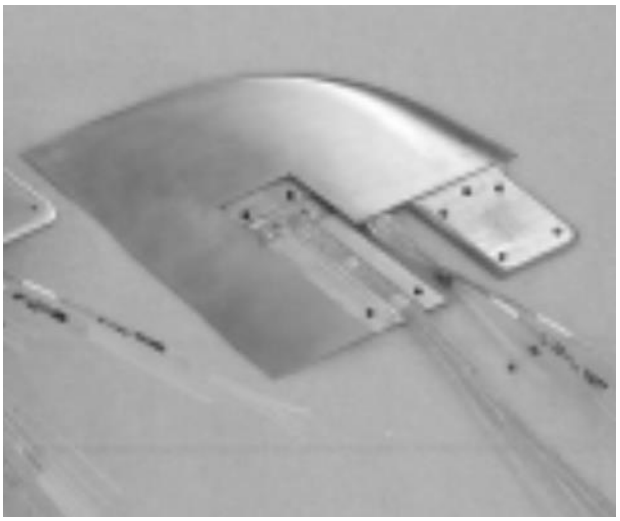

Figure 2.18: Example of Kuchemann wing tips [36]

When the first 3D wing is created the three-dimensional CFD code at Mach and C_L at Design Point is launched (the incidence must be estimated or taken from the two-dimensional exercise), and compared against the target/design values:

- Overall lift coefficient,
- Pressure distributions at grid stations,
- Upper surface isobars.

Then the span-wise lift distribution is examined and the twist is modified accordingly.

Depending on the above, the incidence is changed to $\alpha+\Delta\alpha$ and returned to the CFD code in an iterative fashion.

The process of selecting design variations is carried out by trial and error, relying on the intuition and experience of the designer. Even so, currently

available equipment the turn around for numerical simulations is becoming more rapid that it is feasible to examine a large number of variations. However, it is not at all 100% sure that repeated trials in an interactive design and analysis procedure can lead to a truly optimum design.

The sensitivity of the flow to modest excursions around the design point should be checked.

Finally, the wing must now be exercised throughout the entire ranges of C_L and M_∞, and Reynolds number (concentrating on the important performance points and areas of difficulty including high lift at low speeds). Any problems will require to be addressed. The designer has to consider buffet margins also. Essentially this means the wing C_L has to correspond to a 1.3*g* turn at the highest cruise Mach number without predicting any significant flow separation.

Nacelle/pylon interference has to be addressed. Manufacturing constraints also have to be addressed. Whatever the shape of the wing, it must be manufactured and the manufacturing process places some constraints on the shape and its definition. This means considering the limits to curvature and the manufacturing department's desire for straight-line wrap or ruled surfaces, especially for metal wing skins.

Once the design starts to get close to the desired properties, local inverse methods can be applied to achieve the target pressure distributions.

As new 3D parameterisation technique and optimisation algorithm are continuously developed and computational resources increased, this moved on to analysis of the whole 3D shaped automated wing designs, coupling CFD codes with various numerical optimisation method. Another area of intense research is the use of Reduced Order Modelling (ROM) such as Proper Orthogonal Decomposition (POD) or Adjoint method, in order to accelerate the optimisation process. The POD method could also be used as a low-cost, low-order approximation for aerodynamic shape optimisation. These methods do not require a projection onto the CFD governing equations, but are, instead, a collection of flow snapshots that covers the parameter ranges of interest. The ROM optimisation approach could be used as a low-cost, low-order approximation for aerodynamic shape optimisation in an industrial context. The

technique is able to produce good results in a limited amount of time. It can be applied in particular to a multi-disciplinary environment where CFD is only one part of the optimisation process in a real engineering industrial context. For the assessment of an aircraft configuration it is essential to consider all the relevant disciplines and their interactions at the overall aircraft level. Indeed, by solving the MDO problem early in the design process and taking advantage of advanced computational analysis tools, designers can simultaneously improve the design and reduce the time and cost of the design cycle.

An automated design process is very attractive for the commercial aircraft industry as it greatly reduces the development period. This is of great importance in today's competitive environment because the commercial success depends on the cost and timeliness of products together with quality. That is the reason why industry invests substantial money and resource to the 3D wing shape optimisation. It seems inevitable that a method of this type will provide the basis for aerodynamic designs of the future.

3 Geometry data management in a MDO framework

3.1 Introduction

Product development processes are continuously challenged by demands for increased efficiency. Moreover, at the same time as products become more and more technically advanced the demand for customised variants increases with new product generations and derivatives. These increasing challenges can typically not be addressed by adding more development engineers to the project. Instead, they must be addressed with more efficient development tools, methods for integrated and automated design are needed throughout the development process. Multidisciplinary Design Optimisation (MDO) is one promising technique that has the potential to drastically improve concurrent design. MDO frameworks combine several disciplinary models with the aim of gaining an improved perspective of a system, while capturing the synergies between different subsystems. Geometry plays a crucial role in analysis codes. Among all disciplines, the geometric model is recognised as playing a central role, because it collects most of the data required to any other disciplinary analysis.

3.2 Current limitations

The initial aircraft planform is envisioned and parametrically optimised during conceptual design. A set of design variables typically sizes the major components of the aircraft planform. The resulting abstract geometry representations are sufficient for estimating order-of-magnitude component sizing to satisfy given mission/customer requirements. Until more geometry information becomes available, the initial set of design variables does not completely map into a 3D representation, therefore artistic renderings provide a visual description of the concept. Such depictions are only useful for communicating the concept and are not applicable for preliminary or detailed engineering design or analysis.

The conceptual and preliminary phases of modern aircraft design processes exhibit a gap in analysis and geometry fidelity. In preliminary design and

beyond, however, higher-fidelity analysis is used to completely design the aircraft components and a three-dimensional solid model becomes desirable. The tools and how they are used, and even the people using them, usually change between the phases. Since the geometric representation drives the selection of design and analysis methods, inconsistent geometry models across design phases leads to a segmented design process. Within the current design paradigm it is difficult to implement high-fidelity analysis in the early design phases. The primary reason for the difficulty is that a fully realizable 3D model of the aircraft is usually undefined and unavailable. These circumstances result in a distinction between the geometry representations of one design phase to another. The result is that each phase becomes independent and isolated due to unconnected design methodologies at the geometric level. As the level of fidelity in the geometry improves, the selection of design and analysis methods must comply with corresponding fidelity. Looking at Figure 3.1 that illustrates the aircraft design concept convergence process, a large number of concept configurations are initially generated, and these are eventually narrowed down to a single concept. This is achieved by successive rounds of comparison and down-selection; the level of engineering accuracy and detail increases for each round in order to facilitate differentiation between candidate concepts. The curve gradient decreases with the Maturity Gates (MGs), each of which must be achieved before the next stage can begin. Hence, higher fidelity tools have to be used when increasing the maturity gates. The Layers represent MD toolsets which are appropriate for the various stages of overall aircraft design. The layer numbers correspond with the MGs. Fidelity increases with layer number.

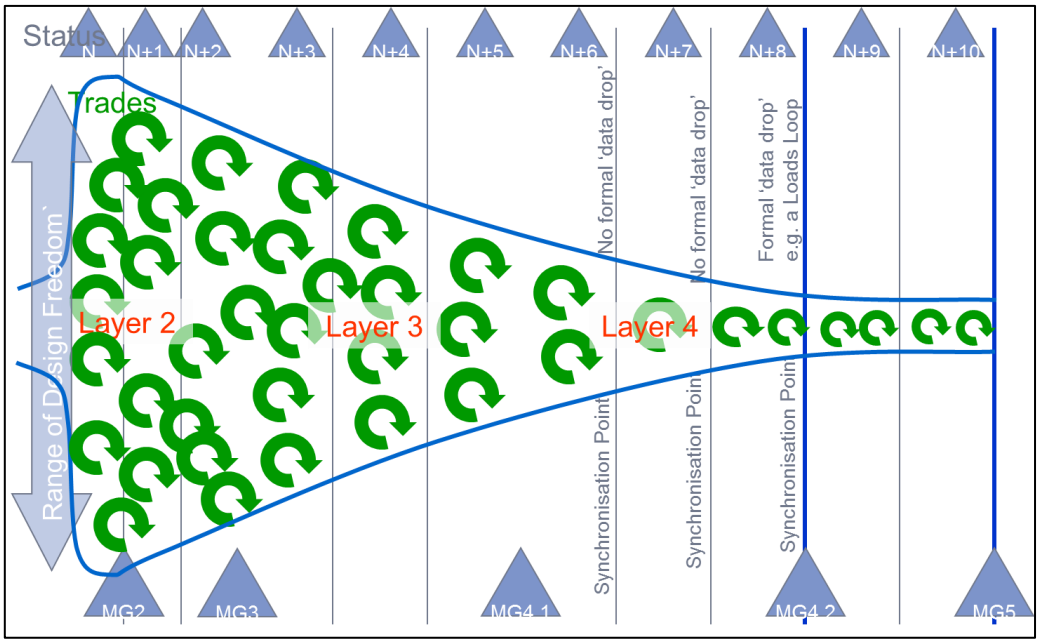

Figure 3.1: Aircraft design concept convergence process

Typically the geometry representation changes from one design phase to the next, therefore a gap in analysis methodology becomes apparent across design phases due to the use of inconsistent geometry definitions.

Thus, the intended seamless design process encompassing the entire lifecycle development of an aircraft actually reduces to a set of modular design phases, wherein independent and isolated design methodologies are defined within the scope of given analysis and geometry fidelity. In conceptual design, the aircraft is defined by a set of parameters that typically size the aircraft planform. This contrasts with the geometry representation in later single discipline design phases, where a 3D model of the aircraft is created via a CAD system. For instance, in the case of aerodynamics and structures, high-fidelity CFD and FEA are typically employed to analyse a 3D model representation of the configuration and its components.

3.3 New Approach

Further advancements in modern aircraft design methodologies and tools currently require a new paradigm for geometry management across the various stages of aircraft design. To avoid these geometry discrepancies, it becomes necessary to employ 3D models of the aircraft containing pertinent geometry

information that evolves throughout the entire design paradigm. The geometry model has to be included in the design optimisation loop. Then, the ability to automatically generate or update the geometric model becomes essential. This can be accomplished by evolving an initial 3D model, defined in the conceptual phase, to contain more geometry information during each subsequent design phase. Such an approach involves a newly revised design paradigm.

For instance, Chang and Silva [37] acknowledged that flexible geometry models are necessary since the design process is by nature iterative and “design changes are frequently encountered in the product development process”. Bowcutt [38] went even further in a paper on future aircraft design methods and tools, in which the author listed requirements that CAD systems should meet to be suitable as MDO enablers from the earliest design phases.

Without a multi-fidelity geometry definition, the multidisciplinary results from earlier phases are not strictly transferable to the later analysis of a fully defined configuration model [39].

Ledermann et al. [40] and [41] make a genuine effort to try to categorize CAD modelling and introduce the benefits of template modelling in CAD tools to develop associative and parametric methods for aircraft design.

Complex products generally have an intricate dependency between geometry, dynamic performance, functionality and cost. Flexible, reusable geometry models are therefore key framework enablers to achieve automated design.

Today, there is already some sharing of models across skill groups. This is typically characterised by exchange of models and adaptation or re-creation of models in different forms, however when skill groups are challenged to collaborate together to solve new problems in tight timescales then cross-skills effectiveness is limited by weak links in this complex network of exchanges and adaptations. In order to improve consistency and sharing of models at the X-skill level, to reduce duplication and time for data conversion and to increase time and effectiveness for engineering innovation is needed introducing a new Common Engineering Model Architecture & Toolset approach.

So let us consider the “today” process for cross-skill models working, and the “to-be” process envisioned by the CEM approach, as in Figure 3.2.

The first step in the Common Engineering Model (CEM) approach is therefore to coordinate needs for common skill models. It means to identify the models that must be shared between skill groups to support key cross-skills integrated processes. The second step is then to establish an architecture for these shared models, and to rationalise the common model elements within this single Common Engineering Model architecture.

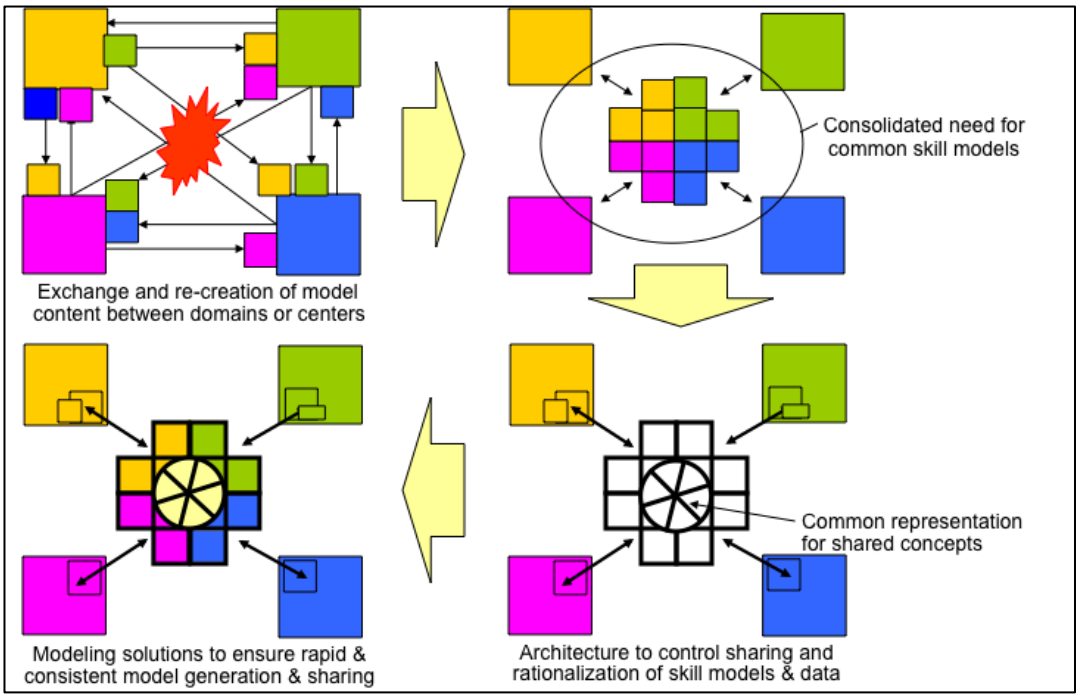

Figure 3.2: "today" process for cross-skill models working, and the "to-be" process envisioned by the CEM approach

The final third step is then adaptation and development of modelling solutions that is methods and tools to ensure rapid and consistent model generation and model sharing. The shared CEM model will include both skill-group owned data to be published to other skill groups, and the common model elements defining product level information fundamental to the working of all skill groups.

The Common Engineering Model approach will be supported by a CEM Methodology and Toolset Architecture in three parts, as in Figure 3.3.

1. CEM Information System Architecture – this is about Methods & Tools at a generic level.

2. Engineering Capabilities Architecture – this is about Aeronautical Engineering models and capabilities.
3. Future Aircraft Programmes – this is about the use of these capabilities to engineer products.

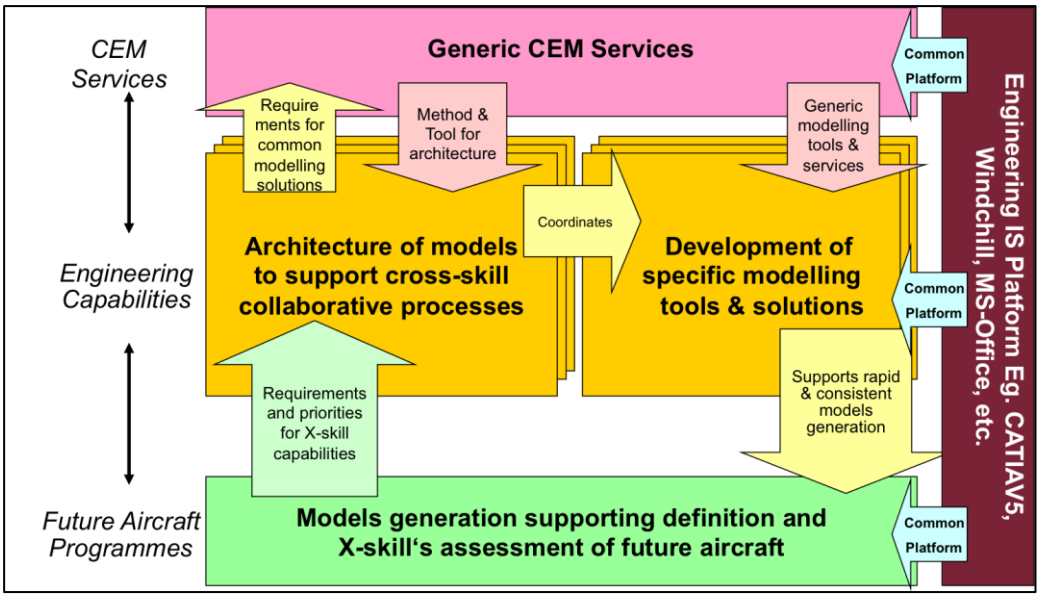

Figure 3.3: CEM Methodology & Tool-Set Architecture

The first component of the Information System (IS) Architecture is a Method and Tool for Models Architecture. This will support the first two steps of the CEM process, to consolidate needs for shared engineering models and to architect skill-group content and common model content. The use of this tool across multiple cross-skill topics will build-up an Engineering Capabilities Architecture, a cross-skill architecture of models to support cross-skill integrated processes.

The second component of the Architecture is library of Generic Modeling Utilities. These will support the specific development of model generation tools in accordance with the capabilities architecture, and facilitate implementation of the common modeling standards necessary for model sharing.

The Capabilities Architecture then provides a recipe book for the Future Aircraft Programmes Architect advising what cross-skill capabilities are available to support key Architecture and Integration activities, and ensuring the participating skill-groups have a joined up set of model generation tools to ensure that these capabilities can be realised rapidly and consistently to

contribute to the concept design studies and engineering work of the aircraft programme.

CEM is a response to a strategic Future Aircraft Programmes requirement for improved cross-skill capabilities and modelling tools. The feed-back and closed-loop control process will ensure CEM evolves as an effective response to this important requirement.

The correct implementation of the above described approach will give an opportunity for improving quality through analysis-based design from initial stage and also an opportunity to increase number of design iterations due to cost/time reduction as depicted in Figure 3.4.

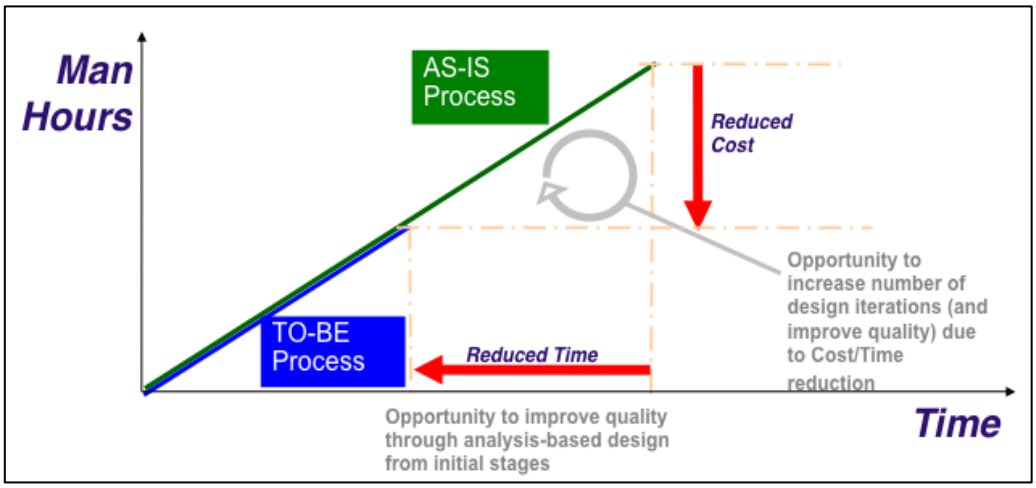

Figure 3.4: Diagram of CEM benefits

To summarise the main benefits of the CEM is its contribution to traceability and coherence across the global aircraft and specific design concept optimisation throughout programme lifecycle. It is an enabler for process and workflow automation at reduced time and cost.

4 Computational Fluid Dynamics (CFD) process

4.1 Introduction

After the parameterisation of the geometry, the next step is the flow solution. CFD analysis is one of the most important tasks to be performed within the optimisation process. In terms of computational cost, it is the most expensive job within each loop of the optimisation, as this work represents about the 90% of wall-clock time required for each completed loop. The stage of flow solution is pictured in Figure 4.1.

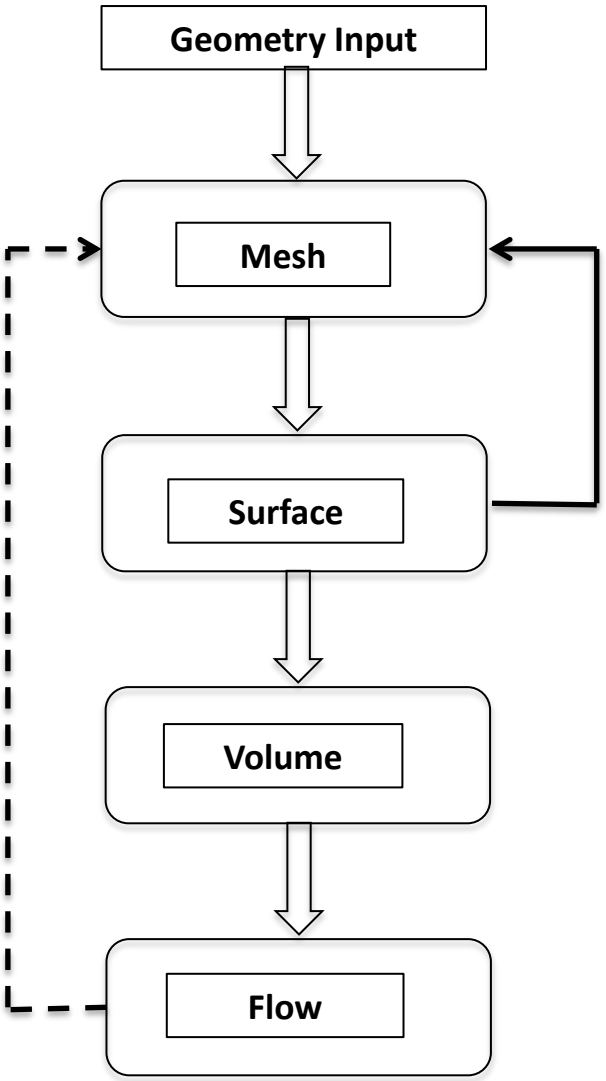

Figure 4.1: the process of 3D flow solution

As seen in Figure 4.1 in order to get the CFD solution, some general steps have to be performed, i.e. meshing generation, pre-processing of the case, and performing the analysis in the solver module. All these steps need to be automated to handle the different geometries and scripting tools need to be used to perform this task. Also, it is shown that the field mesh generation follows after the surface mesh generation. In the following pages the process of mesh generation and the distinction among the different types of mesh is described.

According to the case to be analysed the appropriate CFD method has to be chosen and the 2D or 3D flow solver used. The choice of the appropriate CFD method, of course, depends on several factors such as the usage, accuracy of results required, on the desired use of the results, wall-clock run times etc. After evaluating the flow, the results must to be analysed, in order to validate the accuracy and the reliability of the computational simulation. This is the meaning of the feedback arrow appearing in Figure 4.1, and in case of an inaccurate solution the mesh should be reconstructed through a combination of node movements and edge refinement. Hence, an initially, relatively coarse, mesh is continually adapted during the solution process, considering some flow parameters, in order to do the appropriate adjustments. Also, automated generated meshes may sometimes cause convergence issues and mesh adaptation can cure these problems too. The ultimate objective of mesh adaptation is to achieve the most accurate solution for a given problem for the least computational cost. The solution of complex CFD problems usually requires the use of a large number of grid points. However, the mesh quality depends also on the flow conditions and not only on the geometrical characteristics of the flow. This means that, for the same geometry, the most appropriate mesh can be dramatically different at various Reynolds number. It is clear that the feedback arrow in Figure 4.1 makes sense only for the development of the CFD process and should be not considered in CFD for design where the CFD process has to be already tested and proved to be robust.

4.2 Mesh Generation

The mesh generation around the geometry is the step that follows the parameterisation of the shape in the optimisation design process. In a computational fluid dynamics context, grid generation is as important as the effective solution of the governing equations of the physical problem. Indeed, the grid not only influences the final results of the CFD simulation, but also its generation represents the task that is most challenging and time consuming from a user point of view. Moreover, from a user's point of view, the most challenging stage is to generate and automate this task to function properly and in accordance with the different geometries. Although, many different meshing commercial software are available nowadays some basic understanding of the meshing (grid generation) process is fundamental for an aware and proper use of such tools. The first step in the mesh process is to import the file containing the geometry around which the mesh has to be built and the boundary data. In many cases, however, the domain boundaries are built inside the mesh generator itself. Later points are distributed on the curves that constitute the edges of boundary sections. Consequently a surface mesh is built on the corresponding surface boundary and in the end a volume grid is created. A mesh is defined as a set of points distributed over a calculation field for a numerical solution of a set of partial differential equations. This set can be classified in two categories: Structured and Unstructured. This distinction is made on the bases of the way the points are generated and stored and on the shape of the elements. Main advantages and drawbacks of both the methodologies are presented in the next section.

4.2.1 Structured Mesh

A structured mesh is one in which all the interior vertices are topologically alike, e.g. formed by the intersections of curvilinear coordinate surfaces. An example of a structured mesh around an airfoil is shown in Figure 4.2

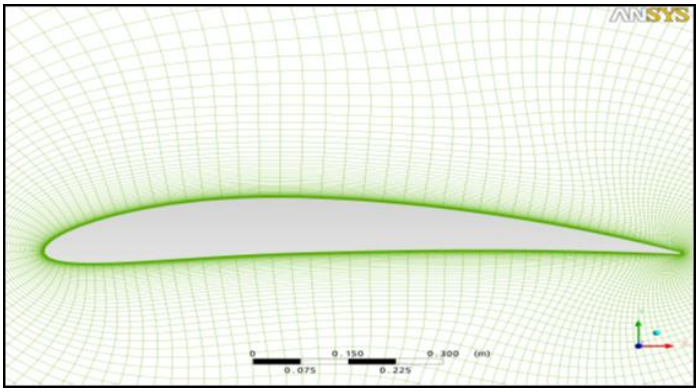

Figure 4.2: Structured mesh around an airfoil

Structured boundary-conforming meshes have been widely used in CFD, both in two-dimension, where quadrilaterals are used, and three-dimension with hexahedra elements.

The advantages of these meshes are:

- Simplicity and easy data access;
- Less computer memory requirements
- Better control over the sizes and shape of the elements
- The generated elements are better aligned with the flow resulting in better quality and faster convergence of the CFD solution.

On the other hand, the generation of such meshes for complex geometry is really complicated and highly dependent on the expertise of the user. This means that the computed solution close to the boundaries of the surface might be quite inaccurate, which is a great drawback, since this area is of high importance. Furthermore, structured meshes do not apply well for selected region grid refinement, due to the fact that such a refinement may be carried over to other regions, leading to a useless increase of resolution in not fundamental zones of the domain.

4.2.2 Unstructured Mesh

Unstructured grids have inherent simplicity of construction in that, by definition, no structure is required. An example of unstructured mesh is presented in Figure 4.3.

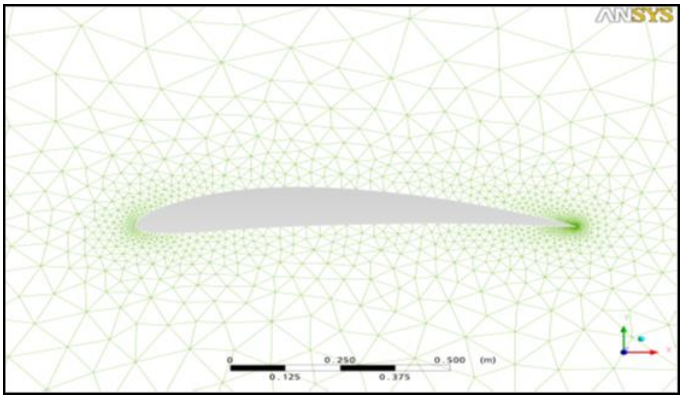

Figure 4.3: Unstructured mesh around an airfoil

The main advantage of these meshes over the structured ones is the much higher level of flexibility when applied to complex geometries in two and three-dimension and in grid adaptation context. As a matter of fact, when the complexity of the geometry increases generating a structured mesh becomes more and more challenging. Often different blocks must be created inside the domain to be able to generate the mesh with the required precision in specific zones of the domain. This feature is fundamental in an optimisation process, since the changes in geometry of the shape to optimise must be supported by a robust and reliable mesh generation method. In addition, grid points density can be increased in zones where resolution requirements differ. Thus, mesh refinement is pretty easily achieved. Since grid point densities are easily modified on a local basis, adaptive refinement is easily achieved, either by addition of new grid points or by the redistribution of existing ones [42]. Due to the large amount of information that needs to be stored, the unstructured grids use much more memory compared to the structured ones. Explicit connectivity information must be saved since neighbouring nodes in physical space appear in storage at non-neighbouring locations and non-constant distances [43]. Besides due to the shape of the elements, triangles in 2D meshes and tetrahedra in 3D ones, these do not result in alignment with the flow, which is an important condition for convection-dominated flows. Thus, to obtain the same accuracy in the solution of a structured mesh the unstructured one must contain a bigger number of points, increasing even more the memory allocation demand. A powerful unstructured grid generation technique is based upon the

Delaunay triangulation, which consists in a set of triangles connecting the points satisfying a specific property that circumcircle of each triangle, does not contain any point of the triangulation [44].

4.2.3 Hybrid Mesh

In the end, the two types of mesh can be combined together obtaining a hybrid Mesh. Using structured meshes in near wall regions, where the solution must be really accurate, and unstructured mesh everywhere else in the domain, where the geometry is quite complex, results in a combination of advantages of both the methods. An example of unstructured mesh is presented in Figure 4.4.

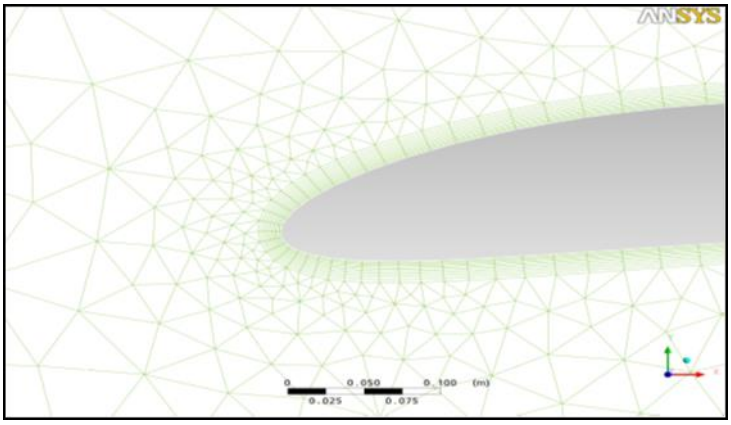

Figure 4.4: Hybrid mesh around an airfoil

The advantage of hybrid grid methods is that you can utilize the positive properties of structured grid elements in the regions which need them the most and use automated unstructured grid techniques where not much is happening in the flow field. The ability to control the shape and distribution of the grid locally is a powerful tool that can yield excellent meshes.

The disadvantage of hybrid methods is that they can be difficult to use and require user expertise in laying out the various structured grid locations and properties to get the best results. Hybrid methods are typically less robust than unstructured methods. The generation of the structured portions of the mesh will often fail due to complex geometry or user input errors. While the flow solver will use more resources than a structured block code, it should be very similar

to an unstructured code. Post processing the flow field solution on a hybrid grid suffers from the same disadvantages as an unstructured grid.

4.3 Flow Simulation Approach

4.3.1 Introduction

Much of the work in applied aerodynamics is concerned with the prediction of these forces. This can be done in several ways, starting with very simple considerations and moving on to the detailed field equations. Regardless of the application, the goal of aerodynamics remains the same, to minimise drag experienced by the body. For an aircraft, minimising the drag ultimately results in an increase in its Lift-to-Drag ratio, which is one of the parameters used to measure aircraft performance. This section gives an overview of the computational tools that are available to analyse fluid flow. The fundamental Navier-Stokes equations of computational fluid dynamics are introduced first. This is followed by the various approaches that can be taken to approximate the solution to these equations, starting with the simple empirical and semi-empirical method and then moving to more advanced numerical methods.

Air flows are governed by second-order partial differential equations (Navier-Stokes) that represent the conservation laws for the mass, momentum (Newton's 2nd law), and energy (first law of thermodynamics). The Navier-Stokes (NS) equations were developed by C. Navier and G. Stokes between 1820 and 1845, see [45] and [46]. To derive the equations of motion for fluid particles we rely on various conservation principles. These principles are entirely intuitive. They are a statement of the fact that the rate of change of mass, momentum, or energy in a certain volume is equal to the rate at which it enters the borders of the volume plus the rate at which it is created inside. Solutions of the full Navier-Stokes equations show the onset of turbulence, the interaction of shear layers, and almost all of the interesting aerodynamic phenomena (with the exception of interacting or rarefied gas flows). This potentially allows CFD to compute the aerodynamics of arbitrary configurations and to provide the designer with information about the physical effects taking place within the flow field. The Navier-Stokes equations are a system of non-

linear Partial Differential Equations (PDE), hence no general closed form solution exits up to date for complex flows. Computational Fluid Dynamics (CFD) is the method of replacing such PDE systems by a set of algebraic equations that are solved using digital computers. CFD is a widely used tool to predict internal and external flows. CFD enables the user to model flows with complex physics and complex geometries and gives an insight into flow patterns that are difficult, expensive or impossible to study using traditional experimental techniques. CFD is a powerful technique to predict how a flow develops with time. To date, CFD is unable to replace experimentation completely, but the amount of experimentation and the overall cost can be significantly reduced by the use of CFD. However, due to the complex behaviour of turbulence, analytical solutions to turbulent flows do not exist. For the cases where the flow variables are known as a function of space and time the NS equations can be solved numerically, these solutions are termed Direct Numerical Simulations (DNS) [47]. However, the instantaneous range of scales increases rapidly with the Reynolds number and as such requires unrealistic computational power. The complexity of fluid flow is well illustrated in Van Dyke's Album of Fluid Motion [48]. Many critical phenomena of fluid flow, such as shock waves and turbulence, are essentially non-linear and the disparity of scales can be extreme. The flows of interest for industrial applications are almost invariantly turbulent. The length scale of the smallest persisting eddies in a turbulent flow can be estimated as of order of $1/Re^{3/4}$ in comparison with the macroscopic length scale. In order to resolve such scales in all three spatial dimensions, a computational grid with the order of $Re^{9/4}$ cells would be required. Considering that Reynolds numbers of interest for airplanes are in the range of 10 to 100 million, the number of cells can easily overwhelm any foreseeable supercomputer. Consequently mathematical models with varying degrees of simplification have to be introduced in order to make computational simulation of flow feasible and hence produce viable and cost-effective methods in the real world. Figure 4.5 indicates a hierarchy of models at different levels of simplification, which have proved useful in practice. Inviscid calculations with boundary layer corrections can provide quite accurate predictions of lift and

drag when the flow remains attached. Procedures for solving the full Reynolds Average Navier-Stokes (RANS) equations are necessary for the simulation of complex separated flows.

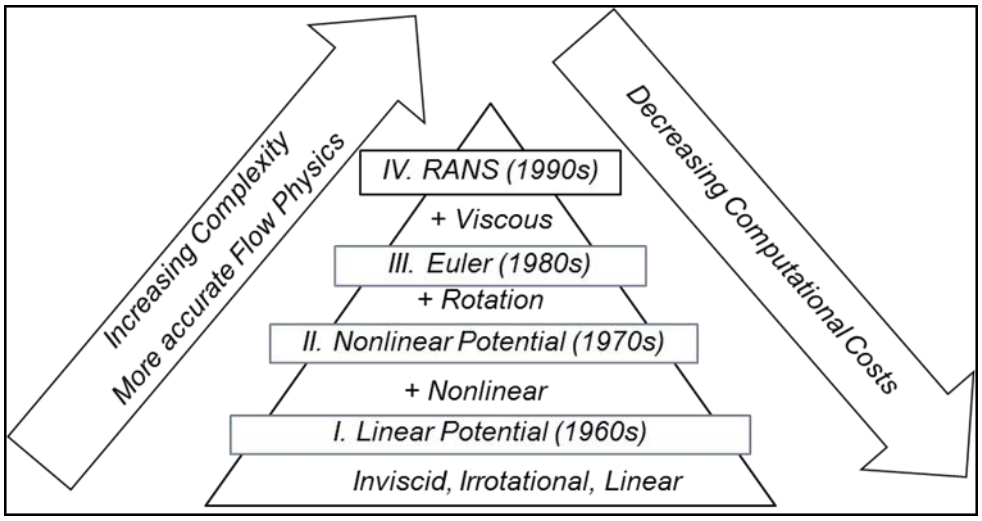

Figure 4.5: Hierarchy of models for industrial flow simulations

In external aerodynamics most of the flows are steady, at least at the macroscopic scale. Computational costs vary drastically with the choice of mathematical model.

4.3.2 Governing equations

The governing equations of a continuous Newtonian fluid flow are the Navier-Stokes equations. These partial differential equations represent the conservation laws of physics and can be used to describe the state of a system. The equation generated by applying the conservation of mass to a system is called the continuity equation (4.1). The second equation (4.2) derived from applying Newton's second law is called the conservation of momentum. The last one (4.3) is the conservation of energy, which represents the application of the first law of thermodynamics. The unsteady compressible three-dimensional Navier-Stokes equations can be written in Cartesian tensor form as follows:

$$\frac{\partial \rho}{\partial t} + \nabla \cdot (\rho \mathbf{u}) = 0 \qquad (4.1)$$

$$\frac{\partial}{\partial t}(\rho \boldsymbol{u}) + \nabla \cdot (\rho \boldsymbol{u} \otimes \boldsymbol{u} + p\boldsymbol{I} - \boldsymbol{\tau}) = 0 \tag{4.2}$$

$$\frac{\partial}{\partial t}\rho e_0 + \nabla \cdot \rho \boldsymbol{u} h_0 = \nabla \cdot (-\boldsymbol{q} + \boldsymbol{\tau} \cdot \boldsymbol{u}) \tag{4.3}$$

The variables $\boldsymbol{\tau}, e_o,\ h_0,$ and $\boldsymbol{q}$ are the viscous stress tensor, the specific total energy, the specific stagnation enthalpy, and the conduction heat flux vector. These can be expressed in terms of the magnitude and gradient of the velocity vector and of temperature as follows:

$$\boldsymbol{\tau} = \mu_l \left(\nabla \boldsymbol{u} + \boldsymbol{u} \nabla - \frac{2}{3} \boldsymbol{I} \nabla \cdot \boldsymbol{u} \right) \tag{4.4}$$

Where μ_l is the molecular viscosity that can be estimated for example from Sutherland's law for air

$$\mu_l = 1.458 \times 10^{-6} \frac{T^{\frac{3}{2}}}{(T + 110.4)} \tag{4.5}$$

and

$$e_o = e + \frac{\boldsymbol{u} \cdot \boldsymbol{u}}{2} = c_v T + \frac{\boldsymbol{u} \cdot \boldsymbol{u}}{2} \tag{4.6}$$

$$h_o = e_o + \frac{p}{\rho} \tag{4.7}$$

$$\boldsymbol{q} = -\frac{c_p \mu_l}{Pr} \nabla T \tag{4.8}$$

Where c_p, c_v and *Pr* are the gas constant pressure specific heat, the constant volume specific heat, and Prandtl number respectively. To complete a closed set of equations, the static pressure is estimated, assuming a calorically perfect gas, as:

$$p = \rho R T \tag{4.9}$$

$$R = c_p - c_v \tag{4.10}$$

From equations (4.6) and (4.9) the pressure can be related to the total energy and the velocity vector as:

$$p = (\gamma - 1)\rho\left[e_o - \frac{\boldsymbol{u}\cdot\boldsymbol{u}}{2}\right] \tag{4.11}$$

Where $\gamma = c_p/c_v$

The Navier-Stokes equations can be written in compact conservative form as follows:

$$\frac{\partial}{\partial t}\boldsymbol{U} + \nabla\cdot[\boldsymbol{F}_c(\boldsymbol{U}) + \boldsymbol{F}_v(\boldsymbol{U})] = 0 \tag{4.12}$$

Equation (4.12) contains the conservative variables vector **U**, the inviscid flux vector ***Fc*** and viscous flux vector ***Fv***, which are defined as:

$$\boldsymbol{U} = \begin{pmatrix} \rho \\ \rho\boldsymbol{u} \\ \rho e_0 \end{pmatrix} \quad \boldsymbol{F}_c = \begin{pmatrix} \rho\boldsymbol{u} \\ \rho\boldsymbol{u}\otimes\boldsymbol{u} + p\boldsymbol{I} \\ \rho\boldsymbol{u}(e + p/\rho) \end{pmatrix} \quad \boldsymbol{F}_v = \begin{pmatrix} 0 \\ -\tau \\ -\boldsymbol{\tau}\cdot\boldsymbol{u} + \boldsymbol{q} \end{pmatrix} \tag{4.13}$$

4.3.3 Approximations

The equations of motion for a general fluid are extremely complex and even if the problem could be formulated it would be impractical to solve. Thus, from the outset, certain simplifying approximations that are often satisfactory are made.

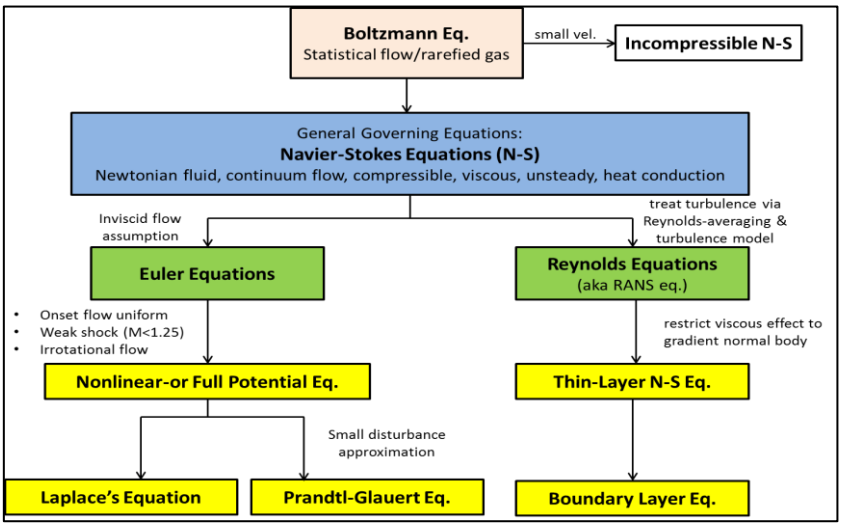

Figure 4.6: Different mathematical modelling based on the assumptions made

The main approximations are here reported and explained:

• *Continuity and Homogeneity*. It is assumed that the fluid is composed of particles, which are so small and plentiful that the statistically averaged properties of interest are the same at any scale. The Boltzmann equation be This works well for gases and fluids under most conditions. It does not work for studying the flow of sand. It does not work when the fluid is so rarefied that the mean free path is of the same order as the dimensions of interest in the problem.

• *Inviscid*. The effect of viscosity may sometimes be neglected or modelled indirectly. For many aerodynamic flows of interest, the region of high shear and vorticity is confined to a thin layer of fluid. Outside this layer, the fluid behaves as if it were inviscid. Thus the simpler equations of an inviscid fluid are often solved outside of the boundary layers.

• *Incompressible* (constant density). When the fluid density does not change with changes in pressure, the fluid is incompressible. Water density changes very little with changes in pressure and is generally treated as an incompressible fluid. Air is compressible, but if pressure changes are small in comparison with some nominal value, the corresponding changes in density are small also and incompressible equations work quite well in describing the flow. The degree to which the fluid density changes with pressure is related to the speed of sound in the fluid. Thus, assuming that the flow is incompressible is equivalent to assuming that the speed of sound is infinite. When the local Mach number is less than 0.3 compressibility effects can often be ignored.

• *Irrotational*. There are two types of motion; translational and rotational. The two may exist independently or simultaneously. If now an element is represented, it may be subjected to deformation. This can be linear or angular. If the motion of the particles is purely translational and the distortion is symmetrical, the flow is irrotational and the vorticity is constant. Kelvin's theorem provides a good understanding for the conditions under which this could happen and how the friction is the source of circulation in fluids.

• *Steady*. When the variables describing the fluid properties at a given point do not change in time, the flow may be treated as steady and the time derivatives in the equations of motion are zero. This condition depends on the chosen coordinate system. If the system is at rest with respect to a body in uniform motion through a fluid the equations in that system are steady, but expressed in a system fixed with respect to the undisturbed fluid, the flow is unsteady. It is often convenient to transform the coordinate system to one in which the flow is steady. This is, of course, not always possible. We will assume that the flow is steady in most of the discussions in this course but unsteady effects are often important in the study of bird flight, propellers, aircraft gust response, dynamics, and aeroelasticity as well as in the study of turbulence.

The Boltzmann equation represents the high level of physical modelling and refers to any kinetic equation that describes the change of a macroscopic quantity in a thermodynamic system, such as energy, charge or particle number. The equation is a nonlinear integral-differential equation, and the unknown function in the equation is a probability density function in six-dimensional space of a particle velocity and position. The Boltzmann equation can be used to determine how physical quantities change, such as heat energy and momentum, when a fluid is in transport, and other properties characteristic to fluids such as viscosity, thermal conductivity, and electrical conductivity can be derived and describes physical phenomena where particles, energy, or other physical quantities are transferred inside a physical system due to two processes: diffusion and convection. From Figure 4.6 it is possible to deduce that under the assumption that the flow is continuum the Boltzmann equation to become the general governing Navier-Stokes equations. If the fluid is considered inviscid the Euler equation can be derived, and in turn if the flow is also considered irrotational the Euler equations become the Full-potential equations. In addition, if the flow is thought to be incompressible another simplification is imposed and the full-potential equations transform into the Laplace’s equation. Otherwise, if only small disturbances are considered, the Full-potentials equations change into the Prandtl-Glauert equations. More

details of the equations coming from these assumptions are given in the next sections.

The aerodynamic performance can be determined in a number of ways. Over the years there has been a gradual incline towards dependency on computers but the traditional method was to manufacture a scale model and test it under the appropriate conditions in a wind tunnel. This would provide the designer with the flow features of the test section. If the need for a similar configuration or condition arose the experimental data could be used to extrapolate or interpolate to the required condition.

Mathematical theories could also be used to estimate the aerodynamic characteristics. Then there are computational tools that simulate the flow over the body. Each of these methods has its own advantages and disadvantages when it comes to representing actual flight conditions and it is down to the designer to choose the most appropriate method for the task.

4.3.4 Empirical and Semi-Empirical Methods

Empirical and semi-empirical methods make use of existing experimental databases together with theoretical models. They are restricted to use for similar configurations and conditions because often they interpolate or extrapolate the experimental data. This means that these methods require very small computational resources and time to predict the aerodynamics characteristics of various configurations, which makes them very popular for aeronautical design.

Most semi-empirical codes are based on component build-up methods, the US Air Force DATCOM and the Engineering Science Data Unit (ESDU) codes are such examples. Simple theory or data sheets are used to estimate the aerodynamics characteristics of an individual component of a configuration, such as the fuselage or the wing. The results are then combined with a further treatment to account for additional effects, such as interference effects between the components, to provide a final solution for the characteristics.

Semi-empirical are limited to predicting forces and pressure coefficients on the surface only and do not predict the solution over the whole flow field. The

methods are also limited to configurations in which the aerodynamics coefficients are of the same order as the interference effects, when the aerodynamics coefficients become much smaller than interference the methods break down. Empirical methods employ theories that rely on numerous simplifying assumptions; they are also restricted to the limited set of date gathered for the experimentally tested configurations and conditions. Analysing any configuration under a conditions for which experimental data is not available results in very inaccurate solutions.

4.3.5 Linear Aerodynamics

The phenomenon with two different forces from different sources enables us to separate the problem of aerodynamic forces. This is usually done by separately assessing the outer problem concerning the pressure forces, and the inner problem concerning friction forces. The forces can be divided into just two types: pressures and shears. Pressures are created at the surface of a body due to (nearly) elastic collisions between molecules of the fluid and the surface of the body. Shearing forces are produced by fluid viscosity. This quantity is a measure of how well momentum is transferred between adjacent layers of the fluid. Although both types of forces are important in applied aerodynamics, pressures are usually the dominant type of force.

The linear aerodynamics is focused on the outer problem, since pressure forces are dominant in certain physical domains. Linear aerodynamics is the field of aerodynamics concerned with linear domain of aircraft behaviour. It has limitations, but is still very useful. This domain is located at small Mach numbers hence the compressible effects can be disregarded. The angles of attack are small to ensure that the lifting surfaces remain well below the stall limit. These limitations make the linear theory impossible to use in some parts of the flight envelope. However, the linear theory is very useful indeed, as every commercial aircraft spends quite a lot of time in the linear domain.

4.3.6 Linear numerical models

Linear methods are used in design requiring generally low computational fidelity. This makes them rapid and thereby ideal for concept design. These

methods make use of singularity element methods and are not valid for compressible flows.

4.3.6.1 Panel methods

The simplest CFD methods are linear solvers. Panel methods are used to solve linear differential equations such as the Prandtl-Glauert equation that represent flows over some rather complex geometry at low-speed. If the body is two-dimensional or axisymmetric, the profile is approximated by a many sided inscribed polygon. If it is three-dimensional, then it is approximated by flat quadrilateral elements. Since the equations solved by panel methods are linear, it is possible multiply a known solution by a scalar and add these results together to form more general solutions. Panel methods may be based on one or more fundamental solutions to the Prandtl-Glauert equation or Laplace's equation. These commonly include source, vortex, and doublet flows. The basic idea is to add up known solutions such as a uniform flow and a point source to produce a streamline pattern that matches the flow of interest. Panel methods are based on this idea. Sources (or doublets or vortices) of some strength are located in the flow such that their combined solutions satisfy the boundary conditions of the problem. The boundary conditions are typically that the combined flow does not go through the surface and that far from the body; the flow approaches the free-stream solution. Each panel is constructed to have some type of singularity distribution. Depending on the accuracy, computational speed and other factors, it is possible to use constant, linear, parabolic or even higher order of distribution of the singularity on each panel. The number of panels can also be varied. Conventional CFD methods require calculations for the entire three-dimensional field about the body under investigation. While, the panel method can calculate the entire three-dimensional field, it requires the calculation over the surface the body, which is a two-dimensional calculation. Moreover the panel method is relatively easy to formulate and compute. Therefore, it requires much less computation than conventional detailed CFD codes. It means that it improves the efficiency of computational speed, the calculation time is order of magnitude shorter compared to classic CFD; seconds vs. hours. [49]. Panel Methods program are used for calculating

aerodynamic forces and moments about an aircraft, for subsonic attached flows where calculation time is important and friction drag can be ignored (optimisation problems, conceptual designs, aerodynamic load generation).

4.3.6.2 Lifting line method

This is a mathematical model for predicting the lift distribution over a three-dimensional wing based on its planform geometry. The method is based on the concept of Prandtl's lifting line theory [33] and Lanchester's contribution of vortex theory during the early 20th century. It also calculates induced drag and downwash velocity. The idea of lifting line theory is to try using 2-D flow results for each section, but correct them for the influence of the trailing vortex wake and its downwash. In this model, the vortex strength reduces along the wingspan, and the loss in vortex strength is shed as a vortex-sheet from the trailing edge, rather than just at the wing tips. It applies to large aspect ratio and un-swept wings at small angle of attack. For incompressible, inviscid flow, the wing is modelled as a single bound vortex line located at the 1/4 chord position and an associated shed vortex sheet. The circulation about the wing that creates lift is represented by bound vortices. Bound vortices are one of the three types of vortices, the other being the starting vortex and the trailing vortex. The strength of the bound vortices, indicated by their vorticity, reduces as they move in the spanwise direction to mimic the real physical wing in every way except that of thickness. When the vortices reach the wing tips they are shed as tip-vortices that form trailing vortices as they extend down into the wake, see Figure 4.7.

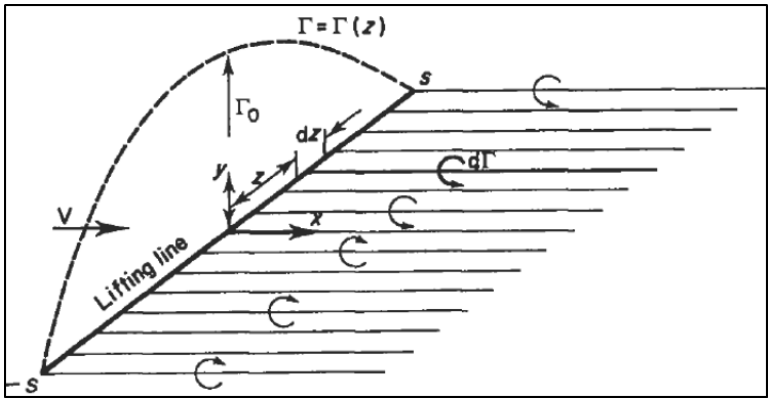

Figure 4.7: Prandtl's lifting line model [50]

4.3.6.3 Vortex Lattice method

The Vortex Lattice Method (VLM) determines the lift and induced drag. It is an extension to the lifting line method that can model straight wings with low aspect ratios as well as wing sweep. The method was first formulated, based on Laplace's equation, in 1943 by Faulkner [51]; however, it was not until the early 1960's, when computational power developed, that the method became a practical.

In a VLM the wing planform is represented by a lifting surface that is divided into a lattice of quadrilateral panels; thickness is not taken into account. Boundary conditions are applied to the panels; the boundary conditions are approximated by linearising and transferring the conditions from the actual surface to a flat mean 'reference'. A control point is located that is used to satisfy the boundary conditions, which in turn allows the relationship between the pressure and velocity to be simplified. These simplifications mean that the lift and thickness contributions can be superimposed and represented by a horseshoe vortex system.

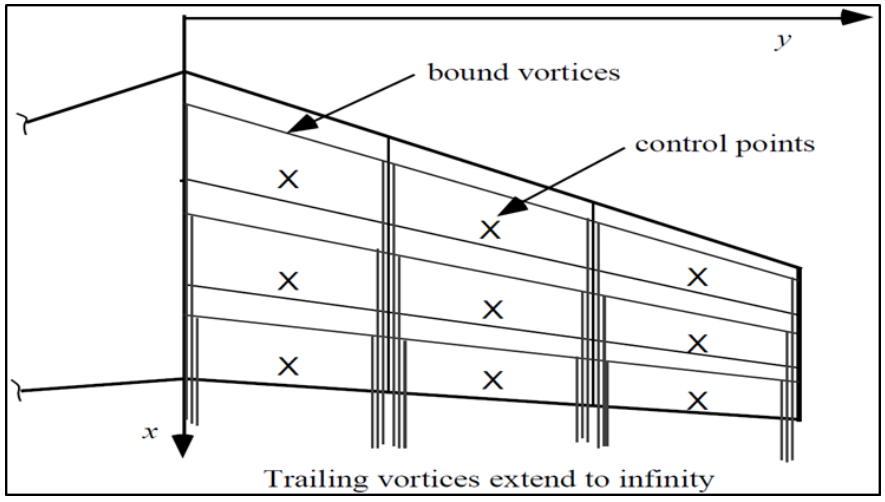

Figure 4.8: VLM method represented by horseshoe vortex [52]

The bound vortex of the horse shoe vortex is placed on the ¼ chord line of each panel. The control point is placed on the ¾ chord point and midpoint in the spanwise direction of each panel, see Figure 4.8. A system of linear equations is then solved to determine the strength of the circulation required to satisfy the boundary conditions.

4.3.6.4 Non-Linear numerical models

The more complex flows, such as transonic or separated flows, can be modelled by non-linear CFD methods that solve the governing equations. Application of these methods can be found in RANS, Euler and full-potential solvers. Many non-linear methods have been developed, the oldest of which is the Finite Difference Method (FDM); it was developed by A. Thom in the 1920s [53]. The applicability of such methods is an important factor and therefore newer methods like the Finite Volume Method (FVM), which has an applicability of around 80%, and the Finite Element Method (FEM), with an applicability of around 15%, have become very popular in industry [54]. It is worth noting that all of these methods require a mesh, which is generated using nodes and cells and requires boundary conditions to be set. How the mesh is used varies for each solver but typically there are two ways the meshes are used, in a structured and in an unstructured way.

4.3.6.4.1 Finite Difference Method (FDM)

In the FDM approximations are applied to the differential equations to yield finite difference equations that can be solved in three steps: first the solution is divided into grids of nodes in a structured grid, then the equivalent finite difference equations are approximated for the first and second derivatives of the differential equation (by truncating a Taylor series expansion), finally the difference equations are solved within the prescribed initial and/or boundary conditions [55]. An example of a finite difference mesh and a corresponding scheme used to discretise the non-linear fluid flow is shown in Figure 4.9.

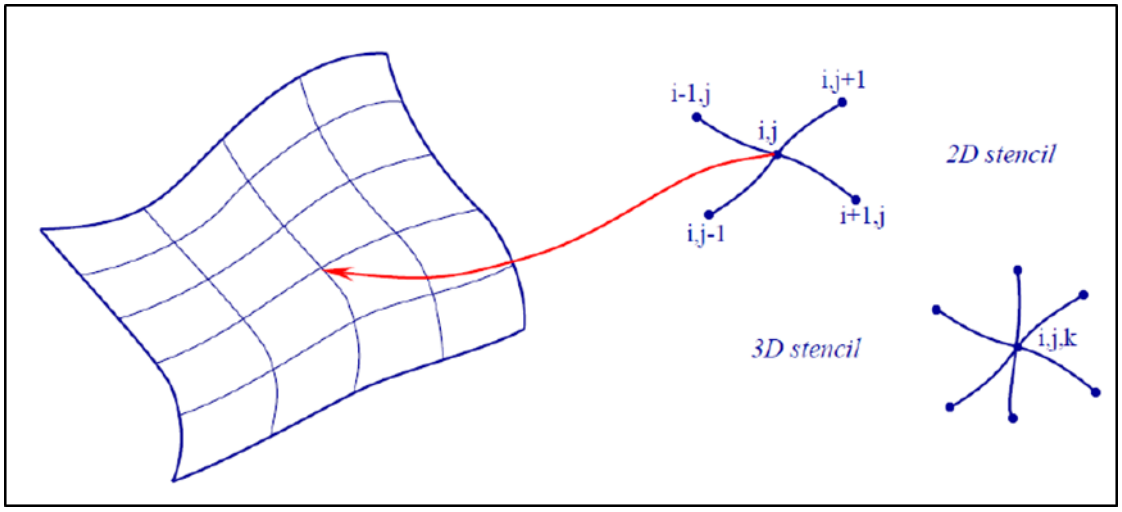

Figure 4.9: Finite Difference mesh and examples of a 2D and 3D stencil [56]

The computational cost of this method depends on the order of the approximations used as well as the number of design variables used. One of the disadvantages of this method is that it requires structured grids, which limits its applicability. The other downside is that it does not conserve moment, energy and mass on coarse grids [54].

4.3.6.4.2 Finite Element Method (FEM)

The FEM is another technique that approximates the solutions of the partial differential equations. Its earliest use was by Courant in 1943, who used it to solve torsional problems [57]. The method was refined over the 60's and 70's for fluid flow analysis. In the FEM approach the field (domain) is subdivided in cells (elements), which can take either a triangular or quadrilateral form, to form a grid, see Figure 4.10.

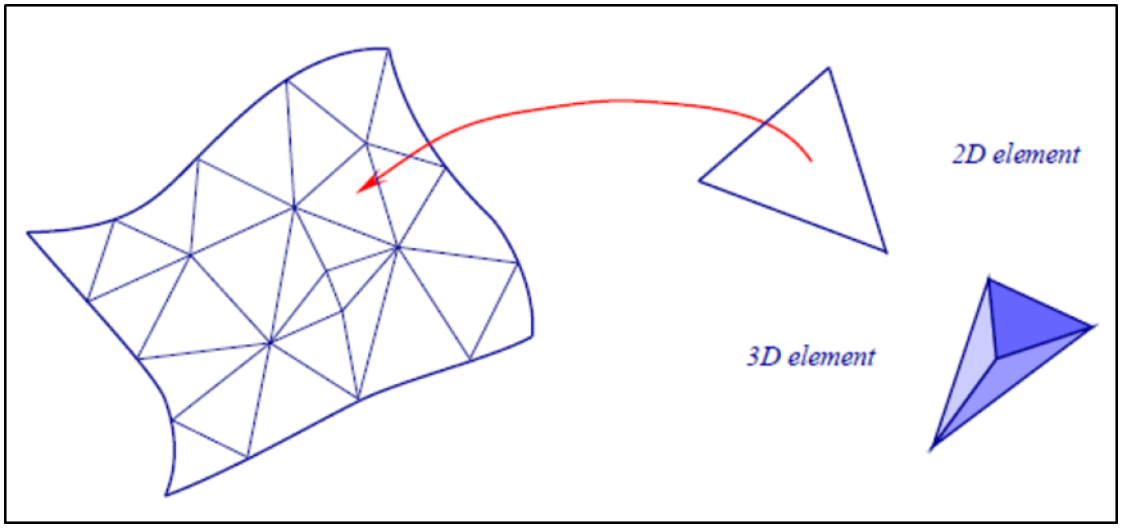

Figure 4.10: Finite Element mesh with examples of a 2D and 3D element [56]

Handling complex geometries is simplified by the fact that the grid does not need to be structured, which is an advantage FEM has over FDM. The solution process looks for a solution of an integral form of the potential differential equations rather than solving them directly. It obtains the integral forms from a weighted residual estimation [58]. This allows the method to deal with arbitrary geometry using different shapes and elements. Out of the three methods FEM has the highest accuracy on coarse grids but solving larger problems can take longer.

4.3.6.4.3 Finite Volume Method (FVM)

The FVM solves for the equivalent integral form of the potential differential equations. The problem is divided into a set of finite volumes in which the nodal points that are used in the computation lie at the centroids of the cells, see Figure 4.11.

Interpolation schemes are used to establish the values at the cell faces, edges and vertices; the most basic interpolation scheme is the so-called upwind approach [59].

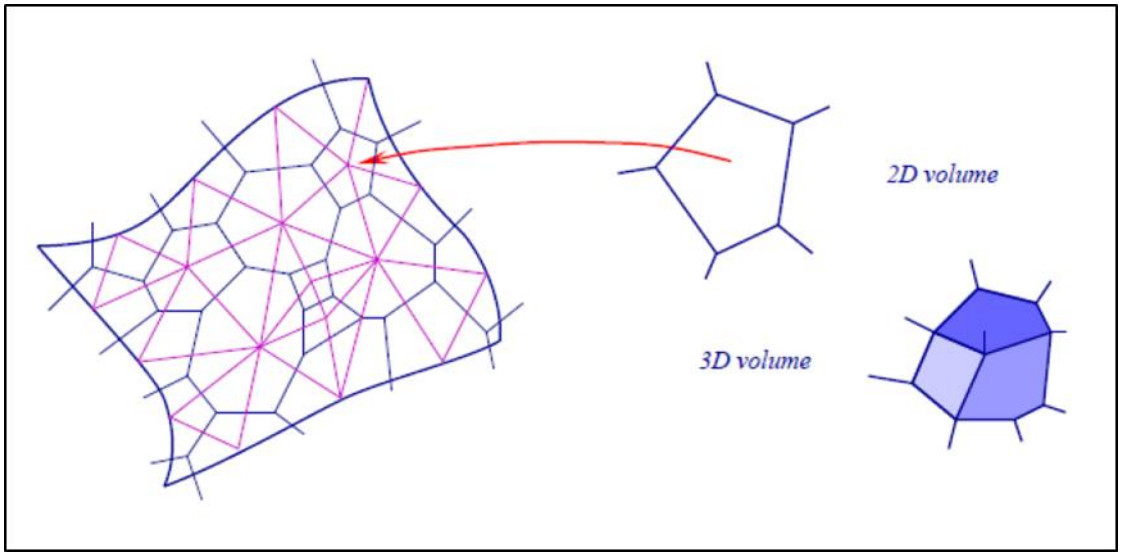

Figure 4.11: Finite Volume mesh with examples of 2D and 3D volume blocks [56]

Finite volume schemes have a number of advantages. Firstly it is applicable to both structured and unstructured meshes; it conserves mass, momentum and energy and they are physically easy to understand. The finite-volume discretization method has the ability to handle near discontinuous flow features. However, taking into account higher order (more than second order) approximations can be difficult to program and false diffusions in the interpolation scheme can also occur and lead to inaccurate solutions [60].

The importance of the discretising and order of approximations must be kept in mind when selecting a solver as these has significant effects on the computations. The solvers do not guarantee that the solution obeys physics and therefore practitioners of these tools should not rely on them blindly.

4.3.6.4.4 Euler Equations

The Euler equations, equation (4.14), are obtained from the Navier-Stokes equations, in the limit of non-viscous and non-heat conduction flows, and represent the highest level of approximation for an inviscid flow system. This approximation is essentially valid for high Reynolds number flows outside the viscous layers, which develop close to the solid walls, as it is known from the boundary layer analysis of Prandtl [61].

$$\frac{\partial}{\partial t}\boldsymbol{U} + \nabla \cdot \boldsymbol{F}_c(\boldsymbol{U}) = 0 \tag{4.14}$$

Neglecting the viscous terms in the governing equations implies a substantial mathematical change in the character of conservation laws. The order of the governing equations decreases from two to one, and consequently the number of boundary conditions decreases as well, but no simplification in the non-linear convective terms [62].

These are combined with the equations of energy and continuity. The equations are often solved by finite differences or volume differences whereby the values of each velocity component, the density, and the internal energy are computed at each point in the flow. From these quantities constitutive relations such as the perfect gas law or the isentropic pressure relation are used to find pressure. Since Euler equations permit rotational flow and enthalpy losses (through shock waves), they are very useful in solving transonic flow problems, propeller or rotor aerodynamics, and flows with vortical structures in the field.

4.3.6.4.5 Euler Viscous Coupled

The accurate and fast prediction of viscous flow over two- and three-dimensional surfaces is an important problem in aerodynamics. The continuing advances in efficiency of numerical algorithms, together with the increasing speed and memory size of computers, are enabling viscous flows to be calculated by methods that solve the full (Reynolds-averaged) Navier–Stokes equations. Whilst Navier–Stokes simulation potentially offers generality, its computational requirements currently limit its use for practical applications, especially within a design optimisation environment [63]. An alternative is to use the older technique of Viscous-Inviscid Interaction (VII), where an inviscid-flow solver is coupled to a viscous boundary-layer calculation method (Figure 4.12). They are based in using interactive boundary layer theory, which involves special techniques to couple the viscous and inviscid regions to find the whole flow solution. VII methods have shown to be very efficient and robust [64]. For many cases of aerodynamic interest the coupled solution matches experimental

data as well as Navier–Stokes simulation, and this at much lower computational cost.

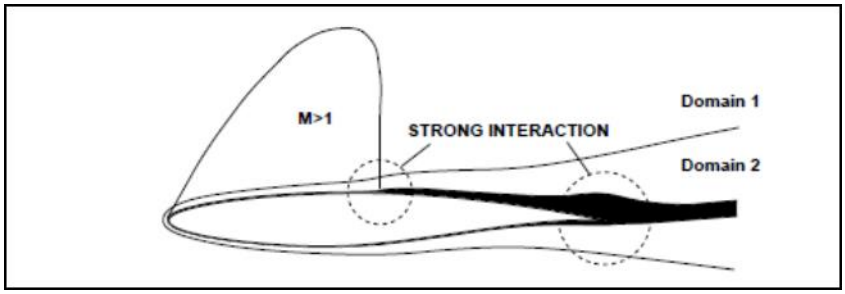

Figure 4.12: Decomposition of flow field into boundary layer and inviscid flow [64]

Since Prandtl [61] introduced his boundary-layer concept in 1904, several VII methods have been developed. An extensive review of different VII methods can be review in [64].

4.3.6.4.6 Reynolds Average Navier Stokes (RANS) equations

Instead of solving for the instantaneous flow-field, the statistical evolution of the flow is sought. The most prevalent approach is to solve the Reynolds-averaged Navier-Stokes (RANS) equations, which compute one-point moments such as mean velocity and turbulent kinetic energy, whilst retaining the effects of compressibility and viscosity [65].

In case of laminar flow, specifying the algebraic relations for the viscosity and the thermal conductivity coefficient as functions of pressure and temperature closes the governing equations. Therefore, the final solution is strongly dependent on the accuracy of these empirical relations.

In case of turbulent flow, most CFD codes do not solve the instantaneous equations directly due to limitations in RAM capacity and processor time. So, the flow variables, varying with time, are divided into mean and fluctuating components.

The principle of this technique is called Reynolds-averaging and applies to a given vector variable as follows:

$$\boldsymbol{u} = \bar{\boldsymbol{u}} + \boldsymbol{u}' \tag{4.15}$$

The mean component $\overline{\boldsymbol{u}}$ is defined as:

$$\overline{\boldsymbol{u}} = \frac{1}{\Delta t}\int_{(n-1)\Delta t}^{n\Delta t} \boldsymbol{u}(x,y,z,t)dt \tag{4.16}$$

where *n* and Δt are the time level and the time step in the CFD computation and the time interval Δt chosen to be long enough with respect to the fluctuations of the turbulent flow and short compared to the time of variations not related to turbulence. By applying this technique to the Navier-Stokes equations, the short-time Reynolds averaged Navier-Stokes equations can be written as follows:

$$\frac{\partial \bar{\rho}}{\partial t} + \nabla \cdot (\bar{\rho}\overline{\boldsymbol{u}}) = 0 \tag{4.17}$$

$$\frac{\partial}{\partial t}(\bar{\rho}\overline{\boldsymbol{u}}) + \nabla \cdot (\bar{\rho}\overline{\boldsymbol{u}}\otimes\overline{\boldsymbol{u}} + \bar{p}\boldsymbol{I} - \overline{\boldsymbol{\tau}} + \bar{\rho}\overline{\boldsymbol{u}'\otimes\boldsymbol{u}'}) = 0 \tag{4.18}$$

$$\frac{\partial}{\partial t}\bar{\rho}\left(\bar{e}_0 + \bar{k}\right) + \nabla \cdot \bar{\rho}\overline{\boldsymbol{u}}\left(\bar{h}_0 + \bar{k}\right) = \nabla \cdot \left(-\overline{\boldsymbol{q}} - \rho\overline{\boldsymbol{u}'h'} + \overline{\boldsymbol{\tau}}\cdot\overline{\boldsymbol{u}} - \bar{\rho}\overline{\boldsymbol{u}'\otimes\boldsymbol{u}'}\cdot\overline{\boldsymbol{u}}\right) \tag{4.19}$$

The short-time averaged turbulent kinetic energy, $\overline{k}$, is defined as:

$$\overline{k} = \frac{1}{2}\overline{\boldsymbol{u}'\cdot\boldsymbol{u}'} \tag{4.20}$$

The form of the continuity equation has not changed after averaging, but the momentum equation has an additional term $-\overline{\rho}\overline{\boldsymbol{u}'\otimes\boldsymbol{u}'}$, which is the Reynolds stress tensor $\overline{\boldsymbol{\tau}}_{\boldsymbol{r}}$. This term represents the influence of turbulence on the momentum equations and depends on unknown fluctuating velocity components. It is far from being a constant fluid property, such the molecular viscosity, but its magnitude and shape depend on the flow pattern. Therefore, the short-time Reynolds averaged Navier-Stokes equations with the equation of state become an open set of equations and it is necessary to develop a turbulence closure model. The purpose of this model is to replace the Reynolds stress $\overline{\boldsymbol{\tau}}_{\boldsymbol{r}}$ with an equation related to the mean flow variables. Using the Boussinesq relationship, the Reynolds stress $\overline{\boldsymbol{\tau}}_{\boldsymbol{r}}$ can be written by analogy with the viscous stress as:

$$\bar{\boldsymbol{\tau}}_{\boldsymbol{r}} = -\overline{\rho}\overline{\boldsymbol{u}'\otimes\boldsymbol{u}'} = \mu_t\left(\nabla\overline{\boldsymbol{u}} + \overline{\boldsymbol{u}}\nabla - \frac{2}{3}\boldsymbol{I}\nabla\cdot\overline{\boldsymbol{u}}\right) - \frac{2}{3}\boldsymbol{I}\overline{\rho}\overline{k} \tag{4.21}$$

where μ_t is the eddy viscosity estimated from a turbulence mode. Because $\boldsymbol{\tau_r}$ has the same form as the viscous stress tensor, this allows writing an effective viscosity as:

$$\mu = \mu_l + \mu_t \tag{4.22}$$

Short-time Reynolds averaging introduces a new term in energy equation due to the influence of turbulence, which is the turbulent heat flux vector $-\rho\overline{\boldsymbol{u}'h'}$.

The turbulent enthalpy transport by turbulent motion $-\rho\overline{\boldsymbol{u}'h'}$ is modelled as being proportional to the short-time averaged temperature gradient, following Wilcox [66].

This gives in the short-time Reynolds averaged Navier-Stokes equations, the turbulent heat flux vector, $\boldsymbol{q}_t$ is modelled by:

$$-\rho\overline{\boldsymbol{u}'h'} = \boldsymbol{q}_t = -\frac{\mu_t c_p}{Pr_t}\nabla T \tag{4.23}$$

Where Pr_t is the turbulent Prandtl number $Pr_t = \frac{\mu_t c_p}{k_t}$

It has been shown that the short-Reynolds averaged Navier-stokes equations contain unknown variables such as $-\overline{\rho\boldsymbol{u}'h'}$ as a consequence of averaging. Therefore, additional mathematical relations are needed to close the system of mean flow equations (4.18 to 4.20) with the equation of state. These mathematical relations can be algebraic, such as the Baldwin and Lomax model, or differential, such as the $k-\omega$ or the $k-\varepsilon$ models. In Table 4.1 is reported the main different turbulence models for closing the system.

Table 4.1: Main turbulence models

Type	Model	Author	Year
Algebraic turbulence model		Prandlt, Clauser	1925/54
		Cebeci & Smith	1967
		Baldwin & Lomax	1978
One-equation model equation (1 partial differential equation)	SA	Spalart & Alarm	1992
Two-equation model based on turbulent kinetic energy (2 partial differential equation)	K-ε	Launder, Spalding,	1972/74
	K-ω	Sharma	1988
	SST	Wilcox	1992
(Explicit) algebraic Reynolds stress model (2 PDEs + Algebra)	(E)ARSM	Pope, Rodi	1975/76
Reynolds stress model (6 partial differential equation)	RSM	Launder, Reece & Rodi	1975
		Speziale, Sarkar & Gatski	1991
		Hanjalic & Jakirilic	1998

The shear stress transport (SST) model, developed by Menter (1992) [67], combines the best qualities of the k-ω and the k-ε models. Specifically, the k-ε model is not able to capture the proper behaviour of turbulent boundary layers up to separation. The k-ω model is reported by Wilcox (2002) [68] as being more accurate than k-ε model in boundary layers under favourable, zero and adverse moderate pressure gradients in the near wall layers and has therefore been successfully applied to flows with moderate adverse pressure gradients. In the modelling of shear flows, the ω-equation shows a strong sensitivity to the values of ω in the free-stream outside a boundary layer. The free-stream sensitivity has largely prevented the ω-equation from replacing the ε-equation as the standard scale-equation in turbulence modelling, despite its superior

performance in the near-wall region. This was one of the main motivations for the development of the SST model. The SST model zonal formulation is based on blending functions, which ensure a proper selection of the k-ω and k-ε zones without user interaction. Menter [67] showed that the SST model exhibits an improved agreement with experiments compared to other two-equation RANS turbulence models for a variety of test cases. The SST model is known to give more accurate predictions in regions of separation in complex flow with a strong pressure gradient.

4.4 Aero Tools comparison

Different Aero solvers have been applied to the same mid-range aircraft, confidential Airbus test case, at cruise condition (M=0.8, α=2.0). Specifically, five different solvers have been used.

1. An aerodynamic model consists of a Truckenbrodt 3D lifting surface method [69], coupled with an airfoil numerical solver for taking into account viscosity and camber effects, for which the inputs are limited to planform geometry and airfoil sections data, i.e. no surfaces information is required. Nine section data have been used.
2. A solver that uses an extended version of lifting line theory, which is a halfway between the lifting-line and the lifting surface theory, proposed first by Weissinger [70] in 1947.
    a. (nine) Sections data calculated with an Euler code
    b. (nine) Sections data calculated with a RANS CFD code
3. A software tool that performs spanwise loading optimisation in the Trefftz plan using a discrete vortex model of the lifting surface, which was first presented by Blackwell [71].
4. A Euler viscous coupled solver (Flite3D+Callisto)
5. A RANS (SST turbulence model) code (TAU)

The results compared in term of lift coefficient versus the wingspan are reported in Figure 4.13. It is clear from the figure that there is not a significant difference between the span loadings calculated with solver based on Weissenger using section data obtained from Euler or RANS solver. Only the Euler Viscous

coupled solver match quite well the results obtained with the RANS CFD code. These last two solvers require a mesh generation and a longer run-time, compared to the others that run in the order of minutes not taking into account the section data required by solver based on Truckenbrodt lifting surface method and solver based on Weissinger theory. For these two solvers the cost of the tool in term of run-time is 99% with the 2D calculations. The choice of the appropriate CFD method, of course, depends on several factors such as the usage, accuracy of results required, on the desired use of the results, and wall-clock run times. The first two methods are suitable for knowing the global and local aerodynamic coefficients, and they should be mainly used for both lateral and longitudinal flight for subsonic flight over a range of Mach number up to cruise Mach number (transonic), but limited for attached flows. These tools are attractive & suitable for performing extensive studies such as MDO or to explore several alternative designs during the early design phases. The third one is used for spanwise target loading optimisation calculation. The Euler coupled solver is accurate enough for loads estimation at early stages in the design process but only in the linear region of the polar. It can be suitable for possible inclusion in a multi-disciplinary, aero-structural numerical optimisation process. Again, each of these methods has its own advantages and disadvantages when it comes to representing actual flight conditions and it is down to the designer to choose the most appropriate method for the task.

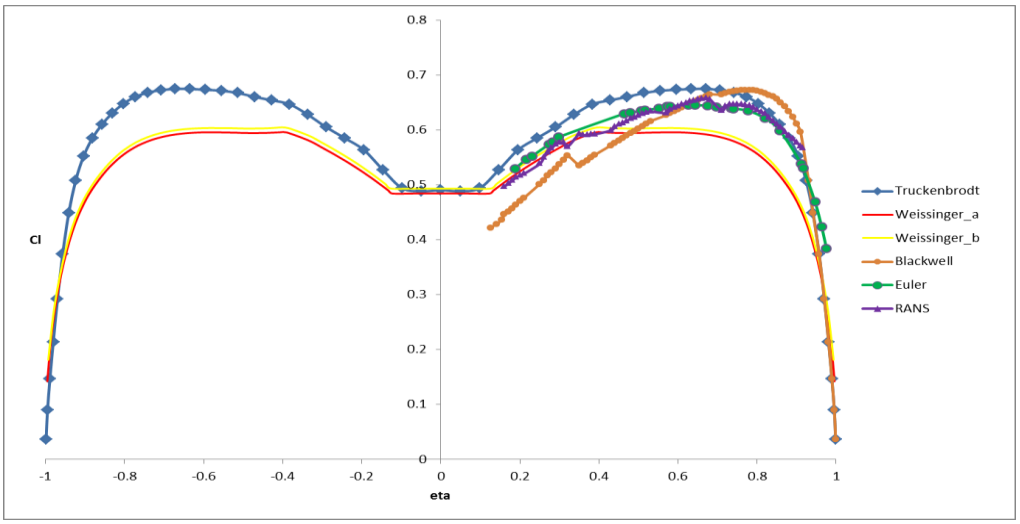

Figure 4.13: Aero Solvers comparison in term of lift coefficient vs. wing span

5 Aircraft Drag

5.1 Introduction

From an aerodynamic point of view the main challenge is to minimise drag due to the huge implications on the performance of the aircraft. One of the remaining areas for significant improvement is aerodynamic drag reduction. Drag prediction is the most important and challenging problem in aerodynamics. Experimental, empirical, analytical and numerical approaches, singly and in concert, have addressed this problem with varying degrees of success. Drag reduction for aircraft has a range of positive ramifications: reduced fuel consumption, larger operational range, greater endurance and higher achievable speeds. Even seemingly minor changes in drag can be critical. In design studies a drag decrease is equated to the decrease in aircraft weight required to carry a specified payload the required distance. The economic viability and future survival of an aircraft manufacturer depends on minimising aerodynamic drag (together with the other design key technologies of structures, propulsion, and control) while maintaining good handling qualities to ensure flight safety and ride comfort.

New designs that employ advanced computational aerodynamics methods are needed to achieve vehicles with less drag than current aircraft. The most recent generation of designs (Boeing 787, Airbus A350, etc.) already take advantage of computational aerodynamics, advanced experimental methods, and years of experience. Future advances in aerodynamic performance present tough challenges requiring both innovative concepts and the very best methodology possible. Initial drag estimates can dictate the selection of a specific configuration concept in comparison with other concepts early in the design phase. The drag projections have a huge effect on the projected configuration size and cost, and thus on the decision to proceed with the design. Drag reduction is a great challenge but there is still room for improvements.

Drag force is the summation of all forces that resist against aircraft motion. The calculation of the drag of a complete aircraft is a difficult and challenging task, even for the simplest configurations.

The variation of total drag force as a function of airspeed looks like a graph of parabola, see Figure 5.1.

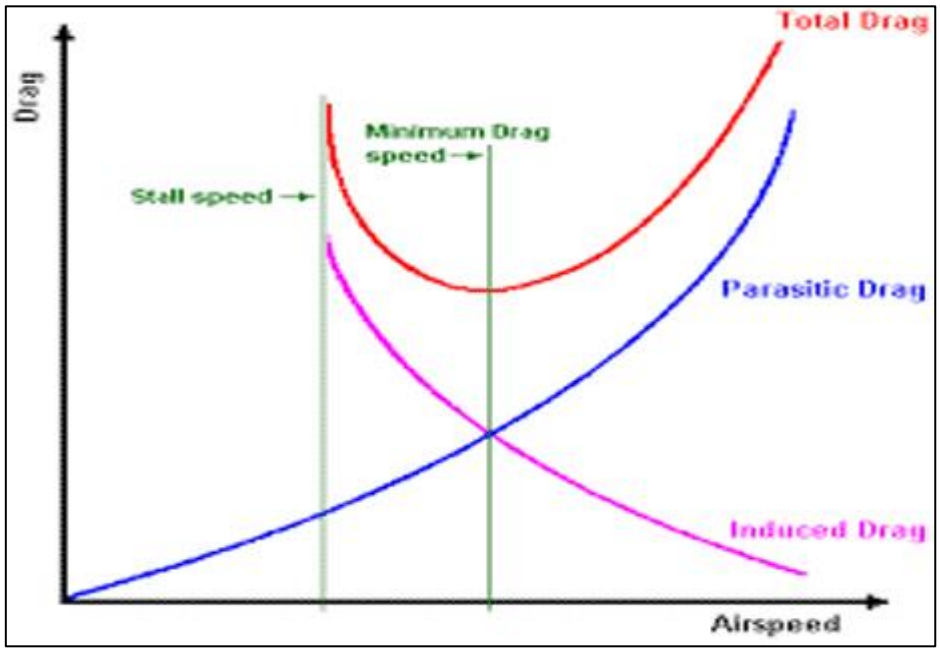

Figure 5.1: Variations of drag versus airspeed [72]

This indicates that the drag initially reduces with airspeed, and then increases as the airspeed increases. It demonstrates that there are some parameters that will decrease drag as the velocity increases; and there are some other parameters that will increase drag as the velocity increases.

There are two key considerations in discussing drag. Firstly, drag cannot yet be predicted accurately with high confidence levels (especially for unusual configuration concepts) without extensive testing. Secondly, nobody is precisely sure what the ultimate possible drag level really is that can be achieved for a practical configuration.

5.2 Basic Concept

Aerodynamic drag generally consists of friction drag and pressure drag. Friction drag is due almost entirely to the state of the boundary layer (laminar, transition or turbulent), and does not vary significantly between subsonic and supersonic flight. On the other hand, pressure drag increases noticeably at supersonic speed due to shock waves; this increased drag is called ‘‘wave drag”.

Aerodynamic drag is also divided into zero-lift drag (or lift-independent) and lift-dependent drag components. To calculate the performance of an airplane it is natural to define drag as the sum of the drag at zero lift and the drag due to lift. This is the approach that leads to the typical drag polar equation:

$$C_D = C_{D_0} + \frac{{C_L}^2}{\pi ARE} \tag{5.1}$$

The zero-lift drag includes all types of drag that do not depend on production of the lift. Every aerodynamic component of aircraft (i.e. the components that are in direct contact with flow) generates zero-lift drag. Typical components are wing, horizontal tail, vertical tail, fuselage, landing gear, antenna, engine nacelle, and strut. The zero-lift drag is a function of airspeed, air density, reference area, and the external shape of the components.

Each term is a function of Mach number, Reynolds number (in practice this is given to the performance group in terms of Mach number and altitude), and the particular geometric configuration (flap deflection, wing sweep, etc.). The drag is not precisely a quadratic function of the lift, and the value of the Oswald efficiency factor, E, in equation (5.1) is defined as a function of the lift coefficient and Mach number: $E = E\ (C_L, M)$. The Oswald factor, or aerodynamic efficiency, is the ratio between the computed induced drag of the aircraft and the ideal induced drag of an elliptic wing of same aspect ratio. Its theoretical maximum, reached only for an elliptic load distribution, is 1.

There is another drag polar approximation that is seen often. This approximation is more commonly used by aerodynamic designers trying to understand wing performance. It is used to take into account the effect of wing camber and twist, which causes the drag polar to be displaced “upward”, becoming asymmetrical about the CL = 0 axis. It is given as:

$$C_D = C_{D_0} + \Delta C_{D_m} + K\left(C_L - C_{L_m}\right)^2 \tag{5.2}$$

In taking into account the effect of camber and twist on shifting the polar, the term represents a penalty associated with using twist and camber to achieve good performance at the design lift coefficient. This equation is for a fixed

geometry. The value of K defines the shape of the polar. C_{D0} represents the minimum drag of the configuration without camber and twist. The values of are functions of the design lift coefficient. In general, friction drag is treated approximately as zero-lift drag, because friction drag is not sensitive in the change of angle of attack. Shock waves are produced by deflections of the flow by airframe volumes, such as the cross-sectional area distribution of the fuselage and the thickness distribution of the wing, and by lift generation. The first corresponds to zero-lift drag and is called ‘‘wave drag due to volume’’. The latter is the lift dependent drag called ‘‘wave drag due to lift’’. Moreover, lift-dependent drag includes a component called ‘‘induced drag’’ at subsonic speed, which is generated by trailing vortices such as wing tip vortices. Classical approaches to reduce wave drag are including area ruling, reduce thickness, wing sweep, wing twist/camber/warp via linear theory and favourable wave interference [73], [74].

Vortex Drag Due to Lift (DDL) is of major interest for both subsonic and supersonics, but this area has not been worked extensively in years except for winglets other tip devices. The classical linear theory approaches of increased aspect ratio, lower lift coefficient and elliptic load distribution are utilised to the extent allowed by structural considerations and overall design [75].

The drag components are shown in Figure 5.2.

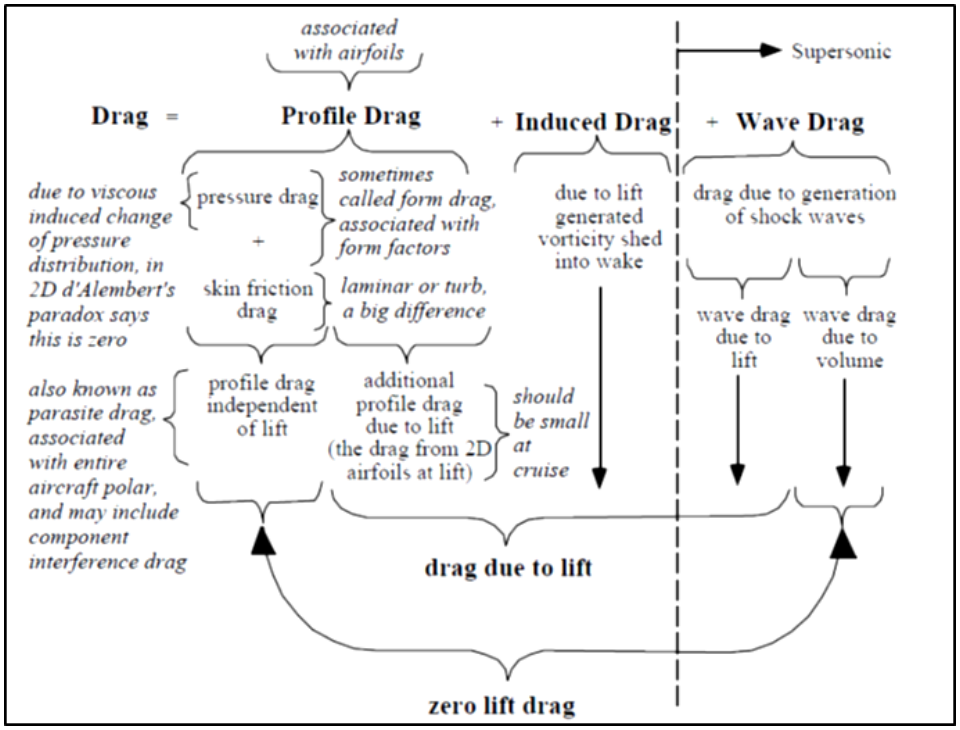

Figure 5.2: A broad-brush categorization of drag [76]

Figure 5.2 provides a basic classification of drag for overview purposes, although the drag nomenclature is frequently quite confusing and sometimes it is matter of technical discussion.

The aerodynamic configuration specific approach to drag is not covered in fluid mechanics oriented aerodynamics texts, but is described in aircraft design books. Probably, the most important overview of aerodynamic drag for design has been given by Küchemann [77] and should be studied for a complete understanding of drag concepts. Figure 5.2 suggests that wave drag appears suddenly at supersonic speeds. A more meticulous examination shows that actually wave drag arises at subsonic speeds when the flow accelerates locally to supersonic speeds, and then returns to subsonic speed through a shock wave. This leads to the presence of wave drag at subsonic (actually, by definition, transonic) free-stream speeds. This initial drag increase, known as drag rise, is followed by a rapid increase in drag, and is an important consideration in the design of wings and aerofoils. The Mach number at which the rapid drag increase occurs is known as the Drag Divergence Mach number, MDD. The increase in drag occurs directly because of the wave drag associated

with the presence of shock waves. However, the drag also increases because the boundary layer thickness increases caused by the sudden pressure rise on the surface due to the shock wave, which leads to increased profile drag. Lynch [78] has estimated that at drag divergence the additional transonic drag is approximately evenly divided between the explicit shock drag and the shock induced additional profile drag. The drag breakdown of a civil transport aircraft shows that the skin friction drag and the lift-induced drag constitute the two main sources of drag, approximately one half and one third of the total drag for a typical long range aircraft at cruise conditions [79]. This is why specific research on this topic has driven researchers towards Hybrid Laminar Flow (HFL) technology and innovative wing tip devices which offer potential for drag improvements, for skin friction drag and lift-induced drag reduction respectively. Aircraft performance improvement can also be obtained through trailing edge optimisation, control of the shock boundary layer interaction and of boundary layer separation.

5.3 Drag prediction methods

Identifying the various sources of transonic aircraft drag alone is not enough to achieve any form of benefits; the drag sources also have to be quantified. Modelling the drag of an aircraft is a vital part of the design process. The drag strongly dictates the range of the aircraft, which is used when the aircraft is marketed to prospective buyers. Therefore getting a correct estimation for the drag, particularly early on in the design stage, is vital. The three physical phenomena responsible of aircraft drag are: Vortex shedding, which gives rise to induced drag; boundary layers and wakes, which give rise to viscous drag; and shock wave formation, which lead to wave drag, see Figure 5.3.

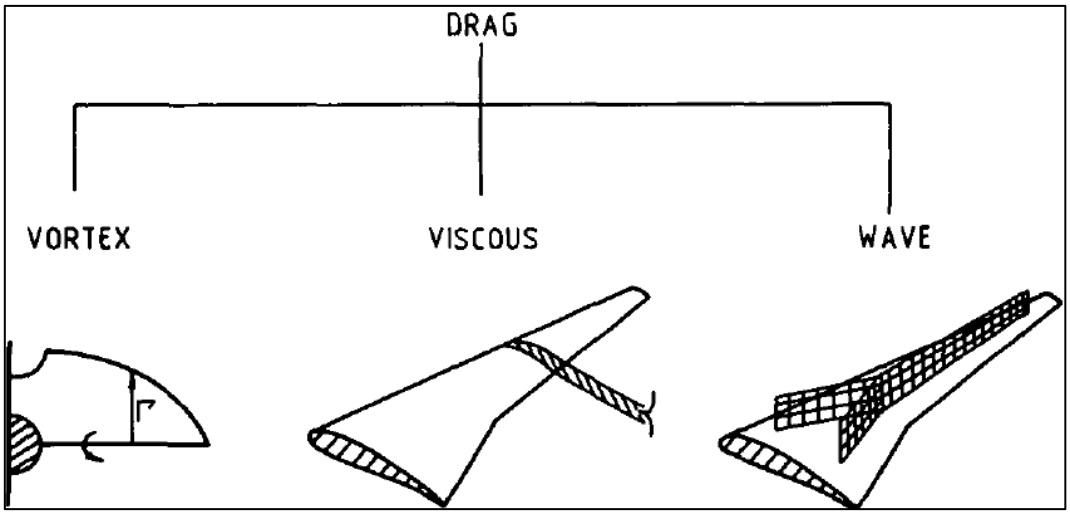

Figure 5.3: Drag components of a transonic wing [80]

The process of quantifying these components is very much reliant on computational methods. There are two different ways in which the drag force can be determined, from the body and from the fluid flow. Accurately determining the drag values using computational methods is considerably more difficult than accurately predicting pressure distributions. The accuracy depends on various factors including: geometry representation, mesh size, flow solver, convergence level, transition prediction and the turbulence model.

5.3.1 Spanwise Integration for Total Drag

The total drag on a wing is made up of the induced, wave and viscous drag components; it can be estimated using the spanwise 'strip method'. It is based on the strip theory that computes the aerodynamic forces and moments on individual 2D sections and integrated across the span to determine the overall forces. Where the strip width is calculated using:

$$\Delta y_i = \sqrt{(y_{i+1} - y_i)^2 + (z_{i+1} - z_i)^2} \tag{5.3}$$

5.3.2 Near-field and Far-field drag method

The surface stress integration method is a near field drag recovery method. Singularity strengths are used to determine the velocity at control points on the surface and the pressures are then computed using a second-order

approximation of the Bernoulli equation. Integrating the pressure coefficients over the surface computes the force coefficients as well as the lift and drag coefficients. The lift coefficients are generally predicted with reasonable accuracy; however, the drag prediction is less accurate. The surface pressure integrations involve cancellations that may lead to loss of accuracy in computing smaller quantities such as induced drag. Determining the position of the forward stagnation point is also prone to error because of the large gradients, particularly for three-dimensional analyses. The far-field method is an alternative method used to determine the induced drag and for which the wave drag can also be calculated. Drag can be extracted from a numerical solution either in the near-field or in the far-field. Far-field drag extraction provides physical and local information about the sources of drag. This additional information are very useful in aerodynamic design.

In the far-field analysis, spurious drag sources can be detected and eliminated. Far-field drag may thus be more accurate than near-field drag.

The localisation, visualisation and evaluation, of the spurious drag sources in the field also provide useful numerical information about the quality of the grid and/or computation.

The near-field computation and the far-field computation approaches should lead ideally to the same results but in practice there is a difference dictated by the numerical errors.

Near-field drag method integrates the stresses at the surface of the aircraft and provides the mechanical breakdown: pressure drag + friction drag

In Far-field drag method the integrals are derived from the momentum theorem, involving control volumes or surfaces within the flow field and provides the physical breakdown: viscous drag + wave drag + induced drag.

The momentum balance is determined over a control volume a large distance from the body. It was suggested by Von Karman that the induced drag could be found by applying the conservation principles to a control volume surrounding a finite wing and determining the residual flow perturbations leaving the control volume. The theory is based on the assumption that viscous drag and wave drag is confined to finite non overlapping surface volume Sv (boundary layer

and viscous shear layer) and Sw (shock layer), and that the flow can be considered as inviscid outside these surfaces.

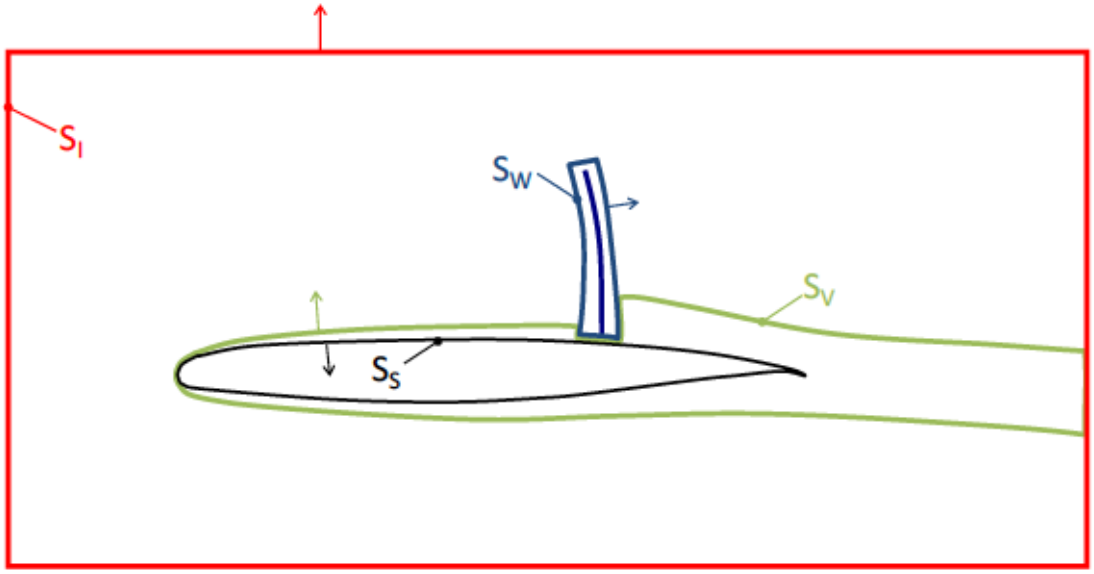

Figure 5.4: Definition of integration surfaces for near-field and far-field drag (Arrows indicate the direction of normal vectors)

The above figure depicts the integration surfaces used for the computation of near-field and far-field drag components for a configuration with no engines, where:

S_S represents all skin surfaces

S_W is the wave drag integration surface (surrounding shock waves)

S_V is the viscous drag integration surface (surrounding boundary layers and viscous wakes, and in which the whole aircraft is included)

S_I is the induced drag integration surface (in which S_V and S_W are included).

Table 5.1 below lists all outputs of the near-field and far-field analysis as well as their definitions and their formulation, using the surfaces defined above.

Table 5.1: Outputs of the near-field and far-field analysis together with their definitions and their formulation

Name	Description	Formulation
Cd_Near_Field	Total near-field drag on all skin surfaces	$D_{skin} = D_p + D_f$
Cdp skin	Pressure drag on skin	$D_p = \iint_{S_s} (p - p_\infty) \cdot n_x dS$
Cdf skin	Friction drag on skin	$D_f = -\iint_{S_s} (\overline{\tau_x} \cdot \vec{n}) dS$
Cd_wave	Wave Drag	$D_w = -\iint_{S_w} \overrightarrow{f_l} \cdot \vec{n} dS$
Cd_viscous	Viscous Drag	$D_v = D_{vp} + D_f$
Cd _viscous pressure	Viscous pressure drag	$D_{vp} = -\iint_{S_V} \overrightarrow{f_l} \cdot \vec{n} dS + D_p$
Cd_induced	Induced Drag	$D_i = \iint_{S_I} \overrightarrow{f_l} \cdot \vec{n} dS$

Where $\vec{f}$ is a dynalpy like-vector

$$\vec{f} = -\rho(u - u_\infty)\vec{q} - (p - p_\infty)\vec{\imath} + \overrightarrow{\tau_x} \tag{5.4}$$

Which can be split into two vectors $\overrightarrow{f}_{vw}$ and $\overrightarrow{f_l}$:

$$\vec{f} = \overrightarrow{f}_{vw} + f_i \tag{5.5}$$

$$\overrightarrow{f_l} = -\rho(u - u_\infty - \Delta\bar{u})\vec{q} - (p - p_\infty)\vec{\imath} \tag{5.6}$$

$$\overrightarrow{f}_{vw} = -\rho\Delta\bar{u}\vec{q} + \overrightarrow{\tau_x} \tag{5.7}$$

With

$$\Delta\bar{u} = u_\infty \sqrt{1 + 2\frac{\Delta H}{u_\infty^2} - \frac{2}{(\gamma-1)M_\infty^2}\left[\left(e^{\frac{\Delta S}{r}}\right)^{\frac{\gamma-1}{\gamma}} - 1\right]} - u_\infty \tag{5.8}$$

Where *ΔH* and *ΔS* are respectively the variations of enthalpy and entropy relative to their free-stream values. $\vec{q}$ is the velocity vector.

5.3.3 Wave Drag by Integrating over Shock Waves

Wave drag in mass-conserving potential flow is known to be the consequence of momentum production across the shock waves in the direction normal to these shock waves [81]. Integrating over the shock i.e. across the flow conditions at the entry and exit from the shock is one approach of obtaining the wave drag. The entropy difference between two planes positioned immediately upstream and downstream of the shock is used to determine the wave drag.

5.4 Geometric variables which affect drag

Drag coefficients are complex functions of profile shape, angle of attack, wing planform, Mach number (M), Reynolds number (Re), and so forth.

Geometry has a large effect on the amount of drag generated by an object. As with lift, the drag depends linearly on the size of the object moving through the air. The cross-sectional shape of an object determines the form drag created by the pressure variation around the object. For a lifting wing, there is a pressure difference between the upper and lower surfaces of the wing. Vortices are formed at the wing tips, which produce a swirling flow that is very strong near the wing tips and decreases toward the wing root. The three-dimensional planform shape affects the induced drag of a lifting wing. Long, thin (chordwise) wings have low induced drag; short wings with a large chord have high induced drag. Wings with an elliptical distribution of lift have the minimum induced drag. Modern airliners use winglets to reduce the induced drag of the wing. Reducing

wing thickness leads to associated reduction in viscous drag. However, thickness reductions have little effect over majority of CL range in term of induced drag. Reducing thickness leads to reduced wave drag over all CL values.

The wing trailing edge has a strong influence on the aerodynamics of a given wing profile. In the subsonic region, increasing camber (increases as thickness decreases or increase with a downward flap deflection) requires less α for a fixed C_L, or increases the coefficient C_L for a constant α.

If we think of drag as aerodynamic friction, the amount of drag depends on the surface roughness of the object; a smooth, waxed surface produces less drag than a roughened surface. This effect is called skin friction and is usually included in the measured drag coefficient of the object. To conclude the flow is very sensitive to particular features of the geometry and that is why designing a wing is not a trivial task.

6 Aero Process in an MD context

A preliminary Multi-Disciplinary (MD) approach would allow Aircraft Architects to study more design alternatives in greater detail. A large number of concept configurations is initially generated, and these are eventually narrowed down to a single concept. Figure 6.1 compares a traditional aircraft design approach with Toyota's set-based philosophy. The latter approach would allow Aircraft Architects to study more design alternatives in greater detail, thus increasing the likelihood of discovering exceptional or flawed designs before the detailed design stage. Ultimately this results in a quicker and more efficient design lifecycle, and offers a potential route to development of superior aircraft.

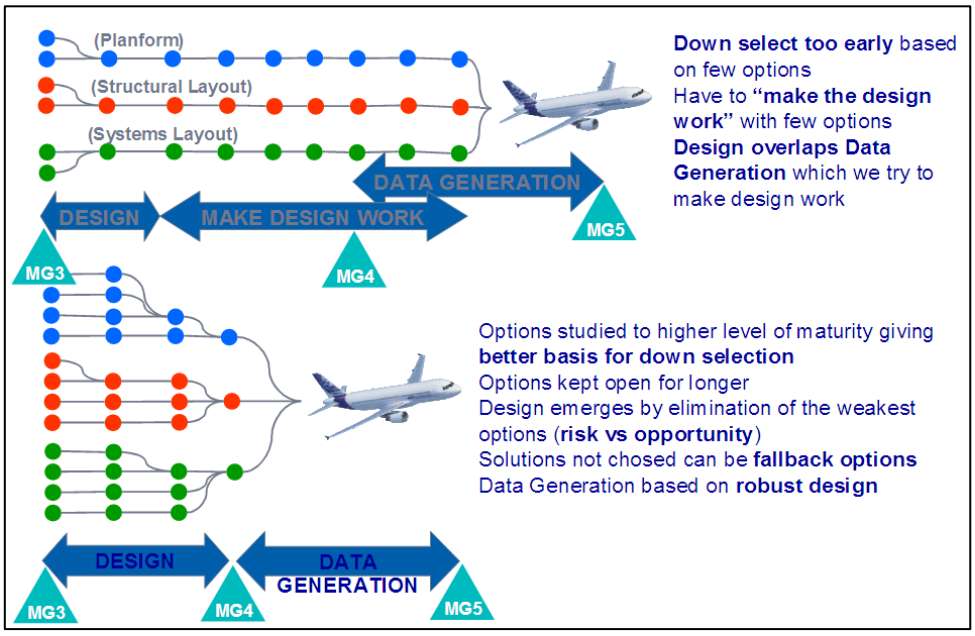

Figure 6.1: Toyota's set-based engineering approach applied to the aircraft design process

This is achieved by successive rounds of comparison and down-selection; the level of engineering accuracy and detail increases for each round in order to facilitate differentiation between candidate concepts. An automated, integrated Aerodynamics Process is a pre-requisite for such a capability, so must be developed if the MD opportunity is to be addressed. This chapter is concerned with the development and enhancement of an industrial MD Aerodynamics Process suitable for preliminary design of aircraft.

6.1 MD project and aero process overview

As previously stated, the step change in performance required by the ACARE 2050 [1] vision for commercial transport aircraft is, in part, dependent on the successful integration of Multi-Disciplinary Design Capabilities (MDDC) at the preliminary design stage. Conceptual design capabilities are now extensively developed and routinely used at conceptual project level. However, the challenge for today is to transition smoothly from conceptual to preliminary design whilst maintaining a true Multi-Disciplinary (MD) approach, as sketched in Figure 6.2.

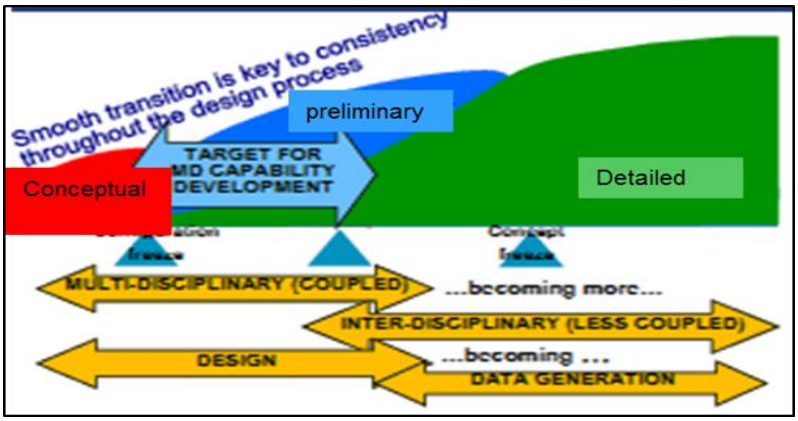

Figure 6.2: Sketch of target for MDDC development

The design space must be progressively constrained, whilst at the same time increasing the level of modelling fidelity and keeping as many design options open for as long as possible, as illustrated in Figure 3.1.

This chapter illustrates the development of an iterative multi-disciplinary Layer 3 design capability using methods with higher level of fidelity than is possible with current Layer 2 that is realised by the Conceptual Design team. Basically, low-order methods that use conceptual design tools to perform trade-studies. At the same time the multi-disciplinary Layer 3 has to be less consuming than methods available at Layer 4 that is realised within the engineering Centres of Competency, during the detailed design phase, who use specialist high fidelity methods to mature design to production. Such methods are typically complex and require long run times. Layer 3 represents an opportunity to enhance the overall design process by introducing MD processes, which use methods

pitched between layer 2 and layer 4 in terms of both fidelity and rapidity. Figure 6.3 shows an overview of the main disciplines involved in a preliminary design stage.

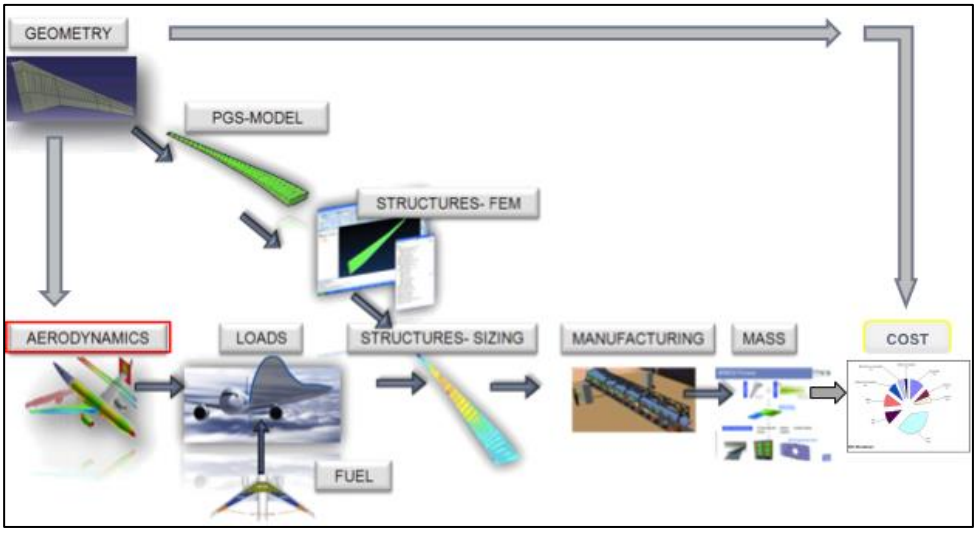

Figure 6.3: Overview of a multi-disciplinary process

The Layers represent MD toolsets, which are appropriate for the various stages of overall aircraft design. Figure 6.4 illustrates how the Layers and domains interact.

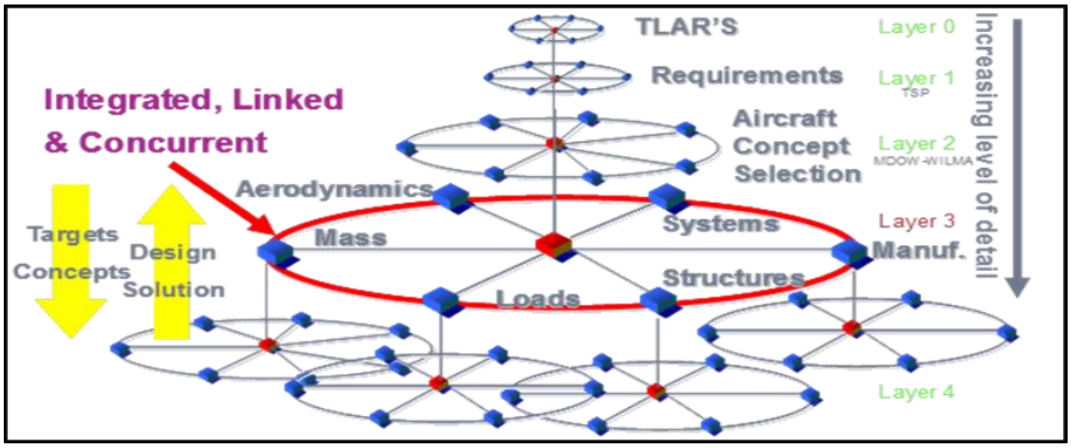

Figure 6.4: The 'Wheels Diagram', interactions between levels and domains

The red boxes at the centre of each wheel represent the collaborative data, which is shared by all domains and is one of the main mechanisms by which the process synchronises the different domains. A design iteration should be

performed within a week, and for this reason a higher degree of automation and deployment of appropriate methods is necessary. As a result the reduction of the development time and cost is possible delivering aircraft with reduced environmental and operating costs and increasing range, payload and passenger comfort. The main benefit expected from this project is the enabling of robust aircraft architectures, i.e. architectures where exceptional or flawed designs will happen in later detailed design phases, where much more engineers are involved and where rework is much more expensive and may not deliver the committed aircraft performance. A Layer 3 MD design capability will ultimately strengthen industry competitive position by reducing development time and costs, and delivering aircraft with reduced environmental, purchase and operating costs. An automated, integrated Layer 3 MD Aerodynamics Process is a pre-requisite for such a capability, so must be developed if the MD opportunity is to be addressed. The project high-level target as previously stated is to go from geometry to cost in a week time frame. As the other domains, the MD Aerodynamics Process within the MD design project must be compatible with these requirements, which means that the time per aero design iteration should be aiming at around 24 hours, fitting with a week-long overall process.

6.2 Description of the automated Aero Process

Within the multidisciplinary design process there is a requirement for a rapid aerodynamic module to enable quicker wing architecture development. This part of the multidisciplinary process will need to provide the aerodynamic data for aircraft performance and aero data for loads. Such process should have increased fidelity over methods available at layer 2 such as semi-empirical and Panel methods, whilst at the same time to be less time-consuming than methods available at layer 4 such as RANS CFD. An Euler coupled with a boundary layer method has been chosen as flow solver kernel. Figure 6.5 shows how the MD Aerodynamics Process should be integrated into the overall multi-disciplinary process. The inputs required are the datum aircraft geometry and flight envelope definitions, which typically include Mach number, incidence

ranges, Reynolds number and air temperature, which are common to all domains.

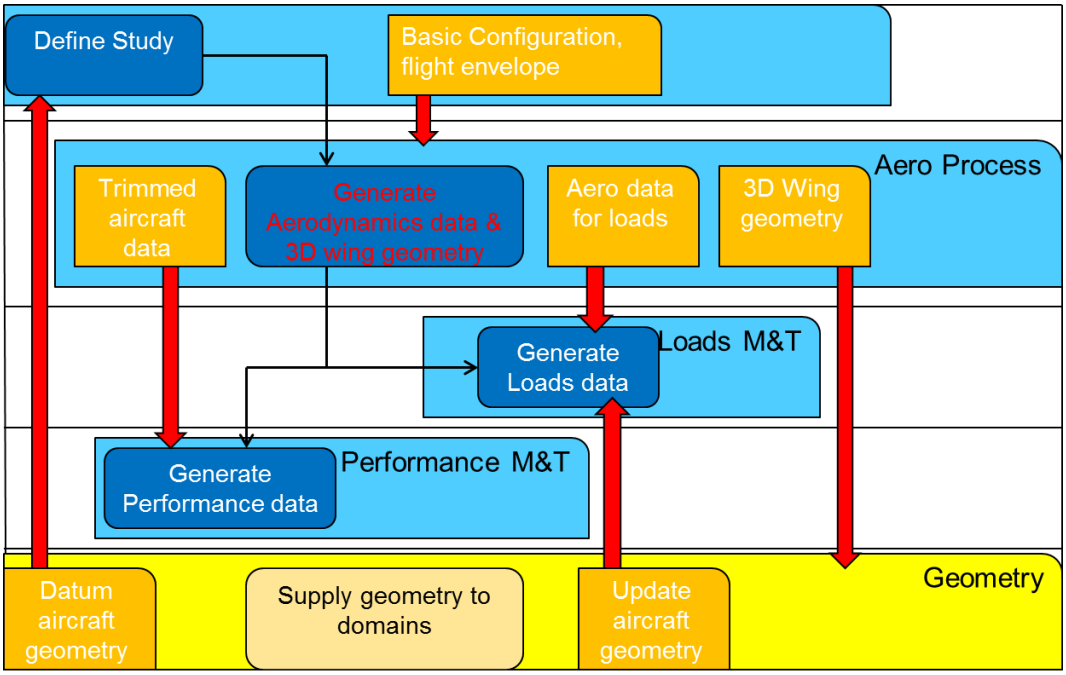

Figure 6.5: Aerodynamics process vision within multidisciplinary context

The MD Aerodynamics Process has to produce aerodynamic data and a new Wing Geometry (see Figure 6.6).

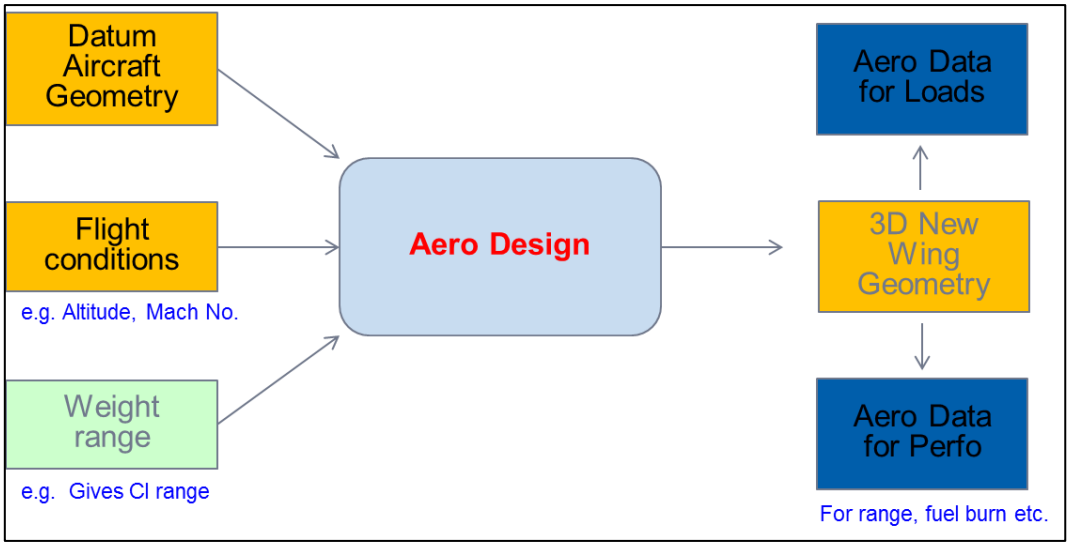

Figure 6.6 Requirements for a MD–TPAACE High Speed Aero Module

The data is passed downstream to the Performance domain and, via Aerodynamic Data for Loads methods, to the Loads domain.

The generalised MD Aerodynamics Process architecture is illustrated in Figure 6.7

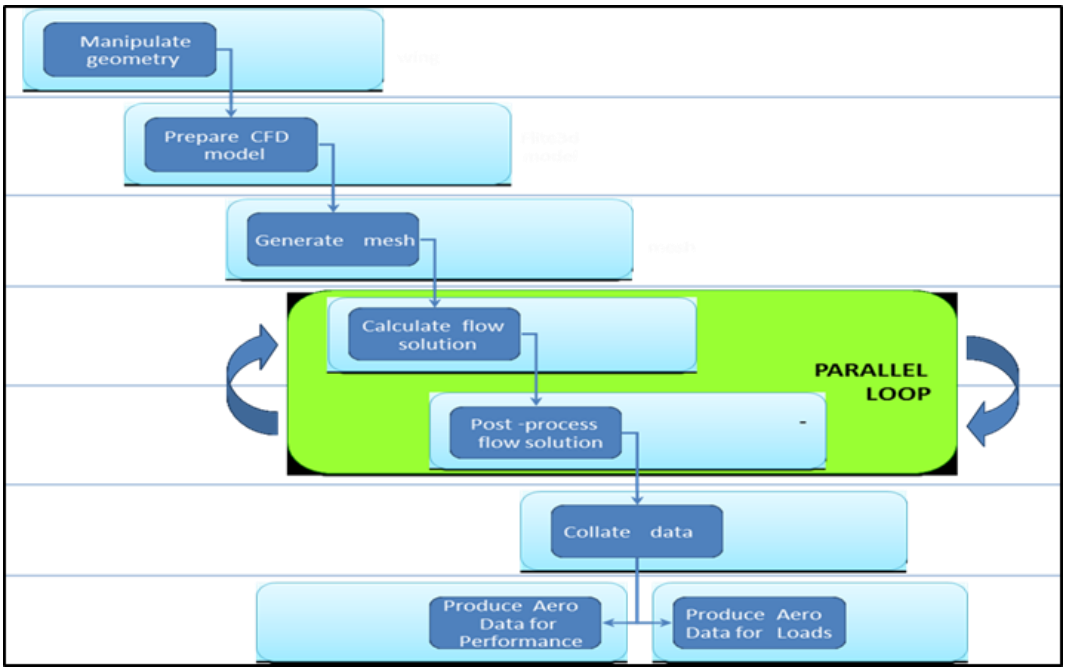

Figure 6.7: Schematic of MD Aerodynamics Process

The Aero Process has been developed and integrated using the commercial software 'ModelCenter', which is an integration/process building environments. It allows any program to be 'wrapped' in a generic, re-usable way to produce a 'component'. A Wrapper is a set of instructions that describe inputs, outputs, and how to execute the analysis. Each module of a process wrapped become a black box component with a set of inputs and outputs, and can be re-used in more than one process or work flow. Components can be connected by linking their output and input variables, forming a 'workflow'. The finished workflow can be run automatically from start to finish and saved as a ModelCenter model. All the components have been wrapped using Python language scripts. A screenshot of the aero process implemented in ModelCenter, in its contracted form, is shown in Figure 6.8.

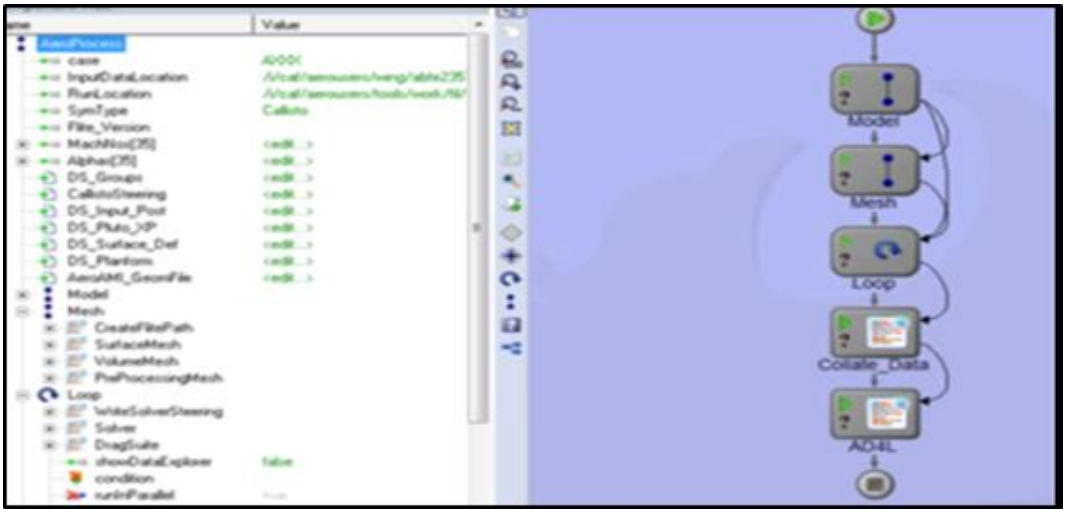

Figure 6.8: MD Aerodynamics Process implementation in Model Center

The first step is to import the new CAD description of the wing geometry from a database using the data management tool. In order to prepare the geometry for the start of the automatic aero process, the geometry needs to be converted from Catia to IGES format using Catia and then from IGES to an *icms file format readable by the pre-processor using an IGES to *icms converter. Once the *icms file is generated, it will be the input for the automatic aero process. The process, as it is shown, is divided in components. The first one is “Model” containing, in turn, other four components. These four components manipulate the geometry and prepare the CFD model. The purpose of it is to generate the model that will be used as input afterwards for the meshing process. See Figure 6.9.

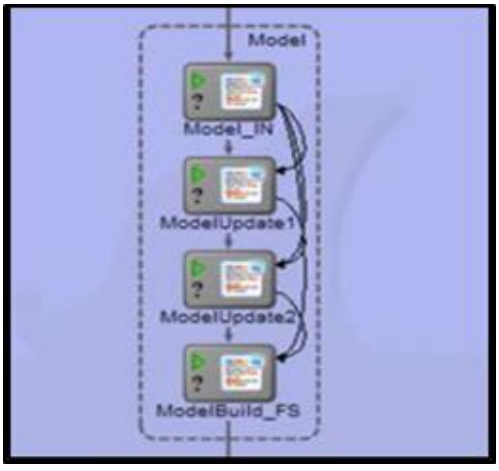

Figure 6.9: “Model” collapsed showing its four components

The first component loads the pre-existing model and the new wing description (ICMS file) into ModelCenter. The second takes the new wing and splits single entity wing into two entities at the trailing edge crank. The third one replaces the two new WING entities in the Model. The last one creates valid model with correct edges and intersections, adding the viscous mesh and the sources needed for the mesh generation. See Figure 6.10.

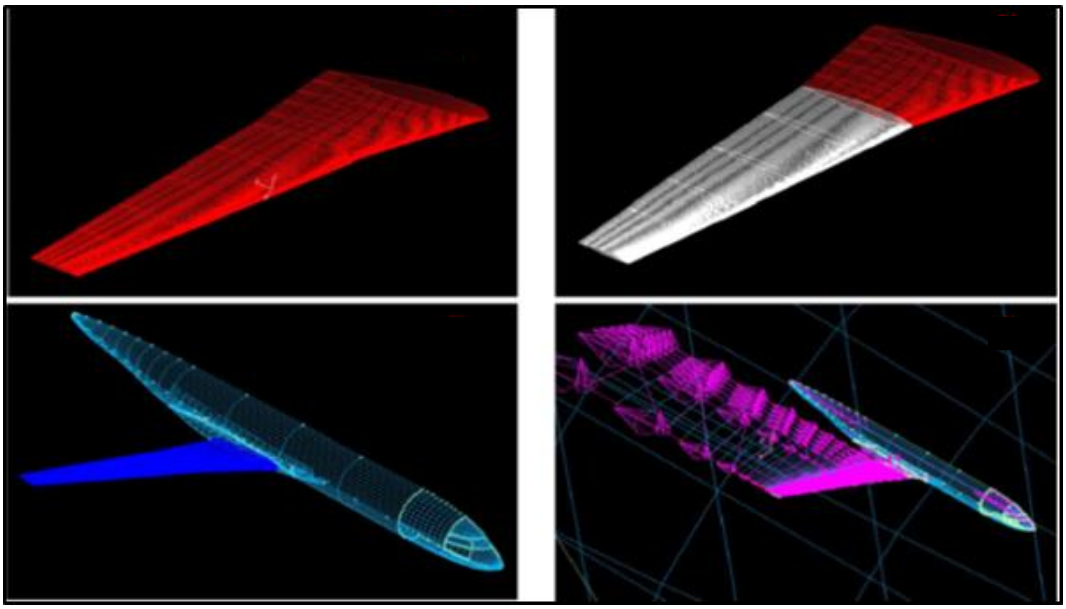

Figure 6.10: Visualization of the four components output

In addition, the fourth component has the capability to transform the wing from jig to flight shape, before running the process. The baseline wing panels are defined with only the design sections. These sections are translated using dx, dy, dz translations and rotations defined in an external text file. The transformed wing panels are re-sampled in a spanwise direction to give a fine distribution of points aiding surface grid generation. Figure 6.11 compares the starting geometry and the flight shape.

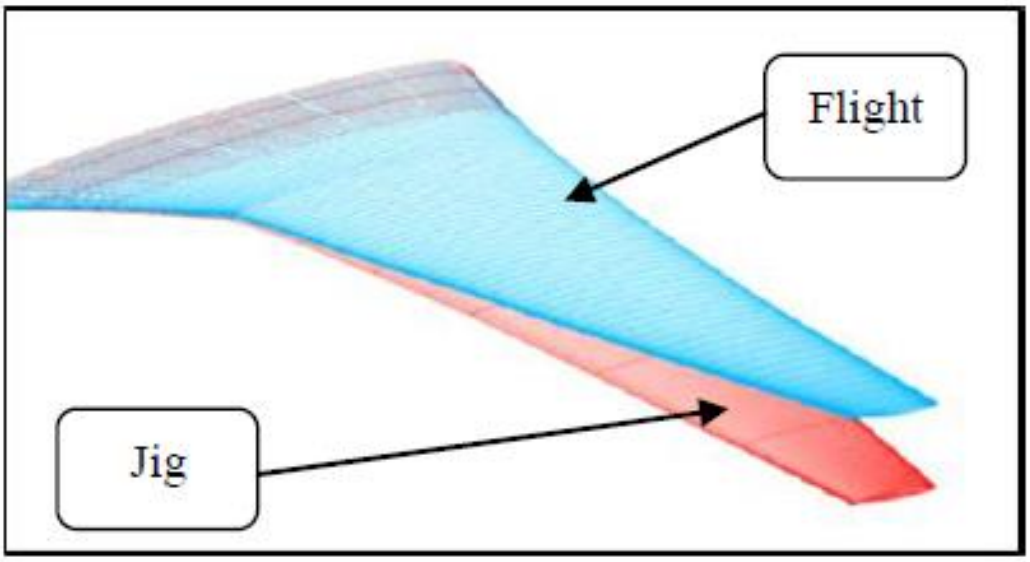

Figure 6.11: Jig (red) to flight shape (blue) transformation

After the model is completed, the next step is the generation of the mesh.

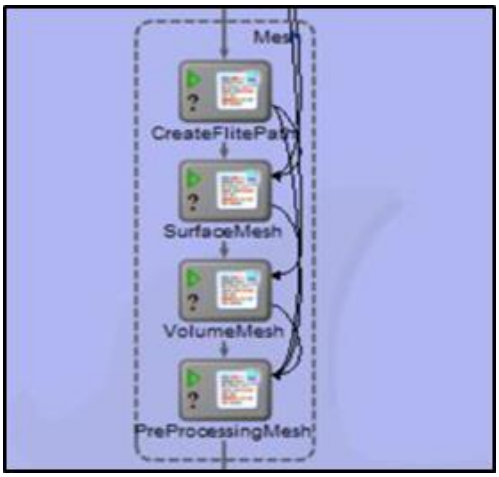

Figure 6.12: "Mesh" collapsed showing its four components

In the mesh module the first component is "CreateFlitePath". It is a simple Python script file that generates a unique path where the results directory is created. The second and third components generate the surface and volume mesh respectively. The last one applies the boundary conditions and gives information about the mesh such as number of cells, quality etc.

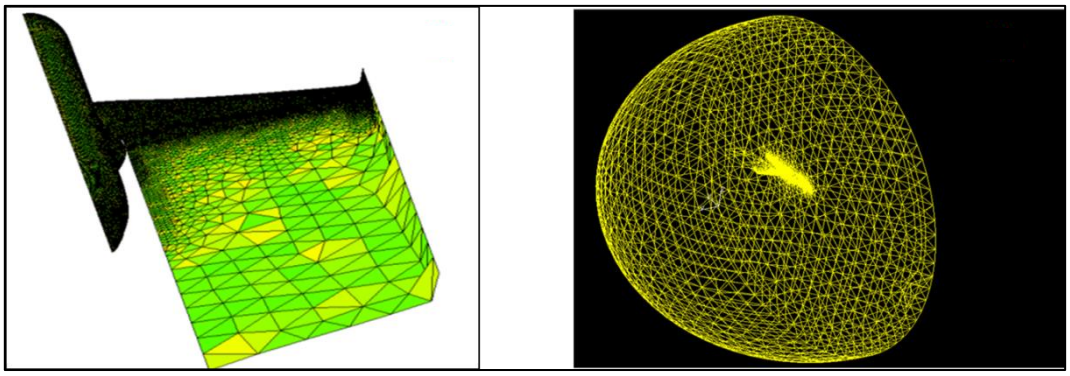

Figure 6.13: Example of mesh generated

The loop module is the Flow solver loop shown in Figure 6.14.

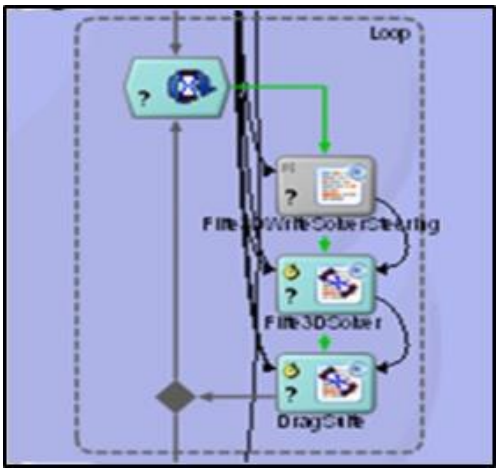

Figure 6.14: "Loop" collapsed showing its three components

In its original version the loop could run in serial mode that means that around 70 hours were necessary to generate aerodynamics data for an flight envelope, which comprise a minimum of 35 operating points (7 incidences at each 5 Mach numbers) required for the calculation of loads. This time to generate the aero data for loads is not compatible with the requirements. This has driven to do more work on the Model Center looping capability. The author has worked in liaison with the Model Center developer to address this issue, testing and reporting all the problems encountered. After a long iterative process, eventually the loop has a parallelization capability that allows running data points simultaneously via grid computing resources. This capability allowed reducing drastically the wall-clock time and consequentially to fit the level requirement of the Aero Process in the Multi-disciplinary context. In the first component

“WriteSolverSteering” are set the input of the simulation, such as number of iterations, Mach numbers and angle of incidence range. The second component is the Euler flow solver coupled with a boundary layer method. At the end of the flow solver the Drag suite component post-processing the flow solution, generating the output file containing the overall forces and drag breakdown, span loading and so on. The last two components of the process assembles the CFD data into polar and extracts the polar data. Specifically, the last tool is used for the production of linearised aerodynamic data for loads calculation, producing aerodynamic data in a suitable format for load methods.

6.2.1 Comparison

In order to check the accuracy of the flow solver, pressure profile results have been compared with RANS data results. The RANS results are for a complete Wing body configuration, including engine, flap track fairings and winglet as in Figure 6.15 (left), although the Model Center geometry is a clean wing. The Model Build component has not yet the capability, at least at the moment, to handle winglet in an automatic fashion. The winglet was added manually using the pre-processor for a more fair comparison with the RANS data. In this thesis some selected results are shown, specifically the chordwise pressure distribution at only four spanwise sections (shown in Figure 6.15) for only the cruise Mach number (M=0.8) and at three different angles of attack, see Figure 6.16, Figure 6.17 and Figure 6.18

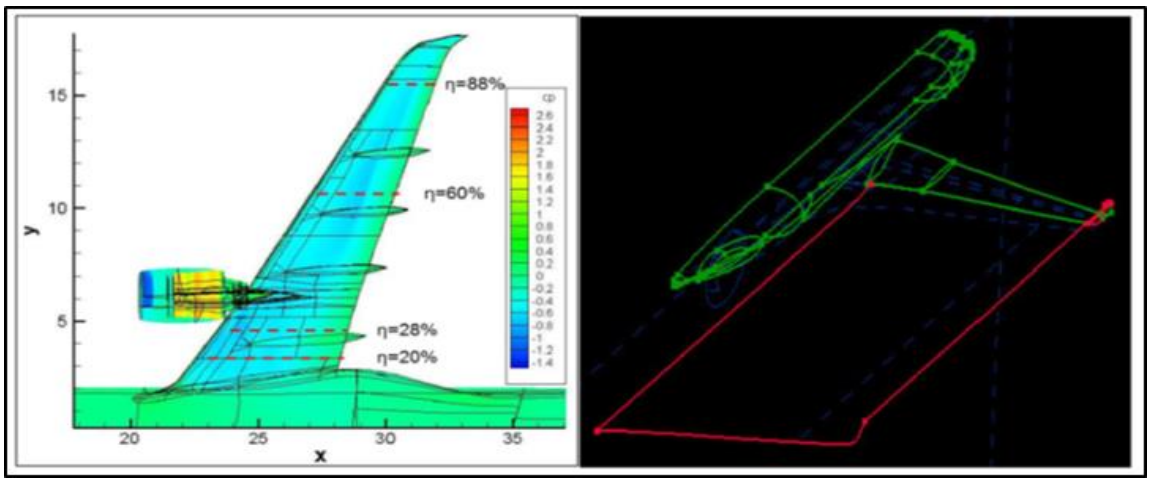

Figure 6.15: RANS model (left) and Euler model (right)

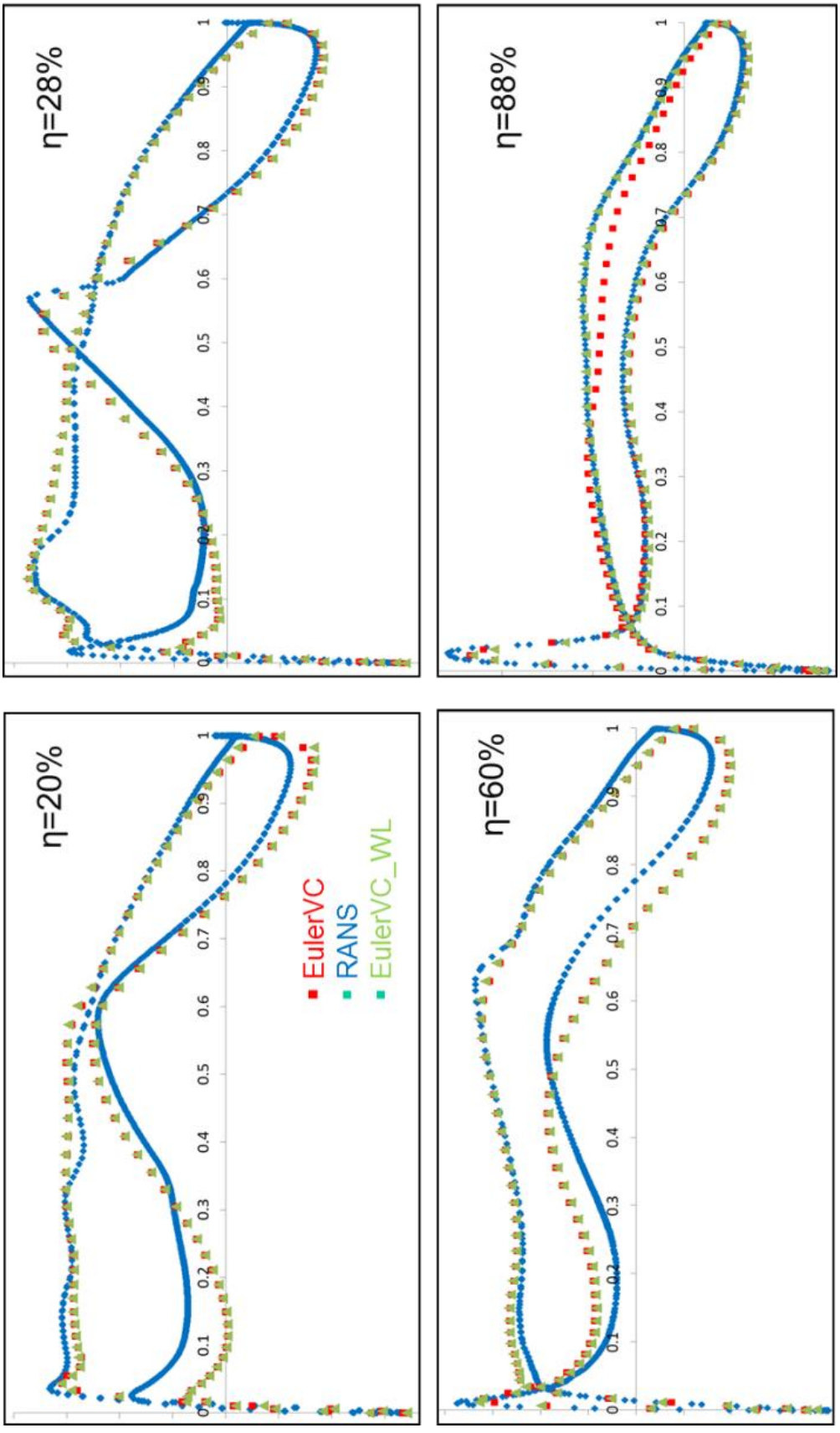

Figure 6.16: Cp distribution at alpha=0

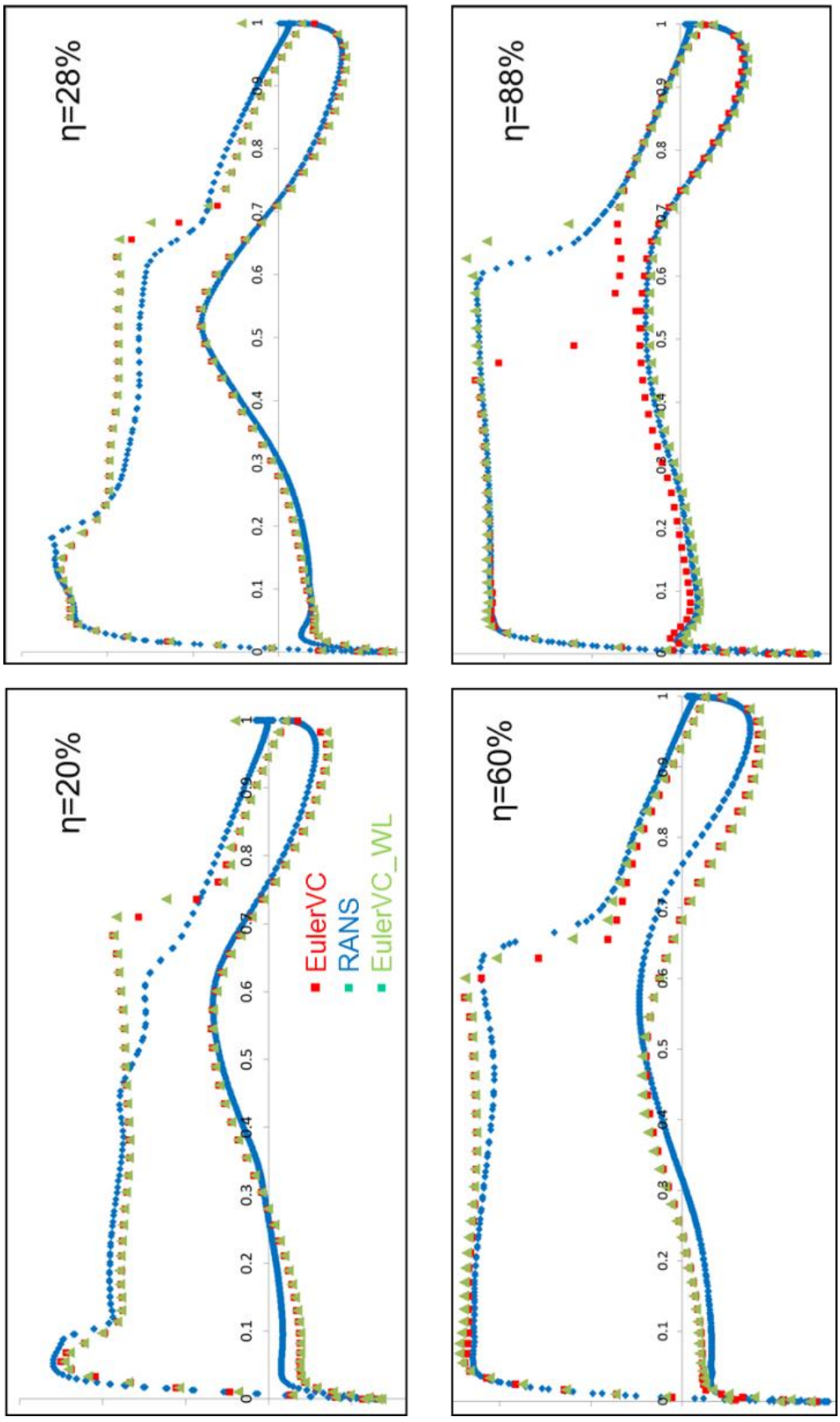

Figure 6.17: Cp distribution at alpha=3

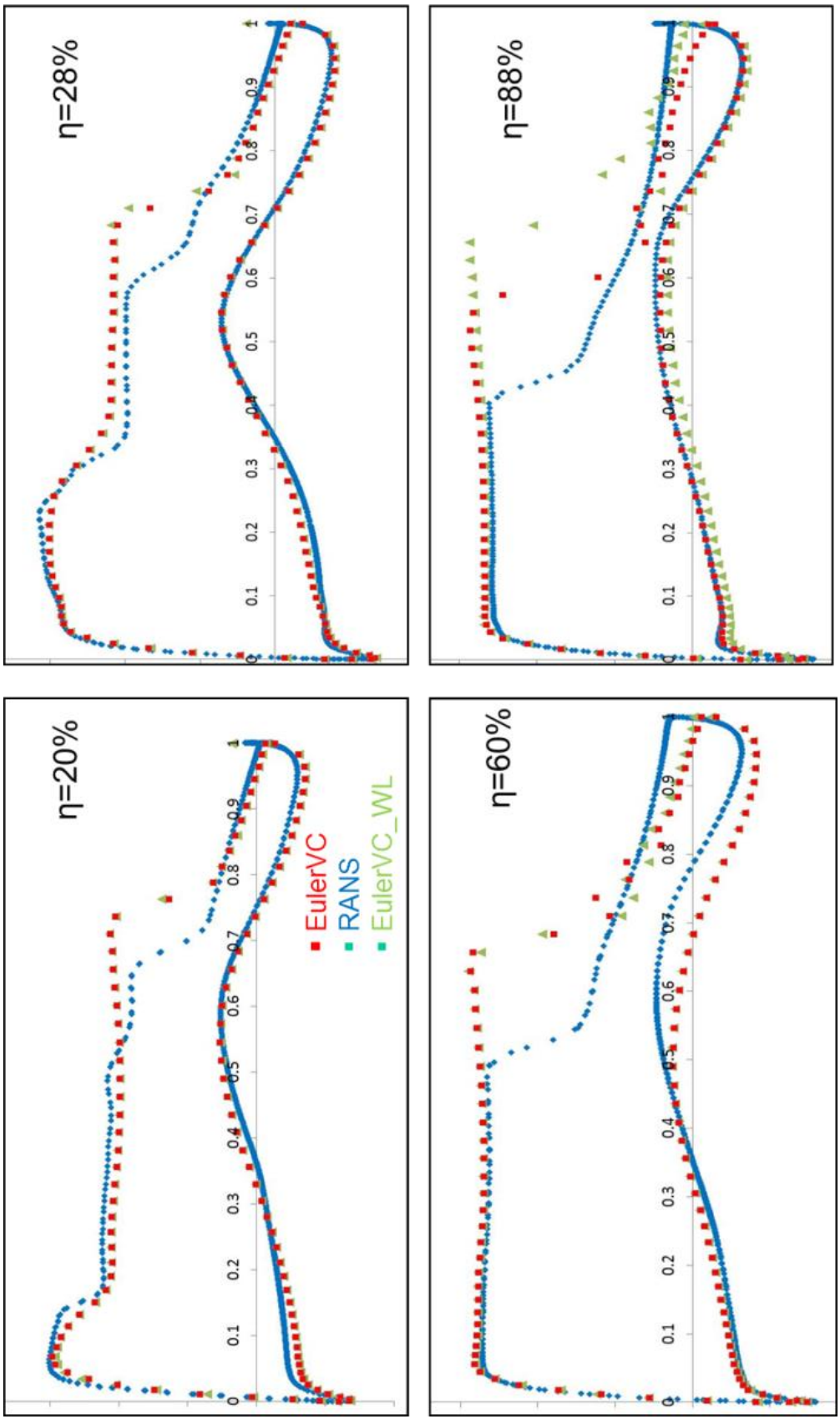

Figure 6.18: Cp distribution at alpha=5

The blue diamond symbols represent the RANS data, the red circle symbols represent the Euler Coupled solver results for a clean wing configuration model without winglet and the green triangle symbols represent the Euler Coupled results for a clean wing configuration including the winglet. Looking at all the plots in the above figures is clear that the winglet has not affected the inboard sections but its effect is quite visible at the outboard section. For alpha equals zero and three (Figure 6.16 and Figure 6.17) the results computed, for the winglet case, within the aero process are in good agreement with the RANS data, also bearing in mind that, as previously stated, the RANS simulation includes engine and flap track fairings that of course perturb the flow field, compared to the clean wing case. At the highest angle of attack (Figure 6.18) the results are not in agreement with the RANS data. This is due to the limitation of the flow solver that does not predict correctly the flow separation that occurs at high angles of attack, hence the solution fails to predict the lift loss due to the separation leading in general to an over-estimation of the loads. For cruise condition, small values of angle of attack, the Euler coupled solver predicts quite well the flow physics and this at much lower computational cost compared to RANS simulations.

6.2.2 Results

The developed aero process runs automatically from start to end, calculating 35 points (7 angles of attack for each of 5 different Mach numbers) in about three hours using 35 different CPUs. Figure 6.19 shows lift coefficient and pitching moment coefficient and their respective slope distribution along the span for some of the simulations performed.

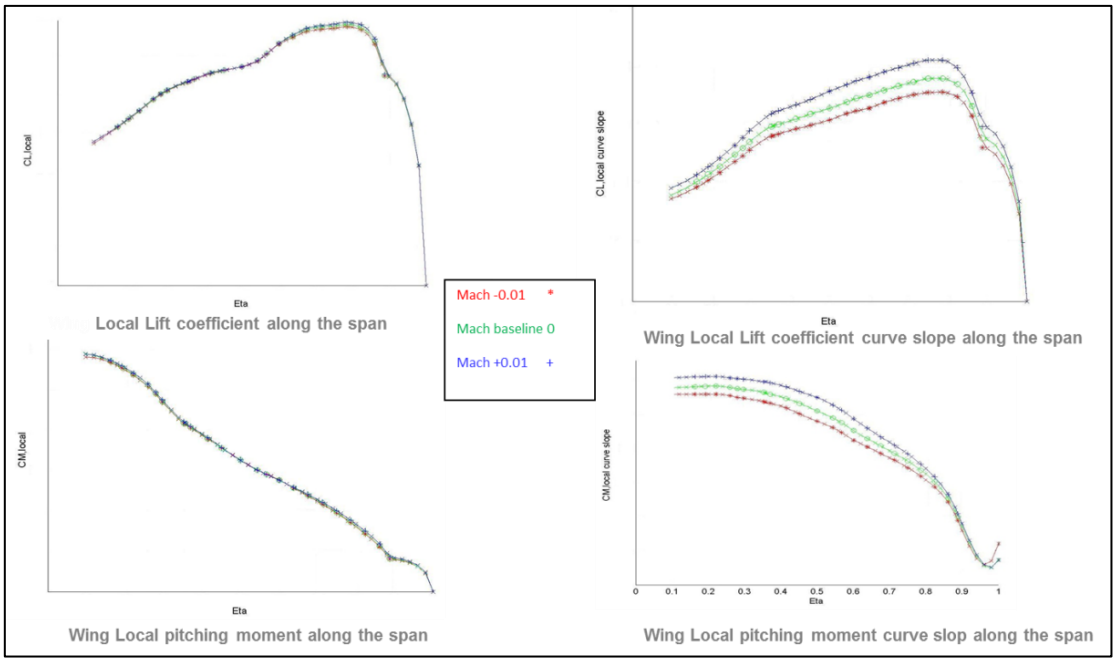

Figure 6.19: Coefficient along the span passed to the load domain for three different Mach numbers

6.2.3 Conclusion and future work

The Aero solution chain has been implemented as a high-speed aerodynamic evaluation capability. However there is not yet an automated complementary Aerodynamic design process. It is possible only to perform this manually at present, and the module to generate the Aero Data for performance has not yet been implemented in the workflow. Hence, further developments are necessary to cover these two aspects, as highlighted in Figure 6.20.

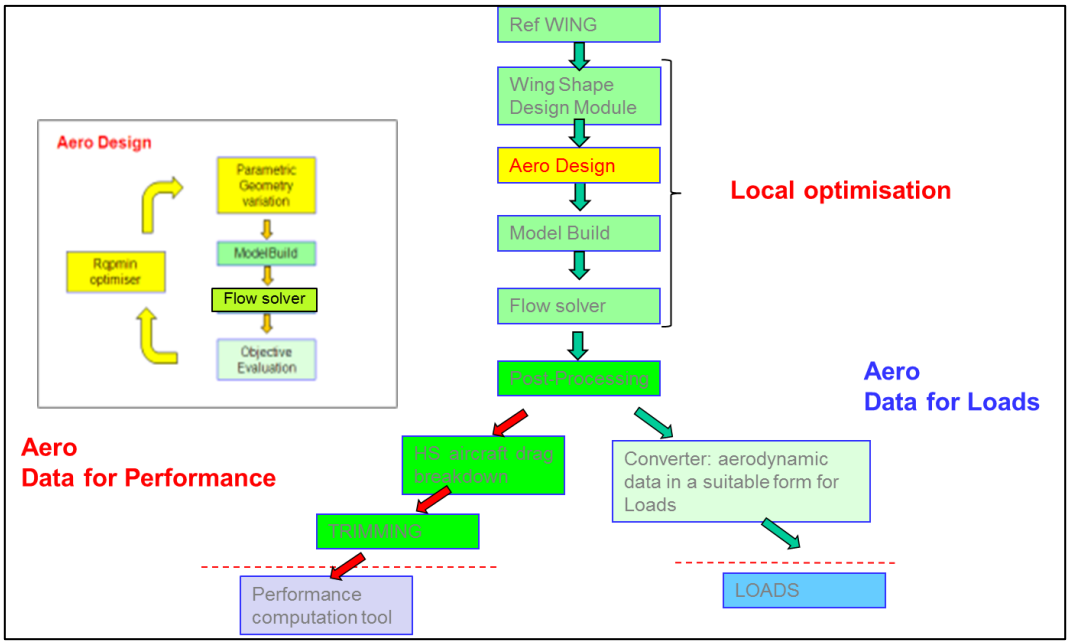

Figure 6.20: Further advances needed on the automatic aero process workflow

Some further modifications will also have to be made to the “ModelBuild” software to allow it to handle winglets. In conclusion, the automatic and integrated aero process developed thus far enables generation of aero data for loads for the cruise phase, in a time frame that is compatible with the requirements of an overall multi-disciplinary preliminary design process at this level. The scheme has already been tested for different aircraft configurations, from single aisle to long-range aircraft, and has been demonstrated to be seamless and robust. Once the further developments discussed are added into the current aero process, it will be ready to be integrated into the overall preliminary multi-disciplinary design process. Such a preliminary multi-disciplinary design approach, should lead to a faster, more efficient design process resulting in both a step change increase in aircraft performance and a considerable reduction in time to market.

7 Geometry parameterisation and application to aircraft configuration

7.1 Introduction

The main aim of an optimisation process is to find an optimal geometry that fulfils the minimisation of the objective functions. Therefore, the first task to be performed is to define some variables, called design variables in the optimisation process, allowing the parameterisation of the wing shape in such a way, which provides enough versatility to generate any kind of wing shape. The selection of the design variables and the freedom to generate new profiles depends upon the parameterisation technique. Hence, the first task to be executed is the parameterization of the geometry. A second task is to define the design space where the optimisation is allowed to set the design variables values, i.e. if the design space is too narrow, the new shape generated may not be good enough to provide any advantage upon the datum profile. Conversely, if the design space is too wide, the geometries generated could be unfeasible and problems will arise regarding other steps of the optimisation process, for instance in the CFD meshing, pre-processor and solver steps. In general, this step is one of the key bottlenecks of the production of an integrated automated optimisation process due to the difficulties of building a tool robust and flexible enough to provide a wide variety of new geometries, allowing for minimal changes, with the minimum amount of design variables.

In addition, since the geometry is continuously changing during the optimisation process, the parameterisation tool must be robust and flexible enough in order to allow the mesh creation around the shape in all the different configurations analysed.

The number of these design variables should be kept as low as possible in order to perform the actual optimisation process. This is necessary due to the fact that the computation time of the whole optimisation is directly proportional to the number of variables used to model the geometry [82]. Due to its fundamental role in the optimisation process, the choice of a parameterisation method will have an enormous impact on the implementation of the whole

design process. The main goal of these methods is to reduce the number of design parameters as few as possible whilst controlling the important aerodynamic features effectively. For this reason an overview of the different alternatives is presented in the next section.

7.2 Literature Overview

The first distinction that can be made dealing with parameterisation techniques is in the way the mesh for the new geometry will be subsequently generated. Two different approaches are available:

- Mesh parameterisation
- Geometry parameterisation

In the first approach the mesh is generated around the initial geometry in a parametric way such that it can be deformed afterwards when the new geometry is obtained from the optimizer. The main advantage of this approach is that alleviates the need for an automatic grid generator, but there are two main drawbacks; a) only small geometry changes are possible, b) this alternative is not feasible to be implemented with the unstructured mesh. Nevertheless, the grid generation approach is much more flexible and allows a wider design space to be analysed from the Optimiser, but it requires the grid to be automatically generated during the optimization process. Hence depending on the optimization process to be performed, the best approach can be chosen.
The geometry parameterisation is much more flexible, and allows for a wider design space, however, it requires the automation of the fluid and structure grid during the process. Thus signifying a higher computational time per step, as the grid generators are the second most time consuming task in an optimisation process, after the solvers one. Hence, the best approach is selected, depending on the nature of the problem to be analysed.
The most common parameterisation methods have been reviewed in this chapter. As stated at the beginning of this chapter, parameterisation is fundamental to optimisation since it has a profound effect on design space. It inherently determines if the optimal solution is discovered in the design space

and affects the optimisation efficiency. The ideal parameterisation method should provide high flexibility on design space; provide a compact number of design variables; and provide a smooth and realistic shape and intuitive physical meaningful design variables.

7.2.1 Parameterisation methods

Basis Vector Approach: proposed by Pickett et al. [83], it defines the shape changes by Equation. (7.1), where $\overline{R}$ is the new design shape, $\overline{r}$ is the datum shape, $\overline{v}_n$ is the design variable vector and $\overline{U}_n$ is the design perturbation vector based on several proposed shapes.

$$\overline{\mathrm{R}} = \overline{\mathrm{r}} + \sum_{\mathrm{n}} \overline{\mathrm{v}}_{\mathrm{n}} \overline{\mathrm{U}}_{\mathrm{n}} \tag{7.1}$$

This technique provides a compact set of design variables when the shape changes are parameterised. Grid generation is not necessary since the grids can be regenerated automatically. The problem with this approach is the generation of a set of basic vectors for multiple-disciplines. Therefore, this method is only a feasible alternative for single discipline optimisations, where there are simple geometrical changes.

Domain Element Approach: this technique is based on linking a set of grid points to an element of the domain, *macro-element*, which is responsible for controlling the shape of the model. Figure 7.1 shows an application example of the method, where a domain element with four nodes is deformed from the baseline. As can be seen the grid points move together with the nodes of the domain. The movement is based on an inverse mapping between the grid points and the domain element. The Domain Element is already available in some commercial software due to its high efficiency and ease of implementation. As in the previous method, also in this case the grid generation is avoided, but this alternative is only useful for cases with simple geometry changes.

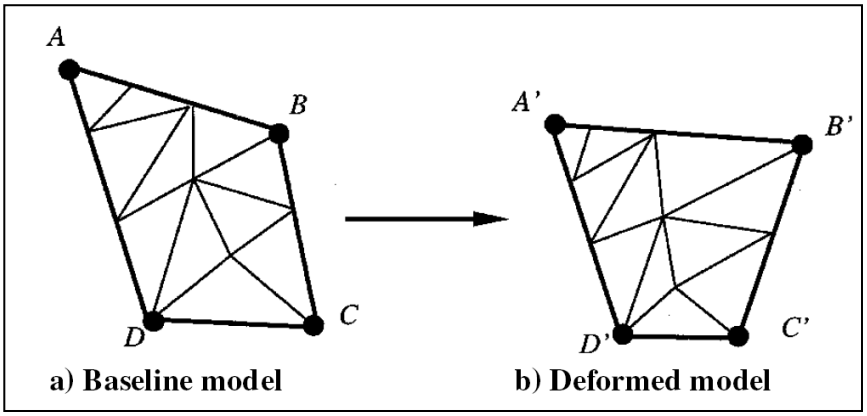

Figure 7.1: Domain element [84]

Partial Differential Equation Approach: Bloor and Wilson (Bloor and Wilson, 1995, cited in [84], p.879) introduced this efficient and compact parameterisation method for the surface generation of an aircraft. The surface of interest is generated as a solution to an elliptic partial differential equation (PDE), so transforming the parameterisation procedure to a boundary-value problem. A small number of parameters are needed to represent even complex three-dimensional geometries due to the fact that surfaces are defined by data distributed around their edges rather than across their entire surface area. This feature makes the tool quite attractive for numerical optimization problems where the computational demand is really high. There are two main drawbacks for this method; firstly it requires a large computation time to achieve the parameterisation of a complex geometry. Secondly, it is not suitable for Multi-disciplinary Shape Optimisation (MSO) since only external geometries can be parameterised, so internal structural elements needed for the structural analysis such as spars or ribs cannot be modelled. Hence, the only feasible option is for single discipline problems with relatively small geometry changes to be performed.

Discrete Approach: it is a really easy method to implement since it uses the grid-point coordinates as design variables (see Figure 7.2). The main drawback is the difficulty in maintaining a smooth geometry moving individual grid points, so that the optimal solution found could be unrealistic. Moreover, for complex geometry models with a large number of grid points, also the design vector

becomes very large leading to difficulties in solving the optimization problem. The flexibility of the method is only constrained by the number of points that define the profile. In addition, this is not a feasible alternative for MSO, as the grid requirements are different for each discipline. Conversely, strong local control and use of an existing grid for the optimisation are some of the advantages of the method.

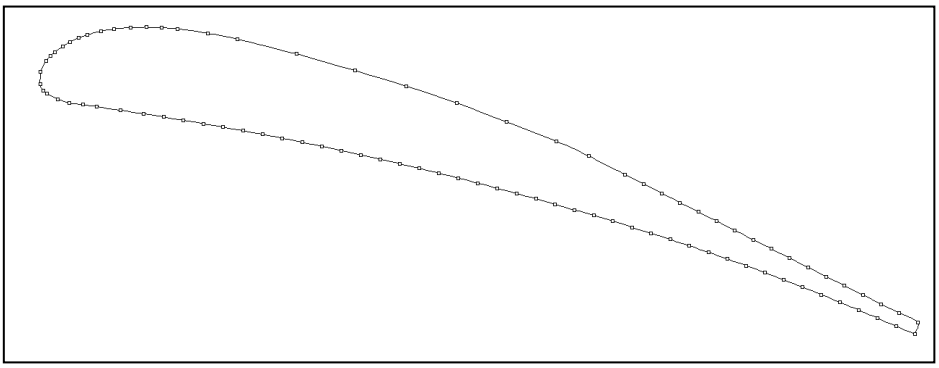

Figure 7.2: Airfoil designed by a set of points [85]

Polynomial and Spline Approaches: they are good alternatives to reduce the number of control points and design variables. It is possible to describe a curve with a few number of design variables using polynomial, (Figure 7.3).

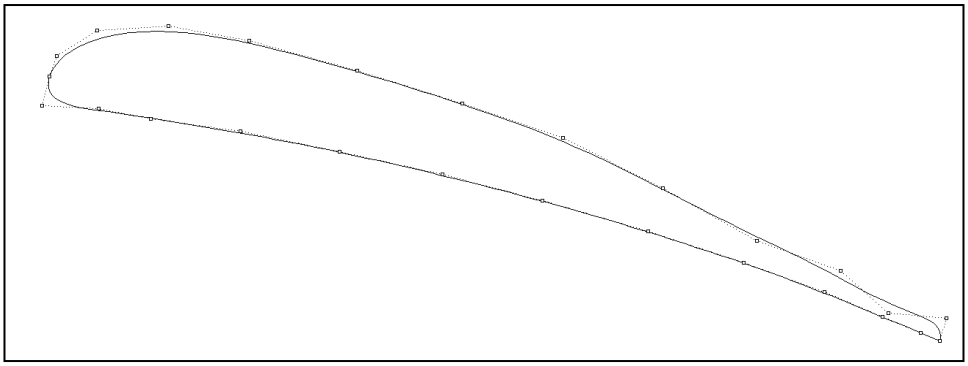

Figure 7.3: Airfoil designed by a set of control points [85]

Mathematically a polynomial can be expressed by Equation (7.2), where $\overline{c}_i$ is a coefficient vector corresponding with the three dimensional coordinates (can be used as design variables), and *u* is the parameter coordinates along the curve. The polynomial form is a compact and powerful method for shape optimisation of simple curves [86].

$$\overline{R}(u) = \sum_{i}^{n-1} \overline{c}_i \, u^i \tag{7.2}$$

One of the first polynomial methods applied for the description of curves and surfaces is the Bezier representation, (see Figure 7.4); it is another mathematical form for describing curves and surfaces, developed by the homonym engineer at Renault Automobile.

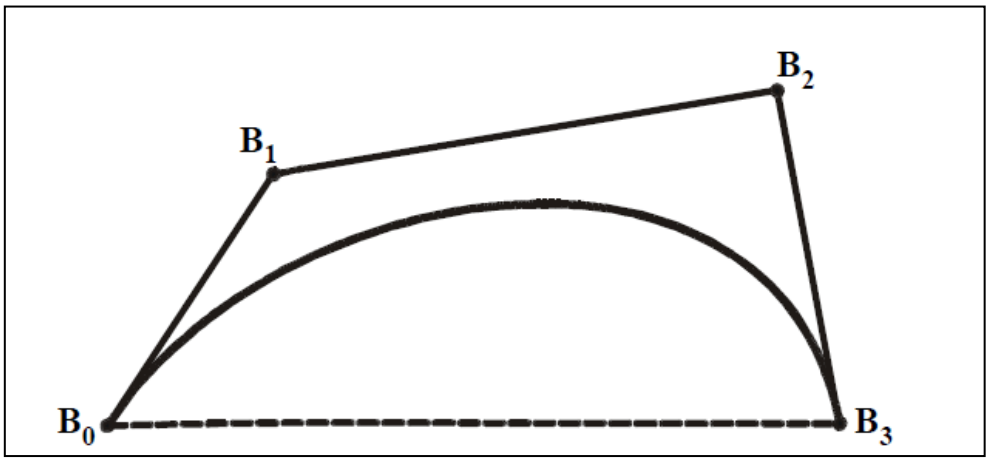

Figure 7.4: A Bezier curve and its control polygonal [87]

Mathematically a Bezier curve can be expressed by

$$\overline{R}(u) = \sum_{i}^{n} \overline{P}_i \, B_{i,p}(u) \tag{7.3}$$

where $B_{i,p}(u)$ are Bernstein polynomials of degree p, n is the number of control points and the coefficients $\overline{P}_i$ are the control points which are usually used as design variables. Several advantages arise from the use of Bezier based polynomial over the power basic one. These include a far better representation due to the fact that control points are more closely related to the curve position and a minimization of the round-off error, due to the way in which Bezier polynomial are built, using “de Casteljau” algorithm. One of the main properties of the Bezier curve is that it is contained within the convex hull of the control polygon (the largest convex polygon defined by the control polygon vertex). This is a very useful property, especially in defining the geometric constraints of the

shape in the context of an optimization process. However, since the order of the curve is one less than the number of control points specified, this representation method has some flexibility limit. Moreover, the Bezier curve has a global nature that is a change in one control points is felt throughout the entire curve. This property eliminates the ability to reproduce local change within a curve. In order to overcome all the limitations of the Bezier representation, a new mathematical description of the curves has been introduced. The so defined B-Spline curve is a composition of low-order Bezier segments that cover the entire curve and it is described mathematically by:

$$\overline{R}(u) = \sum_{i}^{n} \overline{P}_i \, N_{i,p}(u) \tag{7.4}$$

The so defined where $N_{i,p}$ is the *i*th B-Spline basis function of degree p, while the other parameters have been already defined. The only drawback for B-spline is its inability to represent conic sections accurately. The alternative is to use the Non Uniform Rational B-Spline (NURBS), which represent most parametric and implicit curves and surfaces without loss of accuracy [88]. It is the generalization of the previous analytical representation, overcoming all the drawbacks emphasized for the previous methods.

It can exactly represent conic sections and moreover it has additional degrees of freedom compared to the B-Spline due to its definition NURBS are not the cure for everything, as it is not possible to represent some implicit surfaces (e.g. helicoidal and helix), nevertheless, they are not common in aerospace applications, Equation (7.5) shows the NURBS definition:

$$\overline{R}(u) = \frac{\sum_{i=1}^{n} \overline{P}_i N_{i,p}(u) W_i}{\sum_{i=1}^{n} N_{i,p}(u) W_i} \tag{7.5}$$

where W_i are the weights of the control points and, once again, the other terms have the same definition as above. B-Spline is just a special case of NURBS where all the weights are equal. Due to their flexibility and fidelity in representing curves (and surfaces) NURBS are the standard for describing and modelling shapes in computer aided design and computer graphics.

CAD-Based Approach: using the CAD software as the unique tool for geometry creation and modification can potentially save development time, in fact, Feature-Based Solid Modelling (FBSM) CAD systems have made design and modification much easier and faster due to Boolean operations like intersection or union. Even though it is an attractive option for multidisciplinary optimisation, it is still not possible to use it extensively as there are unsolved problems, such as how to calculate sensitivity derivatives or how to choose the design parameters. Furthermore, a lack of confidence in the accuracy of the Boolean operations such as small gaps, free edges, transition cracks, etc. (unseen imperfections) are not a problem for CAD visualization; they could give problems in next steps of meshing (see Figure 7.5). These tools have made design modification much easier and faster but have not yet been proven to be reliable for shape parameterisation inside an optimization process.

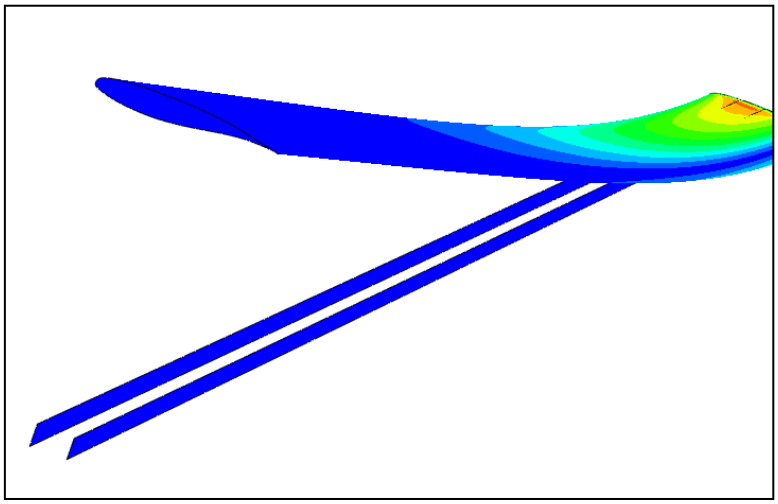

Figure 7.5: example of FBSM CAD based parameterisation problem [89]

Analytical Approach: the formulation of this technique made by Hicks and Henne [90] was based on adding analytical functions defined shape functions to the baseline shape. The analytical functions used are smooth functions based on a set of previous shape designs. The value of the shape functions is evaluated for each design variable to which it is associated. In this way the contribution of each parameter is determined. This method is effective for shape parameterisation but it is difficult to generalise to 3D geometries.

Free-Form Deformation (FFD) Approach: introduced by Sederberg and Parry [91] this technique is known to be powerful for deforming an object regardless of its representation. The FFD algorithm is a subset of the soft object animation algorithms widely used in computer graphics for morphing images and deforming models [92]. This technique enables the deformation of objects by modifying the space around them; space that is controlled by a set of lattice points in a grid, (see Figure 7.6).

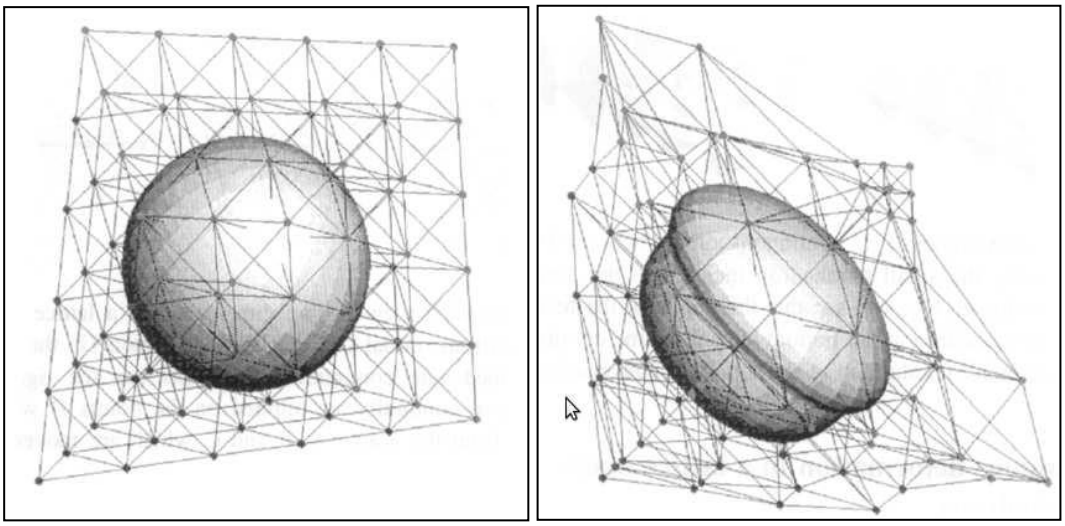

(a) Undeformed Object **(b) Deformed Object using FFD**

Figure 7.6: FFD example [93]

Parametric functions, mainly three-dimensional splines, are used to define the deformations, generating a volume of control points exacerbating the difficulties of establishing how a move should be carried out. The difficulty in controlling shape precisely is mainly due to the control points being extraneous to the object; the deformed object does not follow the control points exactly. Although the movement of the control points gives an indication of the resulting deformation, some shapes are not intuitive to form. For instance, to create a bulge with a flat top it is possible to think to align the control points to a plane, as shown in Figure 7.7. However, it is actually necessary to position the control points as shown in Figure 7.8 to create a flat top.

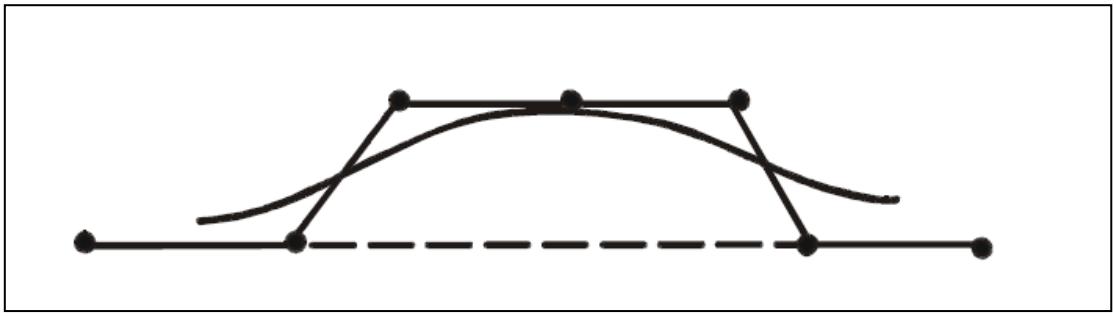

Figure 7.7: The result of a flat line of control points [87]

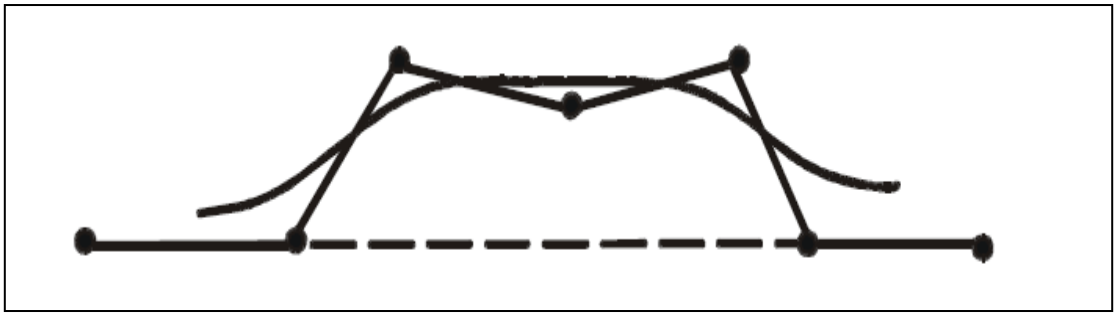

Figure 7.8: The control points configuration to create a flat top [87]

Considering all these points, there are the following problems in manipulating deformations via control points:

- Exact shape is difficult to achieve
- Exact placement of the object points is difficult to achieve
- Users unfamiliar with splines do not understand easily the purpose of the control points and the results of their movement
- The control points are difficult to manipulate when occluded by the object being deformed.

If on the one hand these results in difficulties in controlling the shape of an object under complex deformations; on the other hand it allows the method to work with surfaces of any formulation or degree.

Advantageously, this technique enables the deformation of complex geometries utilizing multiples blocks to model the object. In addition, local deformation is enabled with derivative continuity of any degree; parametric curves and surface remain parametric under FFD. Using Free Form Deformation for the wing parameterisation may be not a good idea because parameters have no real

physical meaning and the generated geometries are not easy to control and as consequence is difficult to introduce constraints.

The PARSEC parameterisation method: targeted at representing subsonic and transonic airfoils was originally developed by Sobieczky [94] and later used in numerous applications. Its key idea is expressing the airfoil shape as an unknown linear combination of suitable base function, and selecting 11 important geometric characteristics of the airfoil as the control variables, in such a way that the airfoil shape can be determined from these control variables by solving a linear system. In his work, explicit mathematical functions were introduced to represent a two-dimensional aerofoil. Intuitive parameters were used in this method. The purpose of the method is to find a minimum number of variables to address the special aerodynamic, geometric and flow features. Sobieczky postulated that the airfoil curvature distribution is strongly linked to the desirable pressure distribution. Therefore, some parameters of curvature were employed to represent an airfoil. In this method, two sixth order polynomials were used to control the upper and lower surfaces of the airfoil, respectively:

$$Z_{up} = \sum_{n-1}^{6} a_n X^{n-\frac{1}{2}} \tag{7.6}$$

$$Z_{low} = \sum_{n-1}^{6} b_n X^{n-\frac{1}{2}} \tag{7.7}$$

Eleven intuitive parameters were employed to explicitly represent an aerofoil, as illustrated in Figure 7.9

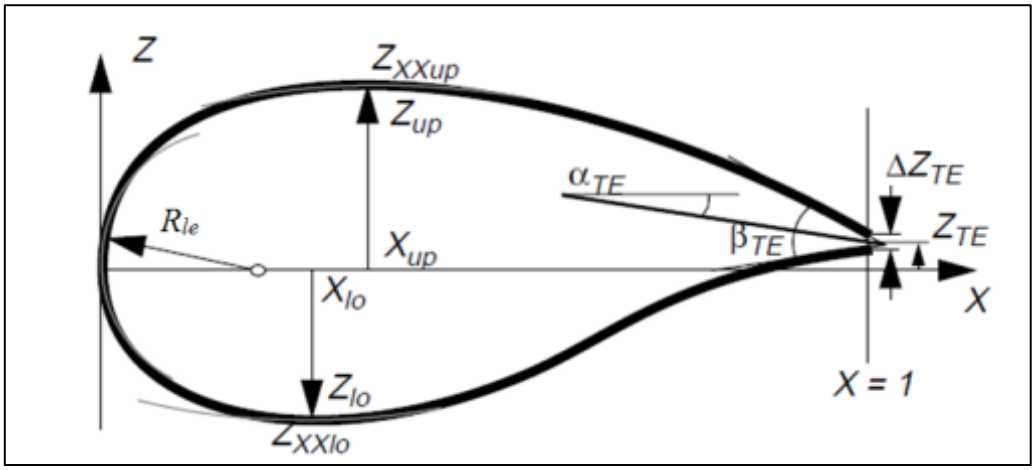

Figure 7.9: Control variables for PARSEC [94]

The parameters are: the leading edge radius (Rle), upper crest position (Xup, Zup), upper crest curvature (Z_{xxup}), lower crest position (X_{lo}, Z_{lo}), lower crest curvature (Z_{xxlo}), trailing edge position (Z_{te}), trailing thickness (ΔZ_{te}) and trailing edge angle and trailing edge wedge angle (α_{te} and β_{te}).

Where Z_{up} is the required z coordinate for the upper surface, Z_{lo} is the required z coordinate for the lower surface and a_n, b_n are the coefficients to be solved from the control variables.

The advantages of the PARSEC method are obviously its intuitiveness and the small number of the design parameters. In the PARSEC parameterisation no baseline shape is needed, a wide range of airfoil shapes can be generated; typical geometric constraints on the airfoil shape (e.g., thickness) can be expressed or approximated by simple bound or linear constraints. Moreover, the impact of individual PARSEC design parameters on the aerodynamic properties of the airfoil can be predicted more easily. Nevertheless, some other key geometrical features between the leading edge and the crest, and the crest and the trailing edge, are uncontrolled, which can impact on the airfoil's performance. For example, for natural laminar flow airfoils, the crest position is related to the transition point, and the slope and curvature between the leading edge and crest are important for keeping the flow accelerating and giving a favourable pressure gradient [95]. For the supercritical airfoil, the shock strength and position are very sensitive to the upper surface curvature in order to maintain a near constant pressure over a large part of the surface to be

terminated by a weak shock or compression wave. The slope and curvature on the upper surface between crest and trailing are significant for the pressure recovery to avoid a large adverse pressure gradient and flow separation [96].

Class/shape function transformation (CST) methods: this new approach proposed by Kulfan [97, 98, 99, 100, 101, 102], is increasingly used in airfoil/aircraft optimisation. The purpose of this method is to develop a universal parameterisation method for complex aircraft configurations, which is not limited just to airfoils. The CST method is initially derived from a mathematical representation of an airfoil with round leading edge and aft-end. For this type of airfoil, the difficulties in representing it mathematically are due to the infinite slope and second derivative requirement at the leading edge and large variations of curvature over the shape. The CST method was intended to overcome these limits and represent the different type of geometries in a generic way. It starts at a general mathematical expression for a two-dimensional airfoil as:

$$\frac{z}{c} = \sqrt{\frac{x}{c}} \cdot \left(1 - \frac{x}{c}\right) \cdot \sum_{i=0}^{N} \left[A_i \cdot \left(\frac{x}{c}\right)^i\right] + \frac{x}{c}\frac{\Delta_{zte}}{c} \tag{7.8}$$

where $\sqrt{\frac{x}{c}}$ describes the round nose, $(1-x/c)$describes the sharp trailing edge, $\Delta zte/c$ represents the trailing edge thickness and $\sum_{i=0}^{N}\left[A_i \cdot \left(\frac{x}{c}\right)^i\right]$ is a general function to describe the detailed shape. $\sqrt{\frac{x}{c}}$, $(1-x/c)$ and $\Delta zte/c$ terms are associated with the basic characteristics of airfoils.

Therefore, this representation form can be rewritten as:

$$\xi(\psi) = C_{N_1}^{N_2}(\psi) \cdot S(\psi) + \psi \cdot \Delta\xi_{te} \tag{7.9}$$

where:

$$C_{N_1}^{N_2}(\psi) = \psi^{N_1} \cdot (1-\psi)^{N_2} \tag{7.10}$$

$$S(\psi) = \sum_{i=0}^{N} \left[A_i \cdot \left(\frac{x}{c}\right)^i \right] \tag{7.11}$$

$C_{N_1}^{N_2}(\psi)$ is the class function, N_1 and N_2 are called class parameters, S(ψ) the shape function and $\Delta\xi_{te}$ the trailing edge thickness ratio. For the general airfoil with a round nose and an aft-end trailing edge, the class parameters N_1 and N_2 are set to 0.5 and 1.0, respectively. In Kulfan's paper, the class function has been demonstrated to have a powerful capability in representing a large number of geometrical types.

Any kind of algebraic polynomial can be employed as the shape function. In the CST methods, the Bernstein polynomial is preferred for use as the shape function, since Bernstein polynomials have the mathematical property of 'partition of unity' and are more numerical stable than power form polynomials.

The aerofoil shape can be represented using the Bernstein polynomial with different weight coefficients. These weight coefficients are then employed as design variables in optimisation. The total number of design variables depends on the order of the Bernstein polynomial, i.e. *n+1.* Eventually, the completed mathematical equation of the CST aerofoil could be written as:

$$\xi(\psi) = \psi^{0.5} \cdot (1-\psi)^1 \cdot \sum_{i=0}^{N} \left[A_i \cdot \binom{n}{i} \cdot \psi^i \cdot (1-\psi)^{i-1} \right] + \psi \cdot \Delta\xi_{te} \tag{7.12}$$

The first weight coefficient of the Bernstein polynomial A_0 corresponds to the leading edge radius:

$$S(0) = A(0) = \sqrt{\frac{2R_{le}}{c}} \tag{7.13}$$

The last weight coefficient of the Bernstein polynomial corresponds to the trailing edge angle and trailing edge vertical position:

$$S(1) = A_n = -\tan\theta + \frac{\Delta_{zte}}{c} \tag{7.14}$$

The details of the derivation of this relation can be found in Kulfan [97] Therefore, the CST method for aerofoils includes two intuitive parameters; the other coefficients in the CST method are non-intuitive. Some properties of the CST method for representing aerofoils have been summarised in Kulfan's paper [97] as follows:

a) Any aerofoil can be represented;

b) This aerofoil representation technique provides a large design space of smooth aerofoils;

c) Every aerofoil in the entire design space can be derived from the unit shape function aerofoil.

8 Optimisation

8.1 Introduction

Modern design techniques seek for the best design to perform the desired tasks. Engineering Optimisation deals with the optimal design of elements and systems in all engineering fields. In an optimisation problem values of the variables that lead to an optimal value of the function that is to be optimised are sought. In order to improve something there must be aspects that can be changed. In design optimisation these are called design variables, and collectively they are grouped in a design vector. Hence, design optimisation is the determination of a set of values for the design variables that minimizes (or maximises) the objective functions and satisfies requirements. The performance characteristics such as cost, weight, speed, power can be called dependent design variables because the designer cannot directly adjust these quantities. The basic stages of an optimisation process are described in Figure 8.1. In this example three different disciplines are considered.

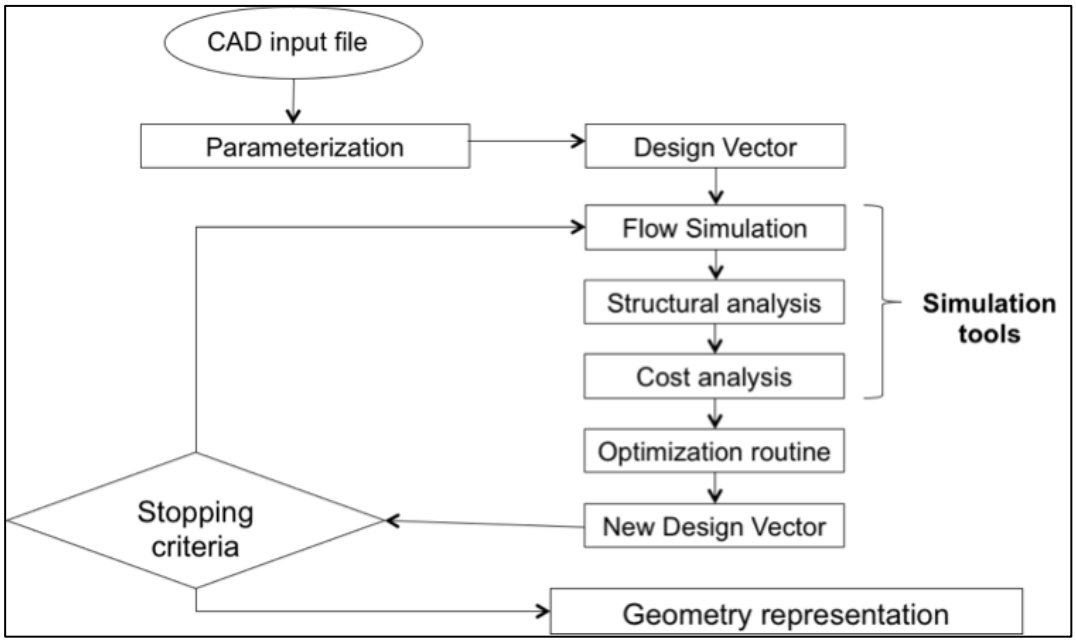

Figure 8.1: Optimization Process – General schematic

The cycle consists of three main steps. The first step of the process is the parameterisation and representation of the geometry, the step in which the

design variables are defined and stored in a correspondent design vector. The number of variables chosen to describe the geometry is kept as low as possible to reduce computational cost, but at the same time the original geometry must be well represented and the smoothness of the shape must be conserved. Once this step has been completed the main optimisation loop takes place. At this point the file containing the initial solution will be the input to the numerical simulation tools. The CFD module constituted by the mesh generator and in cascade the flow solver. A mesh is created around the geometry to allow a CFD simulation of the flow field, after which the metrics are extracted. In this part of the process the aerodynamic objective function(s) will be calculated. Then the initial solution will be the input to structural analysis module. In this module the structural analysis is developed and the definition of the main structural element is performed. The choice of finite element type used and the grid refinement will be assessed. The structural objective function(s) will be evaluated in this step. Again the initial solution will be the input to cost analysis module. In this module the cost analysis is developed and the cost objective function(s) will be calculated. The objective function value and the respective design vector will be passed to the optimiser, which in according to the algorithm implemented will start the search of the optimum solutions. The optimiser is doubtless the “brain” of the system. It is able to control some design variables that define the geometry. The optimiser is the module that performs the search for the improved configuration, basing its decisions on the information collected in previous evaluations of the objective functions. Once the possible optimum design vector, has been found, it will be returned to the geometric modelling system to repeat the process to convergence. When convergence is achieved it will pass for the last time to the parameterisation tool to obtain the final design shape. The last step is to convert the design vectors corresponding to the optimal solutions into a CAD (Computer Aided Design) file in order to visualize the new geometries obtained.

8.2 Multi-Objective Optimisation

Aircraft optimisation often involves the design of a particular shape in order to achieve improvements to a particular performance metric. This type of design process in not new in Aerodynamics and it can be dated back to 1978, when an early research was performed by Hicks and Henne [90]. They assessed the feasibility of applying numerical optimisation for the design of wings. Nowadays, many steps forward have been achieved in the development and utilization of integrated automated optimisation design tool. Both the mathematical formulations and the computational resources are mature enough to perform real-world problem optimisation.

When solving optimisation problems a main distinction can be drawn between the number of objectives to perform:

- *Single-Objective* optimisation
- *Multi-Objective* optimisation

Obviously the first option applies when the aim of the process is to optimize a single objective, obtaining the best possible solution available, defined as the Global Optimum of the problem. However, due to the strong dependence of real-world problems upon different objectives, usually conflicting, the single-objective optimisation has been proved not to be suitable in achieving useful solutions. That is the reason why the multi-objective approach must be considered in performing reliable computational design. Solving a multi-objective problem is much more complicated than finding a solution for a single-objective one. That is the reason why the first approach to the problem has been the introduction in a single-objective method of a composite objective function representing a weighted sum of the objectives. In this way, the problem is relatively easy to solve but has the big disadvantage that the weights must be pre-set, introducing implicitly the user designer pre-conceptions. Moreover, it will be shown later that the solution to a multi-objective problem cannot be a single optimum solution.

8.2.1 Background theory

Mathematically, the optimisation of an engineering problem can be expressed in general terms as:

minimise $f(x); x \in R^n$

$$\text{subject to } c_i = 0; i = 1, 2, \dots, m'$$

$$c_i \geq 0; i = m' + 1, \dots, m$$

where *f*(x) is defined as the objective function, x is the vector containing the design variables and c_i is the set of constraints to which *f*(x) is subjected. Finding a solution to this problem implies the determination of a set of design variables that minimize the value of the objective function satisfying, at the same time, the constraints. In the case of single objective optimisation, a design vector f_1 is considered a "better" solution than f_2 when $f_1 \leq f_2$, thus the solution is unique. For multi-objective optimisation, the size of f is equal to or higher than 2. This problem, instead, is characterized by a family of alternative solutions rather than a single absolute optimum, at this point the concept of *Pareto-optimally* must be introduced. Originally postulated by Ysidro Edgeworth in 1881 [103] and generalized afterwards by Vilfredo Pareto in 1896 [104]. It states that a solution is Pareto optimal if no other feasible solution exists which would simultaneously improve all of the objective functions. The set of all the solutions that satisfy this requirement is defined as Pareto optimal set and consists of all the non-dominated solutions. The concept of inferiority or dominance is explained considering an objective function vector **F**(x) = {f_1(x), ..., f_n(x)}. If no component of the objective function vector F_1 evaluated in x_1 is greater than its correspondent element in F_2 (objective function vector evaluated in x_2) and at least one is smaller, thus x_1 dominates x_2. In the same way if some components of F_1 are bigger than F_2 and some smaller, x_1 is defined as Pareto-equivalent to x_2. In other words, the Pareto-optimal set are the design vectors whose objective functions are Pareto equivalent, i.e. any of design vectors are dominant over the other. The Pareto-optimal set represents the boundary beyond which, no improvements can be achieved without degradation of any of

the other aspects of the overall performance. This mathematical solution does not always coincide with the practical solution. On the contrary a Decision Maker (DM) has to be introduced to choose one final solution among the set of Pareto-optimal ones. Thus, both optimization and decision processes are needed to obtain the solution of a multi-objective problem. Three different DMs can be found in literature:

1. A Posteriori: once the Pareto-optimal set has been created the DM selects the solution from all the possible alternatives. Difficulties in displaying the optimal set arise with high numbers of objective functions;
2. A Priori: a scalar cost resulting from a combination of all the objective functions is generated by the DM. In this way the preferences of the DM are set but also the problem is made single-objective prior to optimisation;
3. Interactive Methods: compromises the advantages of the previous methods since the DM chooses the best solution at some intervals during the process.

Moreover, a high level of confidence is assumed by the DM upon the final solution [105]. An example of Pareto-optimal set is illustrated in Figure 8.2 for a turbo machinery blade multi-objective optimisation process performed by Kipouros et al. [106].

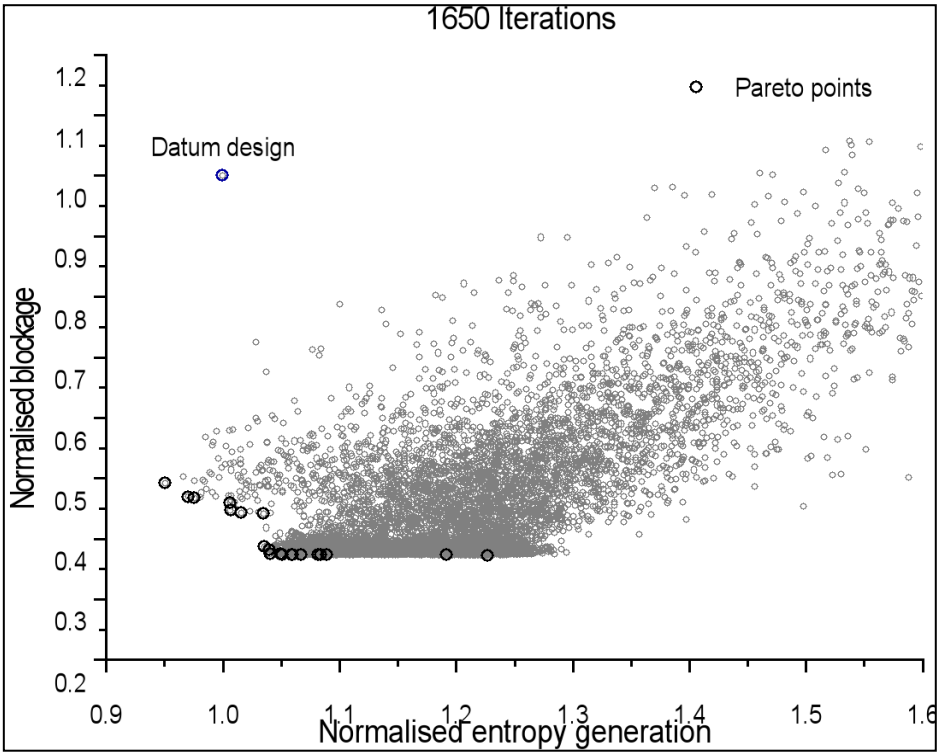

Figure 8.2: Example of optimisation search pattern and Pareto-front [106]

Using the Numerical Optimisation approach in wing design context implies the process has been cast into a well-posed optimisation problem. This means, first of all, that the geometry under investigation has to be parameterised, defining the design variables of the optimisation problem, in order to describe the wing shapes and apply possible constraints. Furthermore, the designer has to define the objective functions to be minimised. The optimiser is the main module of the whole optimisation process and is crucial to the success or failure of producing an improved wing. The performance of the process also relies on the ability of the optimiser to manage these types of problems. Assessing an optimisation, cannot be approached without the use of “computer intelligence”, that is able to manage a large number of design variables and to describe the problem, whilst evaluating the objective functions in order to improve them. In order for this assessment to be feasible, it is necessary to use an algorithm capable of managing the design variables in an efficient manner. Thus, to reduce the resources used in obtaining the solution, it must be able to interpret and acquire guidance from the assessment of the numerical simulation results, previously

collected. In the early years, optimisation was based on experimentation and experience. However, with the advent of numerical simulation, optimisation algorithms are replacing experience in the task to manage the simulation result in an effective manner. Many optimisers have been developed throughout the years with the hope of finding a method able to solve any kind of problem. This is a weakness of the optimiser, as none of them are able to do that task perfectly. The reason for this is that the efficiency of one optimisation algorithm to solve a problem strongly depends on the nature of the problem itself. This is why algorithms are still currently under development. Several methods are appropriate only for certain types of problems. Thus, it is important to be able to recognize the characteristics of the problem in order to identify an appropriate solution technique. Within each class of problem there are different minimization methods, varying in computational requirements, converging properties and so on. Optimisation problems are classified according to the mathematical characteristics of the objective functions, the constraints and the control variables. Probably the most important characteristic is the nature of the objective function. If the relationship between f(x) and the control variable is of a particular form, such as linear, e.g.

$$f(x) = b^T x + c \tag{8.1}$$

where b is a constant-valued vector and c is a constant, or quadratic, e.g.

$$f(x) = x^T A x + b^T x + c \tag{8.2}$$

where A is a constant-valued matrix, special methods exit that are guaranteed to locate the optimal solution very efficiently. These along with other, classification are summarized in the Table 8.1 below:

Table 8.1: Optimisation Problem Classifications [107]

Characteristic	Property	Classification
Number of control variables	one	Univariate
	More than one	Multivariate
Type of control variables	Continuous real number	Continuous
	Integers	Integer or discrete
	Both continuous real number and integers	Mixed Integer
Problem functions	Linear functions of the control variables	Linear
	Quadratic functions of the control variables	Quadratic
	Other non-linear functions of the control variables	Non-linear
Problem formulation	Subject to constraints	Constrained
	Not subject to constraints	Unconstrained

8.3 Optimisation algorithms

Different main strategies in use are Gradient-based algorithms and Stochastic Methods, also known as meta-heuristic methods. The first is a good alternative for smooth problems whose behaviour is well known. In this approach, the success of the optimisation process strongly depends on the initial point, Newton–Raphson method is commonly used for these applications. The second arose as a solution to problems with a higher number of objective functions, whose behaviour are totally unknown and therefore, the optimum solution, is very difficult to find. The existence of numerous relative minimums means that gradient-based methods are not a feasible option, as the optimisation process can easily stuck on local minima giving fake optimum solutions and neglecting from the analysis a big portion of the design space. Moreover, the computational time required by stochastic approach has been found to compare favorably to that of a gradient-based method [108]. There are a wide variety of meta-heuristic methods, each one based on different ideas; therefore, each exhibits a different performance depending on the nature of the problem.

Generally, stochastic optimisation methods are known as Heuristic Methods, which search a good solution, near optimal, at reasonable computation cost without being able to guarantee optimality. Some of the most commonly used are: Genetic Algorithm (GA), Simulated Annealing (SA) and Tabu Search (TS).

8.3.1 Simulated Annealing (SA) algorithm

The Simulated Annealing algorithm, as its name implies, exploits an analogy between the search for a minimum in a general system and the way in which a minimum energy crystalline structure (the annealing process) is generated when a metal cools [109]. The Metropolis algorithm is the base of the Simulated Annealing approach. It simulates the evolution of a solid in a heath bath to thermal equilibrium. The algorithm starts with a given energy value Ei, generates a new status j, applying a perturbation mechanism which transforms the current state into a next state by a small distortion, and compares the two levels of energy. If the energy difference $E_i - E_j \leq 0$ then state j is stored as a new acceptable status. Otherwise the status is accepted with a certain probability, which is given by:

$$exp\left(\frac{E_i - E_j}{K_B T}\right) \tag{8.3}$$

where K_B is the Boltzmann constant and T represents the temperature of the heat bath. More details can be found in [110]. If the lowering of the temperature is done sufficiently slowly, the solid can reach thermal equilibrium at each temperature. In the described analogy, the states of a physical system are equivalent to the solutions of the combinatorial problem. Furthermore, the energy of a state is equivalent to the cost of a solution. The SA algorithm now can be viewed as an iteration of the Metropolis algorithm, evaluated at decreasing value of the control parameter [111].

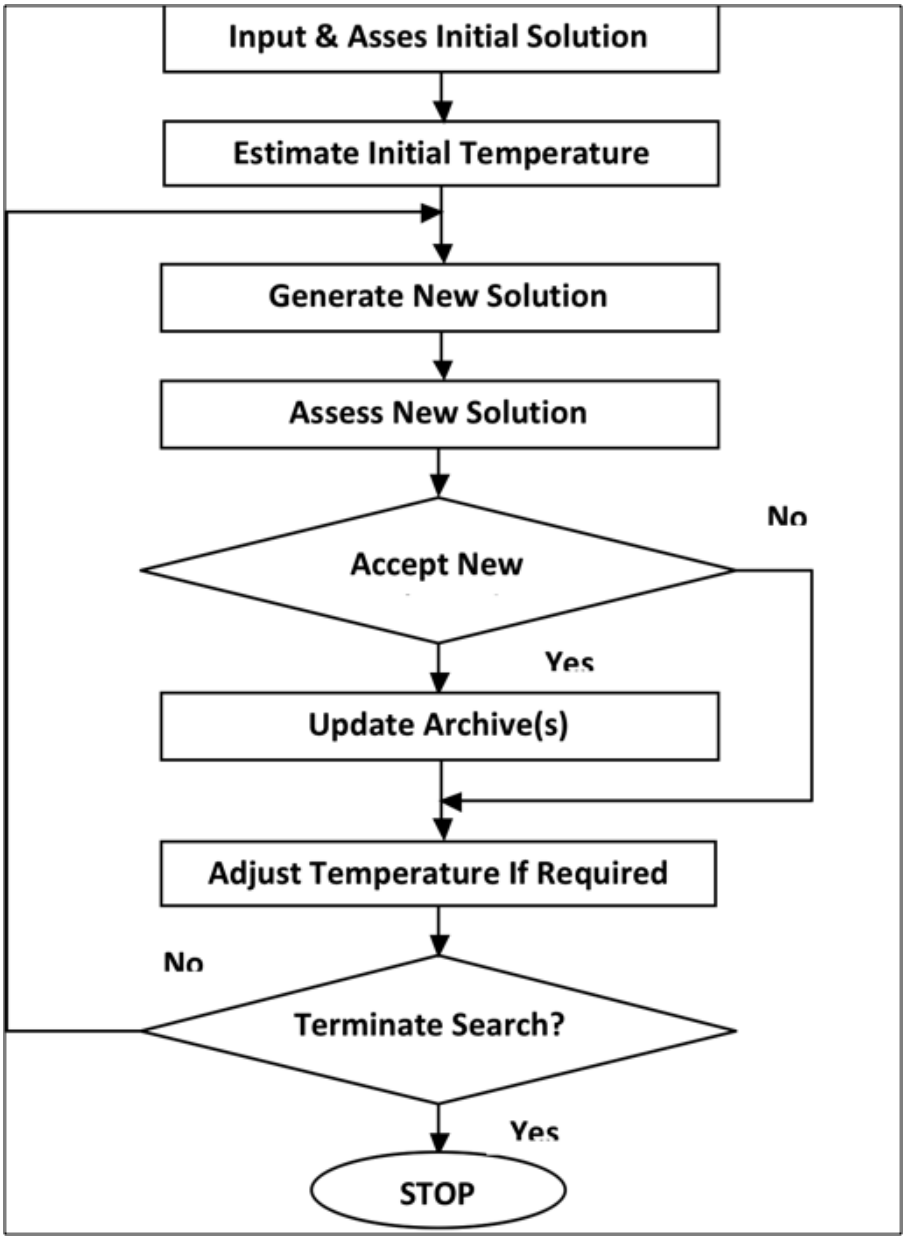

Figure 8.3: The structure of the Simulated Annealing algorithm [109]

In the above flowchart, Figure 8.3, is recognizable the step of archiving. Data management is necessary when a large amount of data is available, and in the real-world optimisation application the data to be stored are considerable. So, the way in which information about the search are recorded is a very important step of the procedure. Obviously, the aim of optimisation is to find the best solution of the problem investigated, which is seldom, the final solution visited in the stochastic search, but a stochastic optimisation method will inevitably explore the search space quite widely and additional information about the

problem being solved may be of value. On the other hand, many thousand, or millions, of solutions will be examined; this means that some discrimination must be applied when storing information to be presented at the end of optimisation. Although, when a large amount of data is available, the data management is necessary, the main advantages of this approach are the ability to avoid getting trapped in a local minima and the straightforward implementation. The general purpose of SA is to get a “good solution” in a reasonable amount of time, rather than the best possible solution in a longer time period.

8.3.2 Genetic Algorithm (GA)

This evolutionary meta-heuristic algorithm was invented by John Henry Holland in 1975, and it was presented in his book Adaptation in Natural and Artificial Systems [112]. Since then, many researchers have been carried out in developing efficient GA methods due to the great capacity of the technique to explore the whole design space. It applies the rules of nature to accomplish the best possible solution: evolution through selection of the fittest individuals, the individuals represent solutions for the problem to be optimised. These types of algorithms are based on the mechanics of natural selection and natural genetics. The starting point is the creation of an initial population by randomly choosing gene values from the given variability ranges. New artificial creatures, defined as strings, are generated in every generation using pieces of the fittest of the old. To add diversity to the genetic characteristic of the population Cross-over and Mutation operations take place. The first contributes to the production of an offspring from two parents, while the latter modifies the genetic material of an individual. Both these processes take place at a certain probability. While randomised, genetic algorithms are not simple random walk. They efficiently exploit historical information to speculate on new search points with improved performance [113]. A flow diagram of the algorithm is shown in Figure 8.4.

To summarise, it starts evaluating a set of random design vectors, then, subsequently tries to improve the initial solution through the application of

repetitive operations called: mutation, crossover, inversion and selection operators.

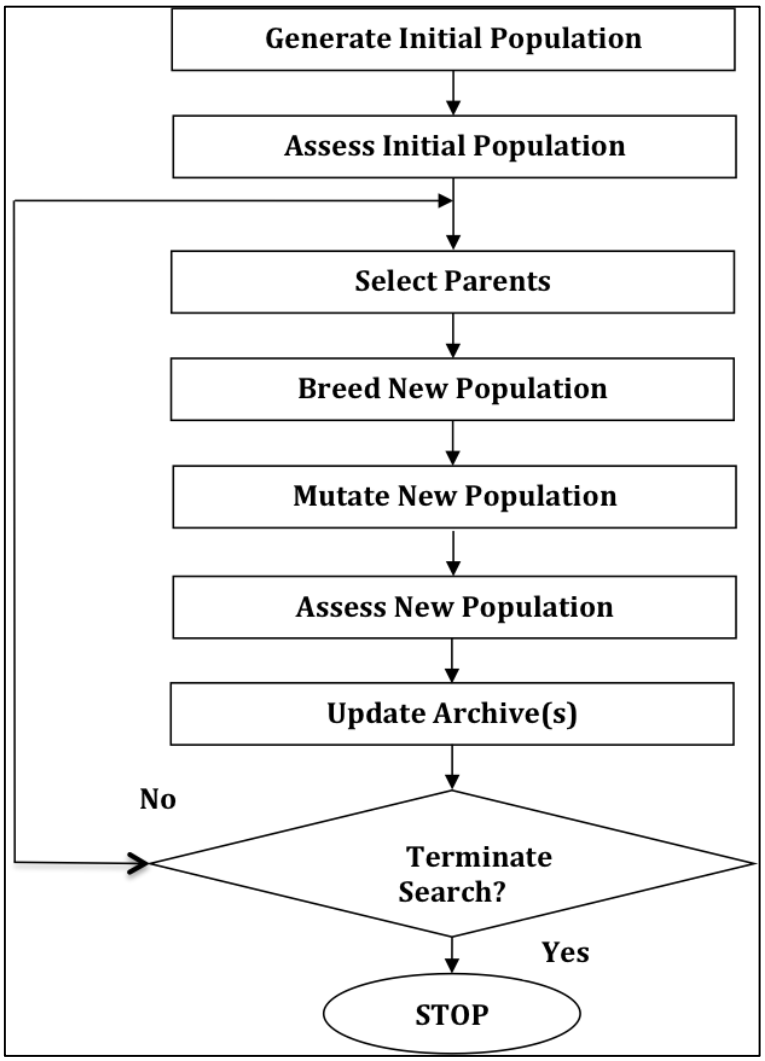

Figure 8.4: The basic structure of the Genetic algorithm [109]

The main advantage of this approach is the effectiveness with which it finds an optimum by scanning a vast design space. The method uses an inductive method, which evolves away from bad circumstances and not towards the best solution. Despite the flexibility of GAs, some drawbacks of the technique are evident. First of all, it uses coding of parameter set and not the parameter themselves. Only the information regarding the objective function is used and no derivatives are calculated. In addition, its probabilistic approach can result in excessive variations of the design parameters. Consequently, this can infrequently causes the solution to get caught in a non-optimal solution.

8.3.3 Multi-Objective Tabu Search (MOTS) algorithm

The MOTS utilised for this work is an enhanced version of a single-objective Tabu Search for discrete optimisation of Conor and Tilley [114], created by Jaeggi et al. [115]. Managing “explicit” and “attributive” types of memories, the code explores the design space in an efficiently guided fashion, avoiding unfruitful moves [116]. “Explicit” memories store the Pareto-optimal solutions and some attractive but unexplored neighbours found during the search, while attributive memory is used for guidance and recording temporal solutions. The name “attributive” is due to the fact that is used for guiding purposes recording information about solution attributes that change in moving from one solution to another. The heart of the algorithm is based on a modified Hooke and Jeeves (H&J) [117] local search method, coupled with adaptive memories to implement intensification and diversification.

The Tabu Search algorithm can be seen as a further development and enhancement of a local search method. The main difference between TS and gradient-based algorithms is the use of adaptive memory to explore efficiently the whole design space avoiding unfruitful moves. MOTS works iteratively, the optimisation starts at a predefined point, defined by the user, and it evolves guided by the information recorded from previous iterations. At each iteration, $2n_{var}$ (where n_{var} are the number of design variables) new points are generated for examination. The points generated are based on the current dominant; a predefined standard size step δ is defined for this task. The new points generated are $x_i \pm \delta$, where x_i are the current dominant design components. The objective functions are then evaluated for each new point. Actually, points that are “tabu” or violate a constraint are removed from the new points generated, thus, $n_{sample} \leq 2n_{var}$ points are evaluated. This feature reduces the number of evaluations performed, which is a good characteristic for real-world problems where a large number of design variables are involved. If there is a point that is dominant with respect to the current one, it is selected as the next point for the iteration. If there are two or more dominant points, one of these is selected randomly from the remaining ones for the next iteration. The other dominant points that have not been selected as a next point base are not discarded but,

instead, stored in an Intensification Memory to be analysed afterwards in the search procedure. The new point, as previously said, is selected randomly because no directionality is to be incorporated in the optimisation, as it can narrow the search capability for the absolute optimum point. Finally, if no dominant points are found, one dominated point is randomly chosen for the current role. In the case of a successful H&J move, a further enhancement is used. It is defined as a *Pattern move*, and incorporates some directionality to the optimisation search. The process will repeat this move, if it is prospering it will continue in that direction, otherwise a normal H&J move is performed. The TS algorithm is characterized by three main stages, each of which is associated with an allocated memory. Recently visited points are recorded in a first-input-first-output (FIFO) fashion in the Short-Term Memory (STM), creating in such a way a tabu list of points that will not be revisited from the progression of the optimisation. The number of recent visited points and consequently the size of the STM, depends on the dimension of the design variables and objective functions vectors and, hence, on the particular nature of the problem.

A Medium Term Memory (MTM) is used to store the optimal or near-optimal points, which are used to perform the *Search Intensification* (SI) strategy. This consists in returning to a region that seems attractive and perform a more intense search but without revisiting the same solutions found. Search intensification occurs if there have been no successful moves for a user-defined number of local search iterations.

Explored points are recorded in the Long-Term Memory (LTM). These data are utilised to perform *Search Diversification* (SD). Figure 8.5 illustrates in a simple example the different memory categories of TS.

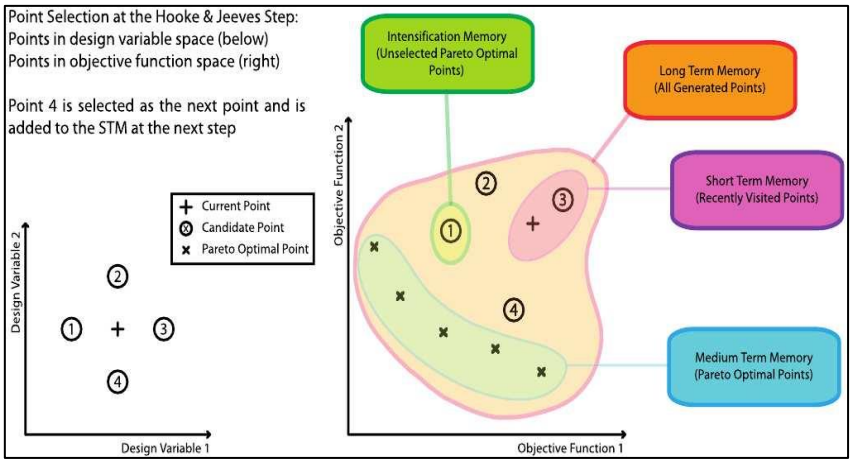

Figure 8.5: Point selection for the Hooke & Jeeves move and Tabu Search memories [115]

While the SI intensifies the search of the optimum in one zone of the design space, the *Search Diversification* strategy moves the search to unvisited or less visited regions. The LTM is used for this purpose, storing the areas, which have been extensively searched by the optimizer. In order to perform such a move the design domain is divided in N sub-domain and the number of points visited in each sub-domain represents its visited index. When SD occurs the search is moved to a random sub-domain with a low visited index. The final stage of the algorithm is the Step Size Reduction (SSR) and happens after a continued lack of successful moves. This strategy is performed to ensure an intensive search in the neighborhood of the current optimal solutions. The step sizes of each design variable are reduced and the search returns to the current “best” solution location in a single-objective case or to a randomly selected point from the MTM. As previous explained, three techniques are involved within the search enhancement; SI, SD and SSR. In order to control the utilisation of these strategies, a new variable is introduced i_{local}. This counter is increased when the current point is not added to the MTM and is then reset when it is added. Therefore, the counter gives information about the temporal success of the optimisation. SI consists of returning to an attractive region and performing an enhanced search with the purpose of finding the optimum solution. The points to be visited are those stored in the MTM. This strategy is performed when i_{local} reaches a predefined value i_{local} SI, the points are selected randomly from the

MTM. SD is based on visiting unknown regions of the design space. To achieve the latter task, LTM information is used, thus this strategy is used when i_{local} reaches i_{local} SD. Intensification strategy is used in the optimisation to improve the exploration of highly successful probability regions, whereas, diversification is utilised to analyse completely unexplored regions. The latter is applied when the current region has been thoroughly analysed, this will happen when the former strategy has been repetitively used to make certain that the current region cannot undergo further improvement. Consequently, it is logical that i_{local} SI < i_{local} SD. SSR and restart the search from the best point found are a coupled strategies utilised to intensify the search nearer to the current optimal solution. For this reason, a point from the MTM is randomly selected and the search is moved to that region. When the step size is raised to a predefined threshold, the initial δ is chosen and the optimisation is restarted from the extreme Pareto-points. A flow diagram of the algorithm is shown in Figure 8.6.

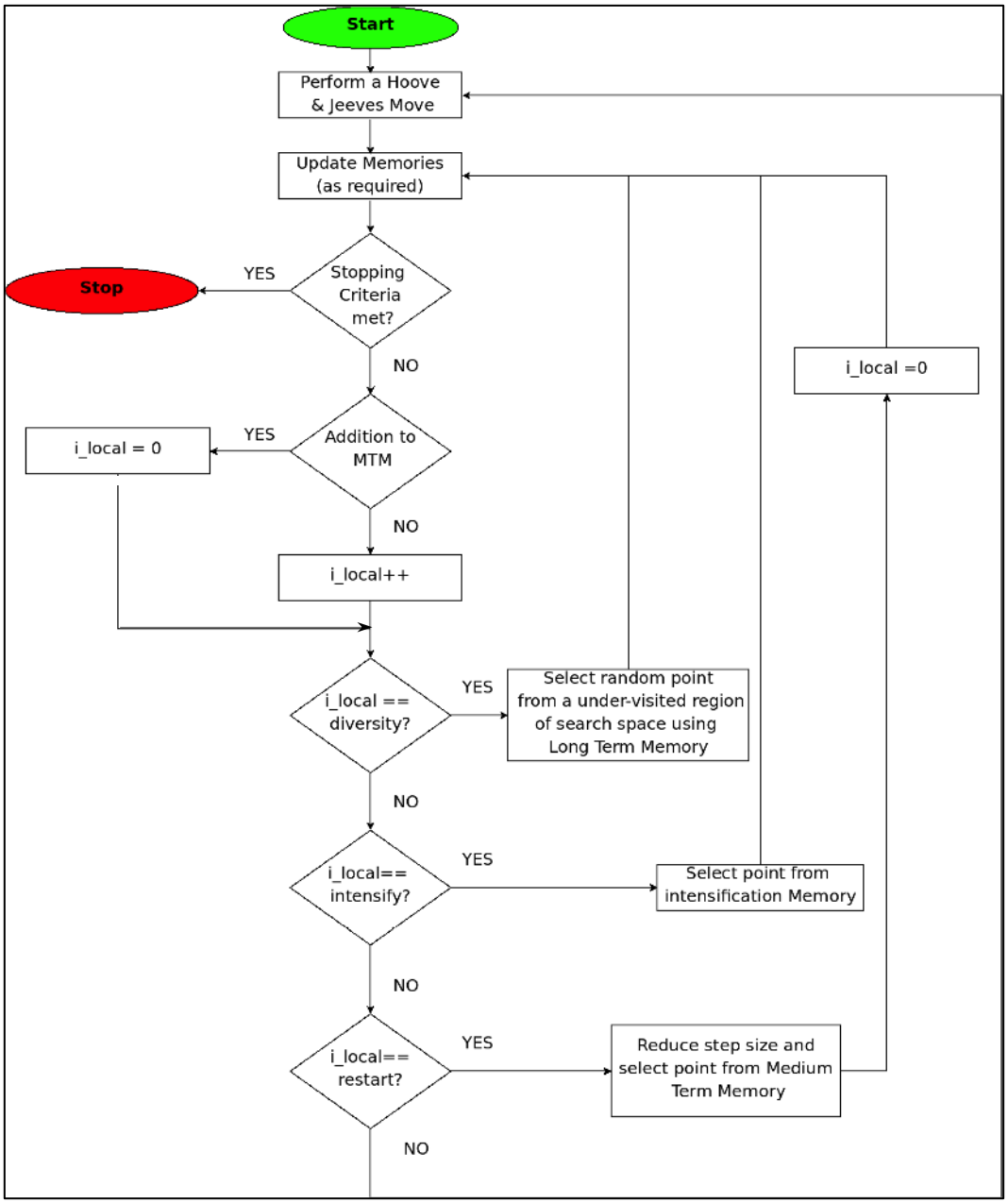

Figure 8.6: Flow diagram of the multi-objective Tabu Search algorithm

Real-world multidisciplinary optimisation involve the handling of a massive amount of data, therefore, in order to assess the optimisation within an reasonable time slot, two strategies have been used in this work, namely Functional Decomposition and Domain Decomposition. To implement the first, the MOTS have been coded in a Master and Slaves fashion. The optimiser code runs within the Master, this is the module that decides what the next step is in the optimisation. It sends the design points to be analysed for each Slave.

Therefore, the maximum number of Slaves used cannot be higher than 2_{nvar} as it is necessary to collect all the information before a new H&J move is performed. The most demanding phases of the optimisation are the flow simulations, and it is for this reason that the second strategy is used. Domain Decomposition is a strategy that divides the flow or structural domain into sub-domains to be analysed separately, providing a multi-level parallelisation capability, which allows a drastic reduction of time completition.

In conclusion MOTS has been developed and proved to be particularly effective on aerodynamic problems [118]. In [102] MOTS algorithm has been compared with a leading Multi-Objective genetic algorithm NSGA II [119], showing that the two algorithm perform comparably. Moreover, the tool has successfully been used by Kipouros and Ghisu [115, 116, 120, 121] in the multi-objective optimisation of an axial compressor. From the flow diagram it is possible to see how the iteration is carried out using a local counter i_{local}, which is reset every time the MTM is successfully updated. The different strategies described in the previous section (SI, SD and SSR) take place when i_{local} reaches user-specified values, selecting randomly a point from the MTM. When a stopping criteria is reached the optimization process in ended and the Pareto-optimal set is found. Such a stop criteria can be either hardcoded into the code, e.g. max iteration number, or be defined by the time available for the optimization task. Both approaches allow the user to visualize the solution set found thus far deciding if the process has to be stopped.

8.4 Surrogates statistically based

Aircraft design, as many other engineering applications, is increasingly relying on computational power. The growing need for multi-disciplinarity and high-fidelity in design optimisation and industrial applications implies a huge number of repeated simulations to find an optimal design candidate. Indeed, a strong effort has been done in the recent past to introduce potentially highly accurate analysis methods both in geometry and physics modelling. The main drawback is that they are computationally expensive. The solution of non-linear steady or unsteady aerodynamic flows by numerically solving the Navier-Stokes

equations implies an amount of data storage, data handling and processor costs that may result very intensive, even when implemented on modern state-of-art computing platforms. This turns out to be an even bigger issue when used within parametric studies, automated search or optimisation loops which typically may require thousands analysis evaluations. The core issue of a design optimisation problem is the search process of an optimal solution. However, when facing complex problems, the high-dimensionality of the design space and the high-multi-modality of the target functions cannot be tackled with standard techniques. Due to these obstacles, long running times and lack of analytic gradients, almost any optimisation method applied directly to the simulation will be slow.

Simulation based analysis tools are finding increased use during preliminary design to explore design alternatives at the system level.

Despite advances in computer capacity, the enormous computational cost of running complex engineering simulations makes it impractical to rely exclusively on simulation for the purpose of design optimisation. To cut down the cost, surrogate models, also known as metamodels, as they provide a "model of the model" [122] are constructed from and then used in place of the actual expensive simulation models. Over the last two decades, there has been an explosion in the ability of engineers to build numerical models to simulate how a complex product will perform. Moreover, the ability to quickly modify these simulation models to reflect design changes has also greatly increased and the potential for using optimisation techniques to improve engineering design is now higher than ever before. However, one of the major obstacles to the use of optimisation is the large running time of the simulations and the lack of gradient information in many complicated simulations. An adequate and general answer to optimisation based on long running and computationally intensive analysis lies in the exploitation of surrogate models.

Surrogate and Reduced Order Modelling (ROM) can provide a valuable alternative at a much lower computational cost. A global surrogate model is generally referred to as a low-cost model able to provide an approximation of a selected objective function over the whole design space. A reduced order model

is a surrogate, which is further able to capture and reproduce the physics embedded in the high-fidelity model by using a low-dimensional basis.

Surrogate models are educated guesses as to what an engineering function might look like, based on a few points in space where we can afford to measure the function values. Recent advances in Surrogate-Based Optimisation (SBO) bring the promise of efficient global optimisation to reality [123] A review of the state-of-the-art constructing surrogate models and their use in optimisation strategies is to be found in references [124, 125, 126].

SBO uses surrogates or approximations instead of the expensive analysis results to contain the computational time within affordable limits. Surrogate models may be usefully exploited through optimisation as they indeed try to provide answers in the gaps between the necessarily limited analysis runs that can be afforded with the available computing power. They can also be used to bridge between various levels of sophistication afforded by varying fidelity physics based simulation code, or even between predictions and experiments. Their role is to aid understanding and decisions taking by exploiting every last drop of information from the analysis and data sources available to the design team and making it available in a useful and powerful way. The basic idea is for the surrogate to act as a curve fit to the available data so that the results may be predicted without recourse to the use of the primary source, the computationally intensive simulation codes. The approach is based on the assumption that, once built, the surrogate will be many orders of magnitude faster than the primary source while still being usefully accurate when predicting away from known data points. This underlines the two key requirements of the approach: a significant speed increase in use and useful accuracy. Obviously these constitute two conflicting requirements and the compromise best suited to the application targeted will drive the choices set. It is worth underlining once again that exploiting surrogates means avoiding to invest one’s computation budget in answering the specific question at hand and instead invest in developing fast mathematical approximations to the long running computer codes, offering a wide potential for trade-offs exploration and physical insight gain.

SBO approaches constitute an adequate engineering practice to tackle the complexity of multidisciplinary design optimisation based on high fidelity simulations. The surrogate model is to be used most of the time, with occasional recourse to the high-fidelity model. More specifically, surrogate-modelling techniques may be classified as:

- ✓ ***Data-fitting models*** (interpolation or regression), which are non-physics-based approximations.
- ✓ ***Hierarchical models***, also known as multi-fidelity, variable fidelity or variable complexity models.
- ✓ ***Reduced-order models***, which can use, for instance, modal analysis or proper orthogonal decomposition.
- ✓ ***Artificial Neural Network*** (ANN) methods.

Data-fitting models are generic but they are not based on the physical properties of the behaviour they are trying to represent. On the other hand, hierarchical models use corrected results from a low-fidelity model as an approximation to the results of a high-fidelity model. These models are physics-based but are of lower fidelity.

Reduced models typically allow gaining a deep physical insight into the leading phenomena. However, it is important to note that many of the existing reduced-order modelling and hierarchical modelling techniques require a priori knowledge of the structure of the high-fidelity model to be approximated. However, in many (surrogate-based) design optimisations, the CFD solvers are used as black boxes and it is therefore difficult to derive low-order models by using classical model reduction approaches, which generally employ a Galerkin projection procedure requiring knowledge of the underlying high-fidelity model. In consequence, such techniques are considered as intrusive.

Non-intrusive reduced order models may also be derived e.g. by combining the use of Proper Orthogonal Decomposition (POD) and data-fitting techniques. Such an approach has the advantage of not requiring an intrusive or code-specific implementation. Such a procedure benefits from the POD to perform the space reduction of the model, whereas generic data-fitting approximations,

like Radial Basis Functions (RBF) or Kriging, can be used for the low-dimensional reconstruction in the design space. ANN is a well-known technique, but needs a large amount of trail-and-error associated with the use of this technique [127, 128].

8.4.1 Proper-Orthogonal Decomposition

Since its introduction in 1901 [129] the POD method has received much attention as a tool to analyse complex non-linear systems. The Proper Orthogonal Decomposition (POD) method has been widely used to obtain low-dimensional approximate descriptions of high-dimensional systems. The technique was proposed by several authors at different times, in different fields and under a variety of names [130]. It is essentially a linear transformation to diagonalize a given matrix. The Proper Orthogonal Decomposition (POD) or Principal Component Analysis (PCA) is an elegant and powerful data-reduction method for non-linear physical systems.

An efficient method for computing PODs for large dimensional problems is the method of snapshots introduced by Sirovich [131]. This technique has been widely applied to CFD formulations to obtain reduced-order models for unsteady aerodynamic applications [132]. A set *[S^k:k=1,…,N]* of *N* observations, called snapshots, is obtained from accurate numerical simulations (e.g. the high-fidelity CFD simulations in the present setting).

POD consists in decomposing each snapshot as a linear combination of modes.

$$S^k = \sum_{j=1}^{N} \alpha_j \varphi_j + \bar{s} \tag{8.4}$$

Where:

- $\bar{s}$ is the mean vector of the set [*S^k:k=1,…,N*]
- *N* is the number of snapshot
- the $\{\varphi_j; j = 1, \ldots, N\}$ are the POD basis vector;
- the $\{\alpha_j; j = 1, \ldots, N\}$ are the POD linear expansion coefficients.

The POD basis is built in several steps. First the snapshot deviation matrix is constructed as

$$S = \left((s^1 - \bar{s}) \dots (s^N - \bar{s})\right) \tag{8.5}$$

Then the covariance matrix C is computed by $C = SS^T$. The eigenvector C determine how to construct the N POD modes φ_j.

Each POD mode contains an energy level, see Figure 8.7. Newman [133] noticed that the most important part of the energy contribution is concentrated in the first modes and the last modes the lower energy. By fixing a certain level of energy a truncation can be performed.

$$S^k \cong \sum_{j=1}^{\tilde{N}} \alpha_j \varphi_j + \bar{s} \tag{8.6}$$

where $\tilde{N} < N$ is chosen to capture the desired level of accuracy.

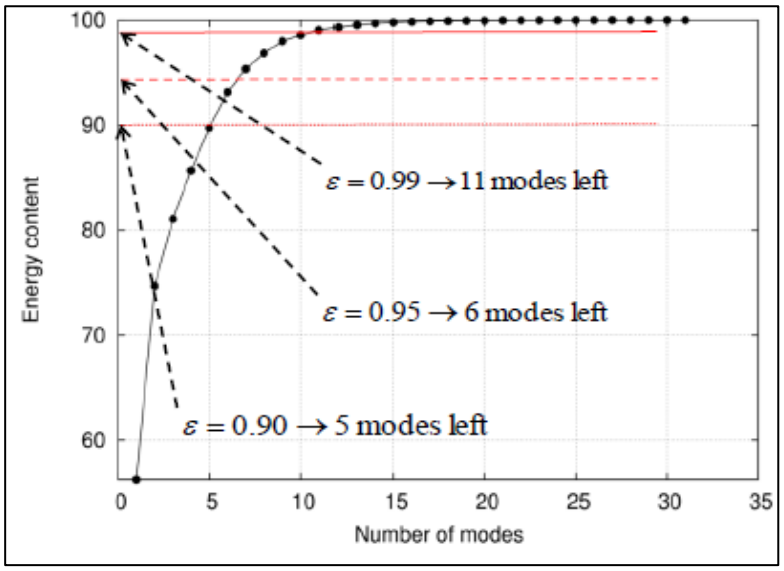

Figure 8.7: Typical cumulative POD energy distribution [133]

The idea behind POD technique is that, given a set of solutions or snapshots, the POD method calculates a set of optimal basis solutions that encompass the most energetic modes of the system (i.e. the modes corresponding to the dominant eigenvalues). Snapshots are generated by varying the design variables in a parametric form. This set is optimal in the sense that the least

square error between the original snapshot ensemble and its reconstruction in the space spanned by the POD modes is minimal. So far the use of POD method has been restricted to finding a basis for the modal decomposition and subsequent reduction of the data obtained by experimental studies or high-fidelity numerical simulations. In the perspective of a fluid dynamic problem, the POD can be defined as a statistically derived process, which provides a mathematical representation of the high-energy components of a fluid flow field. This is done by decomposing the observed structure into a set of uncorrelated linear components, which provide a low-dimensional representation of the problem. The components are the eigenfunctions of a correlation tensor and the expansion is optimal in the sense that the POD eigenfunctions maximize the total energy captured in each co-ordinate direction, subject to orthogonality constraints. Once built the optimal orthogonal basis, reduced-order models can be derived by projecting the model onto the reduced space spanned by the POD modes. Therefore, the original problem, formulated in terms of non-linear partial differential equations as Navier Stokes model, can be converted into a small system of ordinary differential equations, which can be solved efficiently.

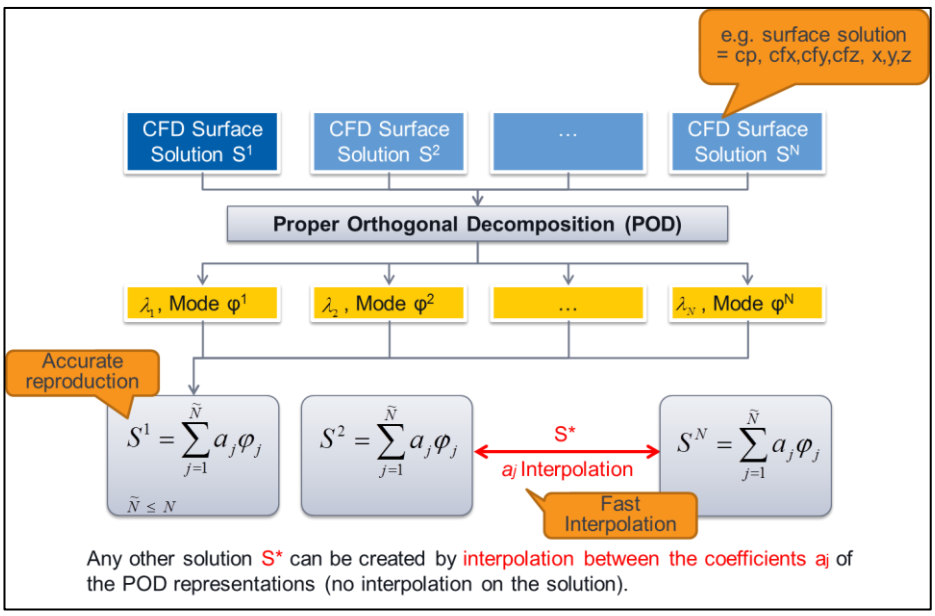

Figure 8.8: Schematic of POD method

The POD technique for basis reduction has been employed in many engineering applications, such as approximate flow modelling in computational fluid dynamics [134, 135], reduced order thermal solutions in hypersonic flows [136], control-oriented modelling of physical processes [137, 138, 139], study of structural dynamics and chaotic systems [140, 141, 142], structural health monitoring [143], load updating for finite element models [144], and multi-disciplinary design optimisation [145, 146, 147]. As mentioned previously, the Proper Orthogonal Decomposition method is a means to obtain low-dimensional approximate descriptions of high-dimensional systems. The mathematical implementation of POD technique involves the use of any of the three very closely related methods: (i) Kosambi-Karhunen-Loéve Decomposition [148, 149, 150], (ii) the Principal Component Analysis [151, 152], and (iii) Singular value Decomposition (SVD) [153]. A wide and comprehensive review of POD-based applications can be found in [154]. A wide and more detailed review of the basic aspect and use of reduced order modelling is provided by Lucia et al [155].

8.5 Integrated Systems for Aerodynamic Shape Optimisation

This paragraph outlines the development of integrated systems to perform multi-objective optimisation for a single element aerofoil test case at fixed flow conditions. The simple airfoil design problem has been defined to demonstrate the functionality of the design systems. Specifically, two different optimisation approaches are investigated, as shown in Figure 8.9.

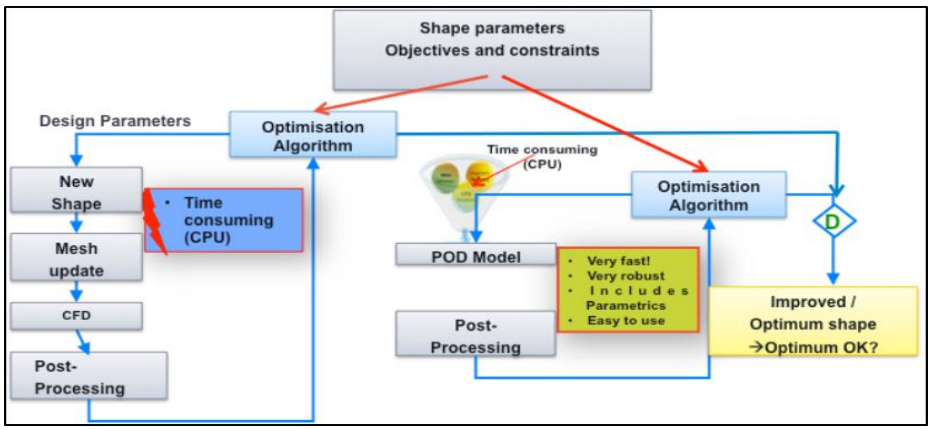

Figure 8.9: Two different optimisation approaches

The first is the direct optimisation approach, and the second makes use of the Proper Orthogonal Decomposition (POD) mathematical technique, in order to accelerate the whole process. A detailed analysis of the methods as well as the results of the comparison between the two techniques is provided. The question of how design acceleration affects the design quality is also addressed.

8.5.1 Description of the test case

The airfoil under investigation is the well-known single element supercritical airfoil RAE2822 [156]. It is shown dimensionless in Figure 8.10.

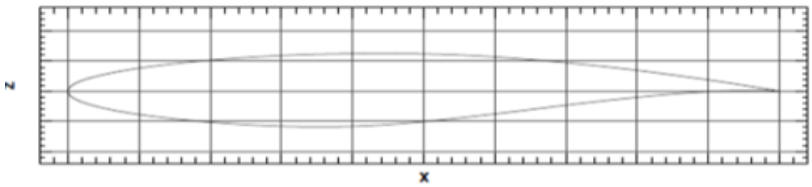

Figure 8.10: RAE2822 airfoil geometry

The analysis is performed for cruise configuration at fixed flow condition. From simple flight dynamics, the thrust produced by the engines of the aircraft has to overcome the drag produced by the motion of the vehicle through the air. The cruise flight phase is commonly the longest one for commercial aircraft; therefore, it is the phase with the highest fuel consumption. In order to reduce the fuel consumed by vehicle, it is possible to improve the Specific Fuel Consumption (SFC) of the engines and/or to improve the aerodynamic performance of the aerodynamic elements. Specifically, the free-stream Mach number is M = 0.75 at a Reynolds number of Re = $6.5 \cdot 10^6$ and the angle of attack is α = 2.3. The objective functions are the lift and drag coefficient to maximise and minimise respectively, under the constraint that the maximum thickness cannot diminishing more than 15% from the datum. This is due to space allocation restriction for the fuel tank volume and to satisfy structural requirements.

8.5.2 Direct Optimisation approach

The flow chart in Figure 8.11 shows the basic stages for the direct aerodynamic optimisation process developed. The system comprise of both, commercial

software and in-house libraries, collated together using a series of code in C++ and exploiting the journaling capabilities of the commercial packages. Several modules constitute the framework. It starts with the parameterisation of the geometry, the step in which the design variables are defined and stored in a correspondent design vector. In this step the FFD technique is implemented. The input is the current design vector from the Multi Objective Tabu Search (MOTS) algorithm. The output is a file containing the subsequent generated airfoil point coordinates. It is necessary to have the datum airfoil configuration (datum.dat) for the algorithm to calculate the deformed one. Once this step has been completed the main optimisation loop takes place. A mesh is created around the geometry to allow a CFD simulation of the flow field. The flow analysis is performed afterwards by mean of ANSYS Fluent flow solver. The Fluent journal file imports the mesh file created in ICEM CFD and defines the solver formulation. After the convergence of the solution, the metrics (and so the objective functions) are extracted. In this case they are the current airfoil geometry and the two objective functions cost: Cd/Cd_{datum} and $-Cl/Cl_{datum}$. The objective function values and the respective design vector are sent to the optimiser that explores the design space generating new design vectors and restarting the cycle.

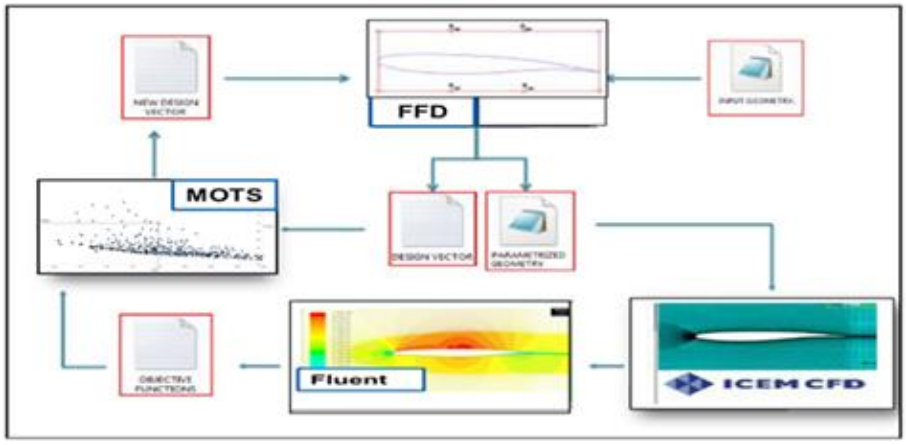

Figure 8.11: Flow chart of the direct optimisation cycle

In order to parameterise the shape profiles, sixteen variables have been set. As can be seen in Figure 8.12, the polygon that controls the shape of the airfoil is highlighted in red. What is more, to maintain the leading and trailing edge points

in their fixed positions, eight design variables in black are fixed to zero over the optimisation process.

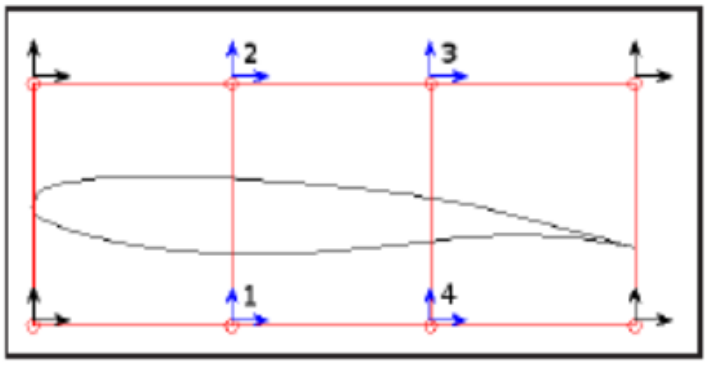

Figure 8.12: Airfoil Design Variables

The shape is modified with the displacement of the eight design variables in blue. The design space limits the variability of the design variables from -0.3 to 0.3 with an initial step of 0.07; this is good enough to have a set of different deformed profiles where all the important parameters that define an airfoil shape have been moved from their datum position. The element shape is then modified following the mesh generation around the airfoil, using an automated process set-up within the commercial package ANSYS ICEM CFD. Feasibility checks are carried out to exclude geometry intersections and low mesh quality from the process. The enhancement of the tool with an Error Checking routine has been encoded, accumulating decisive information about the optimisation evaluations failure. This feature has been added because, in an optimisation process, failures can happen for several reasons at different stage and hence it is important to understand in which phase and why this happen, skipping the failure case and keep continuing the optimisation process. The mesh is, then, transferred to the Flow Solver ANSYS Fluent for the evaluation of the performance. The Fluent journal file imports the mesh file created in ICEM CFD and defines the solver formulation. In addition to the solver formulation, the turbulence modelling approach, fluid properties, discretization schemes, and convergence criteria are also specified. Because real-world multidisciplinary optimisation involves the handling of a massive amount of data, therefore, in order to assess the optimisation within a reasonable time slot, two strategies

have been used in this work, namely Functional Decomposition and Domain Decomposition. To implement the first, the MOTS have been coded in a Master and Slaves fashion. The optimiser code runs within the Master, this is the module that decides what the next step is in the optimisation. It sends the design points to be analysed for each Slave. Therefore, the maximum number of Slaves used cannot be higher than 2•nvar as it is necessary to collect all the information before a new H&J move is performed. The most demanding phases of the optimisation are the flow simulations, and it is for this reason that the second strategy is used. Domain Decomposition is a strategy that divides the flow or structural domain into sub-domains to be analysed separately, providing a multi-level parallelisation capability, which allows a drastic reduction of time completition. Specifically 12 CPUs have been used for the CFD analysis. In this optimisation approach a structured mesh made up of nearly 240000 cells has been generated; it is shown in Figure 8.13. It is fundamental that the domain chosen is inadequate representation of the real-word physical problem. All the boundaries (farfield geometry) are selected in such a way as that the influence of the flow around the airfoils is avoided. Moreover, in order to catch all the peculiar dynamics of the flow field the domain must allow the flow to fully develop downstream.

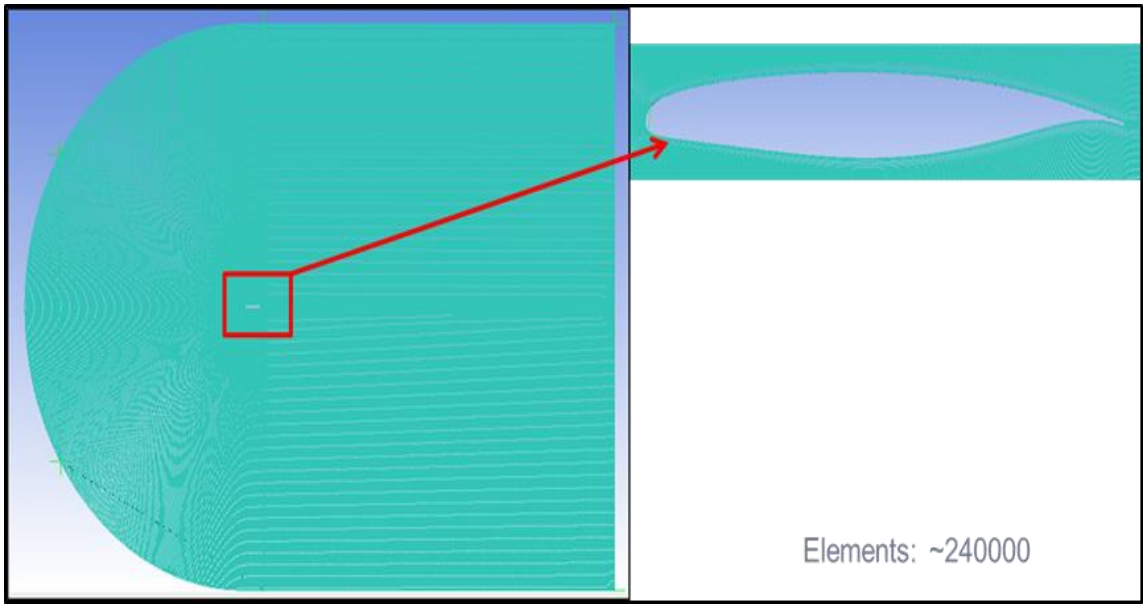

Figure 8.13: Mesh around the airfoil

Table 8.2: MOTS optimisation algorithm setting

Parameter	Value	Description
n_stm	15	Short Tern Memory (STM) size
n_ltm	4	Long Tern Memory (LTM) size
intensify	15	Intensify search after "*intensify*" iterations without adding to the MTM
diversify	25	Diversify search after *"diversify"* iterations without adding to the MTM
reduce_ss	45	Reduce step size and restart after *"reduce_ss"* iterations without adding to the MTM
n_samples	4	Number of points randomly selected at each Hooke and Jeeves move
n_regions	4	In the LTM each variable is divided in n_regions to determine which regions of the design space have been under-explored
max_evals	500	Max evaluations halting criteria

8.5.3 Proper Orthogonal Decomposition

The workflow of the newly developed automated and integrated POD optimisation approach is schematised in Figure 8.14.

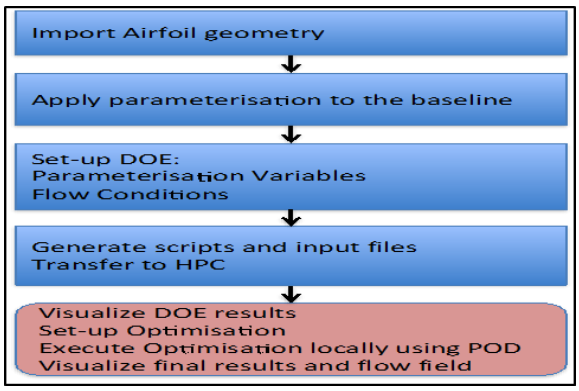

Figure 8.14: Workflow of the offline-online POD optimisation strategy

The Baseline is imported and parameterised using a PARSEC technique, which requires in this particular implementation the specification of 14 parameters. After this first step only 5 amongst the 14 parameters are selected as DVs, see Table 8.3.

Table 8.3: Description of the identified Design variables, their datum value and range of variation for the RAE2822 shape optimisation

Design Variables	Minimum Value	Datum	Maximum Value
ac: airfoil camber parameter 1	-0.00670	$-6.7\ e^{-5}$	0.006700
bc: airfoil camber parameter 2	-0.004800	$-4.8\ e^{-5}$	0.004800
ytc: airfoil camber parameter 3	-0.010000	0.0	0.010000
rle: leading edge radius	0.004290	0.008290	0.012290
teg: trailing edge angle	-9.841870	-6.841870	-3.841870

These parameters are the ones that represent the most critical changes, from a designer point of view, on the airfoil geometry. Next step consists in generating a set of different airfoil shapes. In this case 100 different shapes are generated using Latin Hypercube Sampling (LHS) as Design of Experiment (DoE) algorithm, given that this method provides good uniformity and flexibility on the size of the sample. Examples of partially shapes generated, using the PARSEC technique, are shown in Figure 8.15, in which the deformations have been exaggerated just for figure clarity.

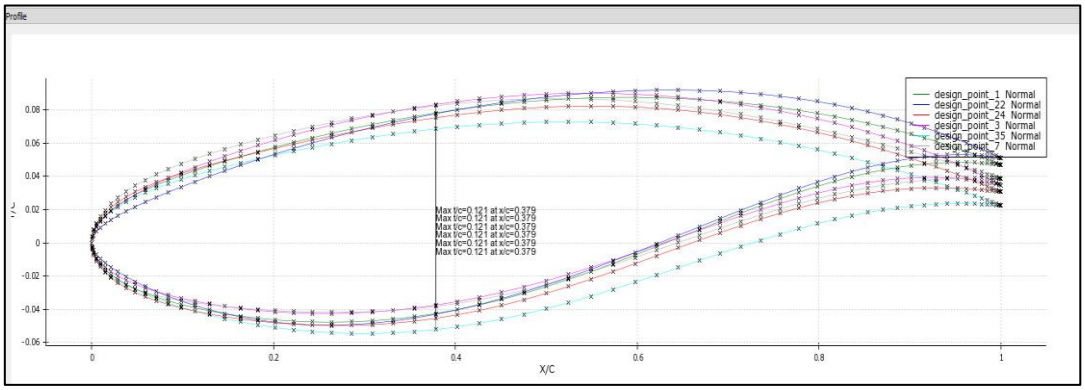

Figure 8.15: Example of aerofoil shapes generated using the PARSEC parameterisation technique

Specifically, a study has been conducted using 25, 50, 75 and 100 snapshots to generate the POD model, in order to assess how many off-line simulations are necessary to achieve an accurate POD-based model. The next four figures show the deviation in term of drag count obtained using the POD model generated using different number of snapshots compared with the direct CFD optimisation.

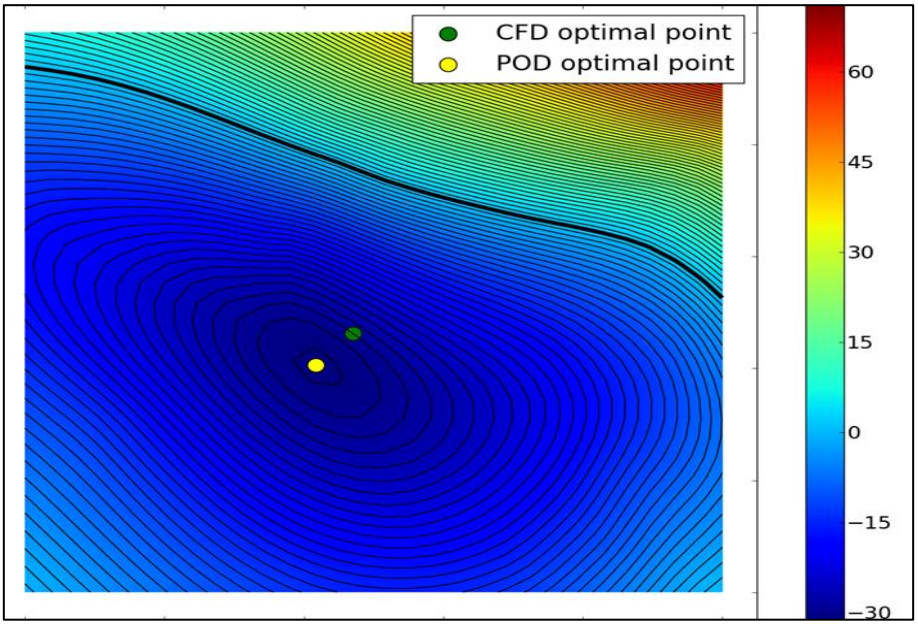

Figure 8.16: Drag count deviation - 25 snapshots

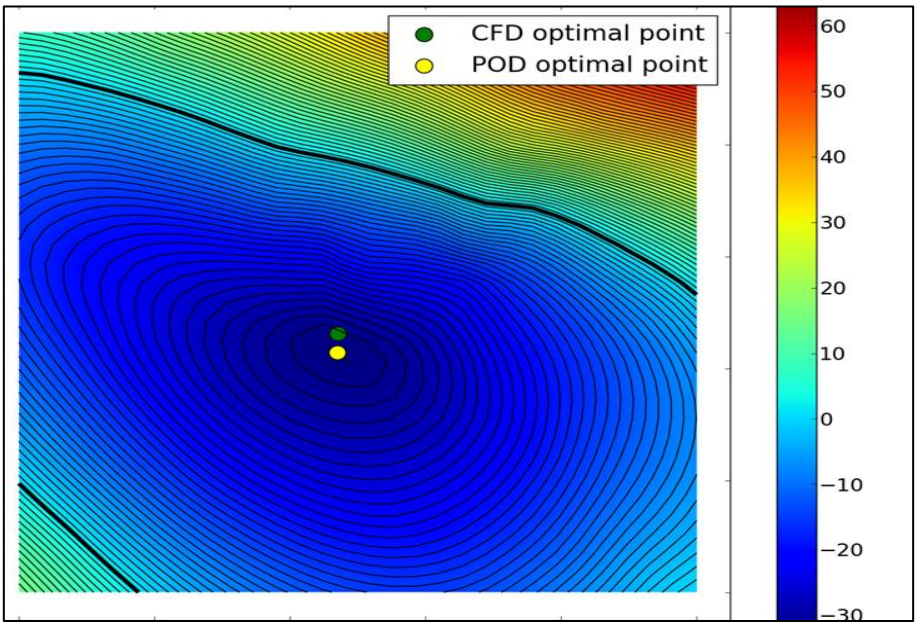

Figure 8.17: Drag count deviation - 50 snapshots

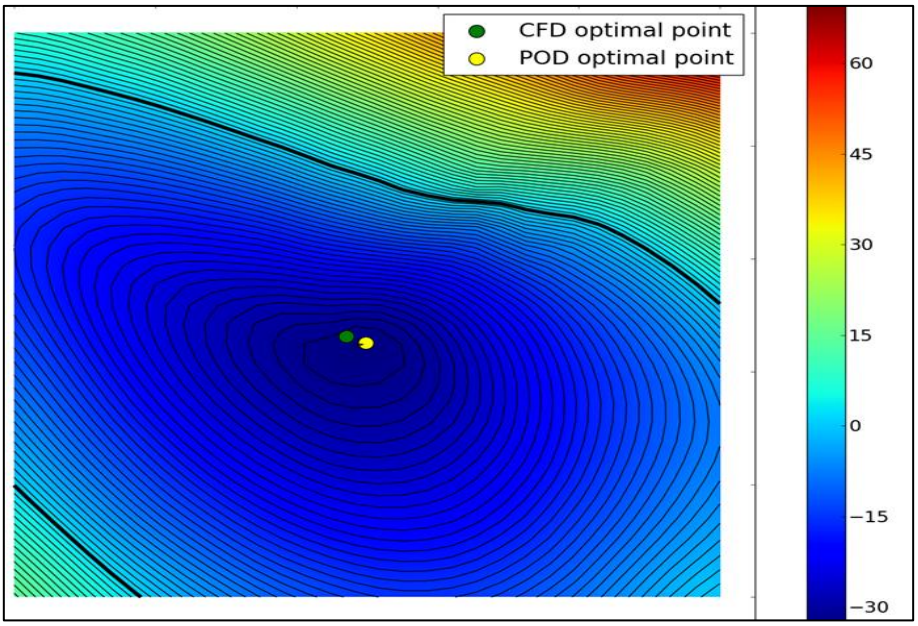

Figure 8.18: Drag count deviation - 75 snapshots

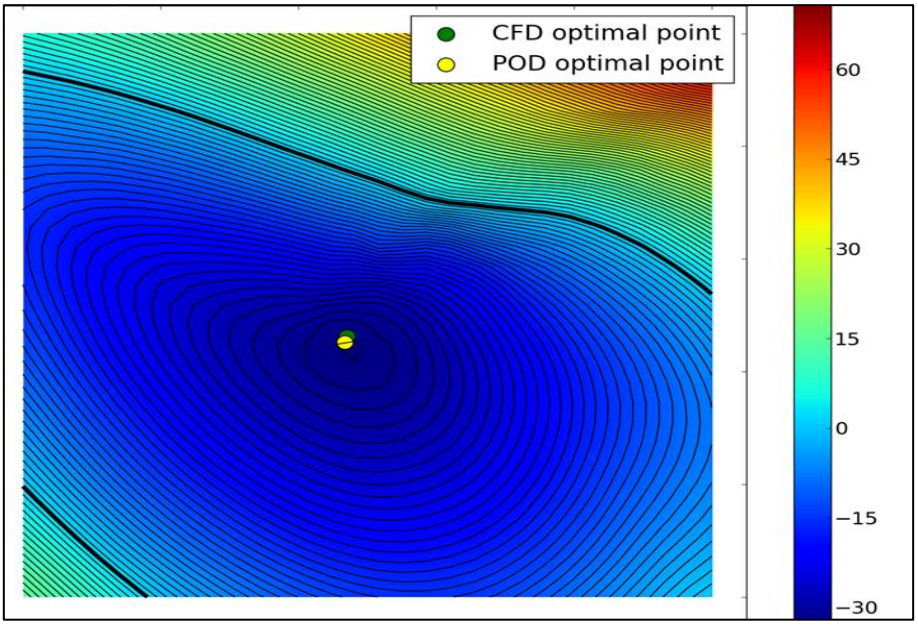

Figure 8.19: Drag count deviation - 100 snapshots

These input files are then transferred to a High Parallel Computing (HPC) cluster, and RANS simulations are performed for each design point, using TAU 2D (DLR RANS code), making use of the Shear Stress Transport (SST) turbulence model, after the meshes are automatically generated. In this optimisation approach a hybrid mesh has been generated. It is structured around the airfoil surface, keeping a y+ < 0.5 all over the surface from the first

cell away from the wall, in order to have a good resolution of the boundary layer. The mesh is shown in Figure 8.20.

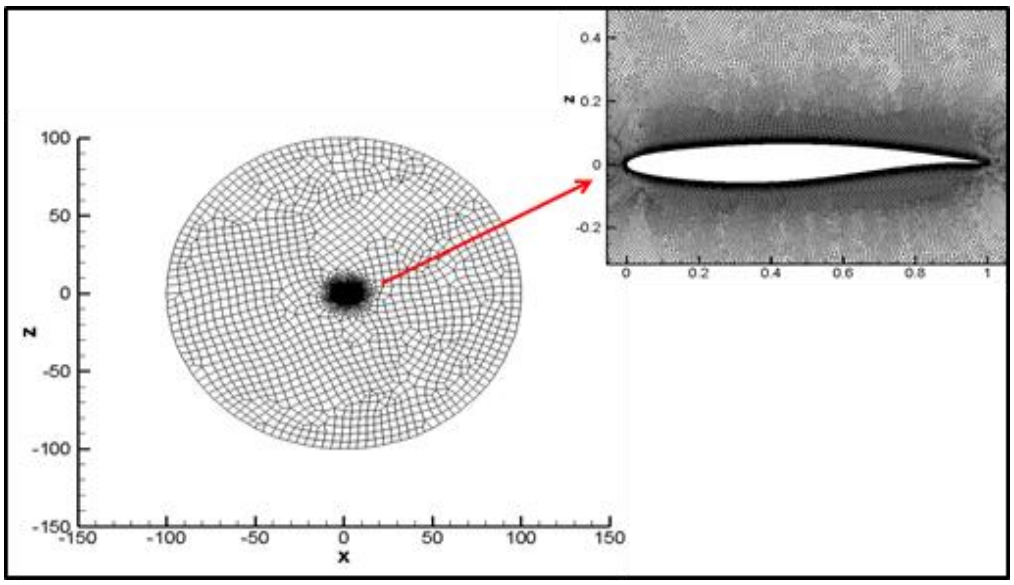

Figure 8.20: Mesh around the airfoil

It is made up of nearly 325000 cells, and the far-field boundary is a circle with a radius of 100 times the chord. A pressure far-field boundary condition has been applied to the external domain and a no-slip condition at the airfoil surface. At the completion of all the converged simulations, the POD approximation is generated using the available “snapshots”. The reduced order model is, afterwards, downloaded to the local machine and the optimisation process can be set-up within the design tool, and executed locally.

8.5.4 Results

Both optimisation approaches run for 500 evaluations, because of industrial needs of reducing the time allocated for the development and execution of such optimisation processes, especially at conceptual and preliminary design stage. The results of the direct optimisation, applying MOTS algorithm, are reported in Figure 8.21, in which the revealed Pareto front together with the optimisation search pattern are shown. The trade-off between the competing objective functions is clearly captured, with 137 designs that improve both objective functions.

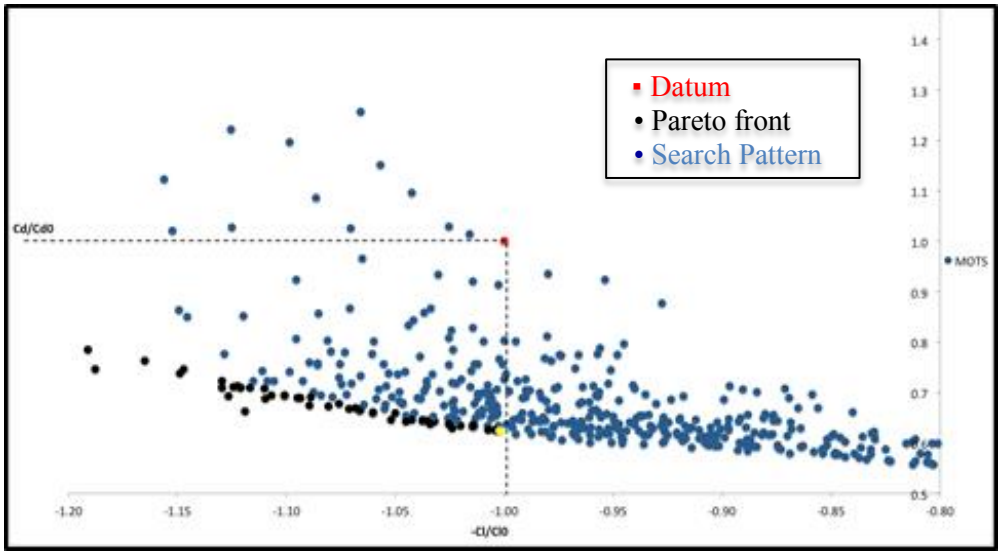

Figure 8.21: Direct optimisation results

The best drag coefficient minimisation improvement at nearly fixed Cl, yellow circle in Figure 8.21, reached a reduction of total drag of 37.4%. The Cl has been improved from the datum of 0.22%. The design point at nearly fixed Cl has been highlighted, because the aero optimisation, for cruise condition, in an industrial context, aims to minimise Cd at fixed Cl, which is usually given by the conceptual design office, coming from a desired wing lift distribution that take into account not only aero consideration. The multi-objective optimisations have been performed for verifying the performance of the algorithms and the robustness of the integrated process when more than one objective functions are considered, as it normally is the case in a real industrial engineering problem. The aerodynamic coefficients for the datum and optimised design are reported in Table 8.4.

Table 8.4: Aerodynamic coefficients comparison

RANS	Cl	Cd
Datum	0.64082	0.0192842
Optimum	0.65582	0.0120539

The results of the POD optimisation, applying both the MOGA and the SA algorithms, are shown in Figure 8.22.

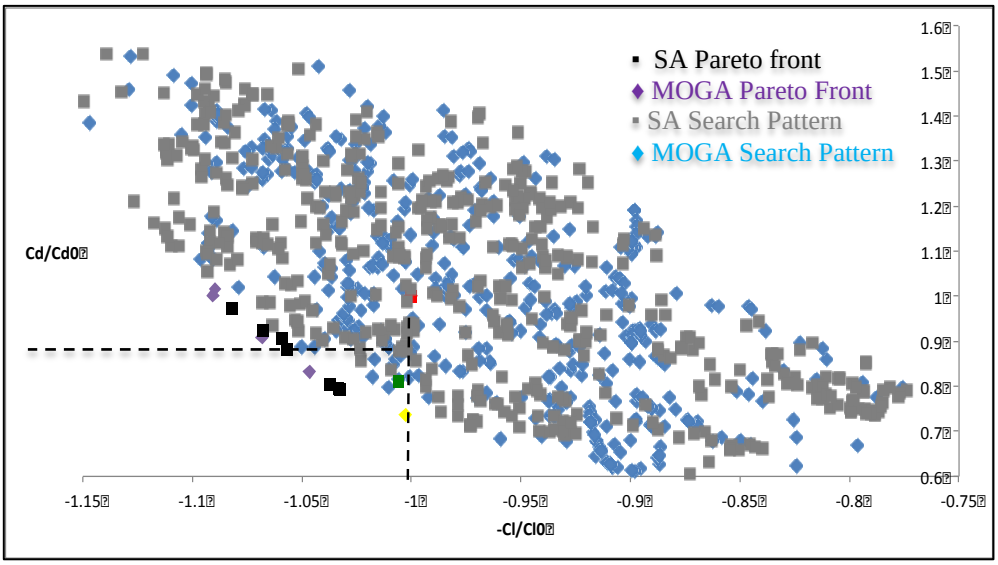

Figure 8.22: POD optimisation results

With both algorithms 40 designs have been found to improve simultaneously the objective functions, and the two algorithms perform comparably. Nevertheless, the best drag coefficient minimisation, at nearly fixed Cl, improvement has been found using MOGA, yellow diamond in Figure 8.21, in which a reduction of total drag of 26.3% has been obtained with a nearly constant Cl, which has been improved from the datum of 0.26%. In this optimisation the initial population is formed by 40 candidates and the optimisation is halted after 10 generations. The crossover probability is set to 0.7, while the mutation probability is 0.1. For clarity the discovered Pareto fronts are reported in Figure 8.23.

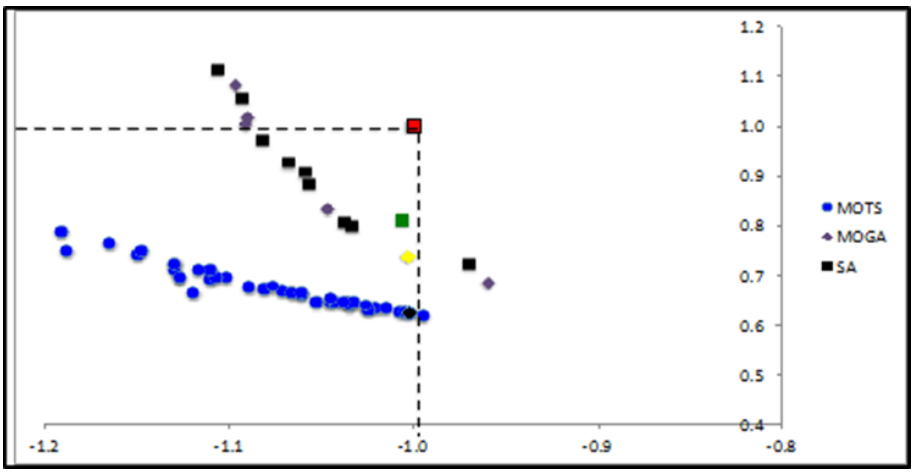

Figure 8.23: Comparison of Pareto front

Looking at the Pareto fronts plotted together in Figure 8.23, clearly is notable a discrepancies between them. But it is important to highlight that to have a fair comparison the same parameterisation technique and same optimisation algorithm should be used for both optimisation architectures. The integrated direct optimisation approach has been developed with tools available at the university, whereas, the POD approach have been developed and integrated used the industrial sponsor tools. For the future clearly a more fair comparison using same algorithms for both parameterisation and optimisation has to be performed.

The identified optimum design, DP325, see convergence Cd history in Figure 8.24 is validated using the full RANS simulation.

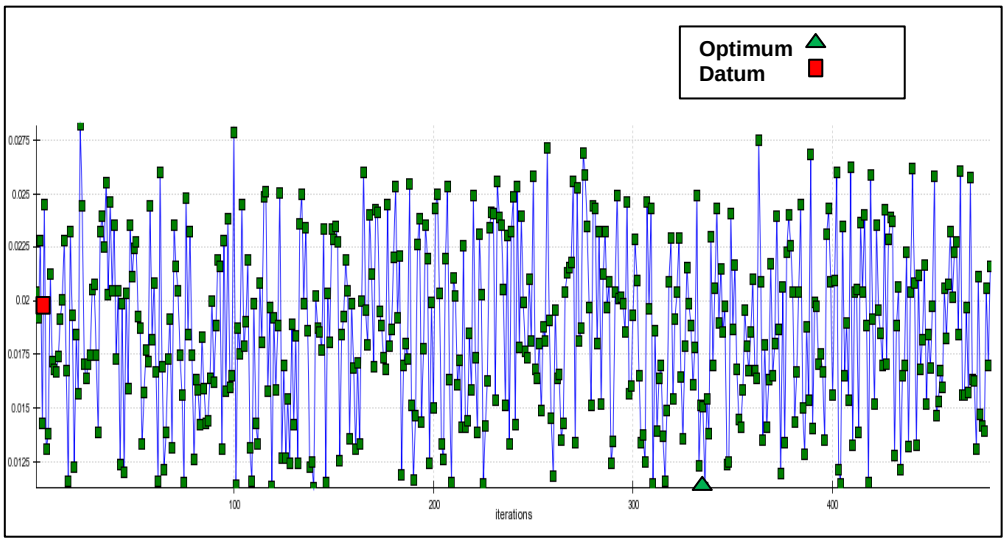

Figure 8.24: Cd convergence history

The resultant pressure distribution is compared with the one predicted by the POD model in Figure 8.25.

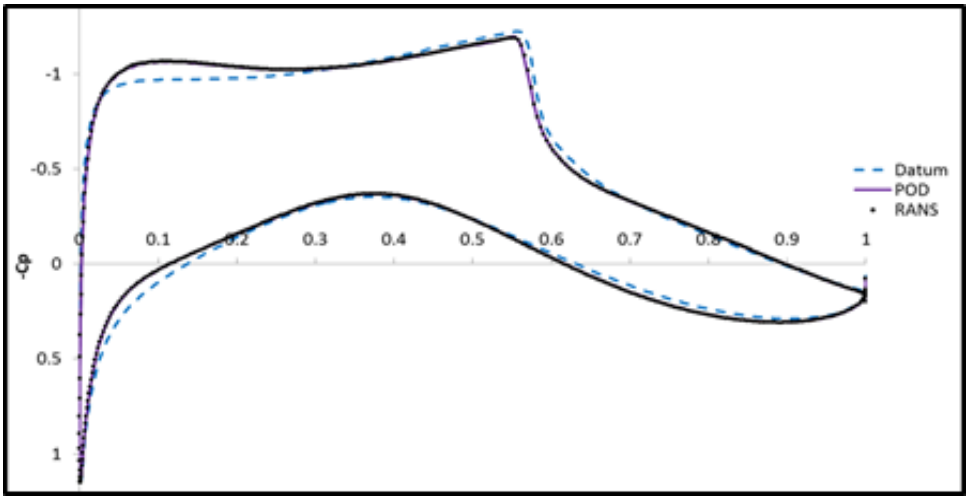

Figure 8.25: Cp distribution comparison

A reduction in the shock intensity is achieved increasing the y_{tc} parameter; see Table 8.5, which effectively results in a reduction of the airfoil angle of attack. The consequent loss in lift is compensated by slightly increase the leading edge radius and the camber at the rear of the airfoil; see Table 8.5 and Figure 8.27. All this is confirmed by the Sensitivity Analysis plot, which is shown in Figure 8.26. It highlights the influence of each design variable on the selected response.

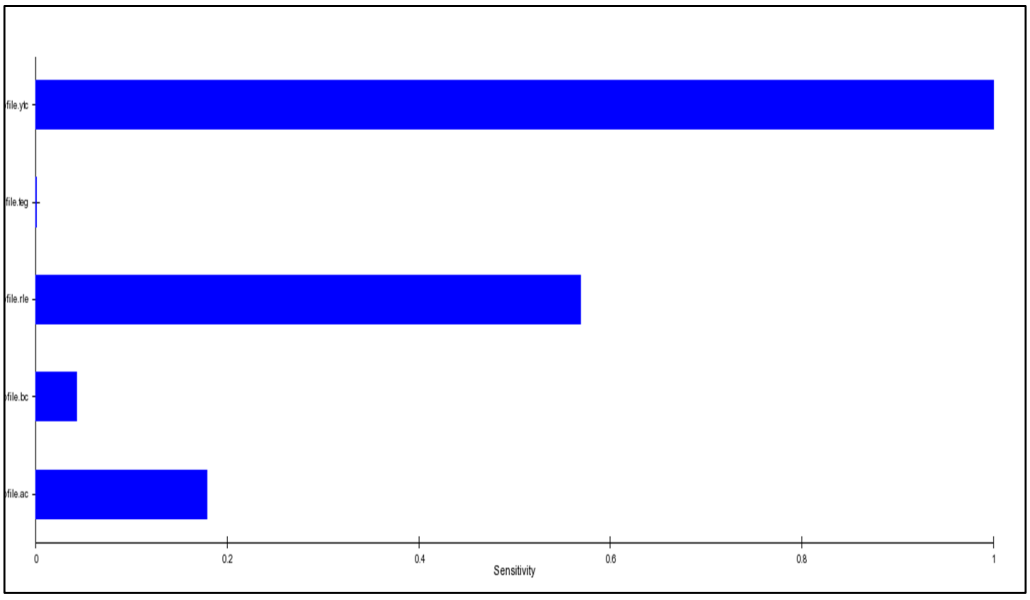

Figure 8.26: Cd sensitivity analysis plot

However a higher down-nose pitching moment is also obtained, which should then be compensated by a higher load on the tail, leading to an increase in the overall aircraft drag.

Table 8.5: Design variables, datum versus optimum

	ac	bc	ytc	rle	teg
Datum	-6.7 e^{-5}	-4.8 e^{-5}	0.0	0.00829	6.84187
Optimum	0.005337	0.004312	0.008964	0.010343	8.92105

Figure 8.27 shows the different profile and camber for the datum and MOGA optimum.

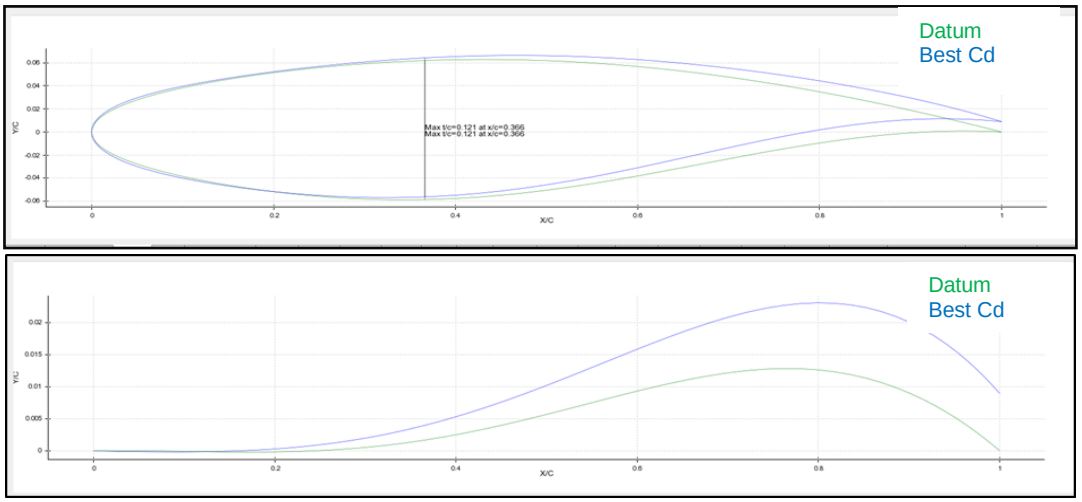

Figure 8.27: Datum and optimum profile and camber comparison

The POD model closely matches the RANS results with only minimal differences on the near-shock region of the airfoil's suction side. The accuracy of the prediction is also reflected in the aerodynamic coefficients that are compared to the RANS simulation ones in Table 8.6.

Table 8.6: Aerodynamic coefficients comparison

RANS	Cl	Cd
Datum	0.6911891	0.0191648
BestCd@FixCl	0.6904577	0.0134195

POD		
Datum	0.69119	0.01916
BestCd@FixCl	0.69029	0.01357

Indeed, the accurate prediction of the shock pattern shown by the POD model indicates a good exploration of the design space by the initial RANS design of experiment. In fact as stated by Lorente et al. [157], in order to derive a good POD-ROM able to deal with moving shock waves a large number of snapshots and POD mode is necessary.

8.5.5 Discussion

Two different integrated optimisation approaches have been developed and compared. The direct optimisation approach has shown a better improved design. From Figure 8.21, it can be seen the outstanding performance of the local search strategy carried out by the MOTS. Just few points of the 500 visited show a worse behaviour than the datum configuration. This shows the effectiveness of local search strategies. A total drag reduction of 37.4% has been reached, whereas, a reduction of total drag of 26.3% using the POD technique applying the MOGA algorithm, which has performed slightly better than the SA optimisation algorithm. It is evident from Figure 8.23 that the optimum solution identified by MOTS outperformed the MOGA one. Moreover, the revealed Pareto front presents a much better spread of the solutions and is also more populated. Indeed the richness of the Pareto front is one limitation of evolutionary based algorithms, since a maximum size implicitly is set once the number of individuals is fixed. This is especially true with a so limited number of evaluations. In contrast, there is no limit assigned to the size of the Pareto front in MOTS. On the other hand, time wise, the POD optimisation has produced results in a sixth of the time compared to the direct one, taking also into account the off-line computation time, which is a sensible reduction of wall-clock time. Namely 3 days against 18 days and in both case the CFD analyses have been run using 12 CPU. This saving in wall-clock time makes clear that this technique when applied to 3D cases will have even more benefit in term of computational

cost, considering that usually a 3D CFD analysis takes on average 6 to 9 times more CPU time than a 2D case.

In any case, it has to be remarked that the use of numerical optimisation technique in aerodynamic design can provide notable increase in performance for the specified deign condition. However the identified optima are often very sensitive to a small variation in manufacturing tolerance and or operating conditions [158]. As result the optimised design could present inferior performance under actual operating conditions, limiting its application to real engineering problems [159]. Uncertainty quantification is therefore becoming an increasingly important aspect of the numerical optimisation assisted design.

Clearly, the choice of the optimisation architecture has a significant influence on both the solution time and the final design. Learning from the experience of previous ad-hoc optimisation implementations within the industrial sponsor environment, this POD architecture is preferred to a RANS-in-the-loop one. In fact, the POD strategy presents several advantages. Firstly, the optimisation process is de-coupled from the RANS execution, reducing the risk of failure during the process. Secondly, the generated POD can be re-used to tackle different optimisation problems, as long as the same set of design variables is used. At the same time the POD approach presents also some drawbacks. The model is not guaranteed to be accurate over the whole design space, especially if the problem tackled is highly non-linear. Besides, the number of snapshots required constructing an accurate POD model increases rapidly with the number of design variables. Additionally, when applying this strategy it is important to consider the existence of a “break-even” point, which expresses the number of online evaluations needed before overall cost savings are obtained using the offline procedure. Finally, the mesh used within the CFD process for the generation of the POD model, has to retain its topology, which implies the use of either a structured mesh or mesh deformation technique. The latter approach is used in this implementation with the associated limitations on geometry deformations. To conclude, automated design process is very attractive for commercial aircraft industry as it greatly reduces the development period, and the POD optimisation approach described could be used as a low-

cost, low-order approximation for aerodynamic shape optimisation in an industrial context, given its ability to produce good results in a limited amount of time. It in particular can be applied in a multi-disciplinary environment where CFD is only one part of the optimisation disciplines in a real engineering industrial context.

9 Cost Analysis

9.1 Introduction

Cost is a factor of success in the product/service of many industries. Reducing cost may be essential for survival in today competitive market. Companies are increasingly required to improve their quality, flexibility and innovation while maintaining or reducing their costs. In short, costumers expect higher quality at decreasing cost. Companies unable to provide meaningful cost estimates at the early development phases have a significantly higher percentage of programs behind schedule with higher development costs than those that can provide completed cost estimates [160]. Understanding the cost of a new project development before it begins can mean the difference between success and failure. Generally, cost refers to the amount of money expended incurred with delivery of products and/or services, and it should cover any expenditure of time, human, and physical resources, from the perspective of total cost management [161].

Cost Engineering is concerned with cost estimation, cost control and business planning. Cost Engineering supports companies with decision making, cost management and budgeting with respect to product development by predicting the cost of a work activity. Cost estimate during the early stages of product development influence the go, no-go decision concerning a new development.

Cost estimators need companywide cooperation and support. Concurrent engineering can assist this process. A concurrent engineering environment has been widely adopted and provides an opportunity to substantially reduce the total cost of a project. A fully integrated product development cycle, with multi-disciplinary teams working together, increase the likelihood of a reduced life cycle cost by avoiding costly alterations late in the design process. In fact, there is now a shift towards the analysis of the influence of cost, as defined in more engineering related terms, in an attempt to link into integrated product and process development within a concurrent engineering environment.

9.2 Context

The UK aerospace industry is one of the most successful manufacturing sectors with a turnover of around £20 billion and producing about 10% of UK manufactured exports, with a consistent trade surplus since 1980 [162]. The industry, both civil and military, employs more than 150,000 people and is second only in size to the US, with a world market share of 13%. Already in the late 1980s, the customer was increasingly being considered more explicitly in the commercial aircraft design process through their demand for reduced operating cost and lead-time, whereas technology had been the dominant driver in the past. Aircraft producers now realise that this demand to reduce cost and lead-time needs to be tackled at the conceptual and preliminary engineering design phase. Typically, it is widely agreed that 65–80% of the total avoidable cost is controllable at the early design stage and indeed many authors agree that conceptual and preliminary design have in hand the greatest cost influence.

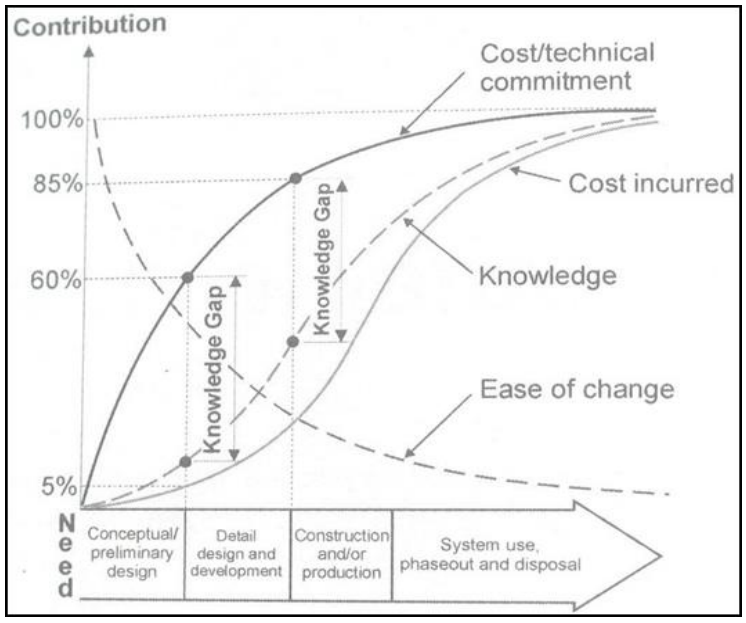

Figure 9.1: The overall aircraft design development process phases related to product life-cycle cost, design knowledge and freedom [163]

Thus, a large proportion of the cost of a new product is committed very early at design stage; long before the actual product development costs occur. In this way the design process accounts for only 10% of the product cost, but indirectly influences up to about 80%. Hence it is important that all the factors, which

contribute to the total cost of the product, are considered at early design stage.

It is claimed that the accuracy of a cost estimate improves with the volume of information available. Cost estimation is a process that provides progressively more accurate information as a project moves from conceptual through final design and construction award. However, cost is not known in advance of production and therefore a cost estimation system is required. As the design cycle proceeds, projects accumulate man-hours of design effort and gain momentum. This makes them increasingly difficult to abort even if a later cost estimate based on the detailed design shows an over-budget condition. Even during these later stages of design, designers typically optimise the functionality and then determine what the cost is rather than doing a full optimisation including costs. If, after the detailed design stage, designs are found to be too expensive, the course of action many companies take is to try to reduce costs by such strategies as changes in manufacturing and the use of different materials, rather than re-designing out the avoidable costs. The likely consequence of this policy is typically a reduction in both cost and quality. Therefore, a wrong decision at this stage is extremely costly further down the development process. Production modifications and process alterations are more expensive the later they occur in the development cycle. Consequently, this results in a more rigorous approach to the issue of cost.

In aerospace engineering there has always been a wide variety of manufacturing alternatives, whether processes, methodologies, or technologies, there are even more materials now available. Data management systems are continually evolving, and improving in computational modelling is being pursued on all fronts, although especially in Computational Fluid Dynamics (CFD) and Finite Element Modelling (FEM) for aerospace applications. However, there is still a basic need for cost tools that help and support engineers in making reasonable and measured design decisions that are cost effective and ultimately, more competitive. Aerospace manufacturers today are searching for techniques to gain a sustainable, competitive advantage in the global marketplace. In the past, technology was the main driver in the aircraft design process. Nowadays, there is a demand of cost reduction in the commercial

aircraft industry to satisfy customers' needs. In recent years, there has been growing emphasis on the need to provide transparency in the costs of engineering programs, leading to growing emphasis on whole-life cost modelling techniques. This has arisen largely due to the increased interest in longer-timescale projects and programs [164]. The main challenges faced by Airlines is to keep low the operating cost, providing high level of service, more frequency of flights to destinations and cheap air fares. Airline companies have to do lot of activities like cutting the cost of maintenance of their fleets and increasing the despatch reliability in order to stay and make money from the business. All this depends upon how the aircraft are designed.

9.3 Cost in Aircraft Design

The importance of engineering costing within aircraft design should have a more directly influential role, for example as part of an integrated process that is embedded within multidisciplinary systems modelling architecture. Ultimately, the goal is that aircraft acquisition is driven by the balanced trade-off between cost and performance leading to affordability and sustainability for operators over the product life cycle. A challenge for the scientific community is to adapt and to exploit the trend towards greater multidisciplinary focus in research and technology, particularly with regard to utilising cost as a metric within the process. Costs are becoming an important factor and aerospace companies are looking forward to reduce the cost without compromising on performance [165]. Cost modelling should be integrated into the design process along with other analyses to achieve efficient aircraft. There is a strong need to understand the cost associate with different competing concepts and this could be addressed by incorporating cost estimation in the design process. This approach can contribute in indicating the cost variation with changes to the design. The aim of the cost estimation methodology is to provide a basis for making a rough cost estimate based on low detail at the early design stage of product design that can later be refined based on greater detail as it becomes available.

The historical objective of minimizing Gross Take-Off Weight (GTOW) in aircraft design is intended to improve performance and subsequently lower operating

costs, primarily through reduced fuel consumption. However, such an approach does not guarantee the profitability of a given aircraft design from the perspective of the airframe manufacturer. Weight based cost estimation relationship however, do not always accurately represent the actual manufacturing cost, and it may not provide accurate sensitivity data for a MDO process. Often a weight reduction will result in a cost increase due, for example, to a requirement for more machining time, closer tolerance etc.

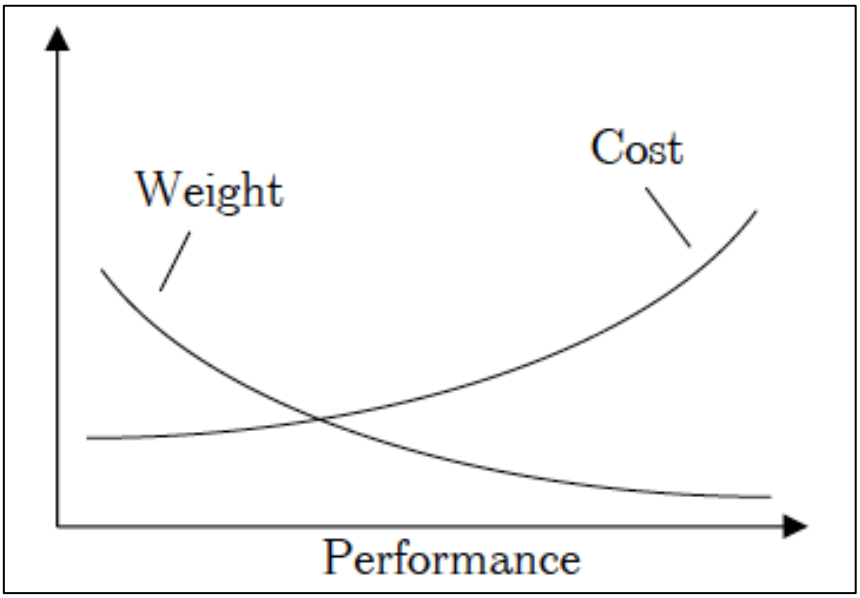

Figure 9.2: Example of Trade-off between cost and weight as a function of the performance of the structural part [166]

Hence, fabrication costs are better correlated to structural layout and complexity than to weight.

Before turning to the field of cost estimation techniques, it is worth to introduce the definitions and concepts of cost as given in Roskam [167].

The cost of an airplane is the total amount of expenditure of resources, usually measured in dollars, needed to manufacture that airplane.

The PRICE of an airplane is the amount of dollars paid for the airplane by customers. PROFIT: PRICE – COST. The evolution of an airplane from design to manufacturing, operational and finally, disposal is referred as airplane programme. It can be divided in six phases:

1. Planning and Conceptual design.

Planning phase consists primarily of mission requirements research. This eventually leads to a mission specification. Conceptual design here consists of the design activities associated with preliminary design (preliminary sizing and preliminary configuration layout and propulsion system integration). Some very preliminary cost studies are also conducted during this phase.

2. Preliminary Design and System Integration.

Refinement of preliminary configuration (layout of wing, fuselage and empennage, weight, drag, polars, flap effects, stability and control, performance verification Landing Gear (LG) disposition, propulsion system integration, cost calculations. Design studies are conducted to find that combination of technology and cost might result in a viable airplane program.

3. Detail Design and Development.

During this phase the airplane and system integration design is finalized for certification flight-testing and production.

4. Manufacturing and Acquisition.

During this phase the airplane is manufactured and delivered to (or acquired by) the customer.

5. Operation and Support.

During this phase the airplane is being acquired by the user and is being operated with the accompanying support activities. (Phase 4 and 5 generally overlap), and as it possible to see from Figure 9.3 it contributes largely at the total cost of aircraft life.

6. Disposal.

This phase marks the end of the operational life of the airplane. This activity can include destruction of airplane and disposal of the remaining material. Disposal becomes necessary when airplane has reached the limit of its technological or economical life.

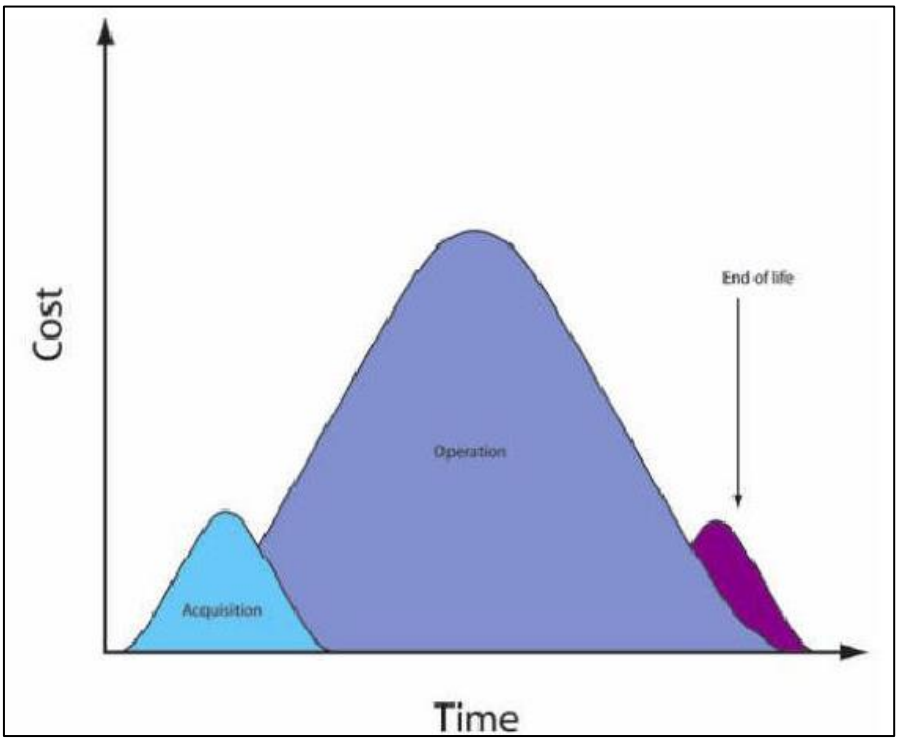

Figure 9.3: Variation of Life Cycle cost over time [158]

The time elapsed during the six phases of an airplane program is called Airplane Life Cycle (ALC). The total cost of an airplane program incurred during the airplane life cycle is called the Life Cycle Cost (LCC), in other words, the overall cost from its conception up to and including its disposal

For preliminary cost estimating purposes the LCC of an airplane program is breakdown into four cost categories:

a) Research and development costs; (Phase 1, 2 3)

b) Production and construction costs; (Phase 4)

c) Operation and maintenance costs; (Phase 5)

d) Retirement and disposal costs. (Phase 6)

Depending on the position in the economic process, a different viewpoint is taken. A part supplier, for instance, might offer his product at the lowest possible price in order to stay competitive. His aim is therefore to minimize the manufacturing cost. The aircraft manufacturer (system integrator), on the other hand, needs to provide his customer with an aircraft that has low design and

manufacturing cost, and that is competitive in terms of operating cost. The operator is finally interested in cost savings throughout the lifetime of the aircraft, i.e. low acquisition, operating and disposal cost.

9.4 Cost Definitions

This section includes a brief explanation of the various cost categories recognised as being incurred by an aircraft producer. The following categorisations are well documented in the literature [169, 170] and are included primarily for clarity and fullness. Some useful classifications that facilitate this process are: (1) direct or indirect costs, (2) non-recurring or recurring

9.4.1 Direct and Indirect Costs

A direct cost is an expenditure, which can be identified and specifically allocated to a product or service. Consequently, they are more easily identified and associated with an end result such as a product, service, programme, function, or project. These costs are typically charged directly to a given contract in the way that procured items can be easily associated with the bill of material (BOM) for a particular aircraft unit. Indirect costs are the opposite of direct, and where direct costs can be allocated directly as the allocation base is known, the allocation base for indirect cost has to be defined. These costs may be difficult either to identify in the first instance or to be associated with a given operation or outcome. Conversely the indirect cost cannot be identified with a specific objective [171]. This means that direct cost can be allocated directly as the allocation base is known, whereas the allocation base for the indirect cost has to be defined. This makes identification and association of indirect cost with a specific objective difficult in the first instance. However, indirect costs are necessary for undertaking an activity and are labelled as overheads or burdens and examples of these are cost of electric power, cleaning, building works, etc.

9.4.2 Recurring and Non-Recurring Costs

Recurring costs are expected to be incurred in a repeating fashion, whereas non-recurring costs are expected to be incurred only once or only at certain

intervals. Recurring costs are repetitive elements of development and investment costs that may vary with the quantity being produced during any program phase. Examples of recurring costs include cost of raw material, engineering efforts required for re-design, modifications, rework, and replacement; tool maintenance, modification, rework, and replacement; labour costs and training. It must be highlighted that the recurring costs per product unit should decrease with the production quantity increasing [172].

Non-recurring costs are those elements of development and investment costs that generally occur only once in the life cycle of a system. A non-recurring cost is typically a capital expenditure, which occurs prior the production. Examples of non-recurring costs include system test, pre-production activities, basic design and development through the first release of engineering drawings and data, basic tool and production planning through initial release, engineering models built for development or test purposes only, and specialized workforce training.

Estimating accuracy is normally improved when repetitive costs are estimated separately from the non-repetitive elements. Costs that have already been incurred and that are not likely to be necessary for the remainder of production, therefore, should be excluded from the estimated cost for the next unit to be produced. If the recurring and non-recurring costs are not properly segregated, then the estimate is likely to be over or understated.

9.4.3 Operating costs of airlines

The operating costs of airlines are generally divided into Direct Operating Costs (DOC) and Indirect Operating Costs (IOC), see Figure 9.4. The direct operating costs are broadly defined as the costs associated with flying operations, and the maintenance and depreciation of the flying material. The indirect operating costs include the operator’s other cost associated with maintenance and depreciation of ground properties and equipment, servicing, administration and sales.

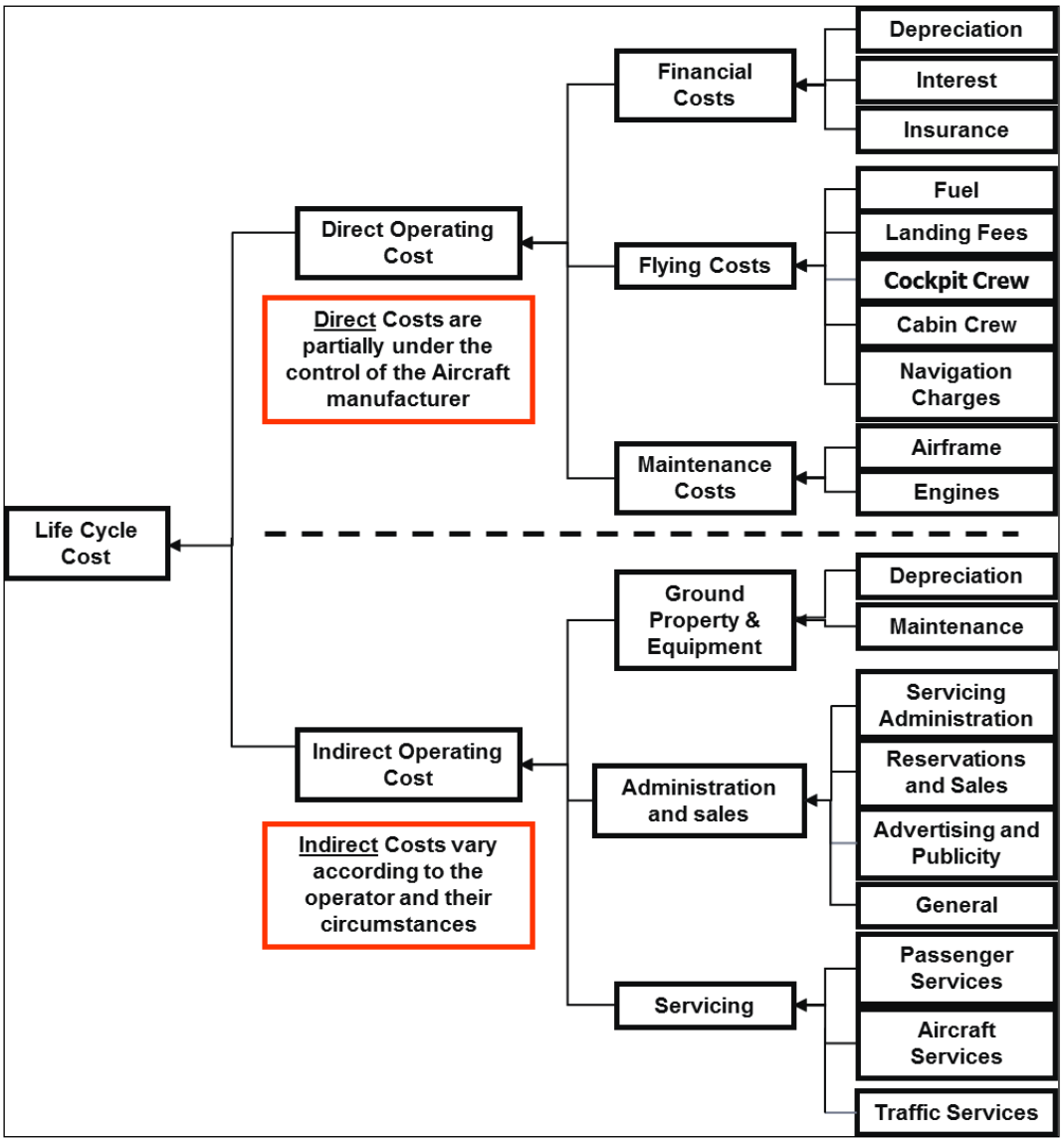

Figure 9.4: Schematic of Airline Operating Costs

The breakdown of the Direct Operating cost is shown in Figure 9.5. The Direct operating cost consists of Financial, Flying and the Maintenance cost. The Financial cost is further decomposed to Depreciation, Insurance and Interest whereas Maintenance cost is decomposed to Airframe and Engine maintenance. The Flying cost includes Fuel, Landing Fees, Cockpit crew, Cabin crew and Navigation charges.

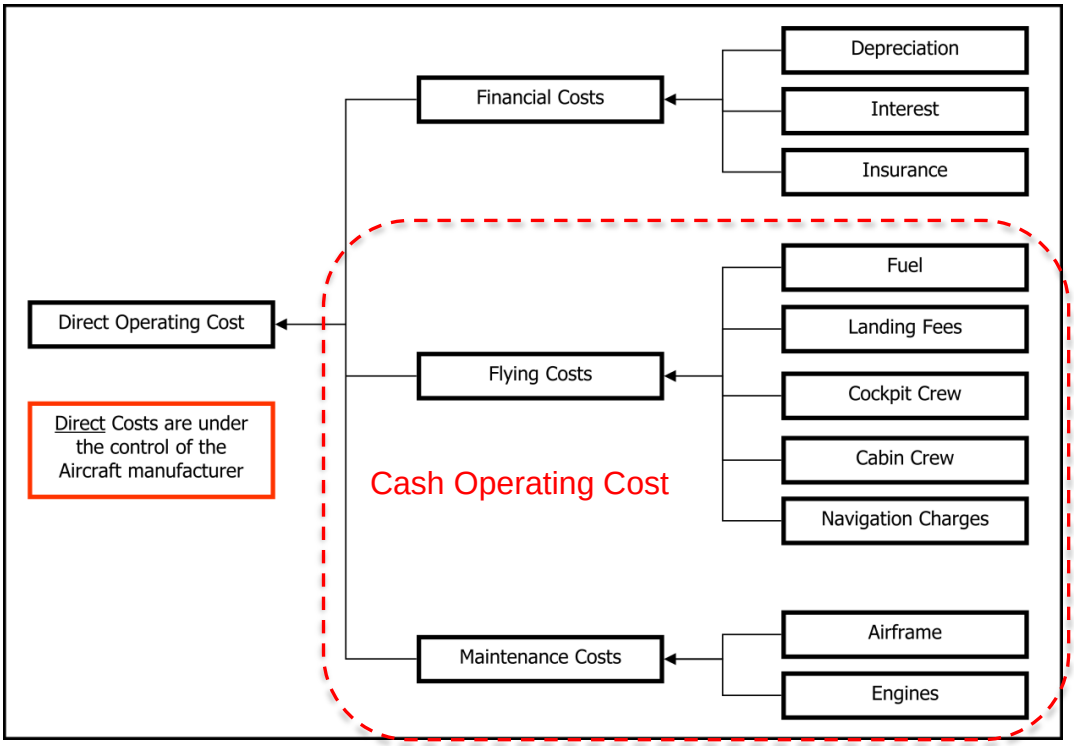

Figure 9.5: Schematic of the Direct Operating Cost

The depreciation, insurance and interest are financially orientated and are then in the cost model generated from the total aircraft price, which is based on the aircraft production cost. The production cost is the summation of the part manufacturing and connection assembly process cost. Both of them include material cost and labour cost. For assembly process, materials refer to additional parts or miscellaneous such as fasteners. The element of crew, fees, and maintenance cost are operating oriented and are consequentially evaluated based on the Airframe weight (AFW). Although the DOC constitute only one aspect of the economic profitability of an airliner, most attention is generally paid to this aspect, for the reason that several factors contributing to the DOC are directly related to the technical conception and operational characteristics of the airplane and as such are under the direct control of the design team [173]. The objectives of a standardized method for the estimation of aircraft operating costs are:

a) to provide a ready means for comparing the operating economics of competitive aircraft and/or aircraft designs under a standard set of conditions

b) to assist airlines and aircraft manufacturer in assessing the economic suitability of an airplane for operation on a given route.

Crew costs form a substantial part of the DOC, but are essentially outside the control of the designer.

Fuel is directly affected by the aircraft engine performance and plane aerodynamic characteristics, but also by the fuel price, which varies significantly geographically and with time. Maintenance cost is an important part of Aircraft Life cycle cost which can reach five times of the ownership cost and accounts for 10-20 % of the Direct Operating cost which makes both the Aircraft manufacturers and Operators to control it. The Airplane Life cycle should summarize the Life cycle cost in Net Present Value (NPV) considering depreciation, taxes and time value of money. The most common element of the life cycle cost, which is used to compare aircraft performance in terms of economic performance, is Direct Operating Cost (DOC) that reflects profit and loss including aircraft depreciation.

In finance, the Net Present Value (NPV) or Net Present Worth (NPW) of a time series of cash flows, both incoming and outgoing, is defined as the sum of the present values (PVs) of the individual cash flows of the same entity. It measures the excess or shortfall of cash flows, in present value terms, once financing charges are met.

Net Present Value can be described as the “difference amount” between the sums of discounted: cash inflows and cash outflows. It compares the present value of money today to the present value of money in future, taking inflation and returns into account. The Internal Rate of Return (IRR) or Economic Rate of Return (ERR) is a rate of return used in capital budgeting to measure and compare the profitability of investments. The term internal refers to the fact that its calculation does not incorporate environmental factors such as the interest rate or inflation.

The internal rate of return on an investment or project is the "annualized effective compounded return rate" or "rate of return" that makes the net present value as:

$$NPV = \frac{NET * 1}{(1 + IRR)^{year}} \quad (9.1)$$

of all cash flows (both positive and negative) from a particular investment equal to zero. In more specific terms, the IRR of an investment is the discount rate at which the net present value of costs (negative cash flows) of the investment equals the net present value of the benefits (positive cash flows) of the investment. In other words, IRR is the discount rate, which equates the present value of the future cash flows of an investment with the initial investment. IRR calculations are commonly used to evaluate the desirability of investments or projects. Return On Investment (ROI) is one way of considering profits in relation to capital invested; Cash Operating Cost (COC) refers to the amount of cash a company generates from the revenues it brings in, excluding costs associated with long-term investment on capital items or investment in securities.

9.5 Overview of different cost modelling approaches

Cost estimation is the process of developing a well-defined relationship between a cost object and its cost driver for the purpose of predicting the cost.
In other words, cost estimating is the process of predicting or forecasting the cost of a work activity. Cost estimation is used to predict costs of alternative activities, predict financial impacts of alternative strategic choices, and to predict the costs of alternative implementation strategies. According to Niazi et al. [174], the first distinction in cost estimation is between qualitative and quantitative cost estimation techniques. Qualitative techniques estimate the cost based on previously manufactured products, and scale the manufacturing cost on the basis of similarities, whereas quantitative techniques are based on design features, manufacturing processes and the material.
Traditionally, there are two main estimates: a “first-sight” estimate, which is done early in the cost stage, and a detailed or bottom-up estimate, to calculate cost precisely later on. The first-sight estimate is largely based on past similar project or purely on experience in costing. To obtain this level of experience take years and considerable input from senior estimators. Although useful for a

rough estimate, this type of estimating is too subjective in today's cost culture; hence more quantified and justified estimates are what is needed. For detailed estimates, cost is based on the number of operations, time per operations, labour cost, material cost and overheads cost. To generate these estimates requires an understanding of the product, the methods of manufacture/process and the relationships between processes. Detailed estimating goes through several iterations because feedback from the relevant departments enables the estimates to be reviewed and improved over a certain timeframe. Curran [172] offers a more detailed classification of estimating methods.

However the most fundamental approaches used in aerospace industry to model cost are the followings:

1. Parametric Cost estimation
2. Generative or analytical Cost Estimation
3. Analogy based Cost estimation
4. Neural-Network-Based Cost estimation

9.5.1 Parametric Cost estimating

Parametric cost models are generally associated with cost estimates or techniques, which deploy 'Cost Estimating Relationships' (CERs) together with mathematical algorithms or logics to establish cost estimates [175]. This methodology assumes that parametric cost modelling is based on data capture. This requires developing required templates and identifying data sources. Most data for parametric cost modelling are obtained from Accountants, Engineers and Process Managers in companies. After the collection of data, there is the need to evaluate variables and respective data attached. By doing this, a decision is taken to identify variables, which change or are likely to change with time. This approach deals with identifying high-level relationships between the cost and the design parameters. The high-level design parameters are usually volume and mass. This approach has positive results towards well-defined class of components. This technique is used to measure or estimate the cost associated with development, manufacture or modification of an end item. This approach has some limitations, the main drawbacks are:

- A significant amount of data is required to identify parametric relationships. It is also difficult the availability of data of adequate quality.
- The cost data should be filtered to remove the effects of inflation, exchange rate etc.
- New manufacturing processes and changes to methods will invalidate the parametric relationships.
- Limited resolution and cannot be applicable beyond narrow class of components.

Nevertheless the above limitations, many industries have adopted parametric estimation as the main means of cost estimation for their design, development and production or implementation phases of engineering projects. In the Aerospace Industry, parametric cost estimates play key role in bidding and target cost estimation, whilst for most component manufacturing industries; parametric cost estimates are used to determine the cost of components [176]. To make good use of parametric models is important highlight that they should not be used outside their database range; they should be used only after they have been verified. In addition they should not be used until a realistic data corresponding to cost drivers can be obtained.

9.5.2 Generative Cost Estimating

This cost estimating techniques use the product definition to get the manufacturing sequence and to estimate the process times. At each phase of the development process, based on technical data, cost related to resource and material consumption are determined. This approach is further divided into Feature recognition and Feature based approach. The feature recognition approach is required when the product model is expressed in terms of design features whereas the Feature based approach requires product definition to be constructed using a pre-defined set of features that have a direct mapping to manufacturing process. The main disadvantages of this approach are:

- This approach depends on rich and detail design definition.
- The algorithms used are expensive and may have narrow capability.
- This approach does not allow the cost to be computed at very early stages of design.

9.5.3 Analogy Based Cost Estimating

The analogous cost modelling method identifies a similar completed product, process or project and reuses cost information associated with this entity to estimate the cost of the new entity, taking into consideration adjustments for the differences between the two [177]. There must be a reasonable correlation between the proposed and the “historical” system. The estimator makes a subjective evaluation of the differences between the new system of interest and the historical system. The analogy method is typically performed early in the cost estimating process. This is early in the life of a potential acquisition program when there may be a limited number of historical data points and the cost estimator may be dealing with technology experiencing rapid technical change. The analogy method is also a very common technique used for cross checking more detailed estimates. In preparing a cost estimate based on the analogy method, start by obtaining a technical evaluation of the differences between the systems from engineers or other experts. Next, assess the cost impact of these technical differences as well as any other factors that may have changed since the existing model was designed and produced (for example increase use of computer aided design and manufacturing). The effectiveness however depends on how accurate the historic data is and how accurate the difference between the two cases is established [178]. A key disadvantage of the analogy method is the subjectivity inherent in quantifying the cost of the technical and other differences between the historical item and the new item. However, the analogy method tends to be relatively fast and inexpensive way of estimating program costs and can be done at a high level of the Work Breakdown Structure with relatively little technical detail about the new system.

9.5.4 Neural-Network-Based Cost estimation

The use of artificial intelligence (AI) system in cost engineering is attractive because there is a good deal of data to handle. The idea is to use computer program that learn the effect of product-related attributes, that is to provide data to a computer so that it can learn which product attributes mostly influence the final cost [179]. This is achieved by training the system with data from past case

examples. The software then approximates the functional relationship between the attribute values and the cost during the training. Once trained, the attribute values of a product under development are supplied to the network, which applies the training data and computes a prospective cost. These systems can produce better cost predictions than conventional regression costing methods. However, in cases where an appropriate cost-estimating relationship can be identified, there are significant advantages in terms of accuracy, variability, model creation and examination. Models can be developed and used for estimating all stages of a product life cycle, provided the data are available for training. A great advantage that a neural network has compared to parametric costing is that it is able to detect hidden relationships among data. Therefore, the estimator does not need to provide or discern the assumptions of a produce-to-cost relationship, which simplifies the process of developing the final equation. Neural networks require a large case base to be effective. This means they are not suited to industries that produce limited product ranges. In addition, the case base needs to be comprised of similar products, and new products need to be of a similar nature for the cost estimate to be effective. They do not cope easily with novelty or innovation, which is actually something we may be trying in our products. With regression analysis, one can argue logically and audit-trail the development of the cost estimate. This is because the analyst creates a cost-estimating relationship based on engineering data, common sense and logic. When considering a neural network, the resultant equation does not appear logical, even if one were to extract it by examining the weights, architecture and nodal transfer functions that were associated with the final trained model. The artificial neural network truly becomes a black-box cost estimating relationship. This is inefficient if your customers require a detailed list of the reasons and assumptions behind the cost estimate.

9.6 Cost requirements in a MDO context

The majority of existing cost models looks at a specific manufacturing process or a particular aspect of maintenance and, hence, do not provide the complete picture. The challenge is to look into all the aspects of cost and to link these into

the decision-making process at the conceptual stage, so that a design-oriented capability can be used to implement product changes that reduce cost [180]. Cost modelling should be integrated into the design process along with other analyses to achieve economic and efficient aircraft [181]. Multidisciplinary Design Optimisation is a tool used in the design process to improve aircraft performance. It considers concurrently different disciplines such as Structures, Aerodynamics, Hydraulics, Propulsion, Weight etc. to achieve substantial benefits. Costs are becoming an important factor and aerospace companies are looking forward to reduce the cost without compromising on performance. Multi-disciplinary design, analysis and optimisation methodologies have traditionally been applied at preliminary design stage often trading weight against drag. The objective was to improve direct operating cost, payload or speed by reducing structural mass without compromising drag. However, whilst lower aircraft weight is important, the process must take into account all the development phases including manufacturing processes and their associate costs. It is essential that manufacturing costs are included in any MDO method that is intended for serious use in the aircraft design. MDO has to enable the trade-off between the cost and performance. There is a strong need to understand the cost associate with different competing concepts and this could be addressed by incorporating cost estimation in the preliminary design process. This could be achieved by having a product definition as an input to the cost model so that any change in the design is reflected in the estimated cost. According to the Aircraft Architects, the Direct Operating Cost (DOC) should be considered and the cost model has to be capable to calculate DOC. The Net Present value (NPV) cost measure has to be adopted and hence the output of the cost model should be in terms of NPV, which is very important from the Airline perspective. The Manufacturing cost should be in terms of features of the components like geometry of the part, number of parts required for assembly etc. This structure is required in order to know what the reasons for the change are in the manufacturing cost. This structure will also assist sensitivity analyses in order to take decisions during the design stage. The maintenance cost should be broken down to scheduled and unscheduled to support the impact of maintenance cost

to be analysed. The manufacturing cost should be broken down to Raw Material costs, Labour costs, Bought out items cost and Profit and Levies. The Flying cost should be broken down to Fuel, Landing fees, Cockpit crew, Cabin crew and Navigation charges. The cost model should be capable to calculate all the above-mentioned flying costs. Moreover, it needs to include recurring and non-recurring costs – e.g. fuel consumption and cost to build first aircraft – including development, tooling, design and production.

9.7 Description of Cost Suite

The analysis of the available cost models indicates that none is well suited for providing a MDO cost model. These existing models have neither the flexibility nor the level of detailed required handling the complex wing design problem. Accurately representing all the details of manufacturing complexity is difficult for a parametric model, given that it must include all the product and process specific parameters that can influence the parametric cost model. The key feature of the cost suite is that it captures the attributes of a design that drive the manufacturing cost, which generally is not only weight, but also the physical geometry of the aircraft. This enables the assembly and detailed manufacturing costs, to be established by means of a relatively detailed component layout by the use of Knowledge Based manufacturing rules. In addition, the parameters from one area have an impact on other areas e.g. the configuration of the Aircraft has a direct influence on the required Design and Production Engineering Effort, as well as the costs required for Tooling. The Model Suite also takes into account the impact of a design on the Operational cost (particularly Maintenance) by taking into account the major features of the Design generated as part of this process. The Model Suite also takes into account the impact of a design on the Operational cost (particularly Maintenance) by taking into account the major features of the Design generated as part of this process. The model is built with the integration of Excel and the Visual basic interface. The tool is designed and intended for use, early in the Design phase of an Aircraft, to estimate the change in cost when different design decisions are made. It is not designed to accurately predict the absolute

cost, which is clearly down to the Finance office. Moreover, the cost suite does not take into account any disposal related cost. New types of flaps have been also implemented, specifically the fixed vain flap and double slotted flap, and new stringer types such as omega and J stringers, to give better clarity to the impact of cost on competing design solutions.

The starting point of any trade is a collection of parameters provided from an external data source. Firstly, a set of parameters is derived from geometric models that are coupled with the cost model spreadsheets. The list of the inputs parameters is reported in Table 9.1. The minimum requirement for the cost model to run is the High Level description.

Table 9.1: List of Top-level inputs

Wing span
Wing Root Chord
Wing Kink Chord
Wing Tip Chord
LE sweep inboard
LE sweep outboard
Trailing edge sweep
Spanwise position of wing root
Spanwise position of wing kink
Position of IB engine
Position of OB engine
Wing Box chord at root
Wing Box chord at kink
Wing Box chord at tip
Inter spar rib pitch
Kink / Span ratio
Wing root thickness / Chord ratio
Wing kink thickness / Chord ratio
Wing tip thickness / Chord ratio
Leading edge chord ratio

Wing area
Slat area
Flap area
Ailerons Area
Spoilers Area
Fuselage diameter
Fuselage length
Fuselage height
Distance between ground and CL of fuselage
Distance between main legs
Area of tail fin (VTP)
Area of horizontal tailplane (HTP)

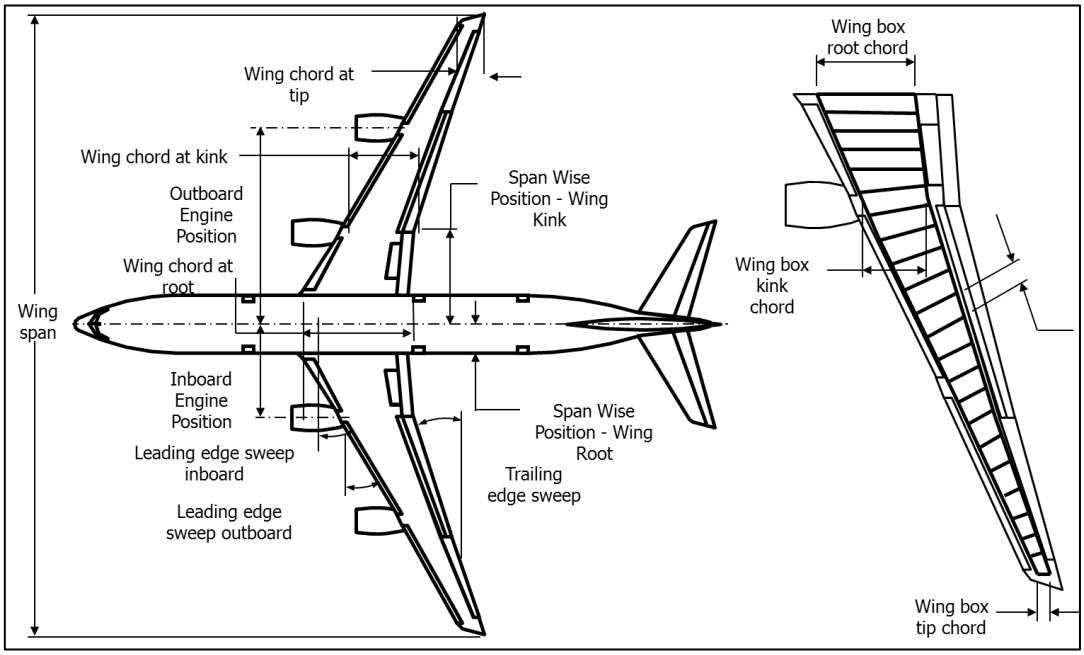

Figure 9.6: Schematic of wing geometry inputs

The geometric parameters are then multiplied with or divided by applicable constants or rates. This is followed by a considerable number of calculations to arrive at cost estimates. These calculations make use of assumed definitions, user-defined definitions and predefined formulas. The user-defined definitions are the values that the user of the cost model can modify to drive the cost

model. They are usually choices that modify the behaviour of the cost model formulas through the use of 'IF-THEN' rules. The cost suite is made up of eight modules as shown in Figure 9.7.

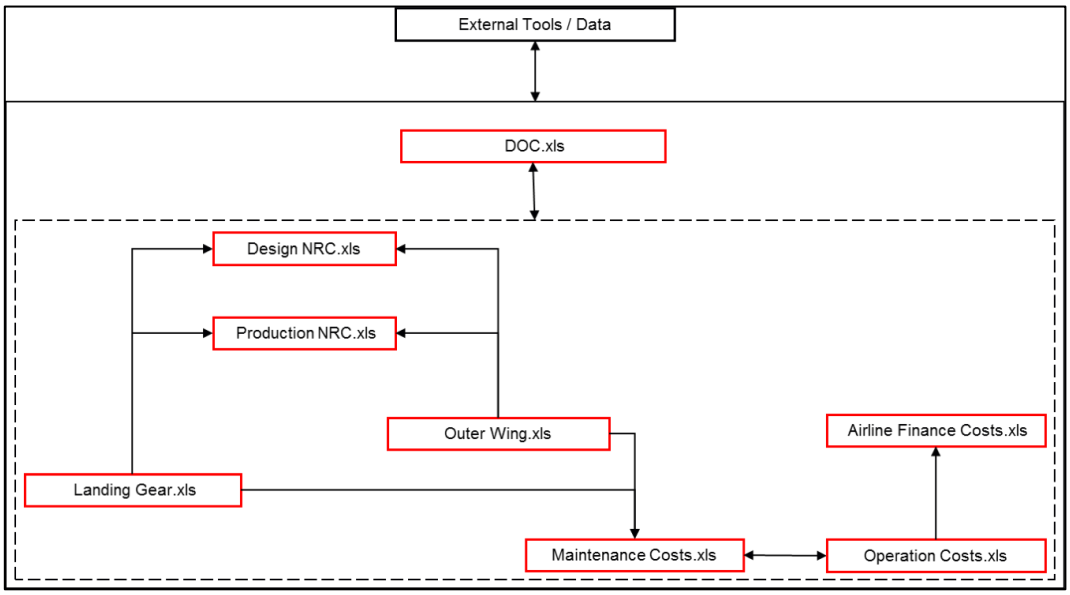

Figure 9.7: Cost model architecture

It is made of two manufacturing modules for Wing and Landing Gear (LG), a design, a production, a maintenance, an operational and an airline finance module, and all these feed the DOC cost modules. All models contain two key sheets: "EXTERNAL – INPUTS": Inputs from other models in the framework.
The individual models will make their own assumptions if an external input is not provided to enable them to be run stand-alone.
"OUTPUTS": Outputs to other models in the framework, and the values required by the DOC model to enable the final outcome of a trade to be generated. The modules receive outputs from a variety of domains, to enable the effects of a physical design change to be estimated. All costs are time based to enable cash flows for both Manufacturer & Airline to be evaluated. This model accounts for only Wing and LG but not consider the fuel and Hydraulics systems in detail.
The manufacturing processes are derived by Knowledge Elicitation/Benchmarking interviews with Production Engineers – Industrial from a wide range of companies, supplying components & assemblies to identify the best assumptions. The process involves the identification of the main features

that drive the manufacturing process. Create a simplified manufacturing process, create the basic manufacturing process models and create the database of assumptions. These assumptions, around 3250, are single values associated to parameters such as time to perform operations based on the features of a part / assembly, machine costs per hour, labour cost per hour, inflation applied to labour cost, assumed percentage procurement levy charged by external supplier etc. Table 9.2 gives an example of assumptions.

Table 9.2: Example of assumption

Description	Short name	Values	Category	Values	Applies To
Set up to X Ray Weld	setUpToNDTIntegralPanel	2.5000 Hours	AdditionalGeneralTimes	2.50000000	Integral Panels
Time to visually inspect weld prior to X Ray	visuallyInspectWeldTime	50.0000 Metres per Hr	AdditionalOpTimes	50.00000000	Integral Panels
Preperation - Set time before drilling Skins to Ribs operations	skinToRibDrillSetTime	4.0000 Hours	AssemblyGeneralTimes	4.00000000	U Box (Stage 2), Stage 1.
Time to produce Countersink	skinToRibCSKHoleTime	0.0167 Mins	AssemblyOpTimes	0.16670000	U Box (Stage 2), Stage 1.
Number of Holes produced before changing tool (metallic)	ribToSparDrillLifeMetal	120	AssemblyProcessAttribute	120.00000000	U Box (Stage 2), Stage 1.
Deburr following machining	spoilerJackBrktDeburrTime	0.1667 Hours	BenchGeneralTimes	0.16670000	Spoiler Jack Brackets
Time for Chemical Milling (Mark up & Mask, etc.	chemiMillSkinLE	0.1400 Hrs per Sq M	BenchOpTimes	0.14000000	Leading Edge pylon skins
Slat Track guide rollers (upper & lower)	defaultSlatTrackRollerCost	126.00 USD	BOFCosts	126.00000000	Slat Track Rollers
The approximate mass of a Top Skin Cleat including Fasteners	approxTopSkinCleatMass	0.0750 Kg	Component Weight	0.00850000	
No of Bushes fitted to jack bracket (2 hinge, 2 jack)	spoilerJackBrktBearingQty	4	ComponentQuantities	4.00000000	
Distance between riblets in D Nose	Riblet_pitch	0.2262 Metres	ComponentSpacing	0.22620000	D Nose Riblets
Time to remove from layup tool & fit to form tool	insertSkinTimeUBox	3.0000 Hrs	CompositeGeneralTimes	3.00000000	U Box
Assumed thickness of single Glass layer	thicknessGlassCloth	0.00025 Metres	CompositeMatlThickness	0.00025000	Top & Bottom Skins (Composite).
Tape Width assumed for smaller wing skin panels (to achieve required part definition)	tapeWidthWingSkinSmall	0.1524 Metres	CompositeMatlWidth	0.15240000	Composite Wing Skins
Time to cut Glass protection layer	cutGlassLayer	100.0000 Metres per Hour	CompositeOpTimes	100.00000000	Various Parts
Capacity of tape spool (typical of AFP Machines)	tapeCapacityAFP	100.0 Kg	CompositeProcessAttribute	100.00000000	U Box Skin
The typical number of seperate orders made per annum	batchesPerAnnum	12	EconomicConditions	12.00000000	Various Parts
Failsafe strap manufacturing time (12 minutes assumed).	failSafeStrapManufTime	0.2000 Hours	FabricationGeneralTimes	0.20000000	Slat Ribs
Profile edge of Access Panel Landing using Router	profileTimePanelLanding	200 mm per minute	FabricationOpTimes	200.00000000	Leading Edge Access Panel Landings
Tag distance	subSparTagSpacing	0.2000 Metres	FabricationProcessAttribute	0.20000000	Sub Spars (L/E)
Swagelock Pin baseline cost (Typically ABS0548VHK5)	Cost_Hilite_med	1.47 USD	FastenerCosts	1.47000000	Various Parts
Typical fastener pitch nut plates Trailing edge panels	fastenPAccessPanelNutPlate	0.0400 Metres	FastenerPitch	0.04000000	
4 per hinge	spoilerHingeFastenQty	8	FastenerQuantities	8.00000000	
Number of faces typical of spar joints	sparJointNumberFaces	6	FeatureQuantities	6.00000000	
Assumed minor dia meter for manhole aperture.	mahnoleMinorDia	0.3500 Metres	FeatureSizes	0.35000000	
Usually self assessed as part of the process.	InspectionAllowanceAssembly	10 %	InspectionAllowances	10.00000000	Various
Average UK High cost machining rate	aveUKHighCostMCRate	159.04 $ per Hour	LabourChargeRate	159.04000000	All High Cost Machine processes (external UK)
Time to machine pin (Trailing edge)	pinMachineTime	0.4500 Hrs	MachineGeneralTimes	0.45000000	
Volume Removal Rate (rough machining)	alGearRibRoughMachineVRR	0.041675 Cu M per Hr	MachineOpTimes	0.04167450	Gear Rib
Assumed Cutter RPM finishing (inter spar ribs)	Rib_RPM_finish_today	25000 RPM	MachineProcessAttribute	25000.00000000	Inter Spar Ribs
The maximum depth of rib (between skins) that can be extruded	maxDepthExtrudeRibs	1.2500 Metres	ManufacturingLimits	1.2500000000	
General density (Titanium)	Density_titanium	4507 Kg per Cu M	MatlDensities	4507.0000000000	
AFP tape for composite top skins	defaultCarbonCostTSkinAFP	120.00 $ per Kg	RawMaterialCosts	120.0000000000	Top Skins & Stringers
Raw material wastage associated with leading edge access panels	panelWasteLE	20.0 %	RawMatlAllowFactor	20.0000000000	Leading Edge Lower Access Panels
Allowance on Length	ribBilletLengthAllow	0.0500 Metres	RawMatlAllowLiteral	0.0500000000	Inter Spar Ribs
Material gauge for side beams	sideWebSheetT	0.0032 Metres	RawMatlGauge	0.0032000000	Flap Support Beam (parts)
Width single TOW	defaultTapeWidthAFP	0.0127 Metres	RawMatlSize	0.0127000000	U Box
Flap Beam Mount to Rear Spar raw material volume	flapBeamMtgBilletVolume	0.000750 Cu Metres	RawMatlWgt&Volume	0.0007500000	
Assumed allowance fo scrap / rework (all components - processes)	allowanceScrapRework	3 %	RecoveriesAndAllowances	3.0000000000	Various
Size of panel where larger Tape widths can be used.	compositeWSkinLargeArea	38.00000 Sq M	SizeFactors&Constants	38.00000000	Composite Wing Skins
Cost per sq metre Krueger as a factor of its area	factorKruegerCost	2323 $ per Sq M	TopDownCost	2323.0000000000	
Ratio of part to raw material for teatments (made from composite parts)	percentVolComposite	95.00 %	TreatmentFactors&Constants	95.0000000000	
Anodise & Prime:	timeAnodiseAndPrime	0.6158 Hrs per Sq M	TreatmentProcessTimes	0.6158000000	Various

While there are many sections in the Wing and LG modules the core "Estimating" sections are illustrated in Figure 9.8 below.

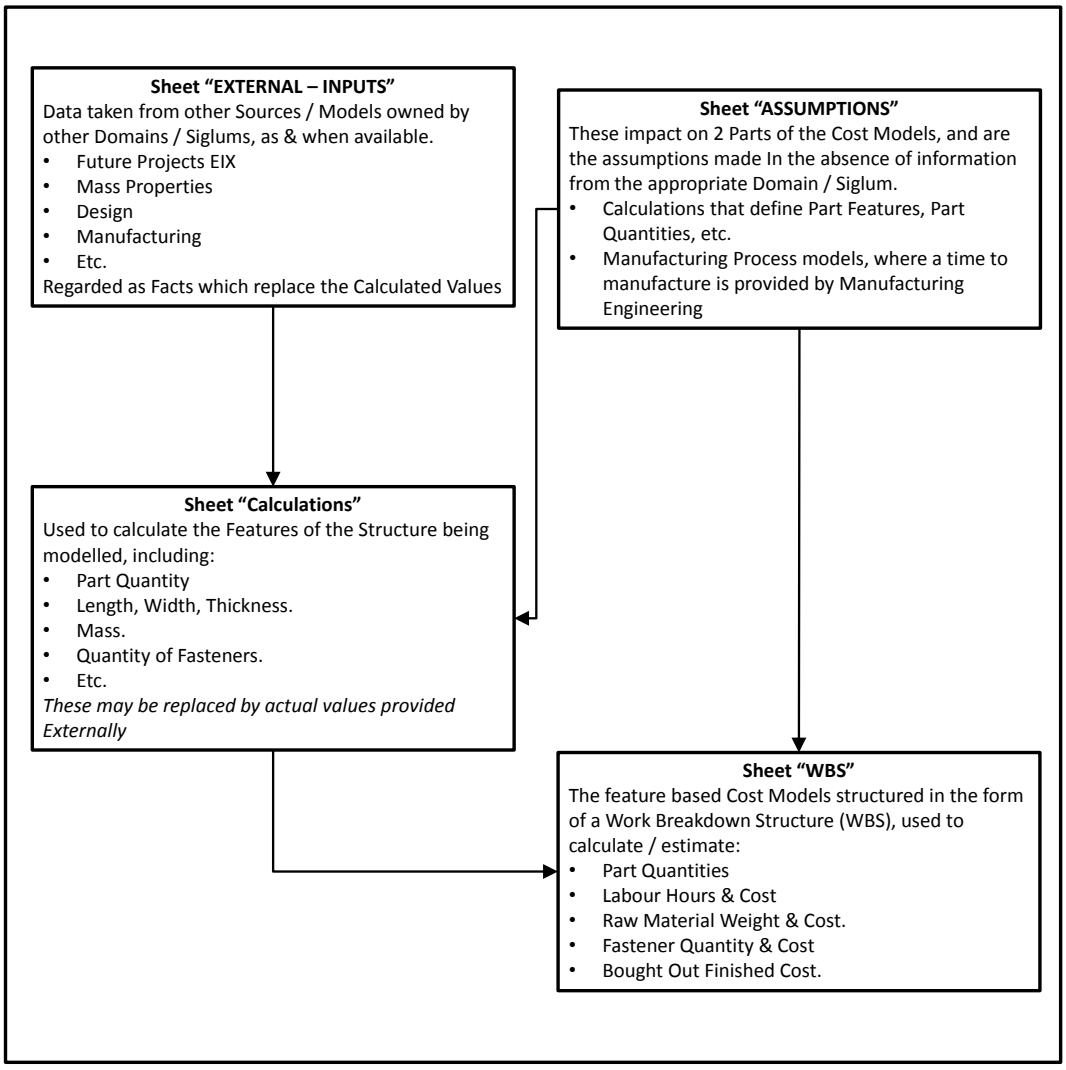

Figure 9.8: Schematic of core estimating sections

9.7.1 Modules Dataflow

Manufacturing modules: These modules enable to consider the cost impact of a number of technologies/design solutions for the structural elements of Wing and Landing gear. Both modules take inputs from geometry, primarily high-level parameters to define the basic airframe, and from other domains to define the physical product such as number of parts, weights and etc. Moreover, they as input require shared project, program & financial assumptions.

They output manufacturing costs for the 100th & development aircraft to DOC model, part count to define physical design task to Design NRC model, parts

lists, part count & process type to define physical production engineering task to Production NRC model. Major structural type (Metallic/Composite) and landing gear configuration (number of legs/wheels) to the maintenance cost model for the wing and landing gear module respectively. The data flow for the Manufacturing Wing module is shown in Figure 9.9.

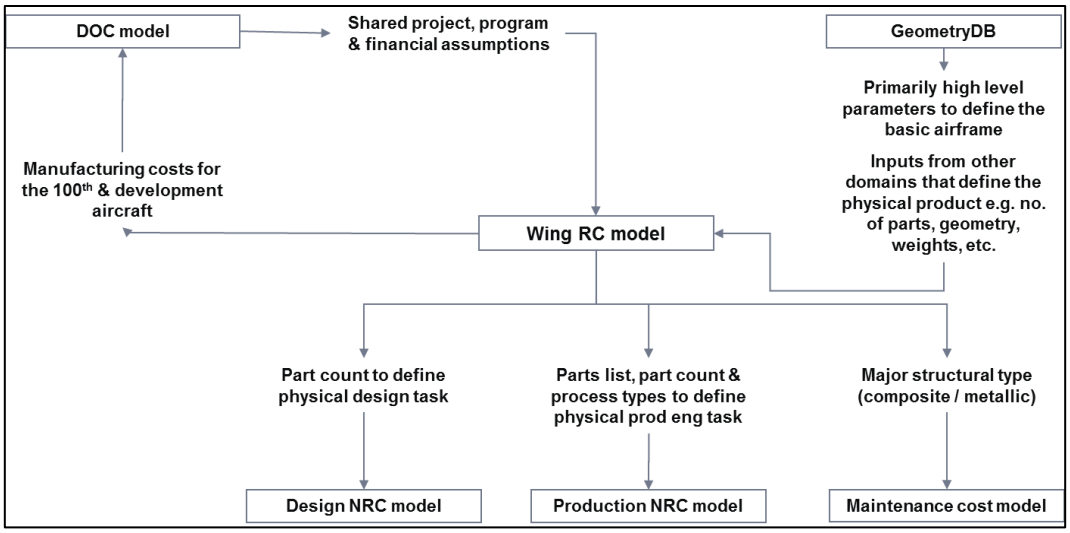

Figure 9.9: Wing RC Data flow

The wing module can be broken down into six basic components:

1. An External Interface Module – Sheet that takes data from a variety of different data sources.
2. A database of Sizing Assumptions & Manufacturing constraints.
3. A Structural Sizing Module that determines configuration of Wing.
4. A series of Manufacturing models compiled in the form of a Work Breakdown Structure (WBS)
5. A database of manufacturing times & material conditions used by the manufacturing processes.
6. A database of cost assumptions built on a single Excel Spreadsheet.

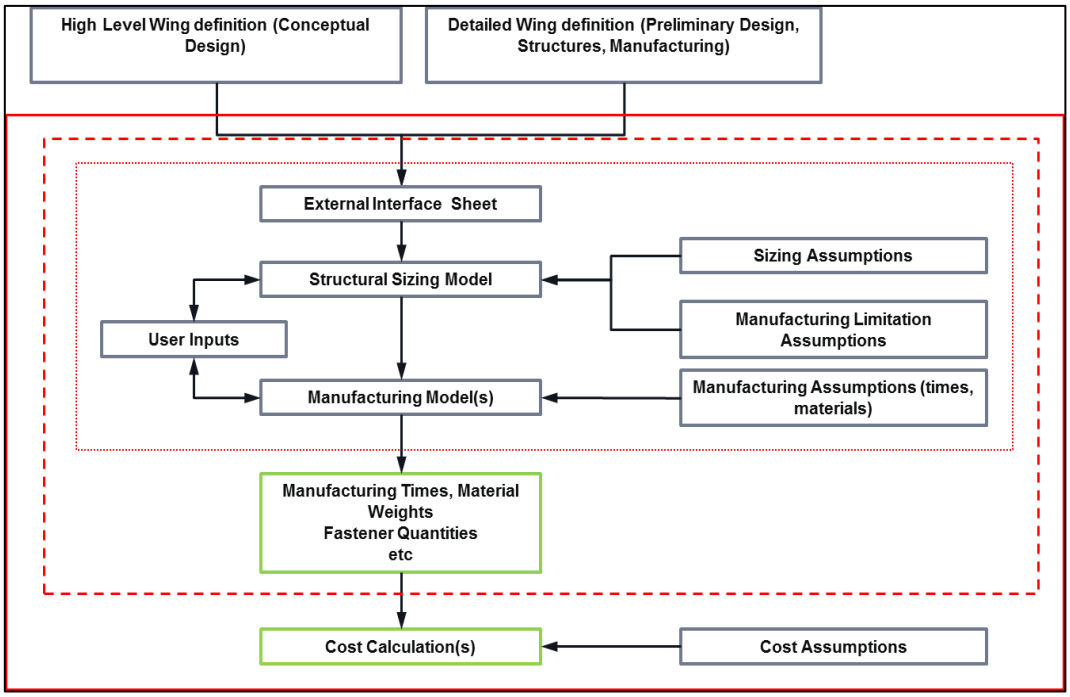

Figure 9.10: Wing module broken down

The main Key element and largest part of the wing module is the structural sizing routines where the configuration of the wing is determined, a sample of which is shown below, this is typical of both the logic flow and level of math. Tool uses the concept of features to drive manufacturing processes. The features may be geometrical, quantity, volume (component, component feature, and raw material), material density, etc. Features derived using Simple Rules of Thumb Heuristics, originally compiled from Knowledge Elicitation Interviews with Functional Design Experts in the areas of leading edge, trailing edge, and wing architects. In Figure 9.11 is reported just an example of wing sizing routine.

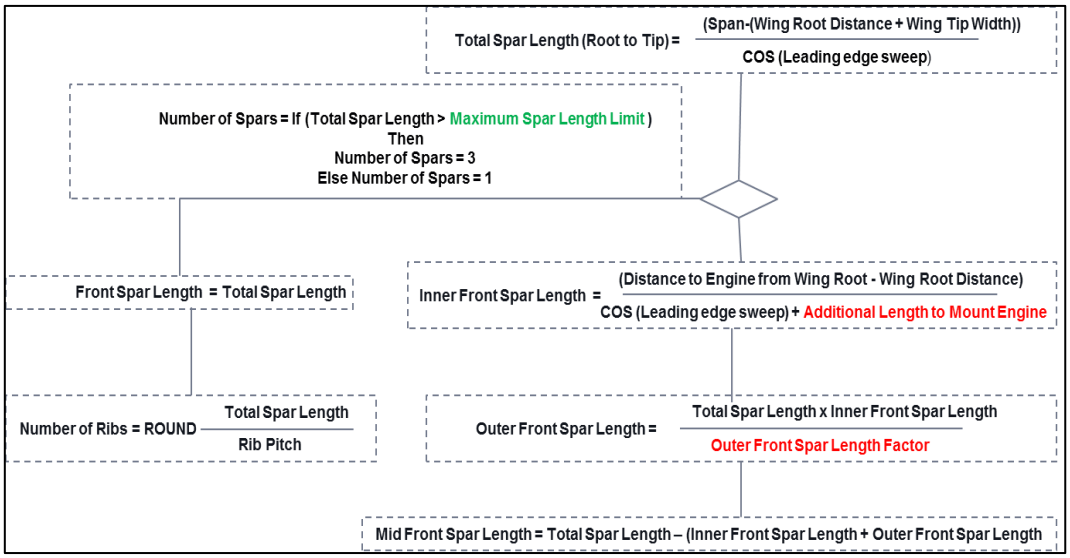

Figure 9.11: example of wing module sizing routine

The data flow for the Manufacturing LG module is shown in Figure 9.12.

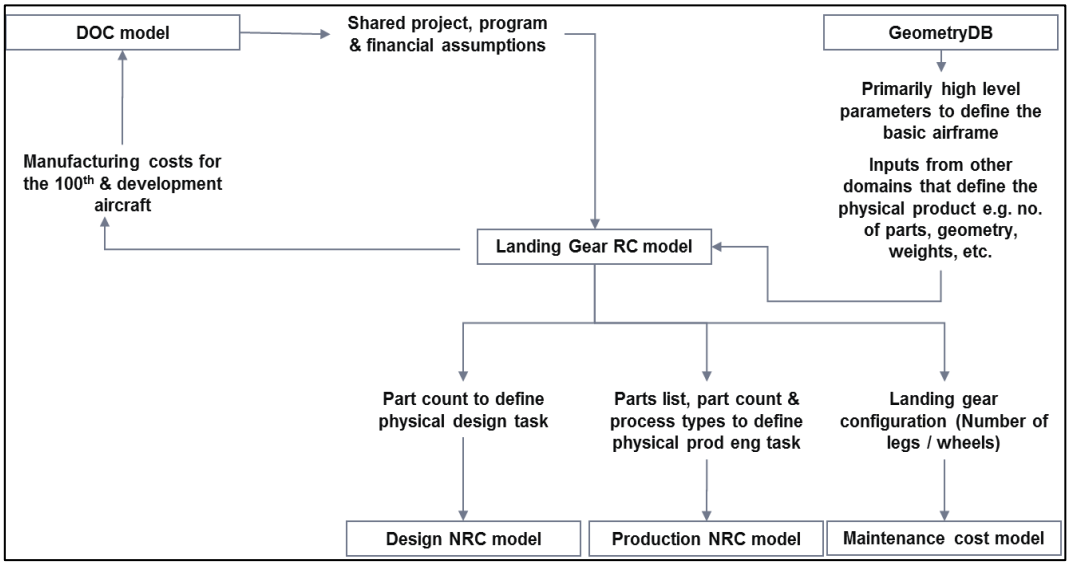

Figure 9.12: Landing Gear RC Data flow

Design NRC: This module enables to calculate the cost related to non-recurring design activities. The inputs required are high level parameters to define basic airframe, number of components that constitute the wing and the landing gear, shared project, program and financial assumption. It outputs the annualised non-recurring cost for all the design activities. Its data flow is shown in Figure 9.13.

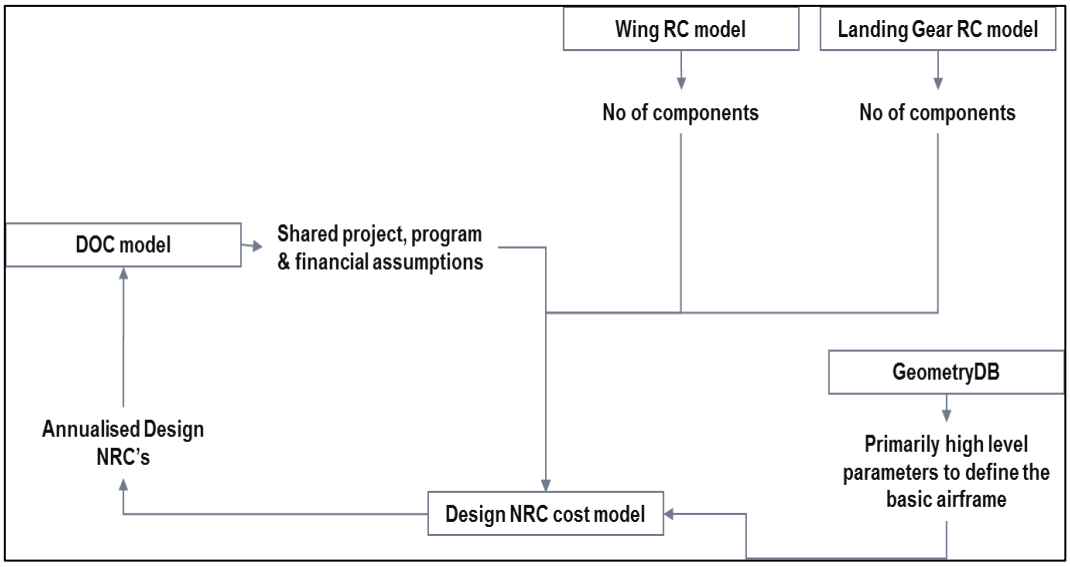

Figure 9.13: Design NRC Data flow

Production NRC: This module enables to calculate the cost related to non-recurring production activities. The inputs required are high-level geometric parameters to define basic airframe, information about wing part quantities, components, process types and manufacturing location to define physical production engineering task. As the other modules it needs shared project, program and financial assumption. It outputs the annualised non-recurring cost for the production activities.

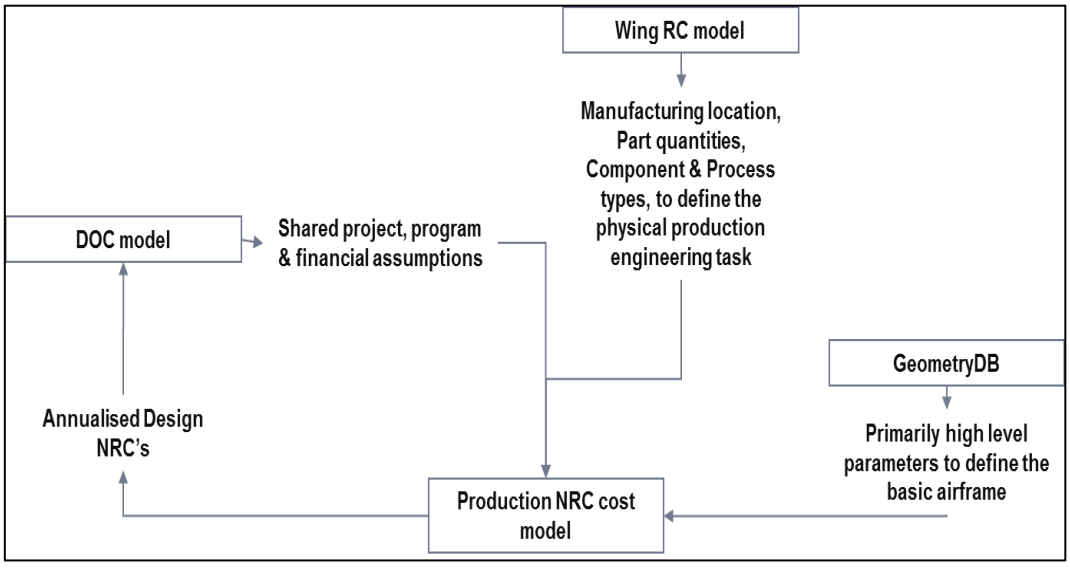

Figure 9.14: Production NRC Data flow

Maintenance: This module enables to calculate the cost related to scheduled and unscheduled maintenance. The inputs required are high-level geometric parameters to define basic airframe, information about wing part quantities, and structure type, landing gear configuration, and shared project, program and financial assumption. It outputs the annualised maintenance cost.

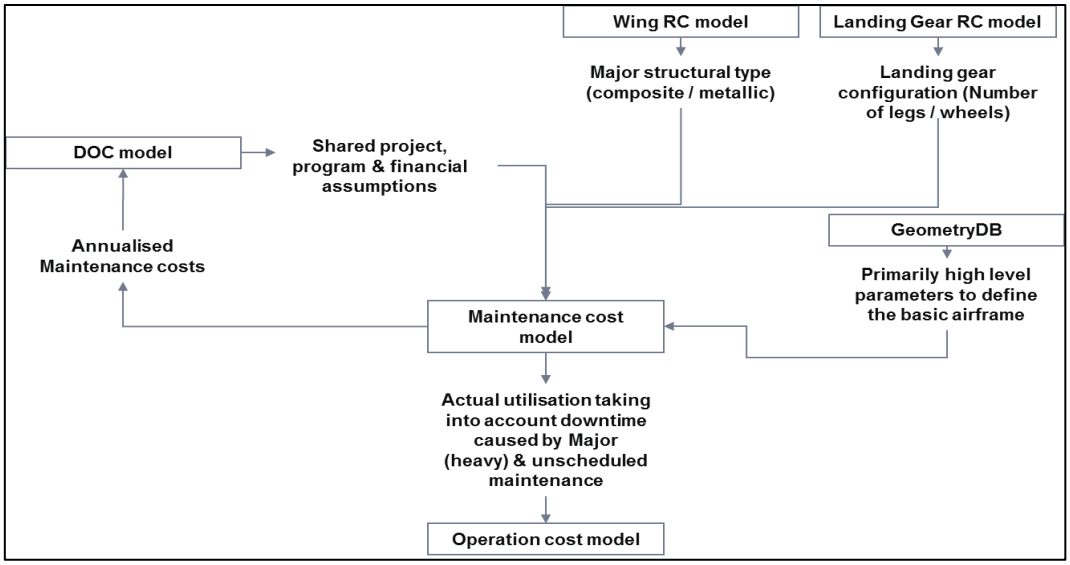

Figure 9.15: Maintenance Data flow

The maintenance cost is broken down into Scheduled and Unscheduled maintenance. The scheduled maintenance cost includes the cost incurred after each transit, daily and weekly maintenance and heavy maintenance whereas unscheduled maintenance includes the maintenance cost for sub systems like APU, Fuselage, Hydraulic etc.

Operational: This module enables to calculate the operational cost. The inputs required are high level geometric parameters to define basic airframe shared project, program and financial assumption and info from the maintenance module such as actual aircraft utilisation taking into account downtime caused by scheduled and unscheduled. It outputs the annualised operational cost.

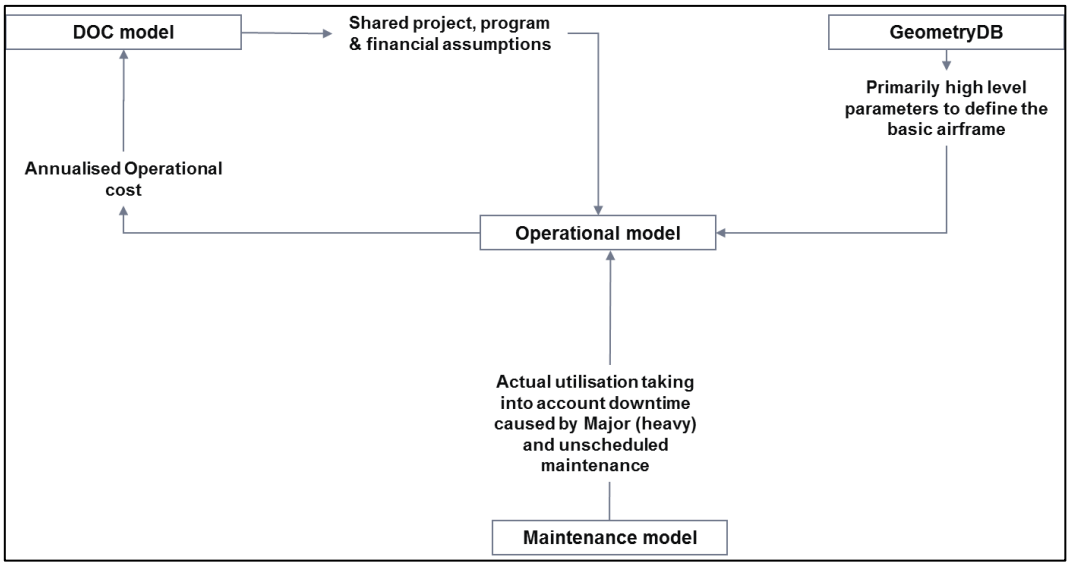

Figure 9.16: Operational Data flow

All the described modules feed the DOC module, as described in Figure 9.17.

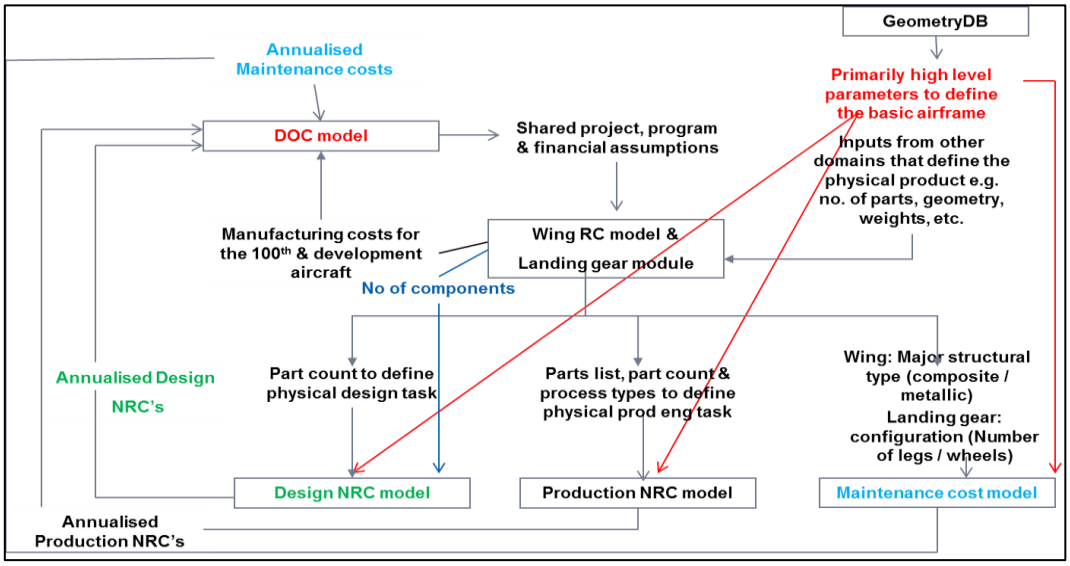

Figure 9.17: DOC Data flow

To summarise, the model is capable of calculating the Direct Operating Cost and provides the output in terms of both net present value and the absolute cost. Direct operating cost is the summation of Depreciation, Flying cost and Maintenance cost. The depreciation is calculated for only wing and landing gear and does not account for Fuel systems and Hydraulic systems. DOC framework considers the cost of development aircraft to calculate DOC. It also accounts

Non-recurring cost limited to design, production engineering and tooling cost, but it does not consider facilities cost.

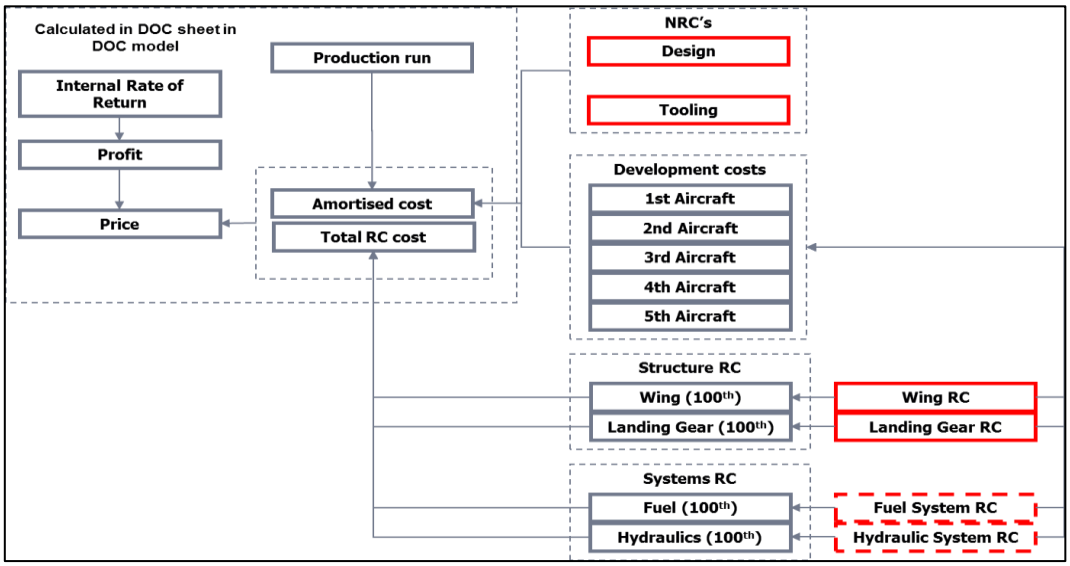

Figure 9.18: Cost breakdown structure (depreciation)

The cost model is partly capable of doing the risk assessments like sensitivity analysis, uncertainty, and probability. It is capable to make a robust Trade-Off between Performance, Weight, Manufacturing and Cost. The model displays the output graphically, which is helpful for the analysis.

9.7.2 Capability Limitations

The Cost suite should not be used to provide a commercial estimate, as it does not take account actual commercial considerations such as specific supplier conditions (Location, Charge Rates etc.). It does not provide a cost for the whole Wing and excludes components that are unlikely to be affected by relatively small changes in configuration and components that where considered unrealistic to model, either because they were too specific to a particular Design/Project or that their contribution has such a small impact to the overall cost. The types of fastener are limited to around 30 different generic functional types, identified as typical for a wing. The manufacturing processes limited to 7 types and treatments only covered at a very high level.

The technologies covered (but not exhaustive) are:

- A Composite Wing (Spars & Wing Skins) using different types of Lay Up (ATL v AFP).
- Conventional Metallic Wing, with provision to configure and compare different methods of Panel Manufacture.
- Advanced Materials for Major Components, Alternative LG Mounting Options.

The financial and economic assumptions are based on 2014 data.

9.7.3 Model Center Version

There are two key software tools that are used to assist generally in the Multi-Disciplinary (MD) integration framework that should be emphasized. The first tool is the general platform that allows data management and navigation to the structural and aerodynamic tools/data, which have been classed as clients. This tool only manages a MD data interface and does not necessary handle the domain specific data transfer between applications, but can be used for this. As such, the tool does not replace the existing data management capabilities within individual domains, but rather acting to enable domain collaboration of data. This is shown in Figure 9.19 along with actual tooling user interface in Figure 9.20.

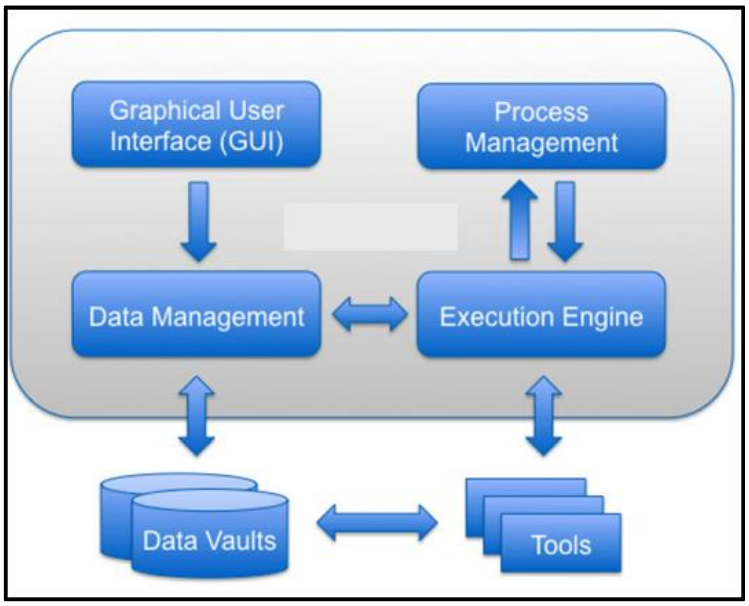

Figure 9.19: Collaboration framework within data management tool

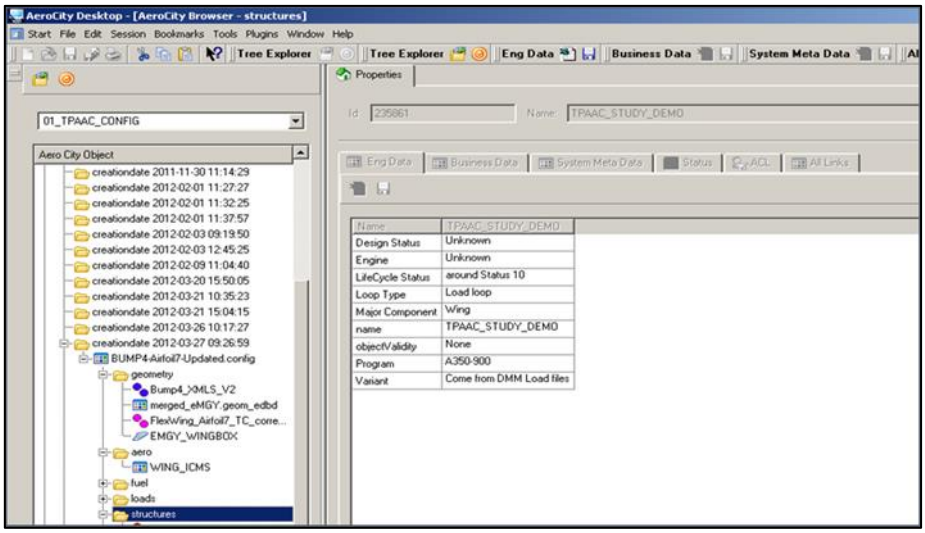

Figure 9.20: User work area of data management tool

The other software tool is Model Center. This is integration/process building environment. It allows other programs and components to be ‘wrapped’ into a generic workflow within it. One of its attributes is that components residing on any connected computer system can be used, including those using different operating systems. Also a designed component only exposes the data, which will be frequently changed by the users. The Cost suite has been integrated in Model Centre integration framework, see Figure 9.21, and automatically can take the input from external domain giving capability to link to other Domains Tool Sets. Changes in one cost model that impact on another model are passed automatically. The Outer Wing Module is the wing manufacturing cost calculations. The Landing Gear Module is the Landing Gear manufacturing cost calculations. The Design NRC Module calculates non-recurring costs for the design process. The Production NRC Module calculates non-recurring costs for the production process. The Maintenance module calculates both scheduled and non-scheduled for maintenance. The Operation module estimates operating costs, throughout the life of the aircraft, except disposal cost.

The Operation module appears twice to resolve circular dependencies between the modules. The first instance is a limited calculation and only provides the variables and calculations required by the Maintenance module. The second instance does the full calculations, using the final results from the maintenance module. The DOC module combines the results from the other modules to

provide total costs. Like the Operations module it appears multiple times to resolve circular dependencies between the modules. The first instance only generates the variables and calculations required by the other modules. The second instance does calculations required to get the aircraft price, required by the Airline Finance module. The final instance does the full calculations, using the final results from all the other modules. The Airline Finance module calculates insurance, depreciation, and financing costs for the operator.

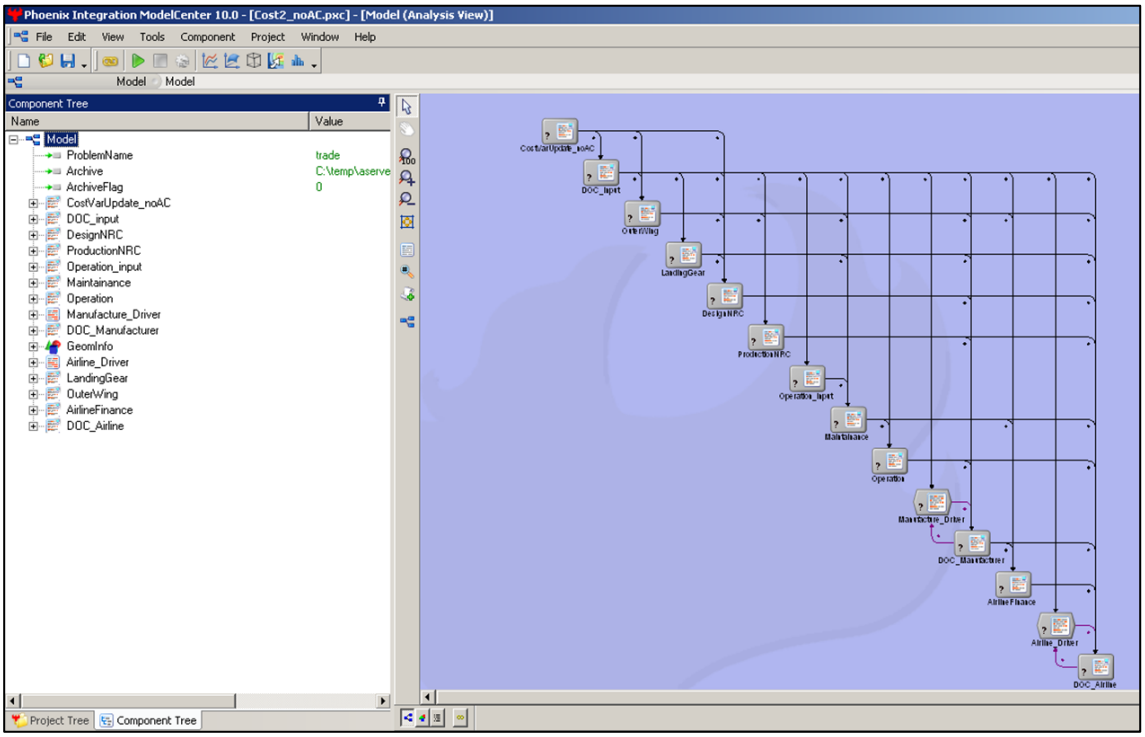

Figure 9.21: Model Center view of the cost suite

In Figure 9.21 is possible to see that two converger components are used, they are called manufacturer driver and airline driver. The converger component provides an easy way to add feedback loops to a Model. The converger component in Model Center employs a fixed point iteration scheme meaning that computed values are directly linked back, unmodified, to guessed values. The analysis is then repeatedly run until the guessed and computed values differ by less than some error tolerance or a maximum number of iterations is reached. In these cases the internal loops run until the desired IRR is reached from both Manufacturer and airline. In other terms the driver modules are used

to iterate the DOC module calculations. This allows profit margin to be set to achieve a desired internal rate of return for the manufacturer, and ticket price to be set to achieve a desired internal rate of return for the operator. When a comparison between a reference aircraft and a concept one is desired to understand if there is any benefit in term of economic profitability, on the second run, using concept aircraft input, the ticket price is kept constant and the IRR left varying.

The start point for any trade is a collection of parameters provided from an external data source. To estimate cost, the geometric features such as the fabrication areas of skin, spars and ribs, and the assembling perimeter of the wing are needed, as well as, mission information

Table 9.3: Mission Information

Number of Flight Crew (if specified)
Number of Cabin Crew (if specified)
Mission (block) time
Number of passengers
Mission fuel burn
Mission Distance

The extraction of these parameters has been implemented in an automatic fashion using again the Model Center integration/process building environments. Figure 9.22 shows the Model Center process for the cost suite input generation.

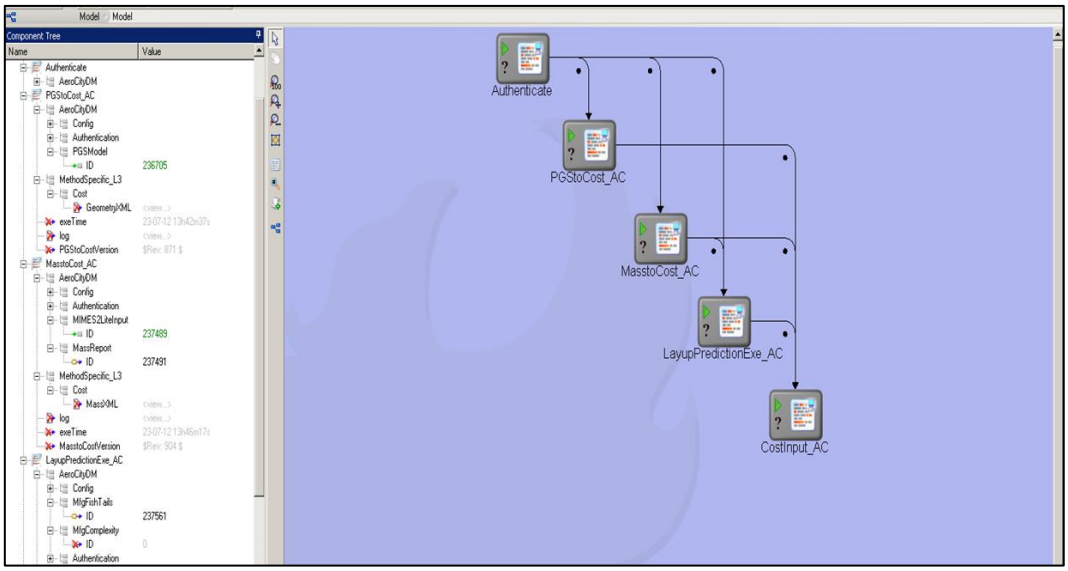

Figure 9.22: Model Center view of the input generation

The first component generates a password string to access the data management tool. The second component consists of a python script developed to extract those geometric features from the 3D CAD model of the wing structure to enhance the product structure and improve the validity of the cost evaluation. In Table 9.1, there is a list of features extracted from the CAD model behind the others wing box geometry inputs listed in Table 9.4.

Table 9.4: Wing Box geometry information

Front spar
The depth of the leading edge spar at the tip
Single piece spar length
Single or Inner Spar maximum spar depth
Rear spar
The depth of the trailing edge spar at the tip
Single piece spar length
Single or Inner Spar maximum spar depth
Top and Bottom panels
Skins
Surface area of wing skin
Leading edge length of panel (inc. growuots).
Trailing edge length of panel (inc. growuots).
Width of panel at the wing root

Width of panel at the wing tip
Ribs
Single Piece
Number of sides
Rib length between spars
Rib depth between skins
Rib thickness over feet
Stringers
The length of individual stringers fitted to the panel
or
The total length of stringers fitted to the panel

The third component is used to extract mass data to enable cost to reflect the actual design. Weight provided from Wing Weight Breakdown, including wing skins, stringers, spars and ribs, as reported in Table 9.5.

Table 9.5: Mass Information

Front Spar Weight
Mid Spar (if any) Weight
Rear Spar Weight
Ribs Weight
Top and Bottom Wing Skin Panels:
Skin Weight
Stringers Weights

The fourth one extracts info on the Manufacturing complexity including process type, process time and raw material weight as reported in Table 9.6.

Table 9.6: Manufacturing Information

Top and Bottom Panel
Process type
Process time
Raw material weight

The last one generates the input file that will be used on the cost suite.

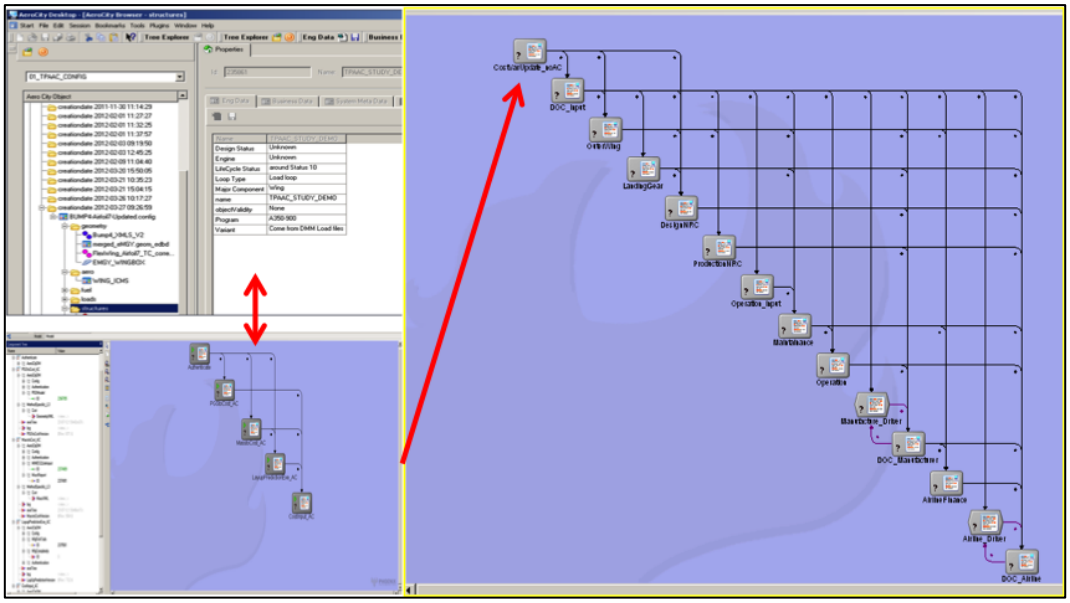

Figure 9.23: Integrated Cost Suite

9.7.4 Integration in SimManager

As simulation business grew, it has been realised that effective management of simulation content is critical to its customers. At the same time there is also the necessity of keeping record of all simulation data and processes from project initiation through final report generation.

SimManager, which is a MSC product, is a web-based simulation data and process management system that manages all aspects of performing CAE simulation. It manages the data independent of application and provides a framework for process execution.

Work has been done to integrate the Model Center version of the cost suite into SimManager. In particular, to launch the process in batch and make the interface between the data management tool and SimManager work smoothly without any user interventions. The integration steps are here explained. Firstly the Model Center workflow has to be developed independent of SimManager and once the process is robust it is uploaded into SimManager for data management and execution. SimManager read from the Aerocity the initial study identifier. Afterwards, SimManager reads the correspondent data required

for the cost suite execution from Aerocity. From SimManager the Model Center Cost process is launched. All data is passed from the SimManager server to the client machine from where the execution of the analysis process takes place. When the process is complete the data is imported back in SimManager and the report is automatically generated and pushed in the Architect Cockpit Tool (ACT). The ACT sits on top of SimManager, providing an alternative interface to the Web User Interface. The ACT interface, which is a Java application, is very much tailored towards the initiation of a study and the selection of alternatives that will comprise the content of that Study/Trade. Its goal is to provide an interface to relevant functionality in a clean interface that is targeted at the operating requirements/desires of the architects, who really wants to see the information without the confusion of additional models/data that is irrelevant to their decision making process. An integration framework integrated with a Simulation Management system ensures complete traceability of the data produced in this multi-disciplinary process and it minimises non-value added tasks in data operations. Thus its importance to multi-disciplinary design is crucial.

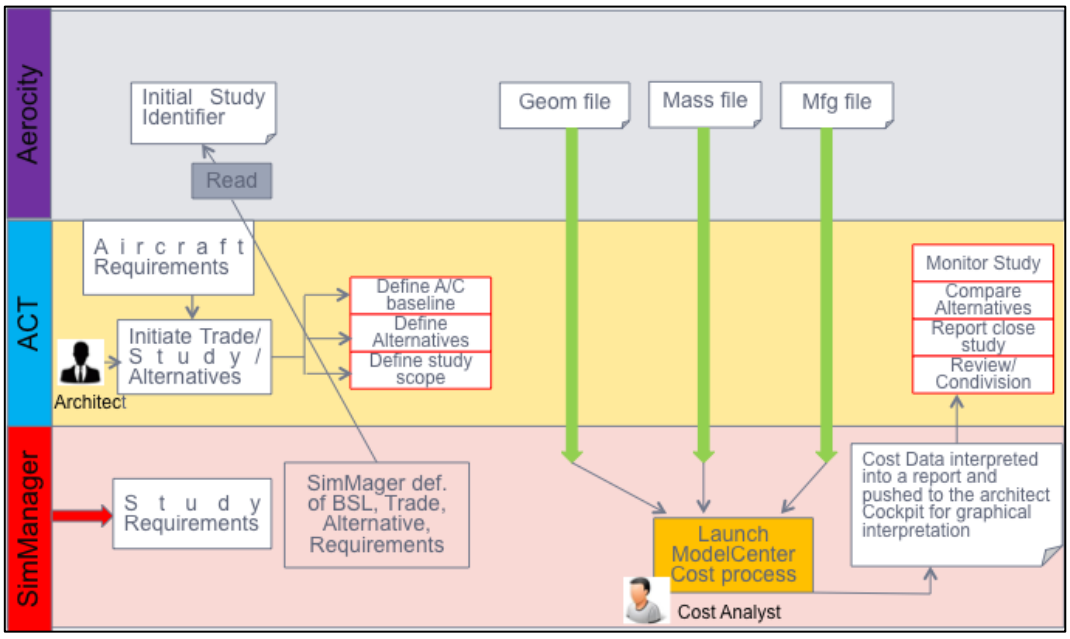

Figure 9.24: Interfaces

Out-of-the-Box, SimManager can provide instant value by maintaining the linkages and pedigree of the variety of data that is input to and output from a simulation and by enabling management to quickly assess the state of simulation tasks in the enterprise. In other words, it eliminates time wasted in searching for data and streamlines the process of distributing standard methods, processes, material properties, and other content. Implementing the discipline of Simulation Process and Data Management gets simulation activities completed efficiently and effectively. In addition, it enables an efficient way to integrate any Computer Aided Engineering tool with High Performance Computing. The client uploads the component models. This can be done using the web client interface and moreover select the method for post-processing and report generation. Once the model is submitted, all the data and process execution are effectively managed between SimManager and the HPC environment. This means that heavy data transfer is done between two systems that are very close connected together so there is not overhead of moving large file around the network, and the processing which require significant resources is executed on the appropriate hardware.

9.7.5 Results

Different trade studies have been performed and cost results produced for different real case configurations. They are not fully reported in this thesis for confidentiality reasons. Some work has been done on the cost results. They have been improved also to be consistent with the output produced by the conceptual design cost model. This will allow an easier comparison between them. Figure 9.25 Figure 9.26 and Figure 9.27 give an example of outputs produced by the cost suite.

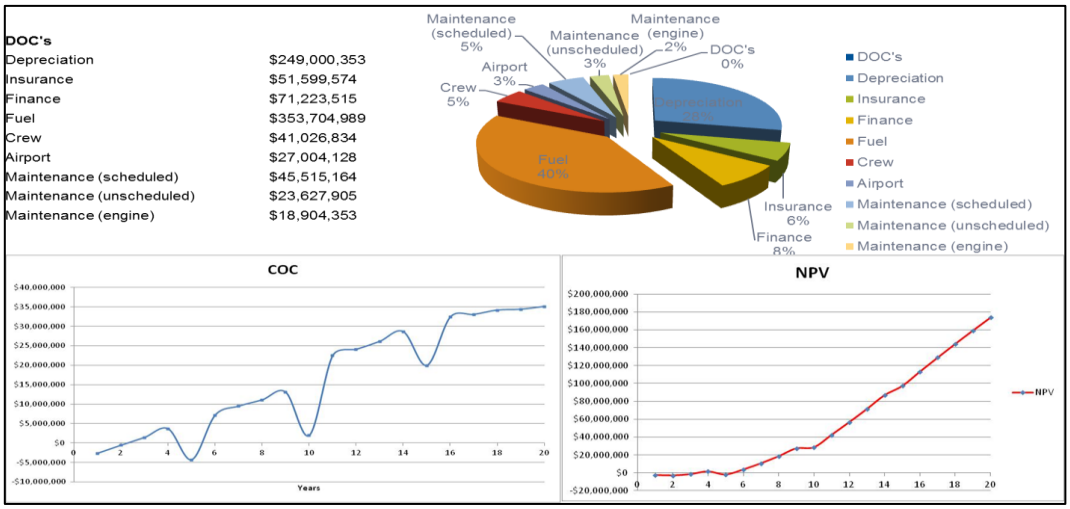

Figure 9.25: Example of output produced by the cost suite from an airline perspective

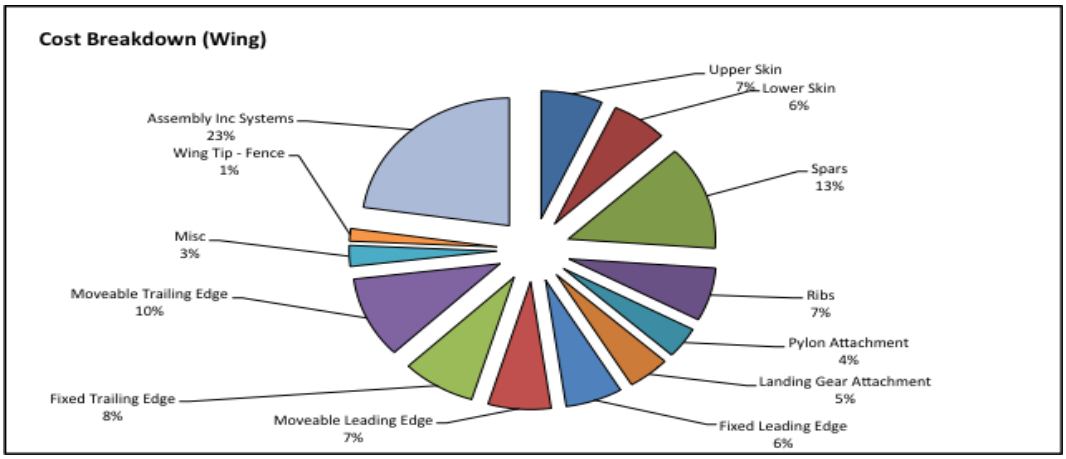

Figure 9.26: Example of output produced by the cost suite from a manufacturer perspective

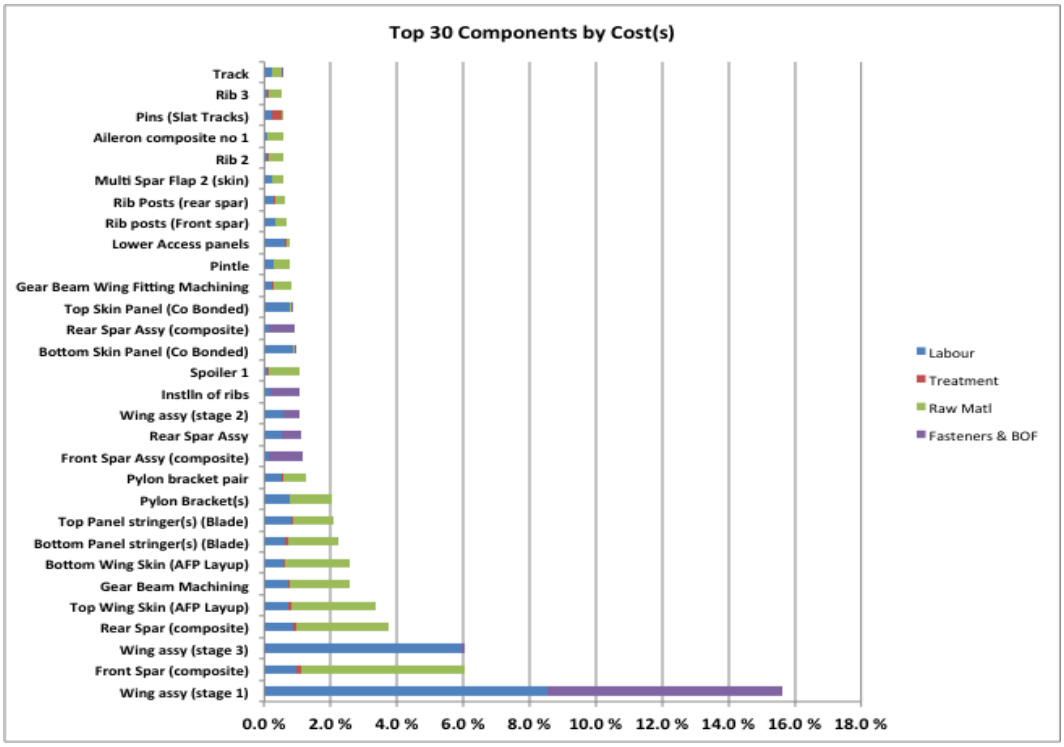

Figure 9.27: Top 30 Component costs

In order to show the capability of the cost model a trade study has been performed on the same aircraft using different wing material, composite versus metallic. In this particular case the ticket price has been kept fixed and the Direct Operating Cost results compared. Figure 9.28 and Figure 9.29 show the DOCs for both configurations, metallic and composite wing respectively.

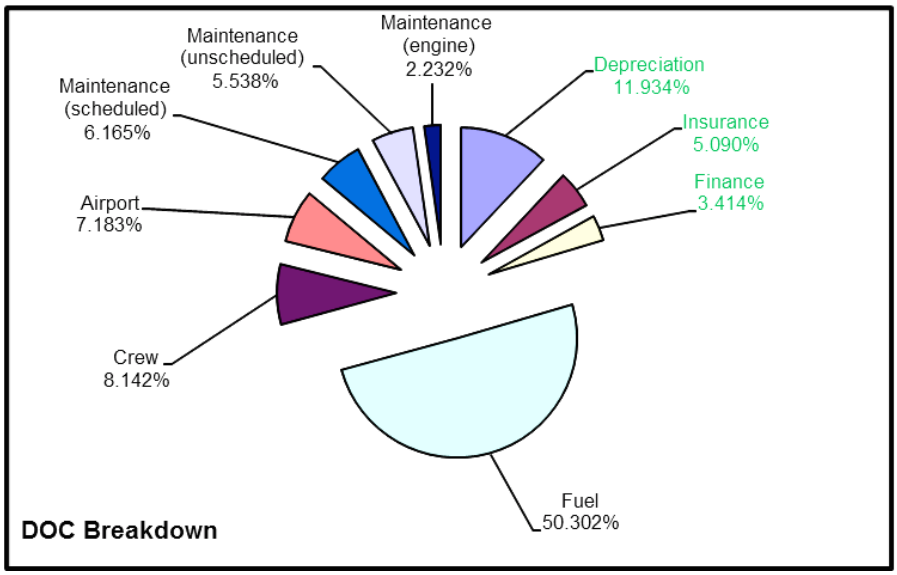

Figure 9.28: DOC metallic wing

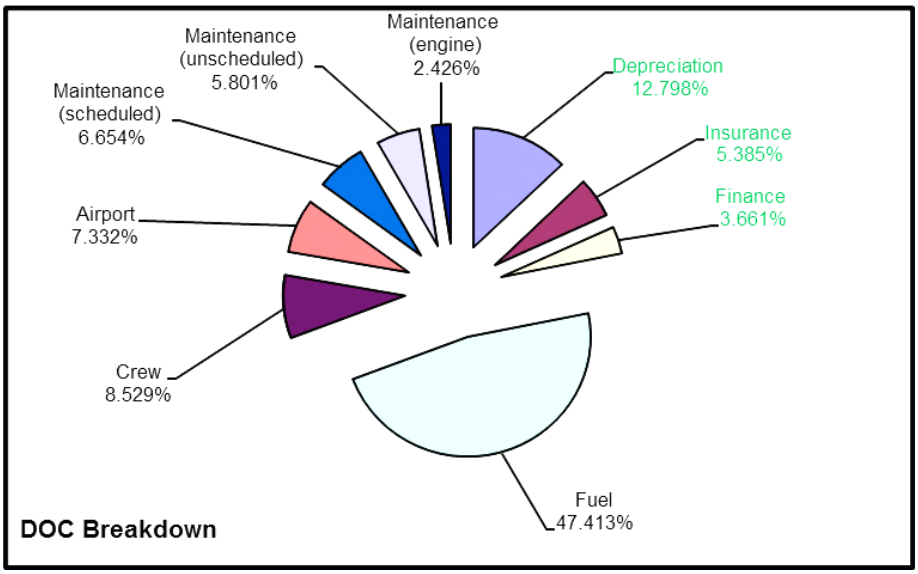

Figure 9.29: DOC composite wing

Although the production cost has increased of about 12%, it has been found an improvement in the operator IRR of about 2% even though the A/C price has increased, but offset by fuel cost consumption. Moreover there is also a benefit in manufacturer profit of nearly 1%.

Another example of study is here reported. In this case starting with a reference wing, the trade study consists to evaluate the effect of span and leading edge sweep angle changes against the economic profitability in term of both manufacturer and airline point of view. Specifically, three alternatives geometries are considered versus the reference one. The first case considers an increase in span, keeping wing area and sweep angle constant, as shown in the followings Figure 9.30.

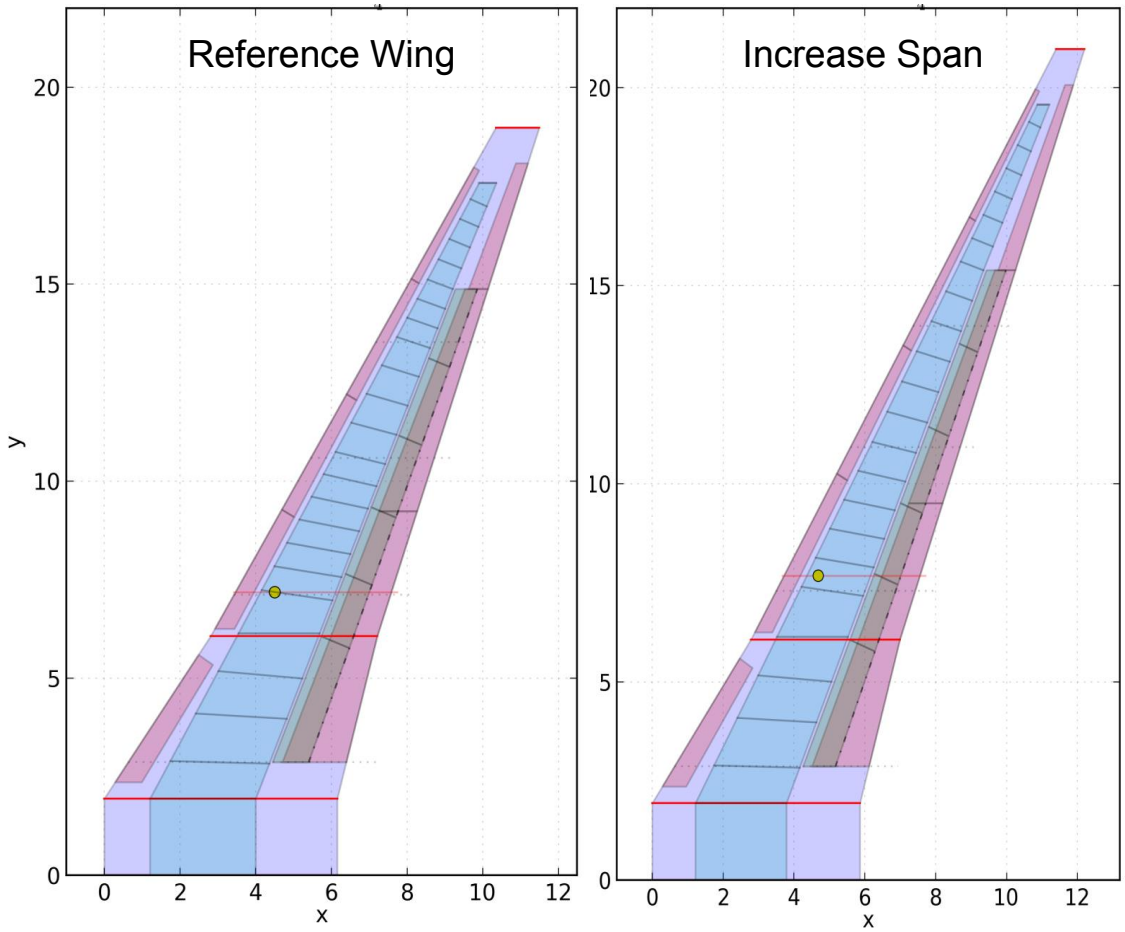

Figure 9.30: Wing geometry comparison

In the second case the leading edge sweep angle has been reduced keeping constant span and wing area, in the third case keeping constant only the wing area the span has been increased and the sweep angle reduced as it is shown in Figure 9.31

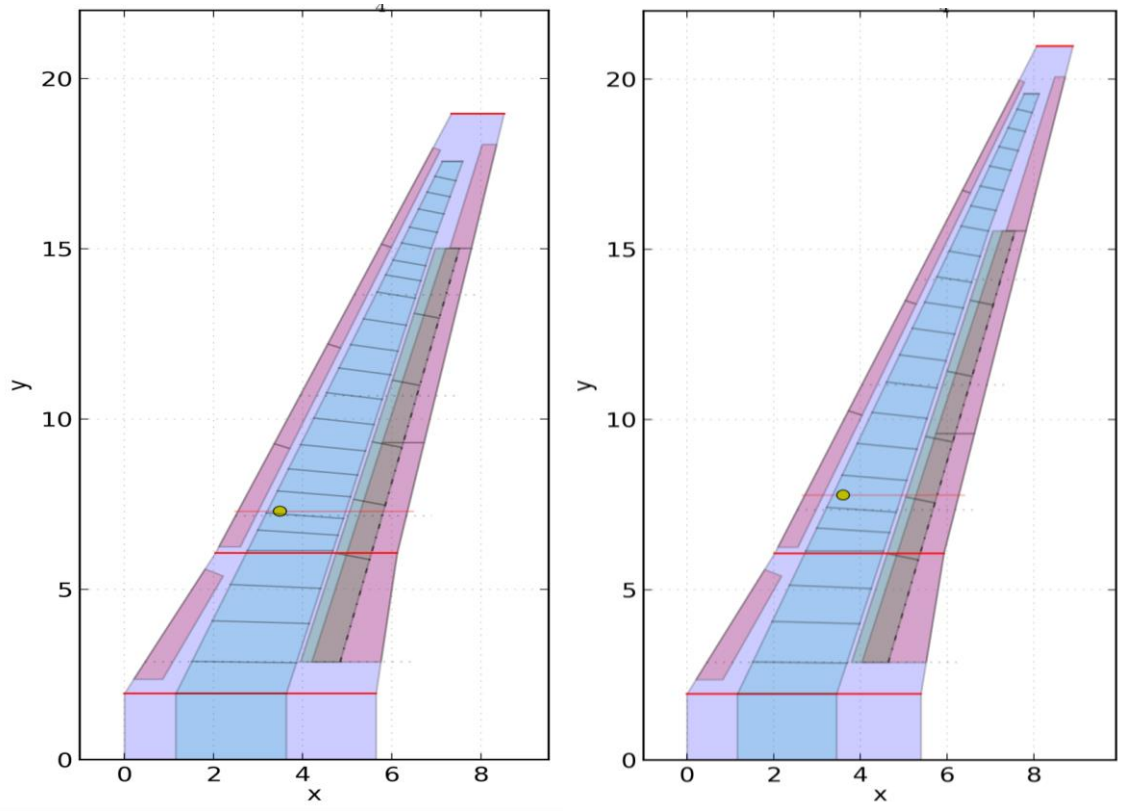

Figure 9.31: Sweep changed (L) Span and sweep changed (R).

After evaluating the reference and all the wing variants it has been found that none of the variants are superiors in term of economic profitability compared to the reference wing both for the airline and the manufacturer, as can be seen in Figure 9.32 where the Net present Value (NPV) is plotted in percentage terms.

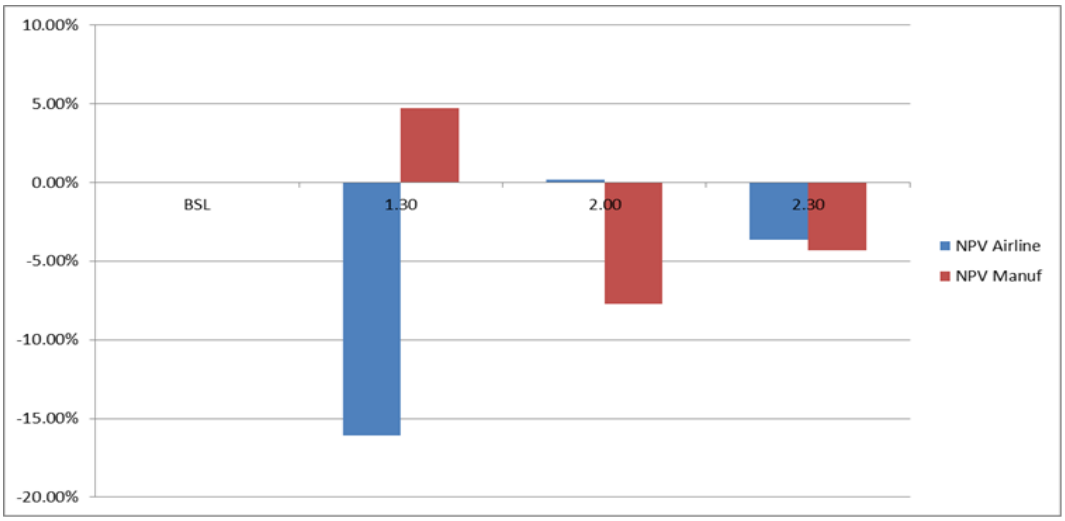

Figure 9.32: Net Present Value comparison

9.8 Cost Optimisation

A series of cost optimisation studies have been conducted making use of the built-in design optimisation capability offered by Model Center that allows automatic search for improved designs. The integration of the cost suite in model center has been slightly modified to consider Recurring and Non-Recurring cost as objectives for the optimisation and to include the optimiser, as shown in Figure 9.33. The optimisation algorithm repeatedly runs the workflow and attempts to find the values for the input variables that best achieve the user's goals while satisfying their requirements. A number of different types of algorithms are included in the Model Center framework (gradient algorithms, genetic algorithms, etc.). In all optimisation case the well-known genetic algorithm NGSA-II (Non-dominated Sorting genetic Algorithm II) [119] has been used.

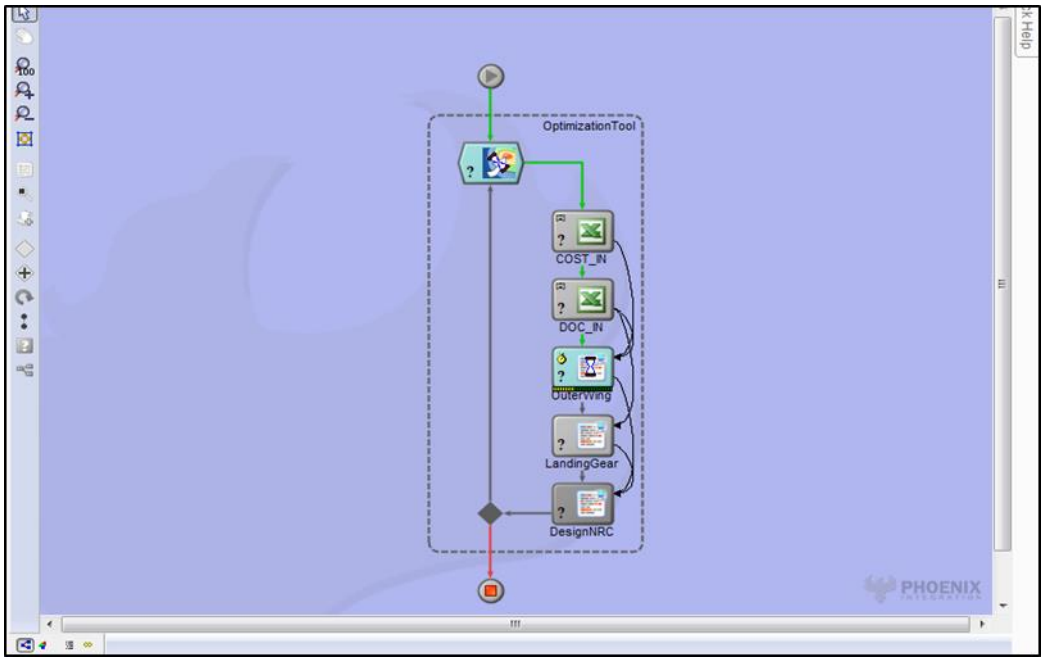

Figure 9.33: Model Center Optimisation set-up

In this optimisation the initial population is formed by 48 candidates and the optimisation is halted after 100 generations. The crossover probability is set to 0.7, while the mutation probability is 0.5, as reported in Table 9.7.

Table 9.7: NGSA-II optimisation setting

Optimisation parameters	
Population	48
Cross-over probability	0.7
Mutation probability	0.5
Stopping Criteria	
Convergence Generations	5
Convergence Threshold	0.001
Max Evaluations	500
Max Generations	100

The test case under investigation is a conventional single aisle mid-range commercial aircraft with composite wing (skin and spars). Fourteen wing design variables have been investigated to understand the effect of these on the wing recurring and non-recurring cost, reported in Table 9.8 together with the correspondent datum value and low and high bound values. During the optimisations only the mandatory input, basically the top-level descriptions are given. This is done to allow the cost suite to calculate the mass information and other geometric data (length, width and thickness) and part quantities by itself.

Table 9.8: Design Variables

	Design Variable	Name	Low bound	Datum Value	High Bound
1	Wing root thickness/chord ratio	tcr	0.113400	**0.1620**	0.210600
2	Wing kink thickness/chord ratio	tck	0.083548	**0.1194**	0.155160
3	Wing tip thickness/chord ratio	tct	0.075202	**0.1074**	0.139661
4	Wing root chord	crt	4.308255	**6.1547 m**	8.001045
5	Wing kink chord	ckt	2.882755	**4.1182 m**	5.353687
6	Wing tip chord	cte	0.802849	**1.1469 m**	1.491005
7	LE sweep inboard	swpi	0.418650	**0.5981 rad**	0.777494
8	LE sweep outboard	swpo	0.369781	**0.5283 rad**	0.686736
9	TE sweep	TE_sweep	0.224102	**0.3201 rad**	0.416189
10	Spanwise position of wing kink	sk	5.026364	**7.1805 m**	9.334676
11	Wing box chord at root	wb_cr	1.920241	**2.7432 m**	3.566162
12	Wing box chord at kink	wb_ck	1.364094	**1.9487 m**	2.533317
13	Wing box chord at tip	wb_ct	0.318669	**0.4552 m**	0.591831
14	Position of IB engine	yengi	4.298954	**6.1414 m**	7.983772

9.8.1 Multi-dimensional data visualisation introduction

To gain maximum value from the optimisation process, designers need to visualise and interpret this information leading to better understanding of the complex and multimodal relations between parameters, objectives and decision-making of multiple and strongly conflicting criteria.

When dealing with large sets of data with many parameters conventional visualisation methods such as diagrams, curves, 2D/3D scatter charts, histograms etc. are often unable to present the data in a meaningful way. In these cases it is possible make use of a multi-dimensional data visualisation tools for interpreting and analysing the results and understand the impact of design changes. Parallel coordinates is a widely used visualisation technique for multivariate data and high-dimensional geometry. Since their first appearance in the scientific literature in the context of Nomography [182], parallel coordinates have become a well-known visualisation for exploratory data analysis [183] and visual multidimensional geometry [184]. To show a set of points in an n-dimensional space, a backdrop is drawn consisting of n parallel lines, typically vertical and equally spaced. A point in n-dimensional space is represented as a polyline with vertices on the parallel axes; the position of the vertex on the i-th axis corresponds to the i-th coordinate of the point. An interesting property of the commonly used parallel coordinates display is the pattern formed by the totality of lines between adjacent axes. These patterns have a direct correspondence to the type of relationship existing between the variables mapped onto the axes in question as well as a salient visual appearance. When most lines between two parallel axis are somewhat parallel to each others, which suggests a positive correlation between these two dimensions. When lines cross in a kind of superposition of X-shapes, which is negative relationship. When lines cross randomly that shows there is no particular relationship.

9.8.2 Results

9.8.2.1 Optimisation study using 3 design variables

The first optimisation study tries to analyse the impact of thickness over chord ratio, t/c, variation along the span on the recurring and non-recurring wing costs. The recurring costs are mainly made by sum of the labour and raw material cost. The Labour cost is function of time needed to perform the operation multiplied with the sum of the cost for the operator, the cost for the machine or facility and some overhead cost (directLaborRate).

$$C_{labour} = f(time, directLabourRate) \quad (9.2)$$

Similar, the volume of the raw material is multiplied with its density and the specific Price.

$$C_{material} = f(Volume, Density, Specific\ Price) \quad (9.3)$$

The non-recurring cost considered in this study is just the Aero design cost.
It depends by the number of part quantity, relative size of the part, weights of material and project duration.

$$C_{AeroDesign} = f(Part\ Qty, Part\ size, Mtl\ weigth, Project\ Duration) \quad (9.4)$$

In this case just three design variables are used, specifically the t/c ratio value at the wing root, “tcr”, the t/c ratio value at the wing crank, “tck”, and the t/c ratio value at the wing tip, “tct”. From their datum value the low and high bound are set to -30% and +30% respectively, keeping constant the remaining 11 design variables to their datum value. The optimisation study has been performed under the geometric constraint that for each design “tcr” > “tck” > “tct”. Figure 9.34 shows the results of the optimisation using the parallel coordinate high-dimensional data visualisation method. Each of the parameters with its range of variation is represented by one vertical axis, (black lines). The parameter name is shown on top of each axis. Each design is represented by a green line that crosses the axes at the ordinates corresponding to the values observed for their respective parameter in that design. The blue lines indicate the datum and best design (bottom line).

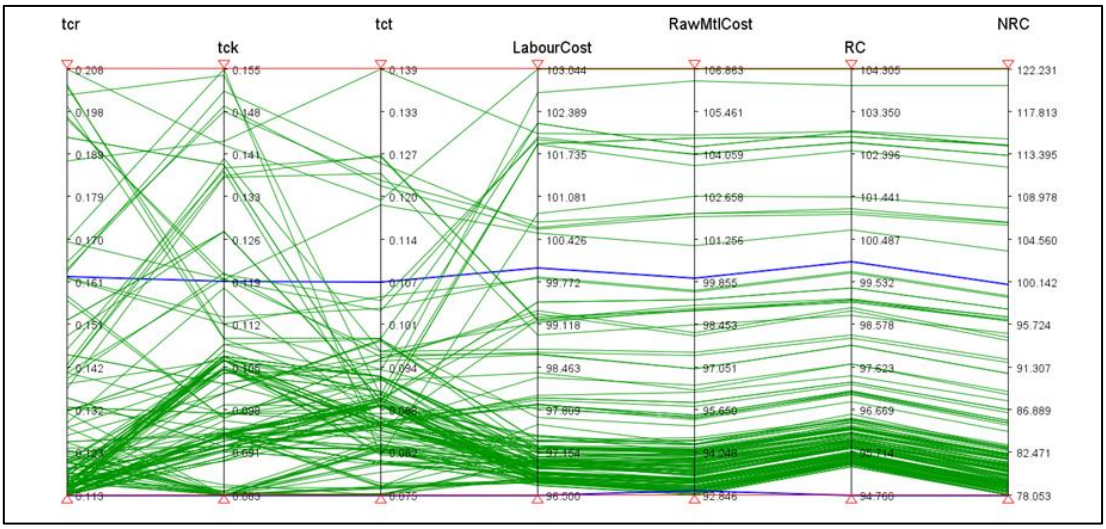

Figure 9.34: Parallel coordinate visualisation: Datum and best design; 3 Design variables

From the picture is possible to see the direct relationship between the Recurring and Non-recurring cost given that lines along x axis are parallel to each others. In fact they are both mainly size driven. The value of the datum and optimised design are reported in Table 9.9.

Table 9.9: DVs and Objectives value for the Datum and optimised design; 3Dvs

	tcr	**tck**	**tct**	N. Parts	Composite Mtl Weight (Kg)	Other Mtl Weight (Kg)	Total Mtl. Weight (Kg)	RC(%)	NRC(%)
Datum	0.1620	0.1194	0.1074	3600	3060	12790	15850	100	100
Optimum	0.1134	0.0835	0.0752	3600	2979	10106	13084	94.76	78.05

As expected the optimum design is reached when the value of the design variables keep their minimum value. Although, the number of parts quantity do not vary with the reduction of t/c, the size of the components decrease, which implies less raw material to be used. Moreover, the quantity of fasteners for any part that attaches to the spars will reduce as t/c decreases; hence fewer fasteners are necessary for the assembly. Consequently, it means less labour time and all this translates in reduction of recurring and non-recurring cost. As

from the table in this case a reduction of recurring cost and non-recurring cost of respectively 5.24% and 21.95% has been achieved. Figure 9.35 and Figure 9.36 displays the sensitivity of variables to one another with respect to the RC and NRC respectively. A main effect is defined as the change in an output variable with respect to an input variable. The graph shows how all the main effects for a given output variable compare to one another. Thus, the input variable with the largest main effect is said to have the greatest influence on the output variable.

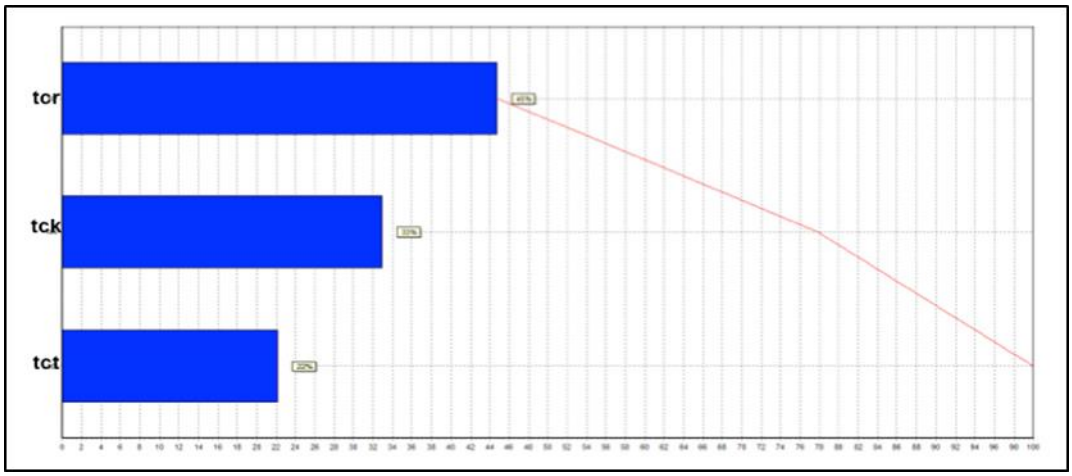

Figure 9.35: Sensitivity data analysis diagram from RC; 3DVs

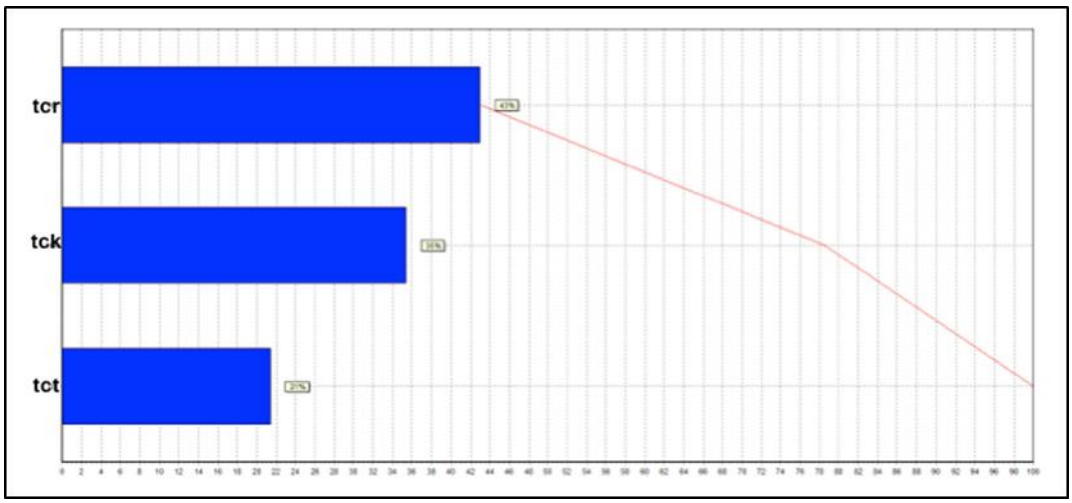

Figure 9.36: Sensitivity data analysis diagram from NRC; 3 DVs

To compute the main effect between a particular input and output pair, these plots take the average output value for all runs with the input at its minimum,

then at its maximum. All the runs where the value is not the minimum or maximum have been discarded. The difference between the two averages is the main effect.

From the above pictures is clear that the thickness over chord at the root has the greatest influence on the outputs, and this is due to the fact that the bigger elements and thus higher cost components that compose the wing are closer to the wing fuselage attachment. This is further confirmed by the next scatter plots figures, in which each design variables is plotted against the objective functions.

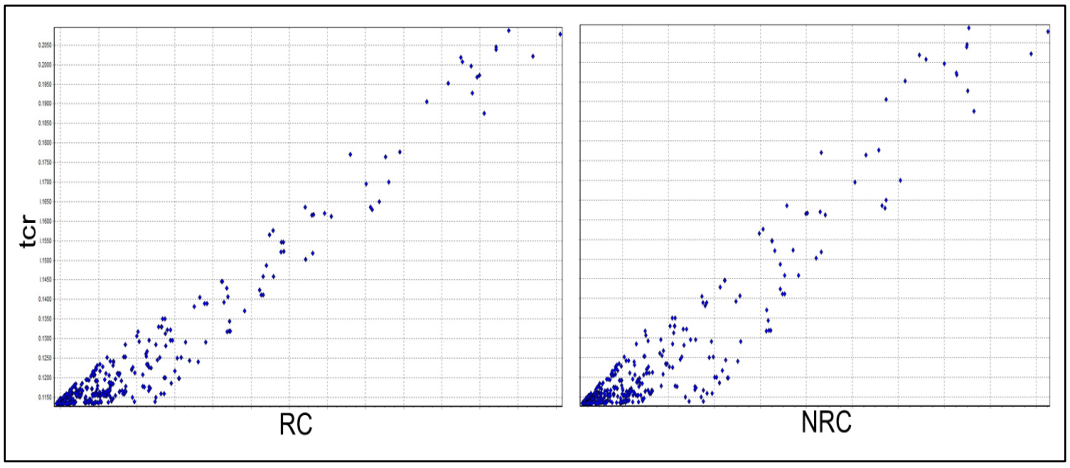

Figure 9.37: Scatter plot tcr vs. RC & NRC

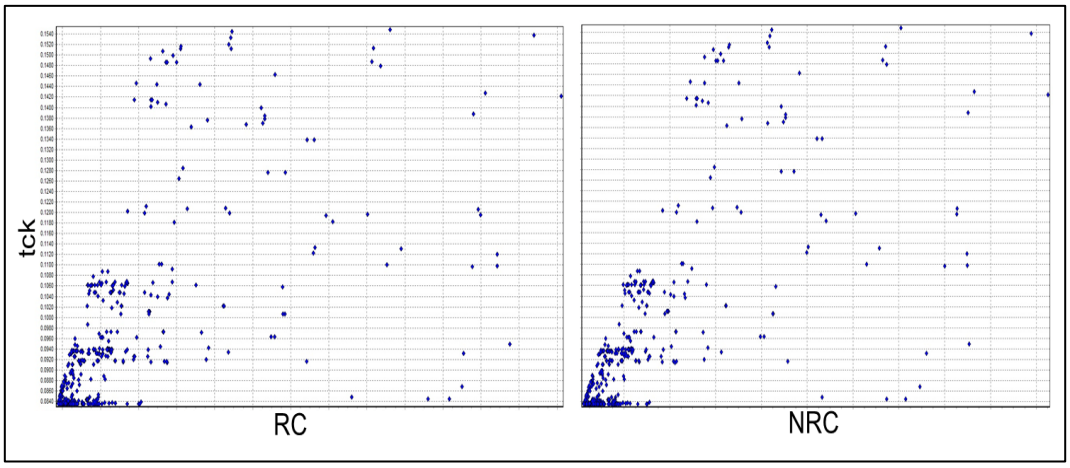

Figure 9.38: Scatter plot tck vs. RC & NRC

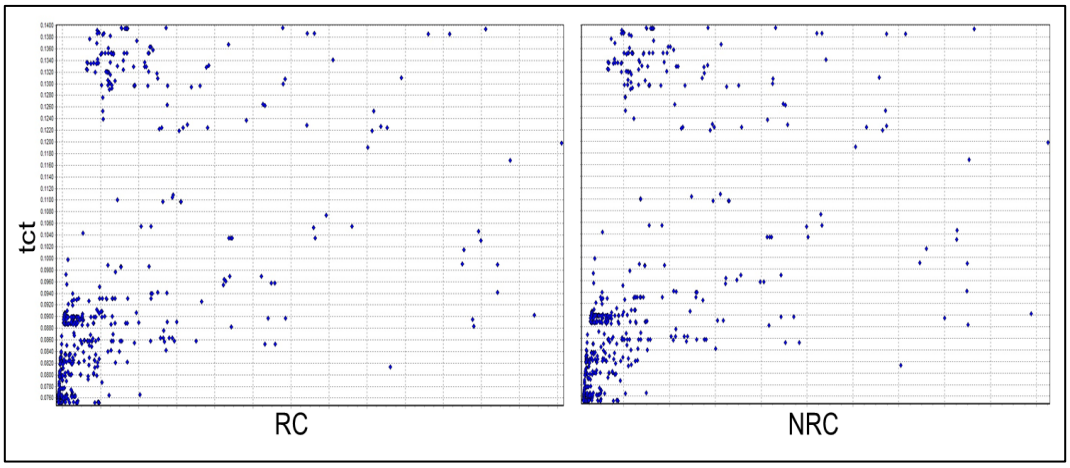

Figure 9.39: Scatter plot tct vs. RC & NRC

Several conclusions can be drawn from these three plots. First, tcr has a big impact on both RC and NRC. Its value has to be low to reduce the objective functions; hence there is a strong correlation with the objective functions, see Figure 9.37. Second, tck and tct define a clear relationship to RC and NRC. While it is possible to reach a low value of the objective functions when tck and tct are close to their respective lower bounds, the objective functions may take any values, once tck exceeds the value of 0.0840 and tct exceeds 0.08.

9.8.2.2 Optimisation study using 7design variables

A second optimisation has been performed varying seven design variables related to the planform geometry. From their datum value the low and high bound are set to -30% and +30% respectively, keeping constant the remaining 7 design variables to their datum value; see Table 9.10, and keeping constant the others.

Table 9.10: Design Variable relative to the Planform geometry

	Design Variable	Name	Low bound	Datum Value	High Bound
1	Wing root chord	crt	4.308255	**6.1547 m**	8.001045
2	Wing kink chord	ckt	2.882755	**4.1182 m**	5.353687
3	Wing tip chord	cte	0.802849	**1.1469 m**	1.491005
4	LE sweep inboard	swpi	0.418650	**0.5981 rad**	0.777494
5	LE sweep outboard	swpo	0.369781	**0.5283 rad**	0.686736
6	TE sweep	TE_sweep	0.224102	**0.3201 rad**	0.416189
7	Spanwise position of wing kink	sk	5.026364	**7.1805 m**	9.334676

The optimisation study has been performed under the geometric constraint that for each design “crt” > “ckt” > “cte” and that the difference between the leading edge sweep inboard and outboard angle has to be less or equal to 3 degrees; |*swpi – swpo*| ≤*3deg.* Figure 9.40 shows the results of the optimisation using the parallel coordinate high-dimensional data visualisation method, where again the blue line indicates the datum design.

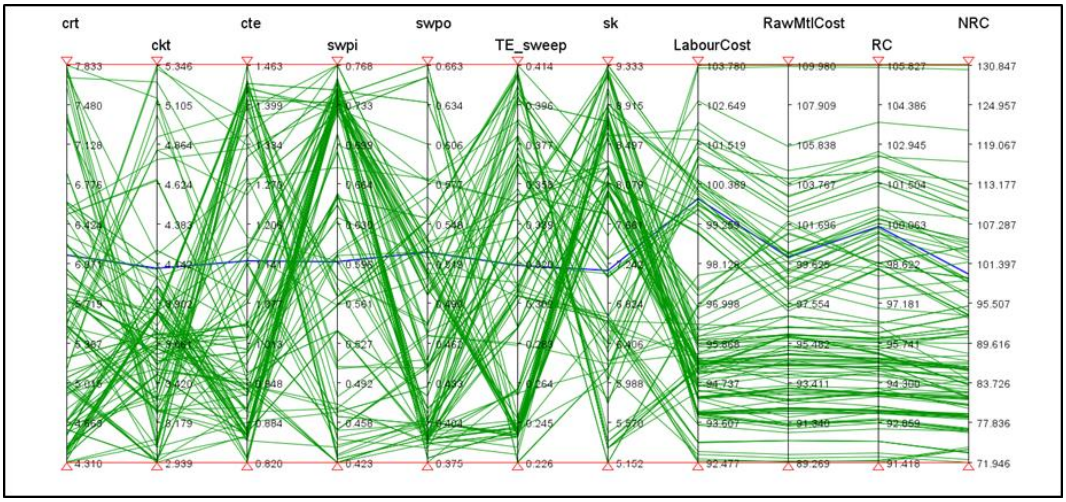

Figure 9.40: Parallel Coordinate visualisation; 7 Design variables

In parallel coordinates, patterns are very often difficult to detect due to the visual clutter caused by too many drawn lines, so it is useful to make a selection of subset of data. Therefore, in order to analyses the data further, so-called filters can be used. These are the small red triangles on the top and bottom of each axis that are connected by red lines. These can be dragged with the mouse and only designs that cross the axis between its filters are displayed. The next Figure 9.41 and Figure 9.42 show respectively the datum and best RC design and the datum and best NRC design.

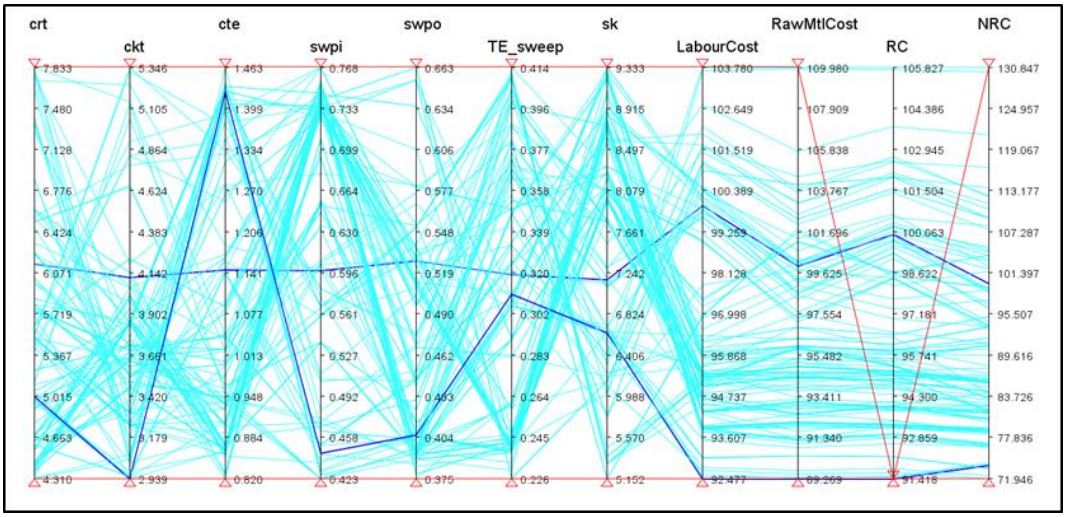

Figure 9.41: Parallel Coordinate visualisation: Datum and best RC design

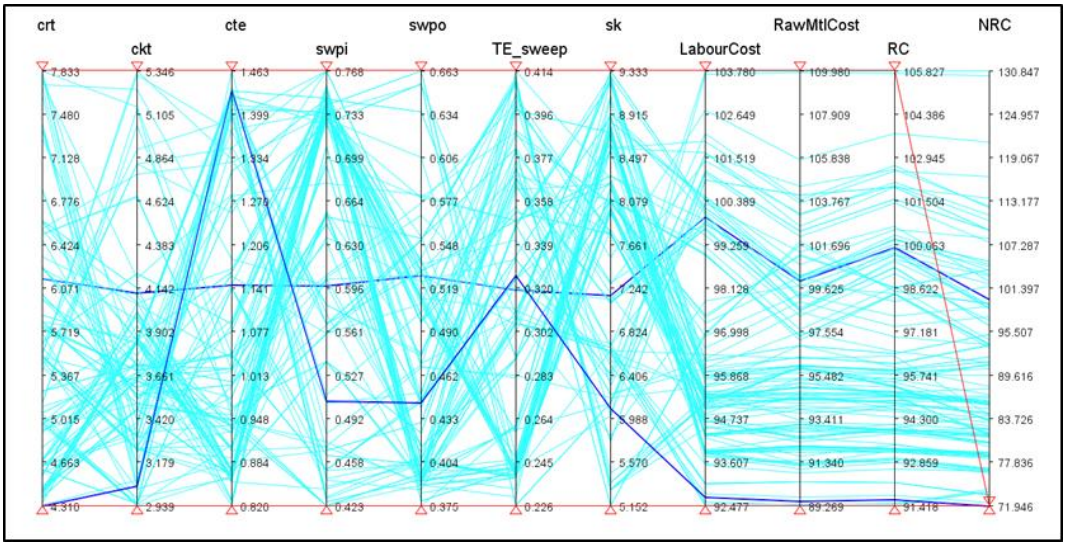

Figure 9.42: Parallel Coordinate visualisation: Datum and best NRC design

The value of the datum and optimised designs are reported in Table 9.11.

Table 9.11: DVs and Objectives value for the Datum and optimised designs; 7Dvs

DVs	Datum	Best RC	Best NRC
crt	6.1547	5.0206	4.3199
ckt	4.1182	2.9412	3.0841
cte	1.1469	1.4261	1.4395
swpi	0.5981	0.4452	0.5111
swpo	0.5283	0.4060	0.5040
TE_sweep	0.3201	0.3108	0.3560

sk	7.1805	6.6451	6.5090
N. of Parts	3600	3538	3546
Composite Mtl. Weight	3060	2763	2851
Other Mtl. Weight	12790	10428	9883
Total Mtl. Weight	15850	13191	12834
RC %	100	**91.42**	91.77
NRC %	100	73.10	**72.41**

Figure 9.43 shows the parallel coordinate plot again, but with the colour scale that indicates the design optimality with respect of the posed problem, with red shadings indicating improved performance.

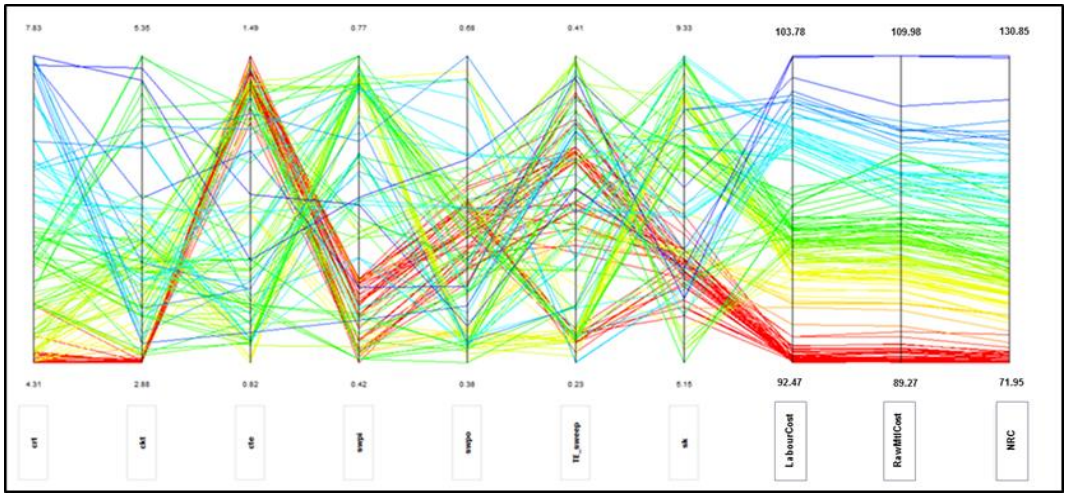

Figure 9.43: Parallel coordinate analysis coloured by optimality of design: 7Dvs

Clearly the above plot shows a general trend, which characterise the optima configurations, as demonstrated by the clustering of red lines. The design parameter TE_sweep varies a lot, which means that does not affect optimality and could be neglected from the optimisation, as it possible to infer for the scatter plot, that show the source of variation of the objective functions with the TE_sweep design variable.

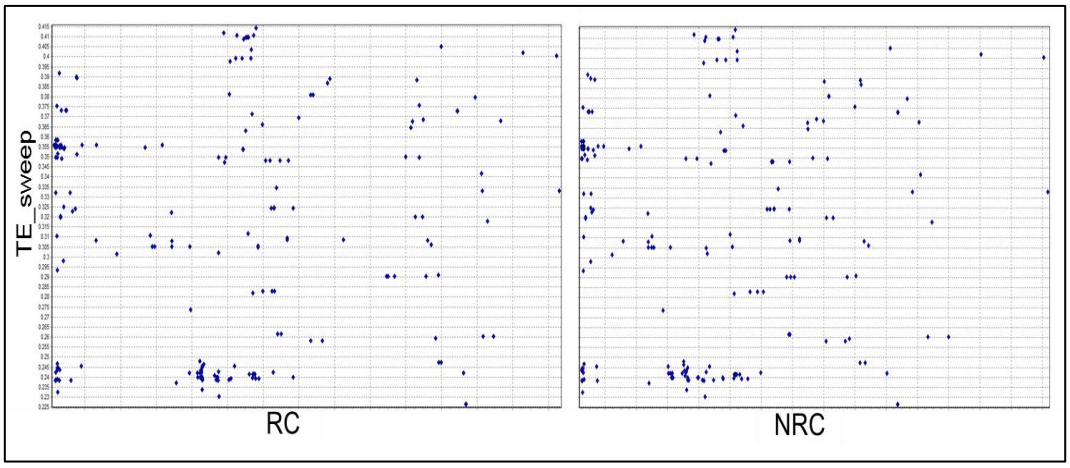

Figure 9.44: Scatter plot TE_sweep vs. RC & NRC; 7DVS

In particular, for these designs, the chord at the tip is enlarged whereas the chord at the root and at the kink are reduced together with the Leading edge sweep angle both inboard and outboard and the spanwise position of the wing kink with comparison to the datum value as depicted in Figure 9.45.

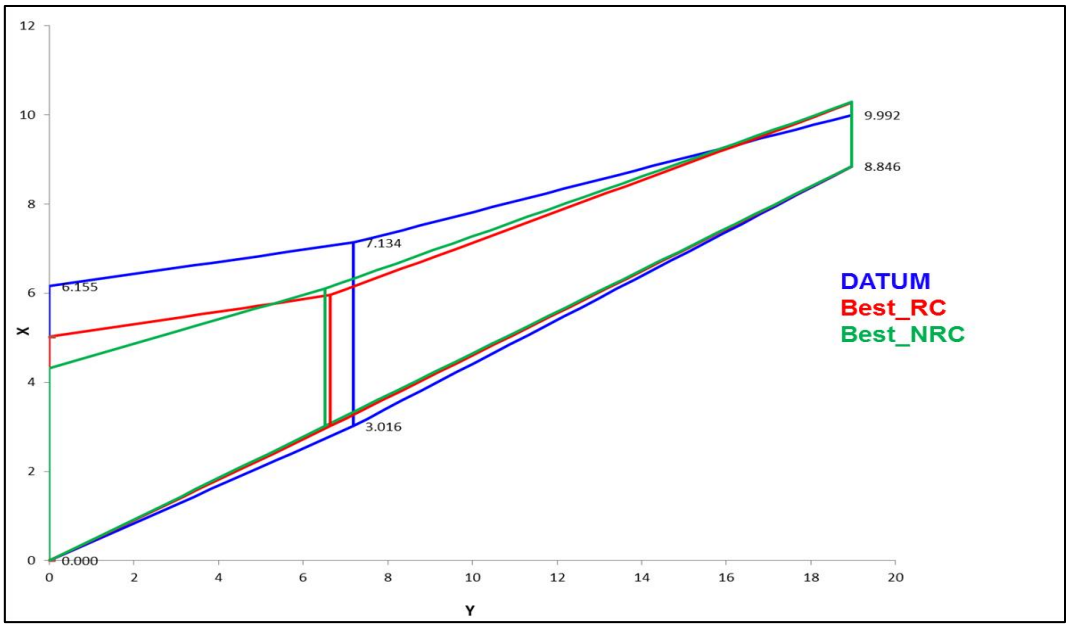

Figure 9.45: Planform comparison

Figure 9.46 and Figure 9.47 displays the sensitivity of variables to one another with respect to the RC and NRC respectively.

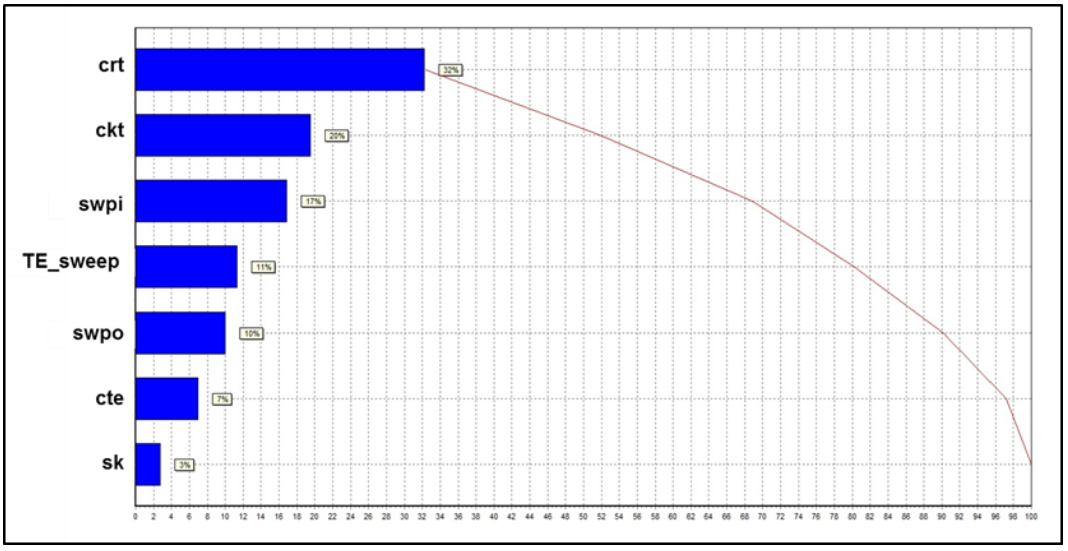

Figure 9.46: Sensitivity data analysis diagram from RC; 7DVs

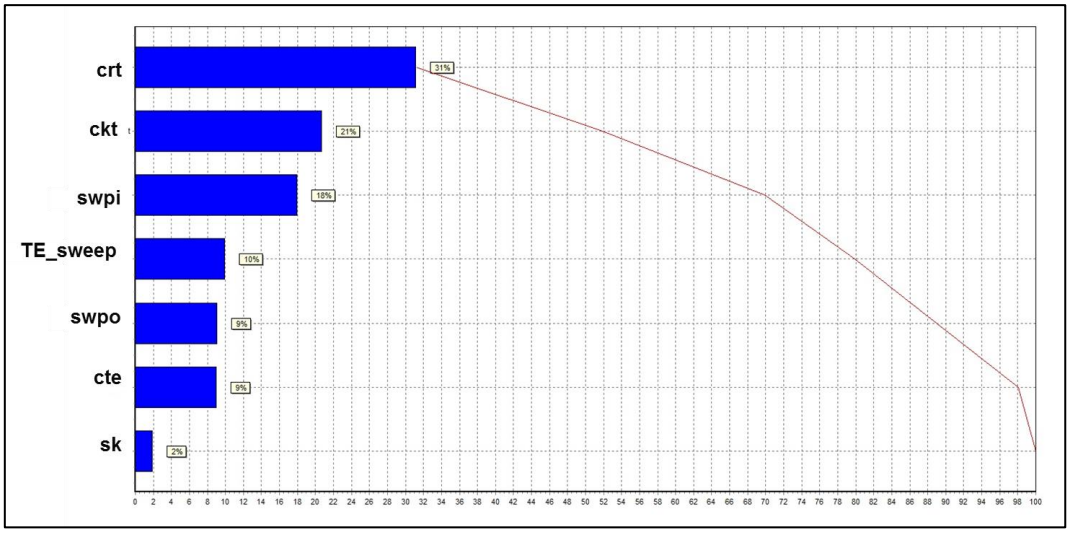

Figure 9.47: Sensitivity data analysis diagram from NRC; 7DVs

The above figures show that both RC and NRC have again a similar behaviour, in term of input variable, which have largest influence on the output variable. The chord at the root and at the kink, hence the size of wing planform affects the objective functions significantly, and clearly smaller wing less costs.

9.8.2.3 Optimisation study using 14 design variables

A third and final optimisation has been performed varying all fourteen design variables that take into account thickness of the wing, planform geometry and wing box geometry; see Table 9.8. The optimisation study has been performed

under the geometric constraint that for each design “tcr” > “tck” > “tct”; design “crt” > “ckt” > “cte”; wb_cr > wb_ck > wb_ct and that the difference between the leading edge sweep inboard and outboard angle has to be less or equal to 3 degrees; $|swpi - swpo| \leq 3deg$. Figure 9.48 shows the results of the optimisation using the parallel coordinate high-dimensional data visualisation method, where again the blue line indicates the datum design.

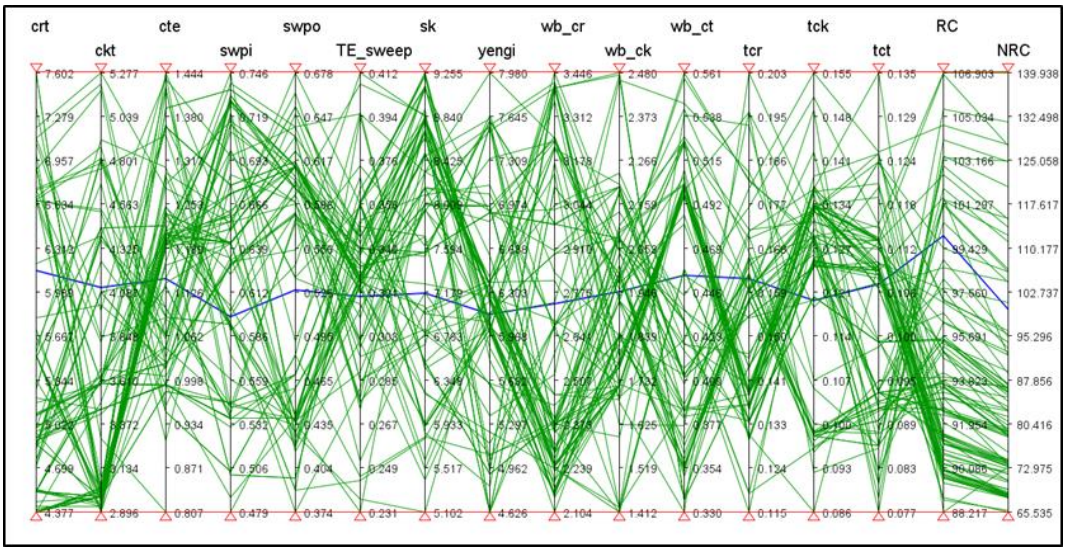

Figure 9.48: Parallel Coordinate visualisation; 14 Design variables

The next Figure 9.49 and Figure 9.50 show respectively the datum and best RC design and the datum and best NRC design.

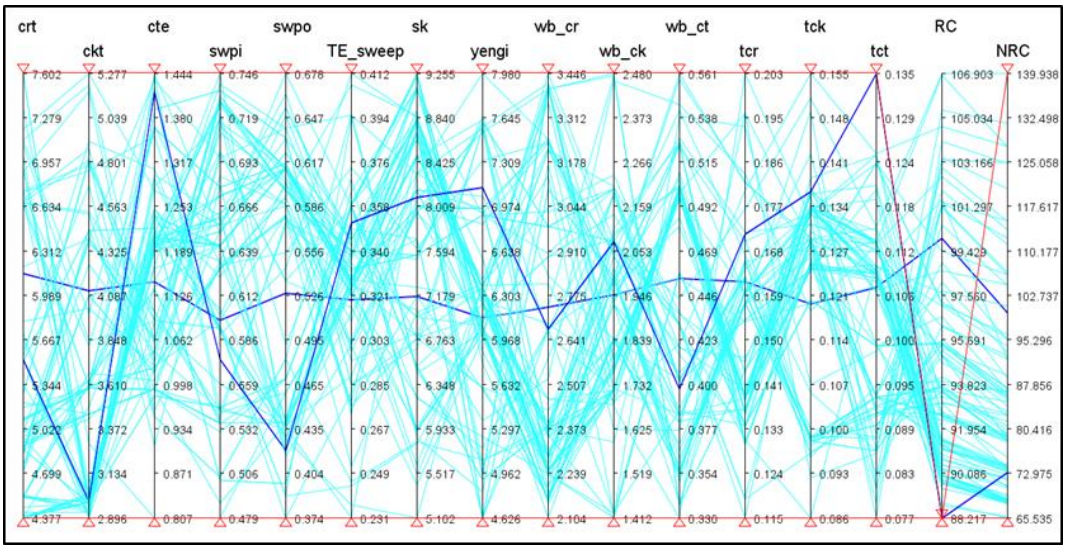

Figure 9.49: Parallel Coordinate visualisation: Datum and best RC design; 14 DVs

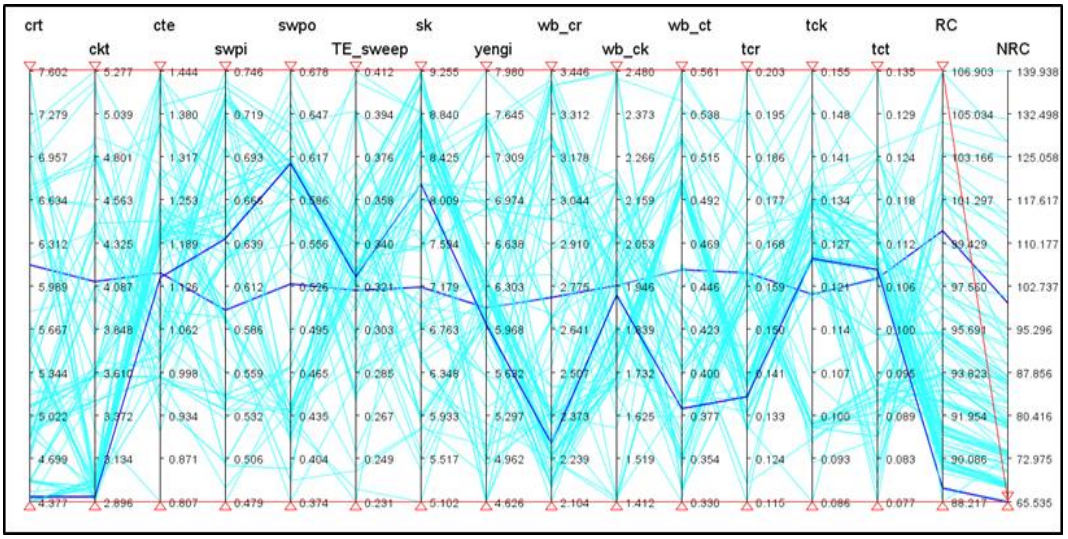

Figure 9.50: Parallel Coordinate visualisation: Datum and best NRC design; 14 DVs

The value of the datum and optimised designs are reported in Table 9.12

Table 9.12: DVs and Objectives value for the Datum and optimised designs; 14Dvs

DVs	Datum	Best RC	Best NRC
tcr	0.1620	0.1366	0.1273
tck	0.1194	0.1342	0.1260
tct	0.10774	0.1086	0.11916
crt	6.1547	4.4235	4.6250
ckt	4.1182	2.9277	2.8956
cte	1.1469	1.2412	1.1412
swpi	0.5981	0.6425	0.64265
swpo	0.5283	0.6128	0.6583
TE_sweep	0.3201	0.3258	0.2820
sk	7.1805	8.1706	8.0271
wb_cr	2.7432	2.2878	3.2293

wb_ck	1.9487	1.9264	1.9323
wb_ct	0.4552	0.3843	0.4778
yengi	6.1414	6.001	6.2544
N. of Parts	3600	3530	3566
Composite Mtl Weight	3060	2831	2604
Other Mtl. Weight	12790	9114	9678
Total Mtl. Weight	15850	11945	12282
RC %	100	**88.74**	89.17
NRC %	100	65.92	**64.83**

Figure 9.51 shows the parallel coordinate plot again, but with the colour scale that indicates the design optimality with respect of the posed problem, with red shadings indicating improved performance.

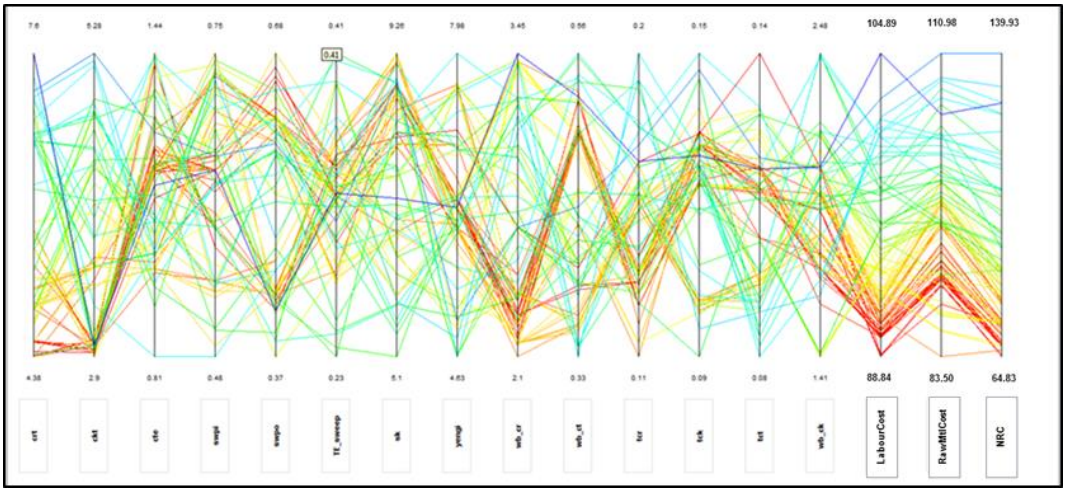

Figure 9.51: Parallel coordinate analysis coloured by optimality of design: 14Dvs

Clearly there is a trade-off between minimum recurring and non-recurring costs.

9.8.3 Conclusion

All optimisations performed have shown that the minimum of RC is found where the Labour cost is minimum, which is more dependent by the number of part quantities; conversely the NRC achieves a minimum value when the Raw

Material cost is minimum, which is affected mostly by the total weight of the components.

Moreover, for all optimisation the heuristic features of NGSA-II are visible, with some design exploring much less promising areas of the design space.

During all the optimisation several runs failed and a number of infeasible designs have been produced. This is a drawback of GAs that, in the effort of extensively explores the design space may incur in designs failure (especially in the early stage of optimisation).

Once again parallel coordinates are useful tool to underpin the geometrical variations that lead to improved designs.

Most importantly, these studies have been able to identify interesting and crucial aspects of the relationships between the design parameters and optimum level of the objective functions under consideration. These findings guide the designer to find answers to questions that could not even be addressed before. In this way, understanding the design leads to more intelligent decision-making and design space exploration.

Clearly, the result of the optimisation is dependent on the quality of the cost model. A limitation of the cost suite, as it is at the moment, is that there is not link between geometrical variables and accurate cost data is necessary to form the input to the cost suite.

10 Aero-Cost Trade study

10.1 Introduction

Engineering and finance are often handled by different groups and at different times. By uncoupling engineering and finance, a company runs the risk of overlooking important interactions between the two. A design system that performs engineering and financial analysis simultaneously may improve upon the efficiency and effectiveness of the traditional methods.

While multidisciplinary analysis and optimisation has seen extensive use for technical design problems in aerospace, there has been less emphasis on applying these techniques to larger scope system design.

Traditional commercial aircraft design attempts to improve performance and reduce operating costs by minimizing take-off weight. However, such an approach does not guarantee the profitability of a given aircraft design from the perspective of the airframe manufacturer. A better design approach also takes into account factors such development and manufacturing costs.

In an increasingly competitive market for commercial aircraft, manufacturers may wish to design for improved financial viability of an aircraft program in addition to technical merit before undertaking such a costly investment. The existing practice of designing aircraft from a technical perspective without simultaneously considering the impact on overall program value is not optimal in a business sense.

The coupled performance/financial framework enable an integrated approach to technical design and programmatic decisions.

The objective of this chapter is to couple aero performance and financial design. Specifically, a trade study is conducted in order to see the impact on the Direct Operating Cost (DOC) and manufacturing cost varying parametrically the wing thickness to chord ratio along the wing span. While the process is not automated, the purpose is to establish a useful foundation for further study and to gain insight into the interactions between technical and program design.

10.2 Use case problem formulation

The test case under investigation is a conventional single aisle commercial aircraft, which is representative of an A320-like aircraft, as in Figure 10.1below, in order to generate realistic aerodynamic performance through modifications to the camber and thickness distributions of the wing.

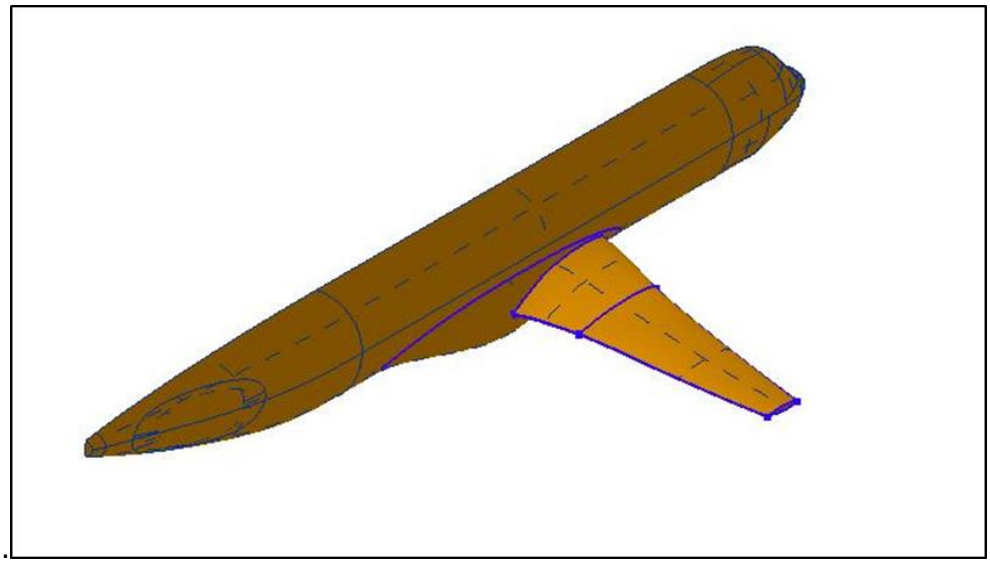

Figure 10.1: Test case, single aisle mid-range commercial aircraft

Starting from the reference geometry, ten new wings with different t/c have been generated. Specifically the thickness over cord along the span has been reduced from the baseline wing respectively of 3%, 5%, 7%, 10% and 12% as can be seen from Figure 10.2

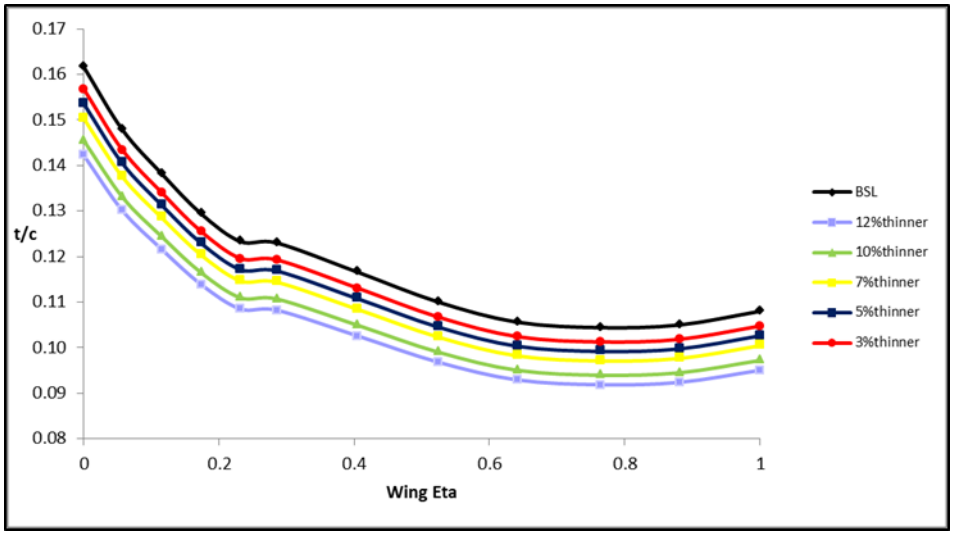

Figure 10.2: Thickness over chord variation along the span

The t/c has been modified in two ways. First, the upper surface has kept constant and the thickness modified moving only the lower surface, see Figure 10.3. Afterwards the thickness has been modified moving both surfaces, keeping constant the camber, see Figure 10.4.

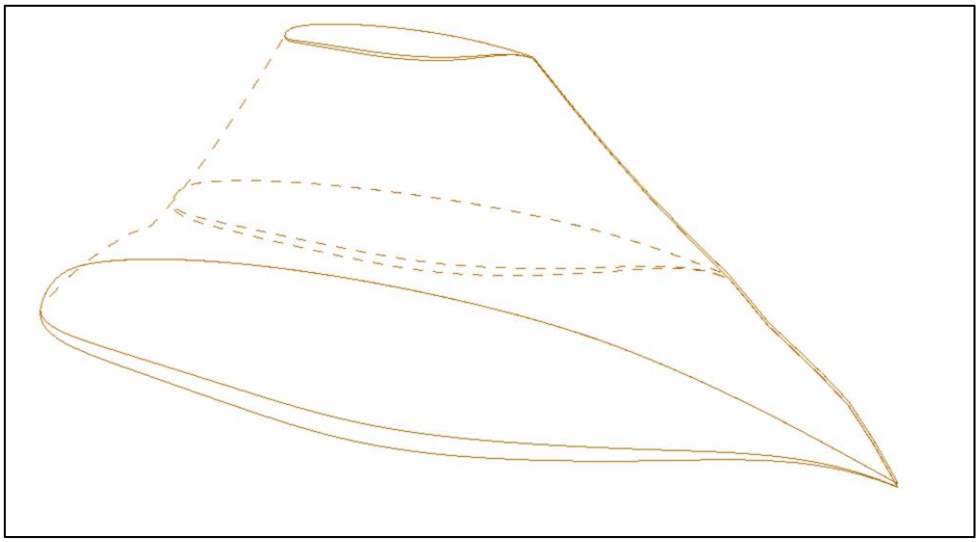

Figure 10.3: Example of t/c modified moving only the lower surface

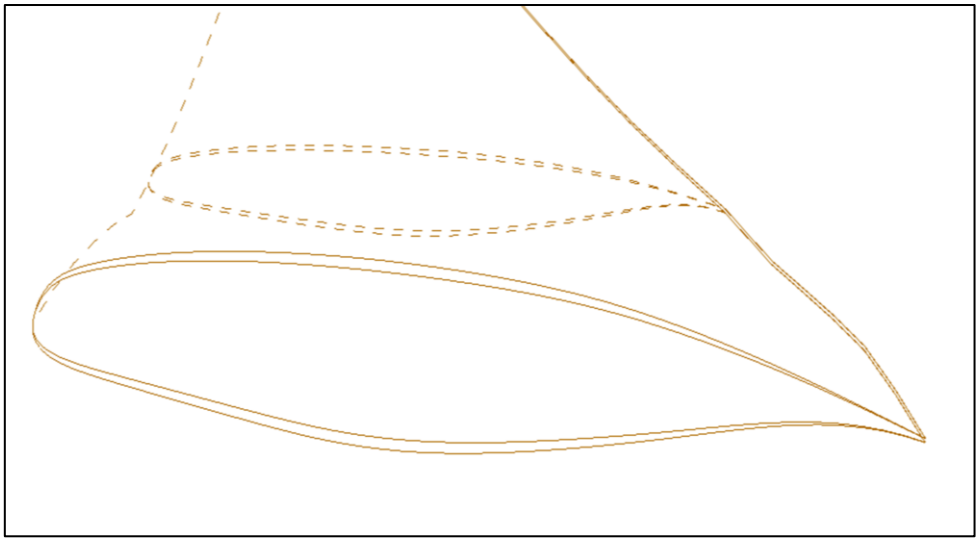

Figure 10.4: Example of t/c modified moving both surfaces

The aerodynamic parameters for the aircraft are calculated using TAU (RANS code) developed by DLR. For this study an unstructured mesh has been generated, for which the surface mesh is made up mainly of quad elements. The mesh is shown in Figure 10.5. It is made up of nearly 2M cells, and the far-

field boundary is a semi hemisphere with a radius of 20 times the wing root chord. A pressure far-field boundary condition has been applied to the external domain and a no-slip condition at the aircraft surface.

In the aircraft's boundary layer the flow gradients are extremely "anisotropic". The gradients normal to the surface through the boundary layer have a very high flow gradient whereas by comparison the flow gradients along the surface are relatively small.

The mesh needs to reflect this and this is the reason for the creation of a "near-field" mesh. The majority of cells in the near-field mesh are very close to the surface and are composed of thin flat hexahedra in order to have a good resolution of the boundary layer.

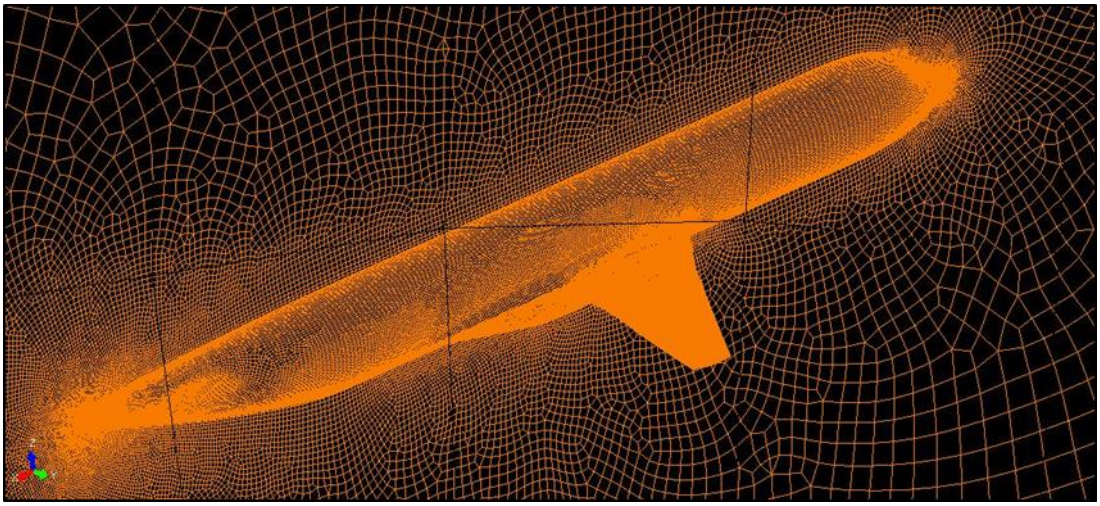

Figure 10.5: Unstructured mesh around the aircraft

The RANS CFD solutions have been run for all the eleven cases from the angle attack range between 0.5 and 4 degrees at cruise speed of M=0.8. The analysis is completed when the lift and drag coefficients have achieved the required degree of convergence. The integral aerodynamics coefficients are extracted at cruise condition. The ratios L/D have been used to calculate the required fuel for the longest flight mission allowable for this aircraft. Since aircraft fuel economy is directly impacted by technology advancement, examining the relationship between fuel consumption and DOC provides a valuable insight into understanding the influence of aircraft aerodynamic performance improvement on aircraft cost.

10.3 CFD Results

The results in term of integral parameters for the baseline and for all cases for which the t/c has been modified moving both surfaces, that from now on for simplicity will be indicated as “both” cases are reported in and figures below.

Table 10.1: Aerodynamic coefficients and the ratio L/D for the baseline and all “both” cases

	Baseline			3%both			5%both			7%both			10%both			12%both		
alpha	Cl	Cd	L/D	Cl	Cd	L/D	Cl	Cd	L/D	Cl	Cd	L/D	Cl	Cd	L/D	Cl	Cd	L/D
0.50	0.369785	0.020849	**17.736342**	0.370346	0.020690	17.899758	0.368744	0.020478	18.006837	0.370116	0.020410	18.134052	0.372056	0.020350	18.282850	0.371779	0.020295	18.318748
0.75	0.401599	0.022001	18.253670	0.402313	0.021799	18.455571	0.400206	0.021563	18.559848	0.401855	0.021498	18.692669	0.403460	0.021415	18.840065	0.403205	0.021330	18.903188
1.00	0.433452	0.023269	18.627874	0.434060	0.023027	18.850046	0.431923	0.022774	18.965619	0.433534	0.022699	19.099255	0.434941	0.022598	19.246880	0.434630	0.022488	19.327197
1.25	0.465378	0.024651	18.878666	0.465976	0.024372	19.119317	0.463715	0.024100	19.241286	0.465382	0.024015	19.378805	0.466585	0.023898	19.524019	0.466202	0.023770	19.613042
1.50	0.497517	0.026180	19.003705	0.498188	0.025862	19.263321	0.495792	0.025572	19.388081	0.497607	0.025480	19.529317	0.498570	0.025355	19.663577	0.498096	0.025217	19.752389
1.75	0.530193	0.027900	19.003333	0.531093	0.027544	19.281622	0.528493	0.027227	19.410622	0.530692	0.027113	19.573341	0.531371	0.026964	19.706683	0.530688	0.026820	19.787025
2.00	0.562955	0.029968	18.785204	0.564253	0.029566	19.084523	0.561629	0.029219	19.221363	0.564409	0.029074	19.412843	0.564994	0.028867	19.572314	0.564245	0.028698	19.661475
2.25	0.595023	0.032426	18.350182	0.597118	0.031997	18.661687	0.594401	0.031601	18.809563	0.598208	0.031456	19.017294	0.599014	0.031186	19.207786	0.598333	0.030982	19.312278
2.50	0.626009	0.035279	17.744522	0.629310	0.034857	18.054049	0.626416	0.034388	18.216122	0.631628	0.034285	18.422867	0.632935	0.033952	18.642053	0.632545	0.033714	18.762087
2.75	0.655082	0.038480	17.023960	0.659971	0.038099	17.322528	0.657069	0.037551	17.498043	0.664200	0.037548	17.689358	0.666377	0.037169	17.928300	0.666421	0.036899	18.060679
3.00	0.680679	0.041928	16.234473	0.687885	0.041652	16.515053	0.685319	0.041014	16.709392	0.694707	0.041178	16.870829	0.698243	0.040785	17.120093	0.699044	0.040498	17.261198
3.25	0.700751	0.045503	15.400105	0.710712	0.045374	15.663420	0.709347	0.044663	15.882207	0.721205	0.045064	16.004017	0.726991	0.044711	16.259779	0.729011	0.044431	16.407711
3.50	0.714594	0.049132	14.544370	0.726638	0.049149	14.784390	0.727308	0.048382	15.032615	0.741029	0.049057	15.105469	0.749845	0.048801	15.365361	0.753771	0.048561	15.522147
3.75	0.724102	0.052807	13.712235	0.737219	0.052951	13.922664	0.739232	0.052119	14.183542	0.753842	0.053064	14.206279	0.765036	0.052916	14.457555	0.770524	0.052726	14.613739
4.00	0.730094	0.056519	12.917674	0.743968	0.056771	13.104719	0.747211	0.055869	13.374340	0.761858	0.057063	13.351173	0.774582	0.057019	13.584630	0.780783	0.056883	13.726122

The lift and drag polar and the relative deltas are reported respectively in Figure 10.6 and Figure 10.7. Neither the magnitude nor slope of lift curve change, but there is an increase in the achievable maximum lift.

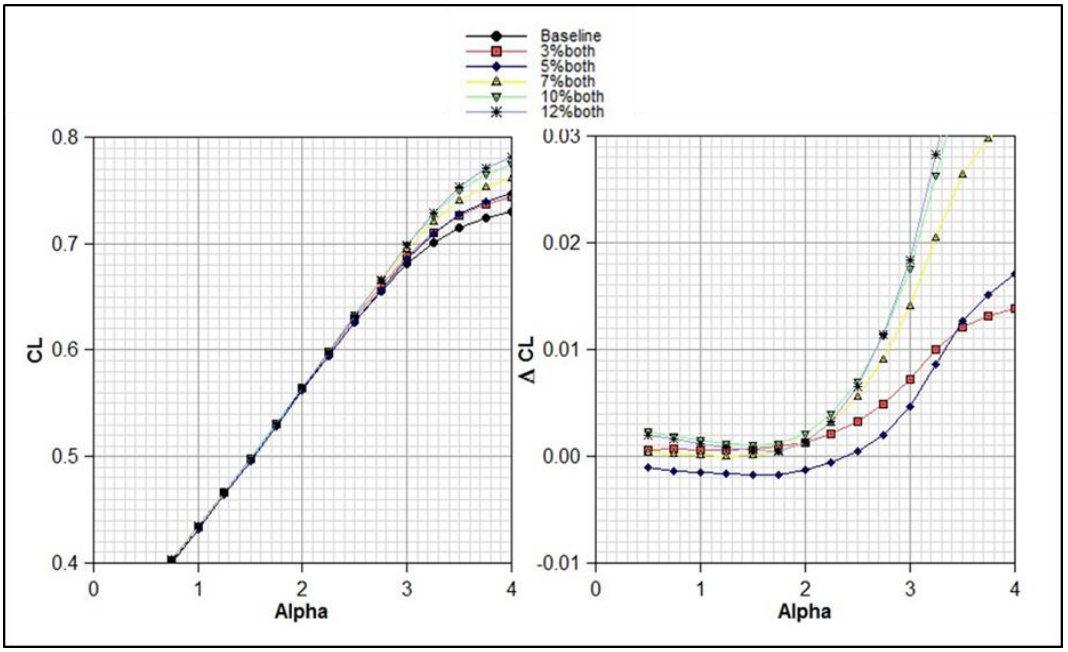

Figure 10.6: Lift Polar and relative CL Delta for the “both” cases

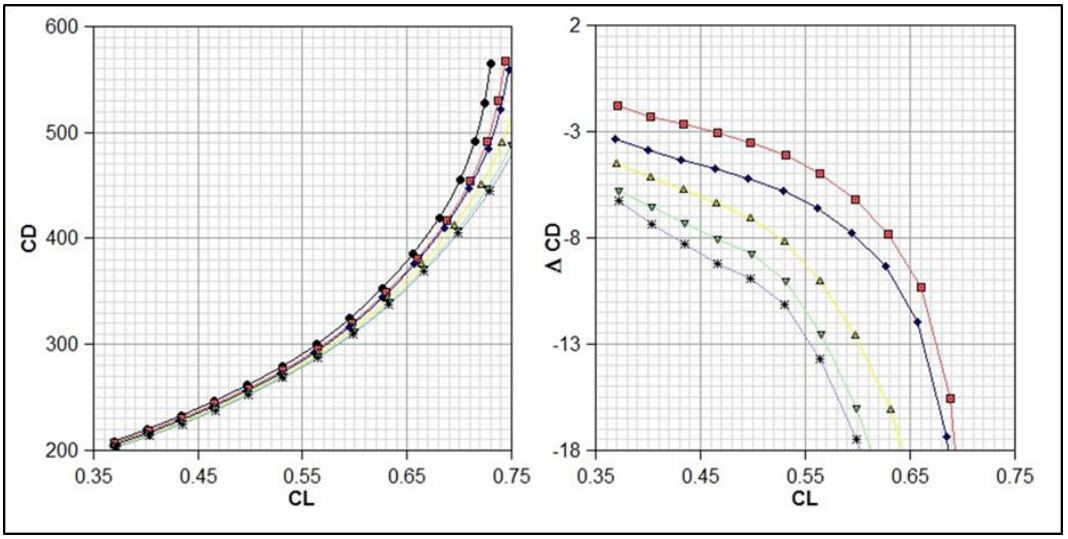

Figure 10.7: Drag Polar and relative Cd Delta for the "both" cases in term of drag count

The total drag has been decomposed in its components using a Drag breakdown tool, that make use of a Far-field analysis, as described in paragraph 5.3.2 of this thesis, and the results reported in term of viscous, induced and wave drag, respectively in Figure 10.8, Figure 10.9 and Figure 10.10.

The drag breakdown shows that the viscous drag and the lift-induced drag constitute the two main sources of drag as expected for a civil transport aircraft, where the lift-induced drag is approximately one third of the total drag.

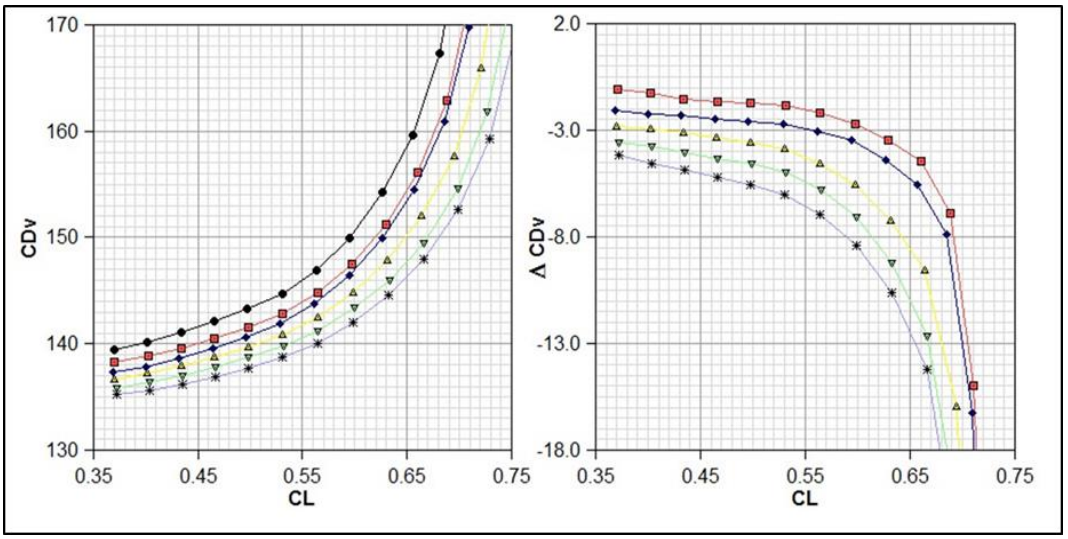

Figure 10.8: Viscous drag for the "both" cases in term of drag count

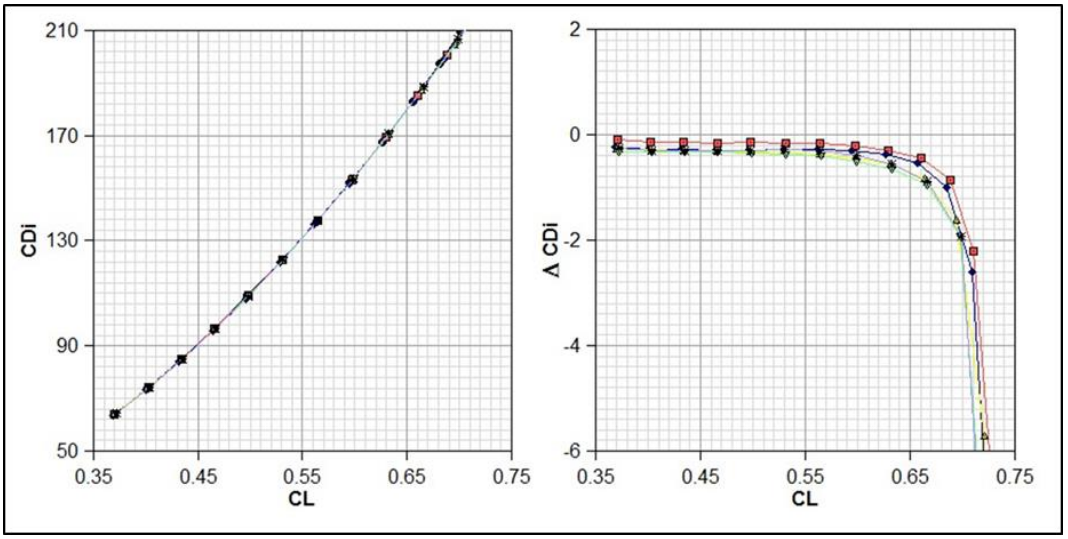

Figure 10.9: Induced drag for the "both" cases in term of drag count

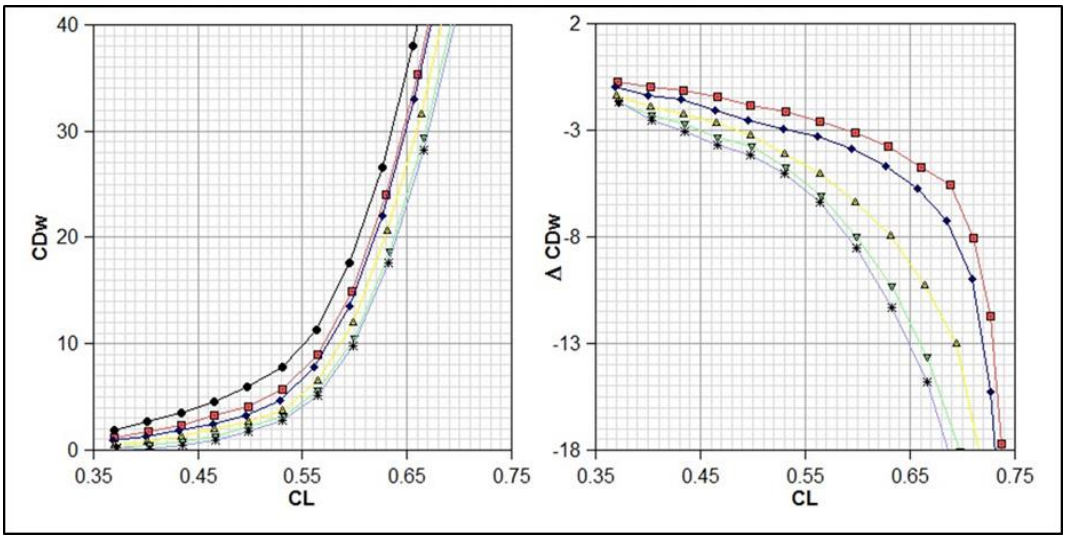

Figure 10.10: Wave drag for the "both" cases in term of drag count

The overall trends suggest reducing thickness leads to associated reduction in viscous drag. Thickness reductions have little effect over majority of CL range in term of induced drag. Reducing thickness leads to reduced wave drag over all CL values.

The results in term of integral parameters for the baseline and for all cases for which the t/c has been modified moving only the low surface, that from now on for simplicity will be indicated as "low" cases are reported in Table 10.2.

Table 10.2: Aerodynamic coefficients and the ratio L/D for the baseline and all "low" cases

	Baseline			3%lower			5%lower			7%lower			10%lower			12%lower		
alpha	Cl	Cd	L/D	Cl	Cd	L/D	Cl	Cd	L/D	Cl	Cd	L/D	Cl	Cd	L/D	Cl	Cd	L/D
0.50	0.369785	0.020849	**17.736342**	0.387732	0.021399	**18.119164**	0.399623	0.021759	**18.365872**	0.407018	0.021921	**18.567492**	0.427575	0.022749	**18.795332**	0.438391	0.023135	**18.949254**
0.75	0.401599	0.022001	18.253670	0.419352	0.022608	18.548832	0.431176	0.023015	18.734564	0.438497	0.023190	18.908883	0.458858	0.024081	19.054773	0.469617	0.024511	19.159439
1.00	0.433452	0.023269	18.627874	0.451081	0.023936	18.845296	0.462707	0.024375	18.982851	0.470001	0.024573	19.126724	0.490332	0.025546	19.194081	0.500994	0.026009	19.262332
1.25	0.465378	0.024651	18.878666	0.482859	0.025377	19.027426	0.494452	0.025855	19.124038	0.501696	0.026071	19.243451	0.521783	0.027109	19.247593	0.532508	0.027611	19.286082
1.50	0.497517	0.026180	19.003705	0.514914	0.026969	19.092810	0.526411	0.027485	19.152665	0.533544	0.027719	19.248313	0.553517	0.028844	19.190022	0.564130	0.029387	19.196584
1.75	0.530193	0.027900	19.003333	0.547416	0.028757	19.035922	0.558821	0.029318	19.060679	0.565916	0.029572	19.136886	0.585612	0.030782	19.024495	0.596179	0.031373	19.002932
2.00	0.562955	0.029968	18.785204	0.579990	0.030891	18.775371	0.591205	0.031491	18.773777	0.598283	0.031763	18.835847	0.617614	0.033053	18.685566	0.628080	0.033686	18.645134
2.25	0.595023	0.032426	18.350182	0.611766	0.033411	18.310317	0.622862	0.034052	18.291495	0.629932	0.034342	18.342904	0.648823	0.035707	18.170751	0.659192	0.036381	18.119128
2.50	0.626009	0.035279	17.744522	0.642387	0.036321	17.686380	0.653250	0.036996	17.657314	0.660345	0.037309	17.699349	0.678478	0.038719	17.523128	0.688765	0.039436	17.465387
2.75	0.655082	0.038480	17.023960	0.670942	0.039562	16.959254	0.681449	0.040265	16.924103	0.688726	0.040612	16.958682	0.705716	0.042031	16.790369	0.715570	0.042764	16.733000
3.00	0.680679	0.041928	16.234473	0.695918	0.043043	16.167972	0.705805	0.043751	16.132317	0.712975	0.044114	16.162103	0.728823	0.045531	16.007182	0.738160	0.046281	15.949526
3.25	0.700751	0.045503	15.400105	0.715398	0.046636	15.340038	0.724527	0.047344	15.303460	0.731570	0.047720	15.330469	0.746300	0.049107	15.197426	0.755117	0.049862	15.144138
3.50	0.714594	0.049132	14.544370	0.729247	0.050277	14.504585	0.740331	0.051077	14.494410	0.744908	0.051364	14.502531	0.759171	0.052734	14.396234	0.767971	0.053497	14.355403
3.75	0.724102	0.052807	13.712235	0.738543	0.053945	13.690666	0.751459	0.054806	13.711254	0.754980	0.055057	13.712698	0.769146	0.056423	13.631781	0.778168	0.057198	13.604811
4.00	0.730094	0.056519	12.917674	0.745477	0.057669	12.926824	0.755518	0.058433	12.929646	0.762172	0.058791	12.964093	0.776830	0.060200	12.904153	0.785724	0.061036	12.873124

The lift and drag polar and the relative deltas are reported respectively in Figure 10.11 and Figure 10.12.

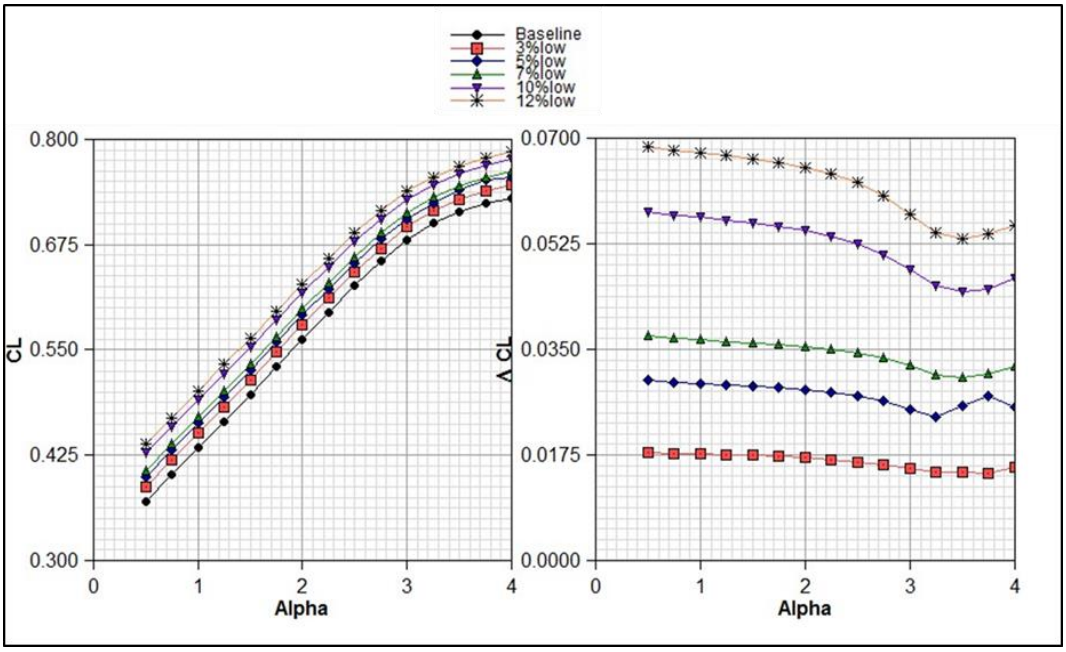

Figure 10.11: Lift Polar and relative CL Delta for the "low" cases

Moving the low surface leads to camber change (increases as thickness decreases). Hence this explains why lift curves are shifted.

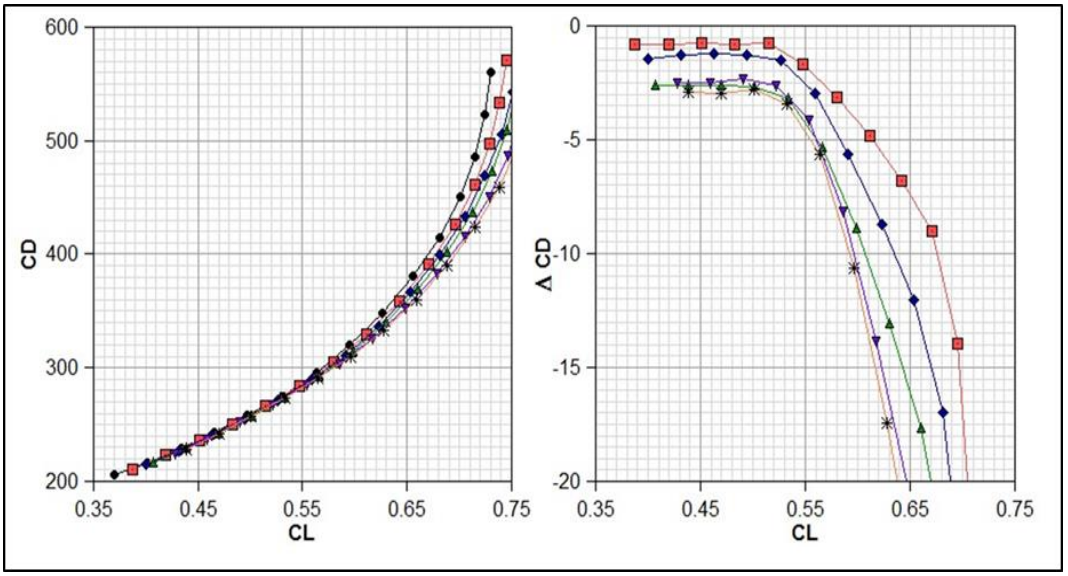

Figure 10.12: Drag Polar and relative Cd Delta for the "low" cases in term of drag count

As in the previous both cases, the total drag has been decomposed in its components using the same Drag breakdown tool, and the results reported in term of viscous, induced and wave drag, respectively in Figure 10.13, Figure 10.14 and Figure 10.15.

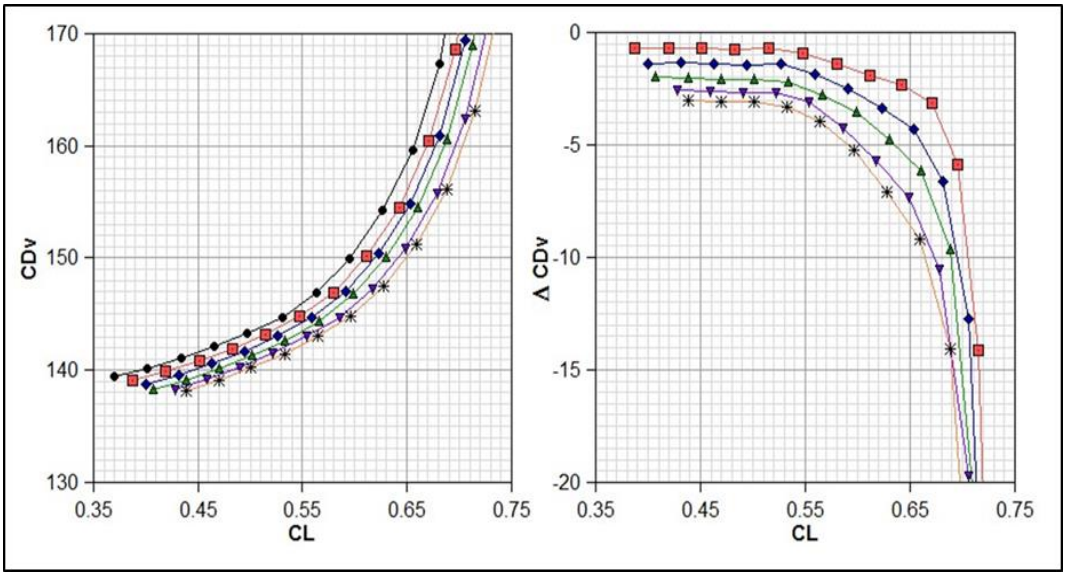

Figure 10.13: Viscous drag for the "low" cases in term of drag count

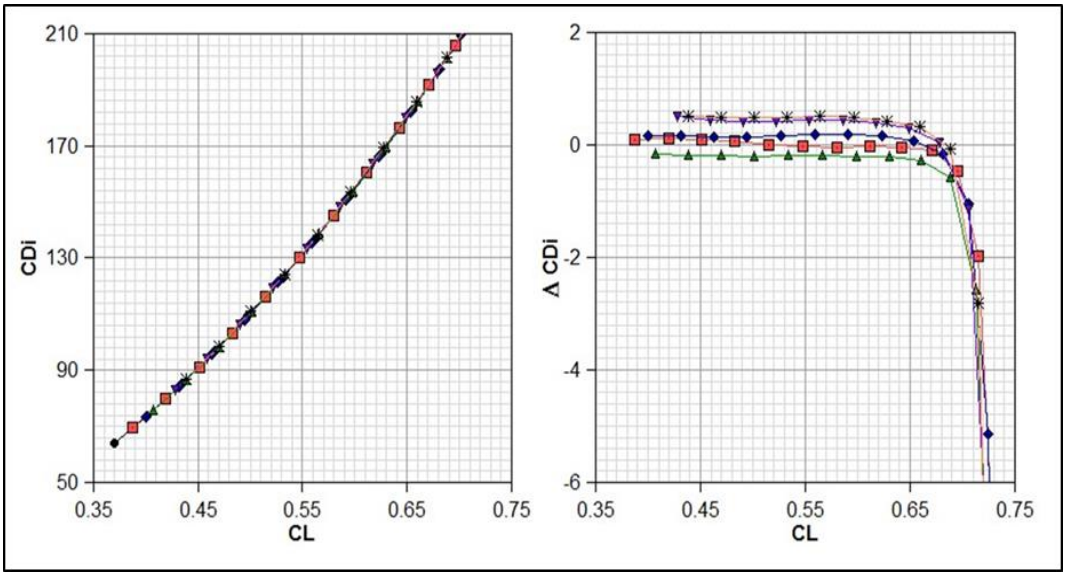

Figure 10.14: Induced drag for the "low" cases in term of drag count

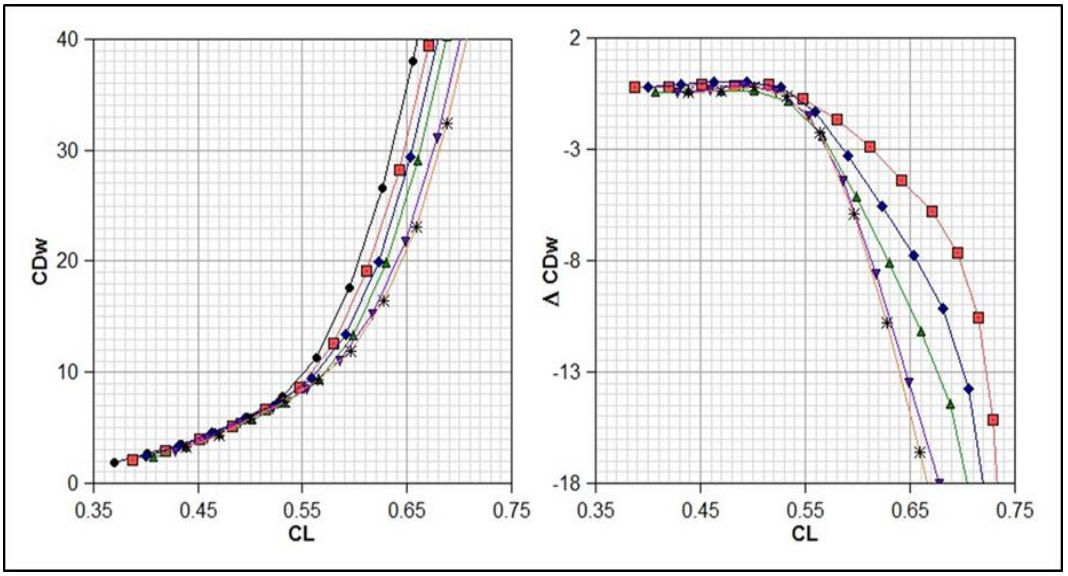

Figure 10.15: Wave drag for the "low" cases in term of drag count

In all cases is found that the lift-induce drag does not vary too much with the thickness variation. This is fairly expected given that lift-induced drag is mainly driven by the planform shape, which has not been modified for all cases under investigation. For the "low" cases the effect on the wave drag is now quite different – does not really reduce wave drag (as expected since wave drag is mainly influenced by the upper surface shocks, upper surface that has been kept the same), but does demonstrate a delay in rapid drag rise.

The required fuel for the flight mission is calculated using the method presented by Roskam [185]. In this method the required fuel for the cruise is calculated using the Breguet range equation. This simplification might lead to inaccurate prediction of the total aircraft fuel consumption. But in this study it is not in any way intended to be exact, but rather to give an order of magnitude, thus some rough assumptions are made. The key assumptions are that Specific Fuel Consumption (SFC), L/D, and flight speed, V are constant, and therefore take-off, climb, and descend portions of flights are not well modelled [186]. This assumption in turn leads to inaccurate calculation of fuel burn, mission range and time, and thus an inaccurate DOC. Moreover, most fuel burn computation focuses more on the cruise portion, which is critical for range missions for commercial aircraft. The analysis exclusively examined the cruise phase of flight, ignoring the climb and descent at the beginning and end of each flight.
The fuel burn has afterwards used as input for the cost suite. The fuselage parameters are assumed to be constant. As for the wing the only parameters modified are the t/c at the root, at the crank and at the tip.

10.4 Financial Results

Once calculated the approximated mission fuel burn, the mission and geometry files input for the cost suite have been updated accordingly and cost analysis launched for all cases and the Direct Operating cost calculated, see Figure 10.16.

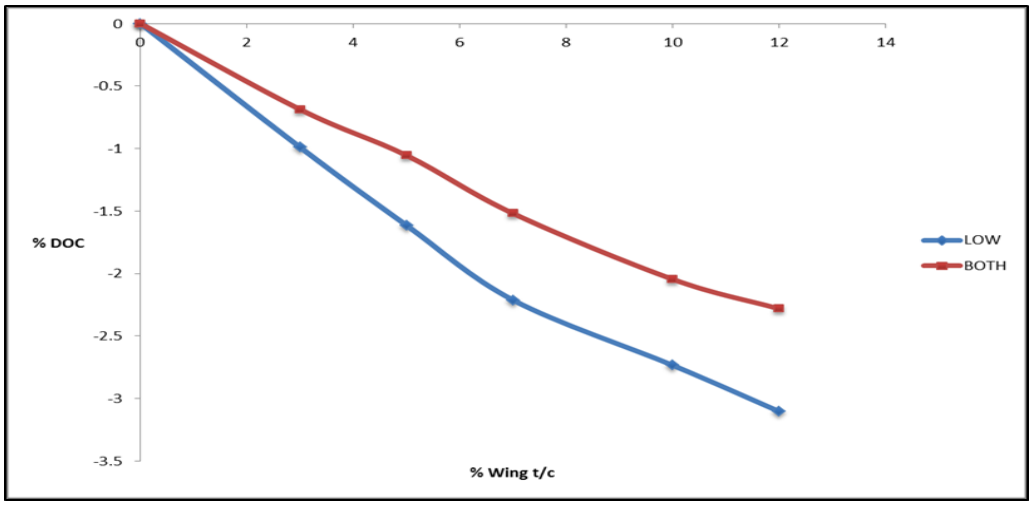

Figure 10.16: DOC function of the thickness over chord variation

The cost analysis has been launched keeping constant the desired Internal Rate of Return (IRR) for the manufacturer. Summary of results are reported in Table 10.3.

Table 10.3: Financial summary results for all cases investigated

	∆Wing Cost (RC)	∆Sale Price	IRR(Airline)	IRR(Manufacture)	∆DOC
BSL	0.00%	0.00%	6.00%	6.00%	0.000%
3%both	-0.61%	-0.69%	6.34%	6.00%	-0.688%
5%both	-1.05%	-0.86%	6.52%	6.00%	-1.056%
7%both	-1.59%	-1.06%	6.74%	6.00%	-1.520%
10%both	-2.29%	-1.34%	7.00%	6.00%	-2.047%
12%both	-2.75%	-1.52%	7.12%	6.00%	-2.283%
3%low	-0.61%	-0.72%	6.48%	6.00%	-0.991%
5%low	-1.05%	-0.86%	6.67%	6.00%	-1.616%
7%low	-1.59%	-1.06%	7.05%	6.00%	-2.213%
10%low	-2.29%	-1.34%	7.31%	6.00%	-2.735%
12%low	-2.75%	-1.52%	7.49%	6.00%	-3.105%

As it is possible to discern from the table above is that wing recurring cost decreases accordingly with the reduction of the t/c and not difference is found between “both” and “low” cases as expected. Although, the number of parts quantity do not vary with the reduction of t/c, the size of the components decrease, which implies less raw material to be used. Moreover, the quantity of fasteners for any part that attaches to the spars will reduce as t/c decreases e.g. Slat Ribs and Hold down Ribs on Leading Edge, Inter Spar Ribs in Wing Box, hence less fasteners are necessary for the assembly. Consequently it means less labour time and all this translates in reduction of recurring cost.

The fact that the IRR for the manufacturer is kept constant means that the aircraft price decrease proportionally. This translates in a better internal rate of return for the customer. Moreover, the better Direct Operating cost achieved is not only due to the better aerodynamic performance that in turn is translated in a less fuel consumption but also to the decrease of sale aircraft price, even if to a lesser extent. Although aircraft price is also influenced by other factors, such as fuel prices, tax rates, and leasing rates as well as airlines’ negotiations with

manufacturers and optional specifications while these external factors are not considered in this study.

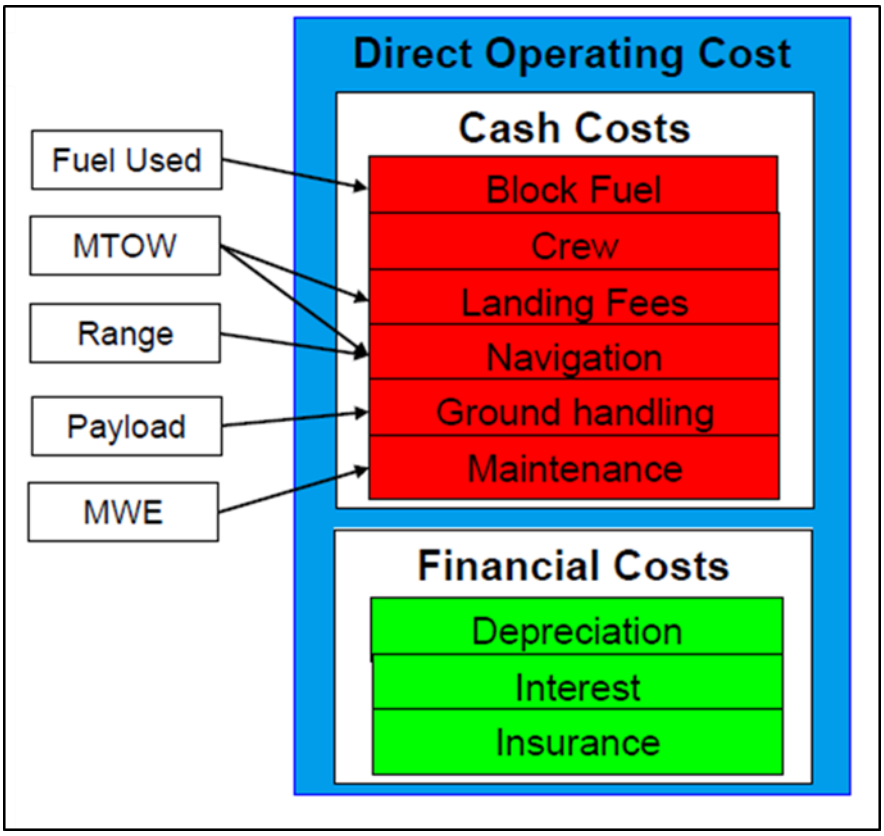

Figure 10.17: Breakdown of Direct Operating Cost

On the other hand it is clearly possible from the manufacturer increases or keeps constant the aircraft price without having a negative effect. In general, airlines are willing to pay higher prices for new aircraft if they can lower operating costs by adopting more-fuel efficient, advanced technology.

A further analysis has been carried in order to check the effect of aerodynamic performance in term of spanwise loading. The next Figure 10.18 and Figure 10.19 show the aerodynamic load over the wing for the “both” and “low” cases calculated at cruise.

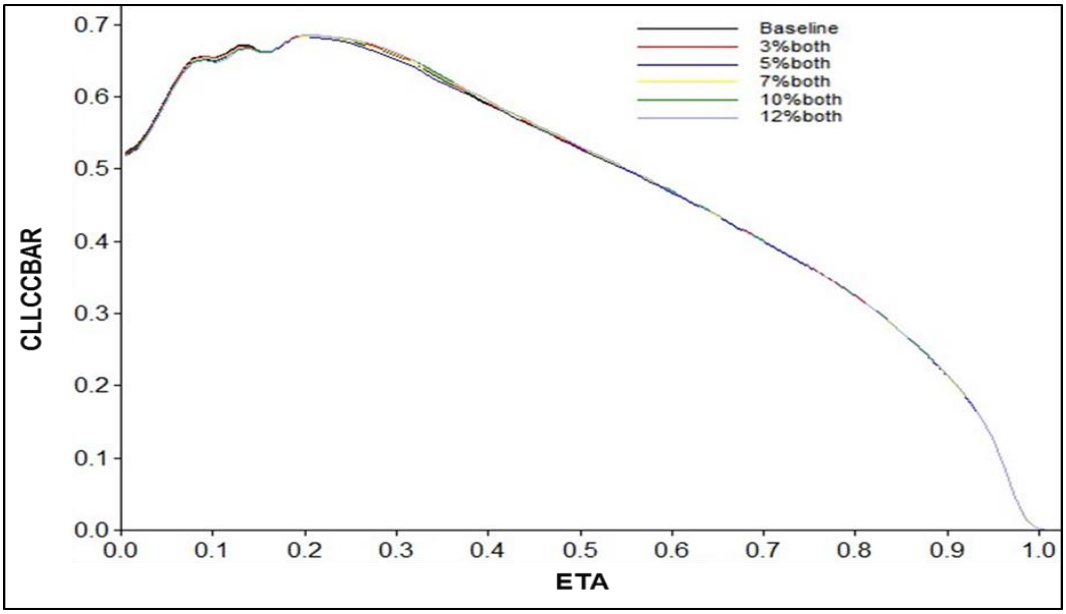

Figure 10.18: Spanwise loading for "both" cases at cruise

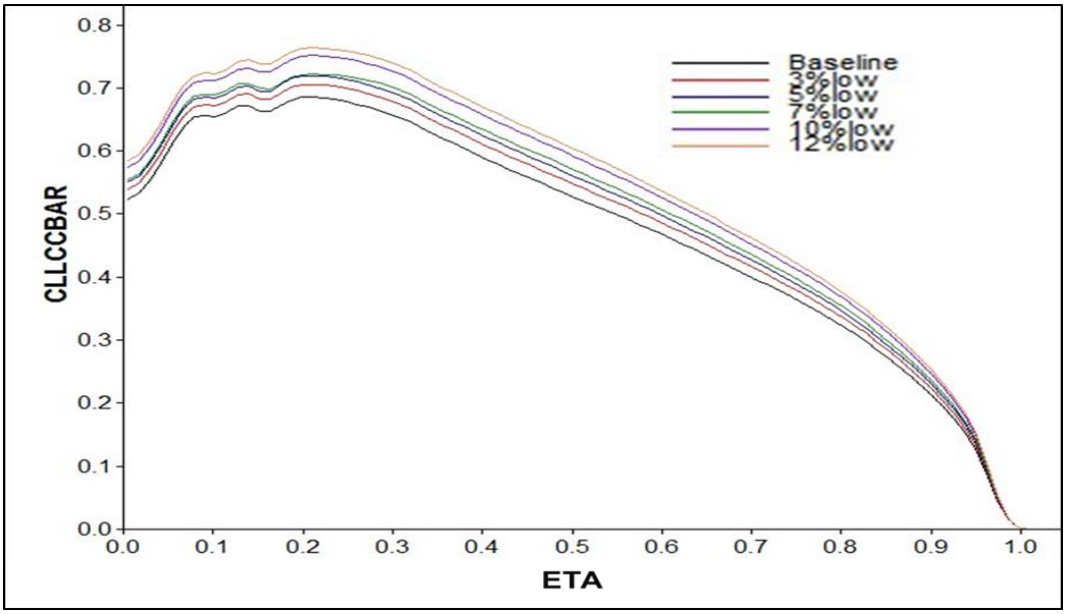

Figure 10.19: Spanwise loading for "low" cases at cruise

It is evident from the figures above that for the "both" cases, the spanwise loading does not vary much with the t/c variation. On the contrary, for the "low" cases the spanwise loading increases when the wing is thinner. This means that the structure has to withstand higher loads and therefore the weight of the wing has to increase accordingly due to a larger wing box sizing. Therefore, the DOC benefit gained due to better aerodynamic performance contrast with higher load on the wing. Hence is clear that to analyse the aircraft performance,

it is important to consider both aerodynamic and structural disciplines simultaneously, to account for the interaction and trade-offs between the two disciplines. To conclude the impacts of aircraft aerodynamic performance on aircraft direct operating cost and price have been quantified. In general, improvements in aircraft aerodynamic performance lead to reductions in direct operating cost. Bearing in mind that economic behaviours have been described by only a few simplified parameters.

11 Conclusion and Future work

Over the course of the last decade a new multi-disciplinary mind-set has been influencing aircraft product development, and this philosophy has now extended throughout all aspects of aircraft engineering design. To mitigate technical and financial risks and compress program time lines, there is an increasing need for more sophisticated tools with capabilities for analysing complex, tightly cross-coupled systems and functions involving a wide range of engineering disciplines. This remains a challenge for the scientific community but a multi-disciplinary approach is essential in the design process of real world applications.

A review of current status of multi-disciplinary design optimisation and current limitations has been addressed in the first chapters of the thesis. Several parameterisation strategies and optimisation algorithms currently used in industry have been presented, highlighting advantages and drawbacks.

The thesis has presented the development and application of an integration/optimisation framework for the preliminary design of high-speed aircraft configuration, involving aero performance and finance jointly in an aircraft program.

An approach is proposed in this work to support the preliminary design for cruise aircraft configurations. For this purpose an integrated 3D automatic aero high-speed framework has been developed, as a process oriented workflow due to the dynamic of input/output.

It thus far enables only generation of aero data for loads for the cruise phase, but in a time frame, which is compatible with the requirements of an overall multi-disciplinary preliminary design process at this level, providing an important fully automatic design capability to the industrial partner.

The scheme has already been tested for different aircraft configurations, from single aisle to long-range aircraft, and has been demonstrated to be seamless and robust. The 3D aero solution chain has been implemented as a high-speed aerodynamic evaluation capability. Although, there is not yet an automated complementary aerodynamic design process, two integrated systems to perform multi-objective aero optimisation have been developed, using two

different optimisation approaches. The first is the direct optimisation approach, and the second makes use of the Proper Orthogonal Decomposition (POD) mathematical technique, in order to accelerate the whole process, for which a lot of work has been done in making it an automated process with a lot of communication between the workstation and the HPC cluster and in the implementation of the POD method for optimisation purposes. A detailed analysis of the methods as well as the results of the comparison between the two techniques, but also between different optimisation algorithms is provided. The multi-level parallelisation of the framework allows the use of accurate RANS simulations for the flow field evaluation, with the associated high level of fidelity.

The POD-based optimisation method presents some clear strength when compared to the classical approach. In fact, firstly, the optimisation process is de-coupled from the RANS execution, reducing the risk of failure during the process. Secondly, the generated POD can be re-used to tackle different optimisation problems, as long as the same set of design variables is used. The substantial gain in computational time for optimisation problem when surrogate model are used was demonstrated. The results of both optimisation processes have illustrated the potential of the proposed approaches, but also their limitations.

The results for the foregoing studies demonstrates that multi-objective integrated design optimisation system can successfully tackle realistic real-world problems, and presenting the designer with a range of designs showing the trade-offs between the objectives under consideration, giving insight into the nature of the design space and suggesting innovative designs for further consideration. In addition, it is revealed that integrated optimisation framework is important in aerodynamic design problems. Even though a few designs might represent the optimum design area, only detailed exploration can manage the appropriate refinements in the optimum shape, in order to achieve a generic performance improvement.

In addition to achieving good aircraft performance, reducing cost may be essential for manufacturer survival in today's competitive market.

For this reason a pre-existing cost model has been examined, tested, improved, and new features added. Afterwards, the cost suite has been integrated using an integration framework and automatically linked with external domain giving capability to take input from other Domains Tool Sets. Therefore, changes in one model that impact on another model are passed automatically. In this way the cost model could be implemented in a multi-disciplinary process allowing a trade-off between weight, aero performance and cost. Besides, the integration of the cost suite in Model Center has been slightly modified to consider Recurring and Non-Recurring cost as objectives for a series of cost optimisation studies performed and results analysed by mean of parallel coordinate multi-dimensional analysis tool. Most importantly, these studies have been able to identify interesting and crucial aspects of the relationships between the design parameters and optimum level of the objective functions under consideration. Visualisation tools, such as the parallel coordinate, of the geometrical design space can potentially reveal hidden aspect of the behaviour of the system under consideration. In this way the geometrical features might be characterised with respect to specific metrics crucial in understanding complex phenomena. These findings guide the designer to find answers to questions that could not even be addressed before. In this way, understanding the design leads to more intelligent decision-making and design space exploration.

Clearly, the result of the cost optimisation is dependent on the quality of the cost model. A limitation of the cost suite, as it is at the moment, is that there is no link between geometrical variables and, accurate cost data is necessary to form the input to the cost suite.

Additionally, studies have been performed to link aerodynamic characteristics with cost figures and results reported.

In the Aero-Cost Trade study chapter, the impacts of aircraft aerodynamic performance on aircraft direct operating cost and price have been quantified. In general, improvements in aircraft aerodynamic performance lead to reductions in direct operating cost. Bearing in mind that economic behaviours have been described by only a few simplified parameters.

The proposed work offers a strong basis for further development.

The modularity of the aero optimisation framework could allow the application of such a technique to real engineering test cases and could be combined with the 3D aero solution chain already developed. Moreover, in order to further reduce the wall clock time the already multi-level parallelisation could be flanked by a multi-fidelity approach. Specifically, CFD methods of different fidelity can be combined in order to accelerate the convergence of the optimisation process. Further development is required on the POD model construction in order to increase its accuracy and range of applicability. In particular, the challenges of producing high quality mesh around the aerodynamic element which retaining its topology (requirements for the POD decomposition) must be addressed. Clearly, this represents a limiting factor in the application of POD-based optimisation to design problems that present a wide range of variability of the design variables. A combination of surrogate models suitable for more efficient search of the design space or for faster evaluation in the design process might introduce a higher quality of intelligence in the design system and therefore increase its efficiency.

In addition, the 3D aero solution chain could be improved integrating the module to generate the aero data for performance and linked to the cost suite, which in turn could be improved linking the geometrical variables.

From the aero cost trade study chapter it has been highlighted that aerodynamic force clearly has an impact on the structure, hence it is clear that to analyse the aircraft performance, it is important to consider both aerodynamic and structural disciplines simultaneously, to account for the interaction and trade-offs between them. The cost modelling methodology for the linkage between manufacturing and design imposes a breakdown of the cost into a number of elements, including material cost, fabrication cost, and assembly cost, so that it could be formulated into semi-empirical equations to be linked to the same design variables as considered in the structural analysis.

For the assessment of an aircraft configuration it is essential to consider all relevant disciplines and their interactions on overall aircraft level.

To conclude, MDO techniques can reduce the weight and cost of an aircraft design concept in the preliminary design phase by fairly minor changes to the key design variables.

REFERENCES

[1] ACARE, “Flightpath 2050 Europe’s Vision for Aviation”, *Report of the High Level Group on Aviation Research*, European commission, 2011.

[2] Markish, J., “Valuation Techniques For Commercial Aircraft Program Design”*. Master’s thesis, Massachusetts Institute of Technology (MIT),* US, 2002.

[3] Reihnardt, D. P., “Break-even Analysis of Lockheed’s Tri Star: An Application of Financial Theory”. *Journal of Finance*, Vol. 28, Issue 4, pp. 821-838, Sep. 1973.

[4] Dickinson, M. W., Graves, S., Thorton, A. C., “Technology portfolio Managment: Optimizing Interdependent Projects Over Multiple Time Periods”. *MIT working paper*, 1999.

[5] Slack, R., “The Application of Lean Principles to the Military Aerospace Product Development Process”. *PhD thesis, Massachusetts Institute of Technology (MIT)*, US, 1998.

[6] Browning, T. R., “Modeling and Analyzing Cost, Schedule, and Performance in Complex System Product Development”. *PhD thesis, Technology, Management and Policy, Massachusetts Institute of Technology (MIT),* US, 1998.

[7] Price A. R., Keane A. J., Holden C. :On the coordination of Multidisciplinary Design Optimisation Using Expert Systems”. *AIAA Journal*, Vol. 49, No 8, 2011.

[8] Ghisu T., Parks G. T., Jarrett J. P. and Clarkson P. G., “An Integrated System for the Aerodynamic Design of Compression Systems—Part I: Development”. *Journal of Turbomachinery* Vol. 133, Issue 1, January 2011.

[9] Ghisu T., Parks G. T., Jarrett J. P. and Clarkson P. G., “An Integrated System for the Aerodynamic Design of Compression Systems—Part II: Application”. *Journal of Turbomachinery* Vol. 133, Issue 1, January 2011.

[10] Wakayama S., Kroo I., “Subsonic Wing Platform Design Using Multidisciplinary Optimization”. *Journal of Aircraft*, Vol. 32, No 4, pp. 746-753, Aug. 1995.

[11] Wakayama S., Kroo I., “The Challenge and Promise of Blended-Wing-Body Optimization”. *AIAA paper* 96-4003, Sep. 1996.

[12] Kroo I., Manning V., “Collaborative Optimisation: Studies and Directions”. *AIAA paper* 2000-4721, Sep. 2000.

[13] Baker A. P. Mavris D. N., “Assessing the Simultaneous Impact of Requirements, Vehicle Characteristics, and Technologies During Aircraft Design”. *AIAA paper* 2001-0533, Jan. 2001.

[14] Perez Ruben E., Liu Hugh H. T., “Flight Dynamics and Control Multidisciplinary Integration in Aircraft Conceptual Design Optimization”. *AIAA Conference paper*, 2004-4435, 10th AIAA/ISSMO Multidisciplinary Analysis and Optimization Conference Albany, New York, 30 Aug. - 1 Sep. 2004.

[15] Peoples R., Willcox K. “A Value-Based MDO approach to Assess Business Risk for Commercial Aircraft Design”. *AIAA Conference paper* 2004-44378, 10th AIAA/ISSMO Multidisciplinary Analysis and Optimization Conference Albany, New York, 30 Aug. - 1 Sep. 2004.

[16] Zang T. A. and Green L., “Multidisciplinary Design Optimisation techniques: implications and opportunity for fluid dynamics research”. *30th AIAA Fluid Dynamics conference*, Norfolk, VA. June 28 - July 1, 1999.

[17] Kipouros T., “Multiobjective Aerodynamic Design Optimization”. *PhD thesis, Cambridge University,* 2006.

[18] Deloitte, “AIAC-Global Aerospace Market Outlook and Forecast”. *Technical report*, Deloitte & Touche LLP and affiliated entities, 2010.

[19] Sehra, A.K. and Whitlow, W.J., “Propulsion and Power for 21st Century Aviation”. *Progress in Aerospace Science*, Vol. 40 pp. 199-235, 2004.

[20] Keane A. J. and Nair P. B., “Computational Approaches for Aerospace Design: The Pursuit of Excellence”. *Book,* John Wiley and Sons, Chichester, UK, 2005.

[21] https://courses.cit.cornell.edu/mae5070/Caughey_2011_04.pdf

[22] John P. Fielding “Introduction to Aircraft design”, Cambridge Press, 1999.

[23] Torenbeek E., “Synthesis of Subsonic Airplane Design: An Introduction to the Preliminary Design of Subsonic General Aviation and Transport Aircraft, with Emphasis on Layout, Aerodynamic Design, Propulsion and Performance”. *Book*, Springer Science & Business Media, 1982.

[24] Sadraey M., “Aircraft Design: A Systems Engineering Approach”. *Book,* chapter 5, Wiley Publications, 2012.

[25] Dimitriadis G., “Aircraft Design course” Universite de Liege Lecture 10 Aeroelasticity.

[26] https://commons.wikimedia.org/wiki/File:Jetliner%27s_main_fuel_tanks.png

[27] D. G. Hull, “Fundamentals of Airplane Flight Mechanics”, Springer, 2007.

[28] Hurt H. H. Jr., “Aerodynamics for Naval Aviators”. *Book*, published by Direction of the Commander, Naval Air Systems Command, United States Navy, reprinted by Aviation Supplies and Academics, Inc., 7005 132nd Place SE, Renton, Washington 98059-3153, 1965.

[29] Harris C. “Supercritical Airfoils A Matrix of Familiy-Related Airfoils”, NASA Technical Paper 2969-NASA Langley Research Center, Hampton, Virginia, EE UU: NASA. 1990.

[30]https://commons.wikimedia.org/wiki/File%3ASwept_wing_w_spanwise_boundary_layer_flow.svg

[31] Prandtl, L., “Applications of modern hydrodynamics to aeronautics,” *Technical rep*ort, NACA Rep. 116 (National Advisory Committee for Aeronautics), 1923.

[32] http://adg.stanford.edu/aa241/wingdesign/images/image332.gif

[33] D.R. H. Introduction to Transonic Aerodynamics of Aerofoils and Wings. 1990;(90008).

[34] Holt, D. R., “Introduction to transonic aerodynamics of aerofoils and wings,” *Technical report*, ESDU (Engineering Sciences Data Unit) 90008, April 1990.

[35] Holt, D. R., “Guide to wing aerodynamic design” Technical report, ESDU, 97017, August 1997.

[36] Mann A., Elsholz E., “The M-DAW Project Investigations in Novel Wing Tip Device Design”, 43rd AIAA Aerospace Sciences Meeting and Exhibit, Reno, Nevada, 2005.

[37] Chang K. H., Silva J., “Design Parameterization for Concurrent Design and Manufacturing of Mechanical Systems”, DETC2001/DFM-21161, *Proceedings of ASME 2001 Design Engineering Technical Conference and Computers and Information in Engineering Conference,* Pittsburg, PA, USA, Sep. 2001.

[38] Bowcutt K.G., "A Perspective on the Future of Aerospace Vehicle Design", *AIAA 2003-6957, 12th AIAA International Space Planes and Hypersonic Systems and Technologies*, Norfolk, VA, USA, Dec. 2003.

[39] Lazzara D. S., Haimes R., and Willcox K., “Multifidelity Geometry and Analysis in Aircraft Conceptual Design”. *19th AIAA Computational Fluid Dynamics Conference*, San Antonio, Texas, 22 - 25 June 2009.

[40] Ledermann C., Hanske C., Wenzel J., Ermanni P., Kelm R., ”Associative parametric CAE methods in the aircraft pre-design”, *Journal of Aerospace Science and Technology*, Vol. 9, Issue 7, pp. 641-651, Oct. 2005.

[41] Ledermann, C., Ermanni, P., Kelm, R., ”Dynamic CAD objects for structural optimization in preliminary aircraft design”, *Journal of Aerospace Science and Technology*, Vol. 10, Issue 7, pp. 601-610, Oct.2006.

[42] Benn M., Eppstein D., “Mesh Generation and Optimal triangulation”. Computing in Euclidean Geometry, Du Z. F., Hwang F. K., eds, World Scientific, 2nd edition, pp. 1-78, 1995.

[43] Anderson J., “Fundamental of Aerodynamics”. Book McGraw-Hill, 2010.

[44] De Berg, Mark, Otfried Cheong, Marc van Kreveld; Mark Overmars, “Computational Geometry: Algorithms and Applications: Chapter 9”, Springer-Verlag. ISBN 978-3-540-77973-5, 2008.

[45] Navier C. “Mémoire sur les lois du mouvement des fluids”. *Mémoires de l’Académie Royale des Sciences de l’Institut de France*, 6:389–440, 1823.

[46] Stokes G.G., “On the theories of the internal friction of fluids in motion and of the equilibrium and motion of elastic solids”. *Transactions of the Cambridge Philosophical Society*, 8:287–319, 1819.

[47] Orszag S.A., “Analytical theories of turbulence”. *Journal of Fluid Mechanics*, Cambridge Univ Press; 41(02):363–86, 1970.

[48] Van Dyke M., An album of fluid motion, Parabolic Press, 1982.

[49] Henne P. A., “Applied Computational Aerodynamics”, *Progress in Astronautics and Aeronautics, AIAA*, Vol. 125, 1990.

[50] Houghton E.L., Carpenter P.W. “Aerodynamics for engineering students”, Butterworth-Heinemann, 2003.

[51] Mason W., “Applied computational aerodynamics”, 1997.

[52] Konstadinopoulo P, Thrasher D. F., Mook D. T., Nayfeh A. H., and Watson L., “A vortex-lattice method for general, unsteady aerodynamics” *Journal of Aircraft*, January, Vol. 22, No. 1 : pp. 43-49, 1985.

[53] Thom A., Apelt CJ. “Field computations in engineering and physics”, Van Nostrand; 1961.

[54] Bakker, “Computational Fluid Dynamics (Course material, Lecture 5: Finite volume solvers)” [Internet]. Available from: http://www.bakker.org/dartmouth06/engs150/05-solv.pdf, 2004.

[55] Morton KW., Mayers DF. “Numerical solution of partial differential equations: an introduction”. Cambridge University press; 2005.

[56] D K. “Introduction to Computational Fluid Dynamics (Course material, Lecture 3: Discretization techniques)”. Institue of Applied Mathematic - University of Dortmund; 2010.

[57] Courant R., “Variational methods for the solution of problems of equilibrium and vibrations”. Bull Amer Math Soc. 49(1):1–23, 1943.

[58] Särndal C-E, Swensson B, Wretman JH. “The weighted residual technique for estimating the variance of the general regression estimator of the finite population total”. Biometrika. Biometrika Trust; 76(3):527–37, 1989.

[59] Keane A, Nair P. “Computational approaches for aerospace design: the pursuit of excellence”, John Wiley \& Sons; 2005.

[60] Blazek J. “Computational Fluid Dynamics: Principles and Applications”. Elsevier; 2001.

[61] Prandtl L., “Ueber Fluessigkeitsbewegung mit kleiner Reibung”. In Verhandlungen des dritten internationalen Mathematischen Kongresses, Heidelberg. pp. 484–491, Leipzig, Teubner Verlag, 1905.

[62] Manna M., “A three-dimensional High Resolution Compressible Flow Solver”, *PhD thesis*, Univesite’ Catholique de Louvain, 1992.

[63] Veldma A. and Coenen, “Interaction Laws in Viscous-Inviscid Coupling”. Domain Decomposition Methods in Science and Engineering, *Lecture Notes* in Computational Science and Engineering Volume 40, pp. 225-232, 2005.

[64] Lock R. and Williams B., “Viscous-inviscid interactions in external aerodynamics”, *Prog. Aerospace Science*, 24:51–171, 1987.

[65] Reynolds O., “On the dynamical theory of incompressible viscous fluids and the determination of the criterion”, *Philosophical Transactions of the Royal Society of London* A. JSTOR, 123–64, 1985.

[66] Wilcox D.C., “Turbulence Modelling for CFD”. DCW Industries California, USA, 1994.

[67] Menter F. R., “Improved two equations k-ω turbulence models for aerodynamics flows”, NASA Ames Research Center, California, Techinical Memorandun 103795, October 1992.

[68] Wilcox D. C., “Turbulence Modelling for CFD”, DCW Industries, 2nd edn. 37, 39, 45, 2002

[69] Truckenbrodt, E., “Tragflachentheorie bei inkompressibler”, Jahrbuch der WGL, pp.40-65, 1953.

[70] Weissinger, J. "The Lift Distribution of Swept-back Wings", NACA Tech. mem. 1120, 1947.

[71] Blackwell J., “Numerical Method to Calculate the Induced Drag or Optimal Span Loading for Arbitrary Non-Planar Aircraft”, NASA SP-405, May 1976.

[72] Sadraey M., Aircraft Performance Analysis, VDM Verlag Dr. Müller, 2009.

[73] Bushnell, D. M., “Supersonic aircraft drag reduction”, *AIAA paper* 90-1596, 1990.

[74] Kcühemann, D., “Aircraft shapes and their aerodynamics for flight at supersonic speeds”, *Adv. Aero. Sci*., 3, 221-253, 1962.

[75] Rokhsaz, K., “A brief survey of wing tip devices for drag reduction”, *SAE paper* 93-2574, 1993.

[76] Hendrickson R., Grumman, with Dino Roman and Dario Rajkovic, “The Dragbusters, Chapter 5, Drag: An Introduction”, 1997.

[77] Küchemann, D., “The Aerodynamic Design of Aircraft”, Pergamon Press, Oxford. 1978.

[78] Lynch, F.T., “Commercial Transports Aerodynamic Design for Cruise Performance Efficiency,” Transonic Aerodynamics, Nixon, D., ed., *Progress in Astronautics and Aeronautics,* Vol. 181, AIAA New York, 1982.

[79] Reneaux, J., “Overview on drag reduction technologies for civil transport aircraft”, *European Congress on Computational Methods in Applied Sciences and Engineering (ECCOMAS*), Jyväskylä, Finland, 24-28, July 2004.

[80] Ashill P. “CFD methods for drag prediction and analysis currently in use in UK”, 1988.

[81] Vandervooren J., “Aircraft drag prediction for transonic potential flow”, *AGARD, Technical Status Review on Drag Prediction and Analysis from Computational Fluid Dynamics:* State of the Art 17 p(SEE N 89-26817 21-02). 1989.

[82] Price A. R., Keane A. J., Holden C., “On the coordination of Multidisciplinary Design Optimisation Using Expert Systems”, *AIAA Journal*, Vol. 49, No 8, 2011.

[83] Pickett R.M., Rubinstein M.F., Nelson R.B., “Automated structural synthesis using a reduced number of design coordinates”, *AIAA Journal* 11(4):489–494, 1973.

[84] Samareh J. *A. “*Survey of shape parameterization techniques for high fidelity multidisciplinary shape optimization*”*, *AIAA Journal*, 39(5):877-889, 2001.

[85] Trapani G., “Multi-Objective Optimization of 2D High-Lift Airfoil Configuration using Tabu Search”, *Master thesis*, Cranfield University, Cranfield, UK, 2009.

[86] Elliott J. and Peraire J., “Practical three-dimensional aerodynamic design and optimization using unstructured meshes”, *AIAA*, Vol. 35, pp. 1479–1486, 1997.

[87] Rogers D. F., “An Introduction to NURBS with Historical Perspective”, Morgan Kaufmann Publisher, 2000.

[88] Farin, G., “Curves and surfaces for computer aided geometric design”, Academic Press Professional, Inc., San Diego, United States. 1993.

[89] Guerrera Vela P. P., “Aero-Structural Airfoil Design Optimisation for Cruising Configuration using Tabu Search”, *Master thesis*, Cranfield University, Cranfield UK, 2011.

[90] Hicks R. M. and Henne P.A., “Wing design by numerical optimization”. *Journal of Aircraft*, 15:407-412, 1978.

[91] Sederberg, T. W. and Parry, S. R., “Free-form deformation of solid geometric models”, SIGGRAPH, pp. 151–160, 1986.

[92] Samareh J. A., “A novel shape parameterization approach”, *NASA* 1999-209116, 1999.

[93] Bechmann D., Bertrand Y., and Thery S., “Continuous free form deformation”, *Computer Networks and ISDN Systems*, 29, p. 1715–1725, 1997.

[94] Sobieczky H., “Parametric airfoils and wings”, *Notes on Numerical Fluid Mechanics*, Volume 68 Vieweg verlag, pp. 71-88, 1998.

[95] Paul, S. and Ruxandra, B., “Two-dimensional aerofoil shape optimisation for aerofoils at low speeds”, *AIAA Modeling and Simulation Technologies Conference*, AIAA 2012-4790, 2012.

[96] Harris, C.D., “NASA supercritical aerofoils: a matrix of family-related aerofoils”, Washington, D.C.: NASA, 1990.

[97] Kulfan, B.M. and Bussoletti, J.E., "Fundamental Parametric Geometry Representations for Aircraft Component Shapes”, *AIAA* 2006-6948, 2006.

[98] Kulfan, B.M., “Recent Extensions and Applications of the CST Universal Parametric Geometry Representation Method”, *AIAA* 2007-7709, 2007.

[99] Kulfan, B.M., “A Universal Parametric Geometry Representation Method – CST”, *AIAA* 2007-62, 2007.

[100] Kulfan, B.M., “Universal parametric geometry representation method”, *Journal of Aircraft,* Vol 45, No.1. 142-159, 2008.

[101] Kulfan, B.M., “New Supersonic Wing Far-Field Composite-Element Wave-Drag Optimisation Method”, *Journal of Aircraft,* 46(5): 1740-1758, 2009.

[102] Kulfan, B.M., “Recent extensions and applications of the 'CST' universal parametric geometry representation method”, *Aeronautical Journal*, 114(1153): 157-176, 2010.

[103] Edgeworth F.Y., “Mathematical Psychics”, P. Keangan, London, 1881.

[104] Pareto V., “Cors D’Economie Politique, Vol I, II”, F. Rouge, Lausanne, 1896.

[105] Kipouros T., “Multiobjective Aerdynamic Design Optimisation”, *PhD, First Year Report*, Jesus College, Cambridge University, UK, 2003.

[106] Kipouros, T., Jaeggi, D. M., Dawes, W. N., Parks, G. T., Savill, A. M. and Clarkson P. J., “Biobjective design optimization for axial compressor using tabu search”, *AIAA Journal*, 46(3):701-711, 2008.

[107] Parks G. T., “Linear Algebra – Optimisation”, *Lecture Notes, Module 4M13*, Cambridge University, Engineering Department, 2002.

[108] Aly, S., Ogot, M., Pelz, R. “Stochastic Approach to Optimal Aerodynamic Shape Design”, *Journal of Aircraft* Vol. 33, No. 5, pp. 956-961, 1996.

[109] Parks G.T. “Stochastic Process and Optimisation Methods”, *Lecture Notes, Module 5R1*, Cambridge University, Engineering Department, 2003.

[110] De Souza X., Suykens J., Vandewalle J., and Bolle D. “Coupled simulated annealing”, *IEEE Trans Syst Man Cybern B Cybern*, 2009.

[111] Aarts E., Korst J. “Simulated Annealing and Boltzman Machines: A Stochastic Approach to Combinatorial Optimisation and Neural Computing”, John Wiley and Sons, 1989.

[112] Holland, J. “Adaptation in natural and artificial systems”, *MIT Press*, Cambridge, MA, 1992.

[113] Goldberg D. E. “Genetic algorithm in Search, Optimisation, and Machine Learning”, *Addison-Wesley Publishing Company*, 1989.

[114] Connor, A.M. and Tilley D.G. “A TABU Search method for the optimisation of fluid power circuits”, *IMechE Journal of System and Control*, Vol. 212, pp. 373-378, 1998.

[115] Jaeggi D. M., Parks G. T., Kipouros T., and Clarkson P. J. “The development of a multi-objective tabu search algorithm for continuous optimization problems", *European Journal of Operational Research*, 185:1192_1212, 2008.

[116] Kipouros T. “Multiobjective Aerodynamic Design Optimisation”, *PhD thesis, Cambridge University*, Cambridge, UK, 2003.

[117] Hooke R., Jeeves T.A. (1961). "Direct search; solution of numerical and statistical problems”, *Journal of the Association for Computing Machinery* (ACM) 8 (2): 212–229, 1961.

[118] Harvey S.A. “The design optimisation of turbomachinery blade rows”, *PhD Thesis, Cambridge University*, 2002.

[119] Deb K., Pratep A., Agarwal S. and Meyarivan T. “A Fast Elitist Multi-Objective Genetic Algorithm: NGSA-II”, *IEEE Transaction of Evolutionary Computation*, Vol. 6 No.2, pp.182-197, 2002.

[120] Kipouros T., Jaeggi D.M., Dawes W.N., Parks G.T., Savill A.M. and Clarkson P.J. “Insight into high-quality aerodynamic design spaces through multi-objective optimisation”, *CMES: Computer modeling in Engineering and Sciences*, Vol. 37 No.1, pp. 1-44, 2008.

[121] Ghisu T., Parks G.T., Jarret J.P. and Clarkson P.J. “An Integrated System for the Aerodynamic Design of Compression Systems: part II Application”, *Journal of Turbomachinery*, Vol. 133 No.1, pp. 011012, 2011.

[122] Kleijnen J.P.C. “Statistical Tools for Simulation Practitioners”, Marcel Dekker, NY, 1987.

[123] Cenaero I. L., “Complements on Surrogate Based Optimization for Engineering Design”, RTO- EN-AVT-167 5 – 167.

[124] Forrester J. and Keane A.J., “Recent advances in surrogate-based optimization”, *Progress in Aerospace Sciences*, Volume 45, Issues 1-3, January-April, pp. 50-79, 2009.

[125] Queipo N.V., Haftka R.T., Shyy W., Goel T., Vaidyanathan R., Tucker P.K., “Surrogate-based analysis and optimization”, *Progress in Aerospace Sciences*, Volume 41, Issue 1, pp. 1-28, 2005.

[126] Forrester A., Sobester A., Keane A., “Engineering Design via Surrogate Modelling” A Practical Guide, John Wiley & Sons Ltd, 2008.

[127] Smith, M. "Neural Networks for Statistical Modeling", Von Nostrand Reinhold, New York, 1993.

[128] Cheng, B. and Titterington, D. M. "Neural Networks: A Review from a Statistical Perspective", *Statistical Science*, Vol. 9, No. 1, pp. 2-54, 1994.

[129] Pearson K., “On lines and planes of closest fit to systems of points in space”, *Philosophical Magazine*, Vol. 2, No. 6, pp. 559-572, 1901.

[130] Loeve M., “Probability theory”, M. Loeve. Springer-Verlag, New York, 4th edition, 1977.

[131] Sirovich L., “Turbulence and the dynamics of coherent structures”, Quarterly of Applied Mathematics, Vol. 45, No. 3, pp. 561-571, 1987.

[132] Hall K.C., Thoma J.P., Dowell E.H., “Reduced-order modeling of unsteady small-disturbance flows using a frequency-domain proper orthogonal decomposition technique”, *AIAA Paper* 99-0655, 1999.

[133] Newman, A. “Model reduction via the Karhunen-Loève expansion, Part I: An exposition”, *Technical Report TR 96-32*, Inst. Systems Research, 1996.

[134] Hall K.C., Thomas J.P., and Dowell E.H., “Reduced order-modeling of unsteady small-disturbance flows using a frequency-domain proper orthogonal decomposition technique", *AIAA Paper*, 99-0655, 1999.

[135] Bui-Thanh T. and Willcox K., “Aerodynamic Data Reconstruction and Inverse Design Using Proper Orthogonal Decomposition”, *AIAA Journal*, Vol. 42, No. 8, pp. 1505- 1516, 2004.

[136] Falkiewicz N.J. and Cesnik C.E.S., “Proper Orthogonal Decomposition for Reduced- Order Thermal Solution in Hypersonic Aerothermoelastic Simulations", *AIAA Journal*, Vol. 49, No. 5, pp. 994-1009, 2011.

[137] Gross A. and Fasel H., “Control-Oriented Proper Orthogonal Decomposition Models for Unsteady Flows”, *AIAA Journal*, Vol. 45, No. 4, pp. 814-827, 2007.

[138] Siegal S., Cohen K., Seidel J., and McLaughlin T., “Proper Orthogonal Decomposition Snapshot Selection for State Estimation of Feedback Controlled Flows”, *AIAA Paper* 2006-1400, 2006.

[139] Hung V. and Hien T., “Modeling and Control of Physical Processes Using Proper Orthogonal Decomposition”, *Mathematical and Computer Modeling*, Vol. 33, Nos. 1-3, pp. 223-236, 2001.

[140] Feeny B.F. and Kappagantu R., “On the Physical Interpretation of Proper Orthogonal Modes in Vibrations”, *Journal of Sound and Vibration*, Vol. 211, pp. 607-616, 1998.

[141] Kappagantu R. and Feeny B.F., “Part 2: Proper Orthogonal Modal Modeling of a Frictionally Excited Beam”, *Nonlinear Dynamics*, Vol. 23, pp. 1-11, 2000.

[142] Azeez M.F.A. and Vakakis A.F., “Proper Orthogonal Decomposition (POD) of a Class of Vibroimpact Oscillations”, *Journal of Sound and Vibration*, Vol. 240, pp. 859-889, 2001.

[143] Kim Y.Y. and Kapania R.K., “”Neural Networks for Inverse Problems in Damage Identification and Optical Imaging Using Orthogonal Arrays and

Principal Component Analysis", *AIAA Journal*, Vol. 44, No. 7, pp. 1628-1634, 2006.

[144] Chock J.M.K. and Kapania R.K., "On Load Updating for Finite Element Models", *AIAA Journal*, Vol. 41, No. 9, pp. 1667-1673, 2003.

[145] My-Ha D., Lim K., Khoo B. and Willcox K., "Real-Time Optimisation Using Proper Orthogonal Decomposition: Free Surface Prediction Due to Underwater Bubble Dynamics", *Computers and Fluids*, Vol. 36, No. 3, pp. 499-512, 2007.

[146] LeGresley P. and Alonso J., "Airfoil Design Optimization Using Reduced Order Models Based on Proper Orthogonal Decomposition", *AIAA Paper*, 2000-2545, 2000.

[147] Toal D.J.J., Bressloff N.W, Keane A.J., and Holden C., "Geometric Filtration Using Proper Orthogonal Decomposition for Aerodynamic Design Optimization", *AIAA Journal*, Vol. 48, No. 5, 2010, pp. 916-928, 2010.

[148] Kosambi D.D., "Statistics in Function Space", *Journal of the Indian Mathematical Society*, Vol. 7, pp. 76-88, 1943.

[149] Karhunen K., "Uber Lineare Methoden in der Wahrscheinlichkeitsrechnung", Annals of Academic Science Fennicae Series A1, *Mathematical Physics*, Vol. 37, pp. 1-79.

[150] Loéve M., "Probability theory", Graduate Texts in Mathematics, Springer-Verlag, New York, 4th ed., ISBN 0-387-90262-7, 1978.

[151] Pearson K., "On lines and planes of closest fit to systems of points in space", *Philosophical Magazine*, Vol. 2, No. 6, pp. 559-572, 1901.

[152] Jolliffe I.T., "Principal Component Analysis", Springer-Verlag, New York, 2nd ed., ISBN 978-0-387-95442-4, 2002.

[153] Golub G.H. and Van Loan C.F., "The Singular Value Decomposition", Matrix Computations, Johns Hopkins University Press, Baltimore, MD, 3rd ed., 1996.

[154] Mifsud, M., "Reduced-order modelling for high-speed aerial weapon aerodynamics", *PhD thesis, Cranfield University* - College of Aeronautics, 2008.

[155] Lucia D.J., Beranb P.S., and Silva W.A. "Reduced-order modelling: new approaches for computational physics", *Progress in Aerospace Sciences*, Vol. 40, pp. 51-117, 2004.

[156] Cook P.H., McDonald M.A., Firmin M.C.P. “Aerofoil RAE 2822 – Pressure Distributions, and Boundary Layer and Wake Measurements”, Experimental Data Base for Computer Program Assessment, *AGARD Report* AR 138, 1979.

[157] Lorente L.S., Vega J.M., and Velazquez A. “Generation of Aerodynamic Database Using High-Order Single Value Decomposition”, *Journal of Aircraft*, Vol. 45, No. 5, pp. 1780-1788, 2008.

[158] Huyse L., Padula S.L., Lewis M.R., and Wu L. “Probabilistic approach to free-form airfoil shape optimization under uncertainty”, *AIAA Journal*, Vol. 40, No. 9, pp.17641772, 2002.

[159] Li. F., Li G., Sun G., Luo Z., and Zhang Z. “Multi-Disciplinary Optimization for Multi-Objective Uncertainty Design of Thin Walled Beams”, *CMES: Computer Modeling in Engineering and Science*, Vol. 19, No.1, pp. 37-56, 2010.

[160] Hoult D. P., Meador C. L., Deyst J. and Dennis M.,“Cost awareness in Design: The Role of Data Commonality”, *SAE Techinical Paper* 960008, 1996.

[161] Humphreys, K.K., “Project and Cost Engineer’s Handbook”, 4th ed., Marcel Dekker, New York, 2005.

[162] DTI. Aerospace & Defence Technology Report, 2006.

[163] Sirirojvisuth A., “Development of a Hybrid Lifecycle cost estimating tool (HLCET) for manufacturing influenced design trade off”, PhD thesis, Georgia Institute of Technology, 2012.

[164] Early J. M. and Price M.A., “Whole-Life Costing for Capability”, *Journal of Aircraft* Vol. 49, No. 3, May–June 2012.

[165] Narasimha L., “Development of appropriate solutions using current costing tools to support Multidisciplinary Design Optimisation (MDO)”, *Master thesis, Cranfield University*, Cranfield, UK, 2009.

[166] Kaufmann M., “Cost/Weight Optimization of Aircraft Structures”, *PhD Thesis, KTH School of Engineering Sciences*, Sweden, 2006.

[167] Roskam J., “Airplane Design: Part VIII, Airplane Cost Estimation: Design, Development, Manufacturing and Operating”, Roskam Aviation and Engineering Corporation, 1990.

[168] Btissame, “Towards a whole Life Cycle Cost Model for ERP projects”, *Master thesis Cranfield University*, pp. 9-11, 2006.

[169] Ostwald P. “Engineering cost estimating”, Englewood Cliffs, NJ:Prentice - Hall; 576pp, ISBN 0-13-276627-2. 1992.

[170] Stewart R, Wyskidsa R, Johannes J. Cost estimator’s reference manual, 2nd ed. New York:Wiley Interscience,1995.

[171] Shuford Jr RH. “Activity-based costing and traditional cost allocation structures”. In: Stewart RD, Wyskida RM, Johannes JD, editors. Cost estimator’s reference manual. 2nd ed. New York:Wiley; p. 41–94, 1995.

[172] Curran, R., Raghunathan, S., Price M., “Review of Aerospace Engineering Cost Modelling: The Genetic Causal Approach”, *Progress in Aerospace Sciences*, 40, pp. 487-534, 2004.

[173] Torenbeek E., “Synthesis of Subsonic Airplane Design”, Delft University Press, Martinus Nijhoff Publishers, 1982. Press, Martinus Nijhoff Publishers, 1982.

[174] Niazi, A., Dai J. S., Balabani S., and Seneviratne L. “Product cost estimation: Technique classiffication and methodology review”. *Journal of Manufacturing Science and Engineering, Transactions of the ASME*, 128(2): 563-575, 2006.

[175] DoD, Parametric estimating handbook, Department of Defence, 1999.

[176] Peoples R. and Willcox K., “Value-Based Multidisciplinary Optimization for Commercial Aircraft Design and Business Risk Assessment”, *Journal of Aircraft*, Vol. 43, No. 4, July–August 2006.

[177] Agyapong-Kodua, K., Wahid B.M. and Weston R.H., “Towards the derivation of an integrated process cost modelling technique for complex manufacturing systems”, *International Journal of Production Research*, 2012.

[178] Asiedu Y. and Gu P., "Product life cycle cost analysis; state of the art review", *International Journal of Production Research* 36(4), pp. 883-908, 1998.

[179] Harding A, Lowe D, Hickson A, Emsley M, Duff R. “The cost of procurement: a neural network approach”, *International conference in construction information technology*. Reykjavik, Iceland; 28–30 June 2000.

[180] Thokala P., Scanlan J. and Chipperfield A., “Framework for Aircraft Cost Optimization Using Multidisciplinary Analysis”, *Journal of Aircraft*, Vol. 49, No. 2, March–April 2012.

[181] Curran, R., Price, M., Raghunathan, S., Benard, E., Crosby, S., Castagne, S.,Mawhinney, P., “Integrating Aircraft Cost Modeling into Conceptual Design”, *Concurrent Engineering: Research and Applications*, Vol. 13, No. 4, pp. 321–330, Dec. 2005.

[182] Maurice D’Ocagne, “Coordonnées Parallèles et Axiales: Méthode de transformation géométrique et procédé nouveau de calcul graphique déduits de la considération des coordonnées parallèlles”, Gauthier-Villars, Paris, 1885.

[183] Wegman E. J., “Hyperdimensional data analysis using parallel coordinates”, *Journal of the American Statistical Association* 85, 411, 664–675, 1990.

[184] Inselberg A., “Parallel Coordinates: Visual Multidimensional Geometry and Its Applications”, Springer, New York, 2009.

[185] Roskam J., “Airplane Design Part I: Preliminary Sizing of Airplanes”, Roskam Aviation and Engineering Corporations, Ottawa, KS, 1985.

[186] Houghton, E. L. and Carruthers, N. B., “Aerodynamics for Engineering Students”, 3rd Edition, Edward Arnold, London, 1982.

Appendix A: Publications

- **D. Di Pasquale, "***Automatic High-Speed Aerodynamics Process for preliminary Multi-Disciplinary design".* Phoenix Model Center International Users Conference, Toulouse, France, 24-26 June 2013.

- **D. Di Pasquale, "***Aero and cost modelling optimisation for aircraft in a Multi-disciplinary context".* The Airbus Flight Physics Distributed R&T Partnership – DiPaRT 'Flight Physics of the Future Wing', Bristol & Bath Science Park, 25th to 27th November 2013.

- **D. Di Pasquale,** C. Holden, T. Kipouros and M. Savill, "*An Automatic Aerodynamic Design Process in an Industrial Multi-Disciplinary Context".* 6th European Conference on Computational Fluid Dynamics (ECFD VI), Barcelona, Spain, 20 – 25, July 2014.

- **D. Di Pasquale**, K. Dunlop, "*Multi-Disciplinary Integrated Analysis study with the assistance of Simulation integration tool and Data Management systems"*. The Airbus Flight Physics Distributed R&T Partnership – DiPaRT 'Multi-Disciplinary Optimisation in Aircraft Design, Analysis Preparation', CFMS Bristol & Bath Science Park, 2nd October 2014.

- **D. Di Pasquale,** T. Kipouros, C. Holden and M. Savill, "*Integrated Systems for Aerodynamic Design Optimisation".* 11th International Conference on Evolutionary and Deterministic Methods for Design, Optimization and Control with Applications to Industrial and Societal Problems, EUROGEN-2015, Glasgow (UK), 14-16 September 2015.

Posters

- **D. Di Pasquale,** *Aerodynamic and Cost Modelling Optimisation for Aircraft Multi-Disciplinary Design.* Airbus PhD Day, Bremen, Germany, October 2014.
- **D. Di Pasquale,** *Aerodynamic and Cost Modelling Optimisation for Aircraft Multi-Disciplinary Design.* DTC poster session, Cranfield University, UK, February 2013.

- **D. Di Pasquale,** *Multi-Disciplinary Design for the Whole Aircraft Application.* Airbus PhD Day, Toulouse, France, October 2012.

Appendix B: Other related work completed

I have been involved in a Research and Technology (R&T) project for which the aim is to develop a new preliminary multi-disciplinary design process by increasing the fidelity of the elements of the existing conceptual design process through exploitation of appropriate domain tools.

Specifically, within it I was responsible not only of the aero and cost part of the process but I have also created the structural geometry file.

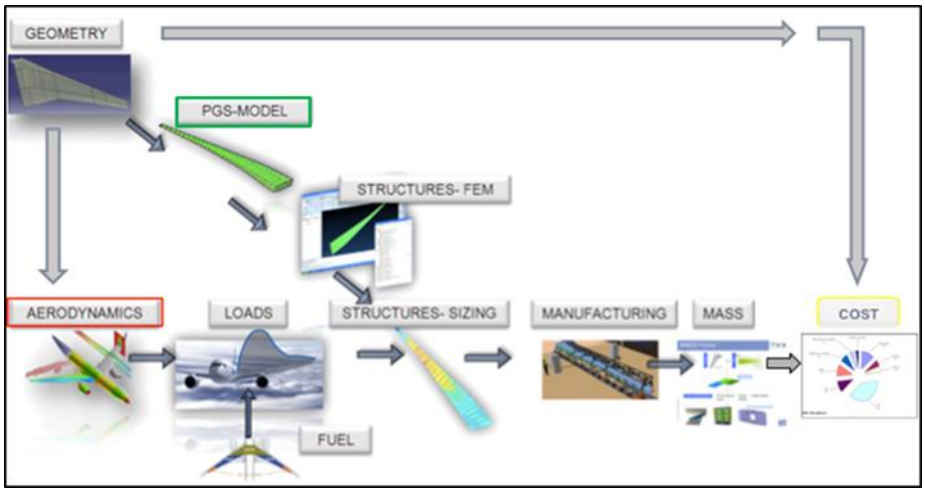

Basically I took the top level geometry delivered and made some changes to it and converted it to a format suitable for the next step of the process, i.e. the generation of the Mesh, later used for the Finite Element Analysis and sizing.

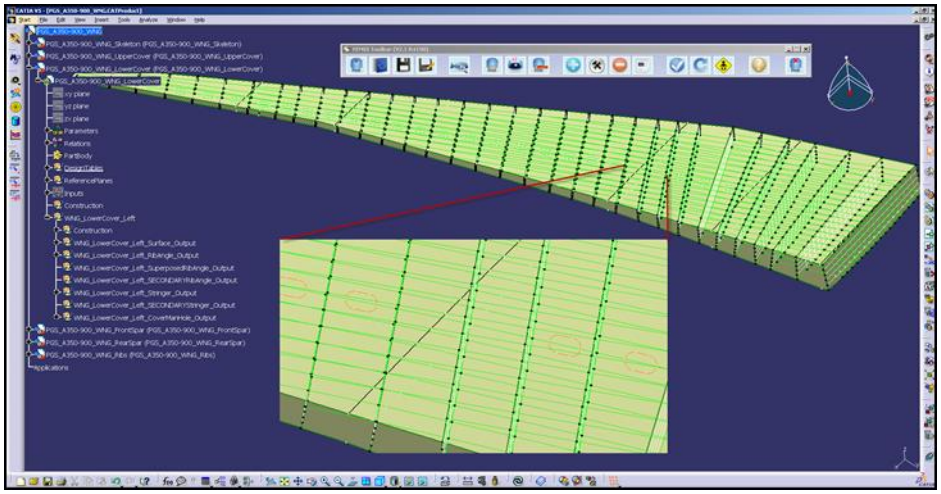

Screen shoot of the structural geometry created during the Wing design process.

I was also in charge of the bump organization that allowed me to improve my management skills. The bump is basically a Demo that lasts two weeks. During this time people from different disciplines gather together in an integration room and everyone does its part of the process, sequentially, with some activities in parallel where appropriate.

In addition to that, I have conducted a survey in order to classify aero tools in terms of the function of the method, usage, mesh type, limitations, accuracy and run time. The aim of this survey was to understand which of them is more appropriate to use for, depending on the MD layers and applications involved. This has been done also because a variety of independent methods are used on different Airbus sites with different granularity. As a result department dependent multiple references used, providing inconsistent not agreed or acknowledged starting points, which decreases the efficiency in collaborations and at MG3 gate reviews. The survey contributes to a convergence and standardisation of Pre-MG3 tools. It will provide an understood status tracking and enables a seamless handover at MG3 and continuation Post MG3 gate reviews. The survey will directly simplify the Airbus aerodynamic prediction landscape and utilise the aerodynamic function knowledge base, which is used/established as knowledge capturing process.